

Designing a chemical “toolbox” for the efficient inhibition of metalloenzymes.

Ryan Antony Hubball

Submitted in accordance with the requirements for the degree of
Doctorate of Philosophy

The University of Leeds
School of Chemistry

December, 2021

The candidate confirms that the work submitted is his/her own and that appropriate credit has been given where reference has been made to the work of others.

This copy has been supplied on the understanding that it is copyright material and that no quotation from the thesis may be published without proper acknowledgement.

The right of Ryan Antony Hubball to be identified as Author of this work has been asserted by him in accordance with the Copyright, Designs and Patents Act 1988.

© 2021 The University of Leeds and Ryan Antony Hubball

Acknowledgements

Firstly, I would like to thank Professor Colin Fishwick for the opportunity to take on this PhD project and for his advice over the years. This project has provided me a wealth of experience in areas of which I had little prior expertise in and which is sure to serve me well in my future endeavours.

I would like to also extend my thanks to all members of the Fishwick group past and present for their valuable advice, with which this project has been all the richer. I would especially like to mention Dr Chris Fitzpatrick and Dr Martin McPhillie for their help with many challenging aspects of this project.

This work would not have been possible without the contributions of the Schofield Group at the University of Oxford, and so I would like to thank Professor Chris Schofield FRS, Dr Karina Calvopina and Alen Krajnc.

Thanks is also due to the BBSRC for funding this project.

Many other members of the School of Chemistry at the University of Leeds have contributed positively to this project. In no particular order, I would like to extend my gratitude towards Luke Trask, Kyle Orritt, Dan Francis, Chris Arter, Lewis Turner, Ryan Gonciarz, Jacob Hauser, Mark Howard, all of the stores and technical staff and everyone else who has contributed in some way towards this work and towards my time at the University of Leeds.

Finally and most importantly, I would like to thank my family, partner and friends for their unwavering support over the course of this PhD project. They might have no idea what it is I actually do, but have supported me nonetheless and without them this would not have been possible.

Abstract

Metalloenzymes, enzymes that utilise a metal ion within their active site for their enzymatic activity, make up a significant portion of known enzymes. In fact, literature suggests that approximately 40 – 50% of all known enzymes may be classed as metalloenzymes. Many of these are implicated in disease and drug resistance. Despite this, there is a significant lack of small-molecule therapeutics focused upon metalloenzyme inhibition.

Metallo- β -lactamases are a family of metalloenzymes that can be found in bacteria. These enzymes cause drug resistance against β -lactam antibiotics, such as penicillin, to emerge in these bacteria. Currently there are no metallo- β -lactamase inhibitors available for clinical use. As such, the World Health Organisation has noted this gap as being a priority for development.

This thesis describes attempts to develop new metal-binding functionalities and to extend the evidence of known functionalities in targeting metallo- β -lactamases. What is learned from this work can then be used to inform medicinal chemists of effective metal-binding moieties when developing small-molecule therapeutics for other metalloenzymes.

Significant *in silico* design has been used throughout to aid with the design of molecules based upon targeting Verona integron-encoded metallo- β -lactamase 2. This has led to the extension of knowledge of a previously identified series of thiol-based metallo- β -lactamase inhibitors. Additionally, work on a series of compounds containing a dithiocarboxylate functional group has identified a novel class of inhibitors of these metalloenzymes, showing micromolar activity in assays against a panel of metallo- β -lactamases. Investigation of the stability of the dithiocarboxylate functional group and possible routes of degradation has also been carried out. It is hoped that this work can contribute to the development of potent, selective small-molecule inhibitors of metallo- β -lactamases and other metalloenzymes.

Table of Contents

Acknowledgements	3
Abstract	4
Table of Contents	5
List of Abbreviations	7
Common amino acids.....	7
Other abbreviations (in order of appearance in text)	8
Chapter 1 Introduction	11
1.1 Bacteria and their mechanisms of resistance	11
1.1.1 Bacterial structure	11
1.1.2 Bacterial defences	14
1.1.2.1 The cell wall, porins and efflux pumps.....	14
1.1.3 How does resistance spread throughout bacteria?.....	19
1.1.4 What is being done to combat resistance?	21
1.2 The history and current state of antibiotics.....	22
1.2.1 The ‘golden-age’ of antibiotic discovery	22
1.2.2 The genomic revolution and why it did not help	26
1.2.3 An overview of recent trends in antibiotic research	26
1.2.4 The rise of resistance	27
1.3 β -lactam antibiotics and β -lactamases.....	28
1.3.1 β -lactam antibiotics.....	28
1.3.2 β -lactamase enzymes	29
1.3.3 Inhibitors of β -lactamases.....	42
Chapter 2 Design, docking & synthesis of metallo-β-lactamase inhibitors	53
2.1 Cyclic boronates.....	53
2.1.1 Introduction	53
2.1.2 Synthesis of cyclic boronate MBL inhibitors	55
2.2 Thiol-based MBL inhibitors.....	63
2.2.1 Introduction	63
2.2.2 Computational docking of thiol-based MBL inhibitors.....	66
2.2.3 Synthesis of thiol-based MBL inhibitors.....	81
2.3 Dithiocarboxylates	92

2.3.1 Introduction	92
2.3.2 Synthesis of dithiocarboxylate-based MBL inhibitors	94
2.4 Anethole trithione	104
2.4.1 Docking & synthesis	104
Chapter 3 Metallo-β-lactamase inhibition assay results & discussion	106
3.1 Metallo- β -lactamase assay platform.....	106
3.2 Biological results	107
3.3 Analysis of metallo- β -lactamase enzyme assay results	114
3.3 Dithiocarboxylate degradation.....	122
3.4 The mass difference problem.....	127
Chapter 4 Conclusions & Future Work.....	129
4.1 General conclusions.....	129
4.2 Thiol-based inhibitors	129
4.2.1 <i>In silico</i> design.....	129
4.2.2 Synthetic development of thiol-based inhibitors	130
4.2.3 Biological results	131
4.3 Dithiocarboxylates.....	131
4.3.1 Fragment validation.....	131
4.3.2 Synthetic development.....	132
4.3.3 <i>In silico</i> design for further elaboration of the series	132
4.3.4 Biological activity.....	133
4.3.5 Stability & degradation	134
4.4 Future work	134
4.4.1 Thiol-based inhibitors	134
4.4.2 Dithiocarboxylates.....	135
Chapter 5 Experimental	136
General information.....	136
Computational.....	136
Synthetic chemistry	136
Biology	137
Experimental notes	138
List of References	181
Appendix.....	203
Linear regression analysis plots	203

List of Abbreviations

Common amino acids

Ala – Alanine

Arg – Arginine

Asn – Asparagine

Asp – Aspartic acid

Cys – Cysteine

Glu – Glutamic acid

Gln – Glutamine

Gly – Glycine

His – Histidine

Ile – Isoleucine

Leu – Leucine

Lys – Lysine

Met – Methionine

Phe – Phenylalanine

Pro – Proline

Ser – Serine

Thr – Threonine

Trp – Tryptophan

Tyr – Tyrosine

Val – Valine

Other abbreviations (in order of appearance in text)

OMVs – Outer membrane vesicles

PBPs – Penicillin binding proteins

OmpC – Outer Membrane Protein C

MDR – Multi-drug resistant

rRNA – Ribosomal ribonucleic acid

VGT – Vertical gene transfer

HGT – Horizontal gene transfer

DNA – Deoxyribonucleic acid

CDC – Centers for Disease Control and Prevention

GSK – GlaxoSmithKline

HTS – High-throughput screen

WHO – World Health Organisation

SBL – Serine- β -lactamase

MBL – Metallo- β -lactamase

TEM – TEM β -lactamases

KPC – *K. pneumoniae* carbapenemase

ESBL – Extended-spectrum β -lactamase

CTX-M – Cefotaximase

OXA – Oxacillinase β -lactamase

BLI – β -lactamase inhibitor

IMP – Imipenem resistant metallo- β -lactamase

VIM – Verona integron-encoded metallo- β -lactamase

NDM – New Delhi metallo- β -lactamase

EDTA – Ethylenediaminetetraacetic acid

NMR – Nuclear magnetic resonance

ACE – Angiotensin-converting enzymes

RT – Room temperature

THF – Tetrahydrofuran

LC-MS – Liquid chromatography-mass spectrometry

TFA – Trifluoroacetic acid

TFAA – Trifluoroacetic anhydride

TLC – Thin-layer chromatography

DCM – Dichloromethane

SPM-1 – Sao Paulo metallo- β -lactamase

MIC – Minimum inhibitory concentration

PDB – Protein Data Bank

Cryo-EM – Cryogenic electron microscopy

SP – Standard precision

XP – Extra precision

IFD – Induced fit docking

IC₅₀ – Half maximal inhibitory concentration

R² – Coefficient of determination

T – Kendall's tau rank coefficient

μ - Population mean

σ – Standard deviation

GUI – Graphical user interface

HRMS – High resolution mass spectrometry

IR – Infrared spectroscopy

pKa – Acid disassociation constant

HMBC – Heteronuclear multiple bond correlation

RBF – Round bottom flask

UV – Ultraviolet spectroscopy

HPLC – High pressure liquid chromatography

ppm – Parts per million

DEPT – Distortionless enhancement by polarisation transfer

COSY – Correlated spectroscopy

HSQC – Heteronuclear single quantum coherence

FTIR – Fourier transfer infrared spectroscopy

Chapter 1

Introduction

1.1 Bacteria and their mechanisms of resistance

Bacteria are a vast domain of microorganisms and can be found in every environment on Earth.

They are prokaryotic, lacking a membrane-bound nucleus, amongst other differences in internal structure that separates them from eukaryotic organisms. They are also separated from the domain of *Archaea* due to differences in internal structure, although these differences are more subtle (as such, *Archaea* and bacteria were not formally separated until the 1990s)¹.

Prokaryotes lack distinct intracellular organelles, membrane-bound structures that lie within the cytoplasm that are used to carry out cellular functions. Prokaryotic structure is somewhat simpler compared to that of eukaryotes, which do possess obvious intracellular organelles, however the functions that are usually performed by these specialised organelles are instead carried out within the cytoplasm by organelle-like structures, which are nevertheless less complex than that of their eukaryotic relations². These simplifications allow bacteria to be amazingly highly adaptable; they are able to reproduce through mitosis rapidly, conferring them an evolutionary advantage through vertical gene transfer (the process by which cells pass genes down to further generations)³.

1.1.1 Bacterial structure

The shape of individual bacteria varies greatly, but can generally be reduced to three main types: spherical (*coccus*), rodlike (*bacillus*) or curved (*vibrio*, *spirillum*, or *spirochete*) (*Fig. 1*). They are the smallest living organisms, with particularly small examples sometimes being 0.1 µm in width and 1 µm in length (*Mycoplasma pneumoniae*) but some examples can reach sizes of 750 µm in diameter (*Thiomargarita namibiensis*) and are viewable by the naked eye³.

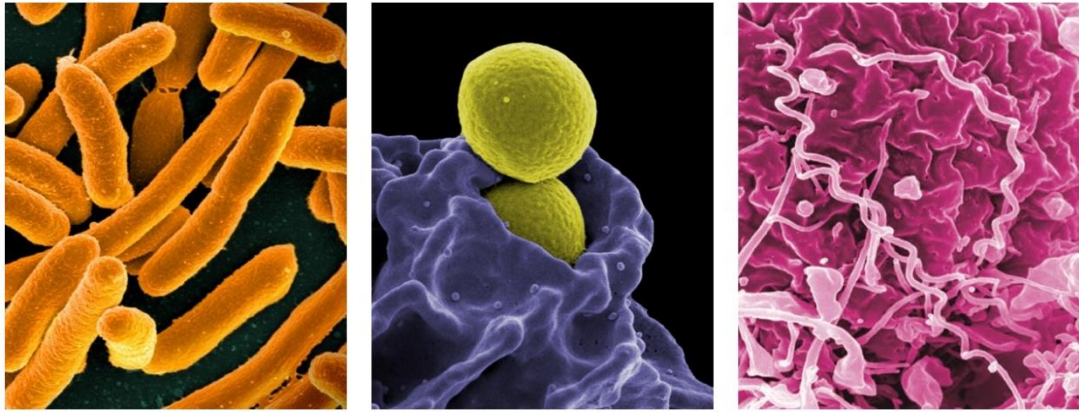


Figure 1. Images of rodlike *Escherichia coli* (bacillus), spherical *Staphylococcus aureus* (coccus) and curved *Treponema pallidum* (spirochete) bacteria. Images taken from National Institute of Allergy and Infectious Diseases⁴.

Since the invention of the eponymously named Gram stain in 1884, bacteria have been divided according to being Gram-positive or Gram-negative. Gram-positive bacteria retain this violet stain (a crystal violet – iodine complex) when washed, whilst Gram-negative bacteria are cleared of it but are subsequently stained red by a complementary stain (carbol fuchsin or safranin). The reason for this lies in the differences in their cell membrane structure⁵.

1.1.1.1 Gram-positive bacteria

Gram-positive bacteria feature a cytoplasmic membrane and single, relatively thick peptidoglycan cell wall, to which secondary polymers are attached. The majority of the mass of this cell wall is made up of anionic polymers, teichoic acids, and it also features many proteins which are responsible for various functions, such as intercellular signalling and regeneration of the cell wall^{6,7}.

The Gram stain can penetrate this cell wall and the charged crystal violet-iodine complex sticks to it. During the subsequent washing step the Gram-positive bacteria retains the dye, on account of its thick peptidoglycan layer, and therefore retains a purple hue. During the subsequent dyeing step, the carbol fuchsin or safranin dye is unable to adhere to the cell wall as the bulky crystal violet-iodine complex blocks it^{8,9}.

1.1.1.2 Gram-negative bacteria

Gram-negative bacteria have a relatively more complex cell envelope, compared to their Gram-positive relations. This consists of an inner cytoplasmic membrane, a central peptidoglycan cell wall, and most strikingly

a lipopolysaccharide outer membrane. This outer membrane is unique to Gram-negative bacteria and affords them a greater deal of resistance to many drugs that would otherwise penetrate the bacterial wall (Fig. 2).

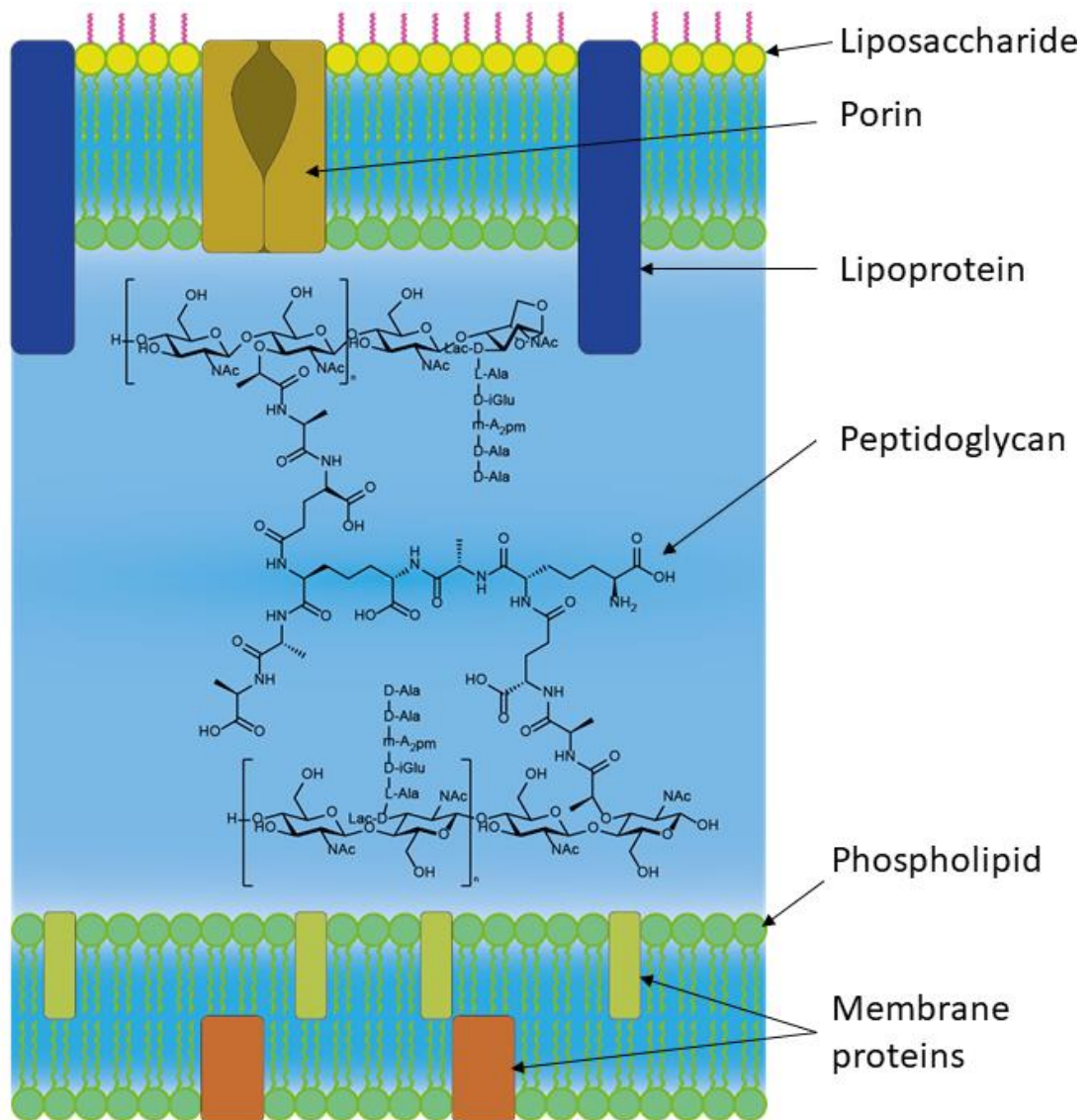


Figure 2. The cell wall of a typical Gram-negative cell. The outer membrane consists of a liposaccharide outer layer and a phospholipid inner layer and holds porins, controlling cellular entry, and lipoproteins that perform various functions. The periplasm between the membrane layers contains peptidoglycan chains. The inner membrane is made up on phospholipids and membrane proteins. Whilst Gram-positive bacteria share the peptidoglycan cell wall, the liposaccharide membranes are unique to Gram-negative bacteria.

The lipopolysaccharide membrane is a bilayer cell wall, but it differs from the peptidoglycan cell wall in the molecules it is constructed of. Whereas the peptidoglycan cell wall is constructed of sugars and amino acids the lipopolysaccharide membrane consists of, as the name would suggest, lipids

and polysaccharides. The two main categories of proteins that lie in this membrane are lipoproteins and β -barrel proteins. Whilst lipoproteins are generally not transmembrane proteins, many of the β -barrel proteins are and these are what construct the porins, allowing molecules to enter the cell⁶.

The peptidoglycan cell wall that lies beneath the liposaccharide membrane in Gram-negative bacteria is largely similar in structure to that in Gram-positive bacteria but is far thinner. It is due to this lower peptidoglycan content that the Gram-negative bacteria do not retain the crystal violet – iodine complex when being washed of the Gram-stain. The bacteria are decolourised by the alcohol rinse, which disrupts the glycoprotein outer-membrane, and then take up the carbol fuchsia or safranin, staining them red^{5,9}.

A unique ability of Gram-negative bacteria is their ability to create outer-membrane vesicles (OMVs). These OMVs are formed at the cellular envelope are intentionally released from the cell during active growth, as opposed to being a by-product of cell lysis. This releases a lipid-enclosed particle into the bacterium's environment, which can carry bacterial enzymes outside of the usual range of the bacterium. This provides a number of advantages, such as the greater dissemination of genetic material *via* distribution of enzymes and plasmids within their environment that can then in turn be taken in as exogenous material by other bacteria¹⁰.

1.1.2 Bacterial defences

Bacteria can be hazardous to health, and for that reason we have developed antibiotics to kill them. However, for antibiotics to function they need to accumulate within the bacteria and reach an effective concentration. Thus, they must pass through the protective cellular envelope and remain in the cell until they are able to overcome any defences and destroy it. Bacteria have a range of options at their disposal to prevent this.

1.1.2.1 The cell wall, porins and efflux pumps

The cell wall is a bacterium's first line of defence. For an antibiotic to have an effect, it must first enter the bacterium. This is generally not an issue in Gram-positive bacteria, which is quite amenable to penetration by hydrophilic molecules of up to 50000 Da¹¹.

Both Gram-positive and -negative bacteria feature the peptidoglycan cell wall. This cell wall features many proteins which perform various functions. Foremost amongst these are the penicillin-binding proteins (PBPs), which are responsible for the constant regeneration of the cell wall and without which the cell cannot survive, as constant degradation of the cell wall means an equal or higher rate of constant regeneration is also required. DD-transpeptidase is the PBP responsible for joining together glycan chains into the larger peptidoglycan wall. It does this by attaching itself to the N-terminus of the peptidoglycan chain, in turn enabling a glycan to displace this and extend the chain (*Fig. 3*)¹².

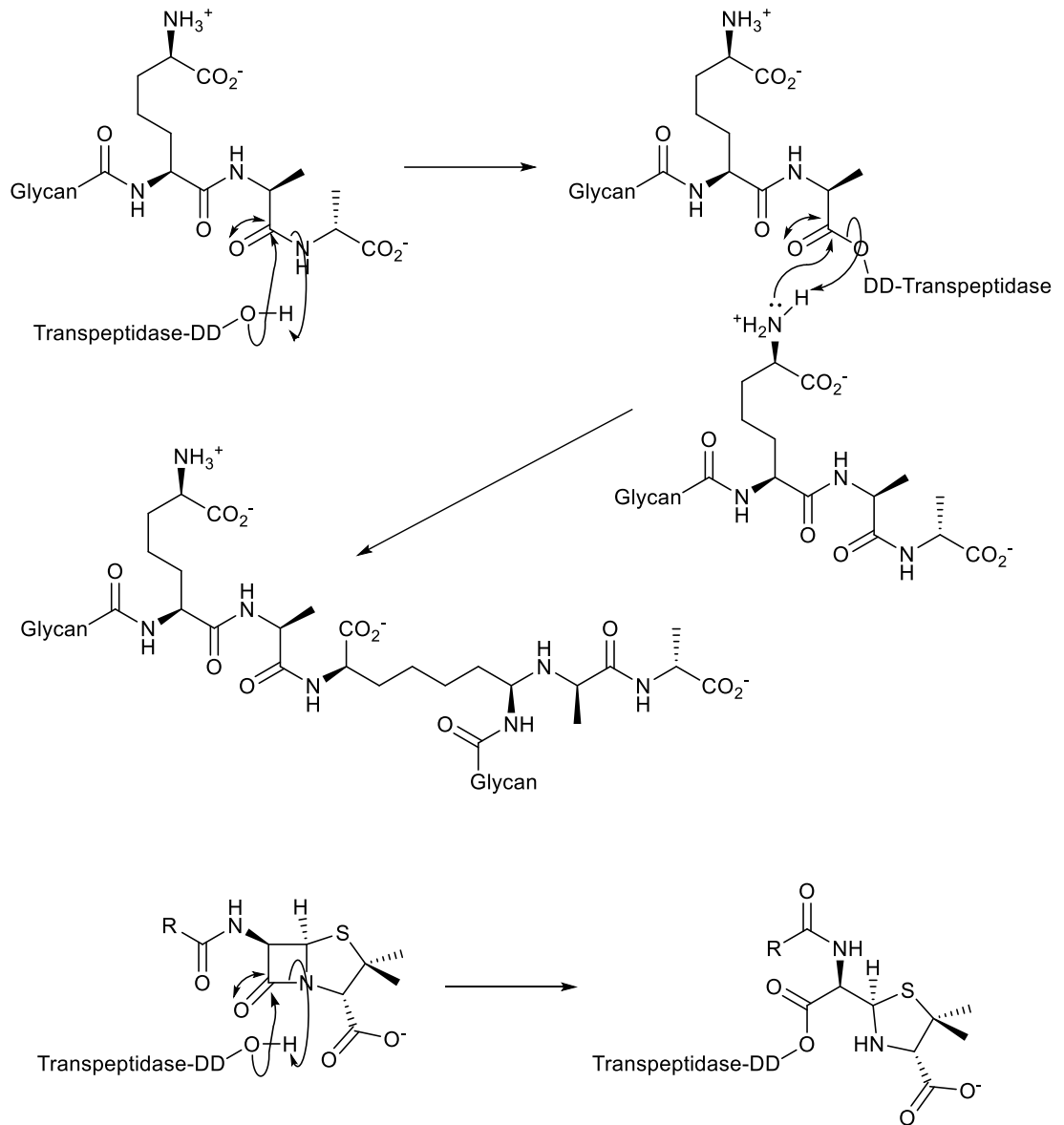


Figure 3. The mechanism of peptidoglycan cell wall biosynthesis. a) The carbonyl group of an amide bond at the N-terminal end of peptidoglycan is attacked by a transpeptidase enzyme via a hydroxide moiety. The nitrogen atom adjacent to the carbonyl gains a proton and leaves as a molecule of alanine. b) A nearby glycan attacks the newly formed ester group via a diaminopimelic acid residue, displacing the enzyme. c) The glycan strands are now joined together in a peptidoglycan chain. Below this shows what happens when a penicillin molecule is introduced. The penicillin's β -lactam ring mimics the amide group that is attacked in a), but the enzyme cannot detach from this and so its action is inhibited and the cell eventually dies through cell wall thinning¹².

Changes in cell wall structure can reduce permeability to antibiotics, meaning drug molecules find it more difficult to access the bacterial cell¹³. However, this is rarely, if ever, the sole reason for resistance to antibiotics arising in Gram-positive bacteria¹¹.

Gram-negative bacteria are naturally less permeable to antibiotics than Gram-positive bacteria, due to their more complex multi-component cell wall which features a glycolipid outer layer that is not found in Gram-positive bacteria. This liposaccharide outer layer is more hydrophobic than a typical phospholipid bilayer and has low fluidity¹⁴.

Cellular entry is instead controlled by porins which span the outer membrane. Thus, cellular accumulation is reliant on the ability of molecules to pass through these channels¹⁵. Porins are β -barrel in structure, are size restricted, typically only allowing molecules that are below 600 Da through, and are generally preferable towards allowing the passage of hydrophilic charged compounds¹⁶. Decreased permeability can arise through more selective porins being developed, reducing the ability of drugs to cross this barrier and perhaps rendering them ineffective to any Gram-negative bacteria. This has been seen in β -lactam resistant *K. aerogenes* and *K. pneumoniae*, where a Gly to Asp mutation in the L3 loop of the OmpC porin confers resistance (this is also implicated in meropenem-vaborbactam resistance)¹⁷.

Another mutation that antibiotic resistant bacterial isolates have shown is decreased porin production. By reducing porin expression the bacteria take in less toxins, thereby reducing the concentrations of these toxins within the cells and becoming more survivable. Alongside this, an increase in the regulation of efflux pumps has been found in these bacteria, indicating that the influx and efflux mechanisms of bacteria are linked¹⁵.

Efflux pumps are trans-membrane proteins found in Gram-negative bacteria that can recognise foreign molecules and eject them from the cell. For this to confer resistance, the output of toxins must exceed the input¹⁸. Thus, if these pumps act upon antibiotic molecules, reducing their concentrations within the cytoplasm, they can be rendered ineffective. Efflux pumps can be specific for certain molecules or act upon a broad range, depending on their structure¹⁹.

Many efflux pumps are effective against a wide range of molecules, giving rise to multi-drug resistant (MDR) bacteria. Due to their large protein structures and ability to handle diverse compounds, these are especially hard to inhibit using small molecules²⁰. If an efflux pump does not recognise an antibiotic and it is effective, that does not mean it will not evolve to do so (as seen in *S.*

typhimurium, where a substitution caused ciprofloxacin resistance). Whilst the mutation of these massive proteins has a large metabolic cost, it can still be beneficial for bacteria to pay this when under pressure¹⁸.

1.1.2.2 Target site modification & protection

Another common method of antibiotic resistance is a change in the target site, be this through enhanced target site protection or a change in structure of the target site itself¹⁹.

Modification of the target site can decrease the affinity of the substrate for its intended target. This could be due to a change in the spatial location of certain residues, or a change in what residues are present. These changes can occur through single-step point mutations or multiple mutations occurring over time, with each successive one raising the minimum inhibitory concentration of the drug slightly, so making the bacteria more survivable at each step¹⁹. As an example of point mutation conferring resistance, multidrug resistance has been seen due to expression of the chloramphenicol-florfenicol resistance (*cfi*) gene in *Staphylococcus aureus* and *Escherichia coli*. This encodes a methyltransferase that modifies the 23S rRNA of nucleotide A2503. Because of this methylation at the binding site, five antimicrobial drug classes bind with lower affinity to the target and thus the bacteria harbouring this mutation are resistant²¹.

Target protection mechanisms do not always require mutation of the encoding gene of the target site. For example, they can occur *via* protein-protein interactions whereby an antibiotic resistance protein binds to the drug target site with greater affinity than the drug molecule, preventing the drug molecule from binding and so stopping any inhibitory effects²². This has been found as a mechanism behind resistance in tetracycline, fluoroquinolones and fusidic acid¹⁹.

Bacteria are also able to develop a completely new active site in the enzyme that completes the biochemical functions of the inhibited target site, but are not inhibited by the drug molecule. This means that whilst the original target site may be successfully bound to, the bacterial activity is successfully retained. One example is of strains of *S. Aureus* that have gained resistance to methicillin by acquiring an exogenous PBP (PBP2a), which has low affinity

for all β -lactams and thus is able to continue cell wall biosynthesis in their presence¹⁹.

1.1.2.3 Enzymatic inactivation of antibiotic molecules

If bacteria can deactivate antibiotics then this will also cause resistance. Enzyme catalysed modification is relevant in many resistance mechanisms, such as hydrolysis of β -lactams (a class of antibiotic compounds including penicillin) by β -lactamases²³. These enzymes hydrolytically cleave vulnerable chemical bonds such as esters and amides. This can inactivate the antibiotic functionality of the drug molecules.

β -lactams become covalently associated with the active site in PBPs. This causes the PBP to hydrolyse the β -lactam ring, the structural commonality between all β -lactam antibiotics, but the turnover rate is very slow. In contrast, β -lactamases hydrolyse β -lactams with much higher turnover rates. Hence, when β -lactamases are secreted into the periplasm (where PBPs are active) then bacteria become resistant to β -lactam antibiotics²⁴.

With so many methods of resistance available to them, bacteria have shown themselves to be extremely versatile and difficult to combat without continually producing new ways to kill them, or by blocking inhibition mechanisms.

1.1.3 How does resistance spread throughout bacteria?

Over time, bacteria evolve to combat threats to their survival. These threats include man-made antibiotic drugs. This occurs *via* Darwinian evolution, where advantageous mutations in the genome lead to more survivable specimens reproducing and so passing their more successful genes down (this is known as vertical gene transfer (VGT))²⁵.

Resistance can also be transferred to other populations *via* horizontal gene transfer (HGT). This means genes are not only passed to related bacteria in a parent to child fashion, but can also be transferred to unrelated bacteria. HGT can happen through several mechanisms, such as conjugation, transformation and transduction²⁶. In addition to this, Gram-negative bacteria have shown the ability to transfer resistance genes through OMVs²⁷.

Bacterial conjugation occurs *via* genetic material being transferred directly through the physical contact of two cells (*Fig. 4*) This involves a plasmid

transferring genetic material across the two cells, which then integrates itself into the genome of the recipient cell²⁸. If this genetic material contains the required genes for antibiotic resistance, then the recipient bacterium will become resistant.

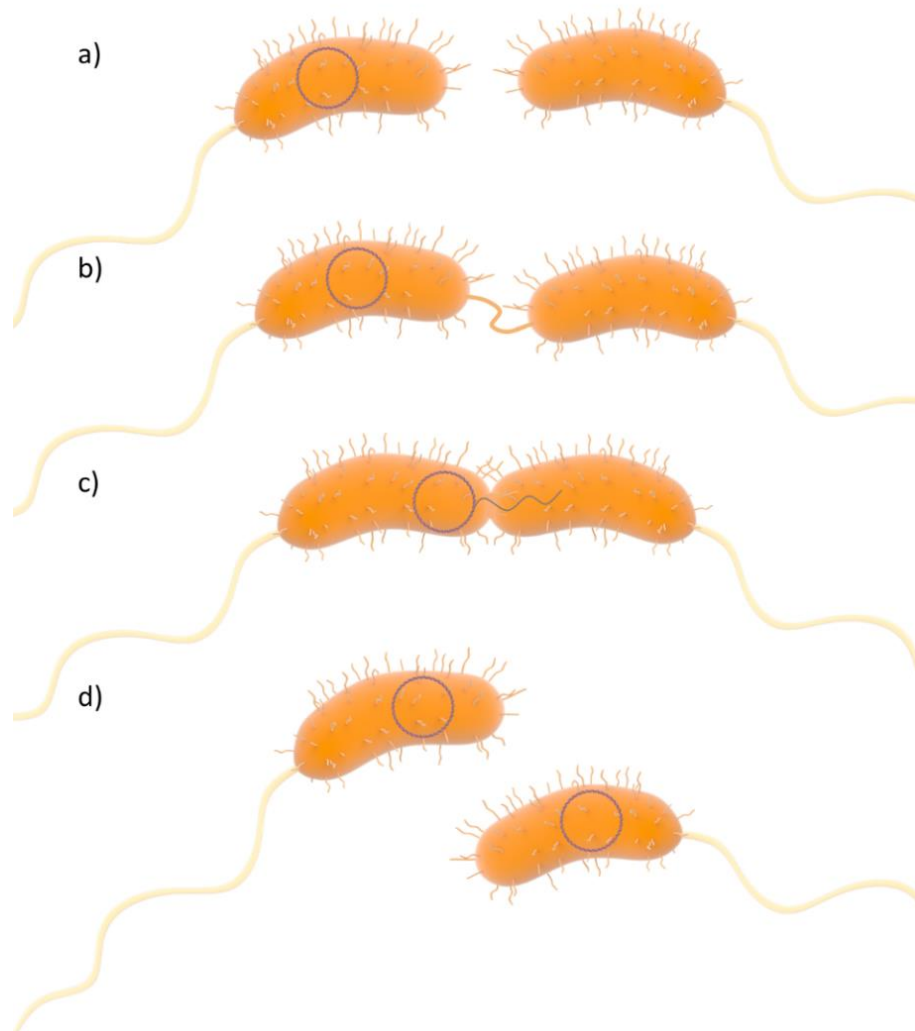


Figure 4. The sharing of resistance mechanisms through bacterial conjugation. a) Two bacteria encounter each other; one contains the plasmid encoding a resistance mechanism whilst the other does not. b) The bacteria grow pili and connect. c) The bacteria join together and genetic material is transferred from the resistant bacterium to the non-resistant bacterium. d) The bacteria disconnect and now both bacteria are resistant due to the transferred genetic material.

Through transformation, the bacteria acquires a section of exogenous genetic material from its surroundings and incorporates it into its genome. If this exogenous genetic material is part of the genome from a resistant bacterium that causes resistance, then the bacteria incorporating it will become resistant too²⁹.

Bacterial transduction is the transfer of host DNA, mediated by phage particles. Bacteriophages are viruses that infect bacteria; when passing between organisms they can transfer the host DNA, therefore implanting it in the new hosts genome. This is thought to be the major cause of the spread of antibiotic resistance in some organisms, such as *S. aureus*³⁰. There are three forms of transduction: generalised, specialised and lateral³¹.

Generalised transduction occurs when phages simply randomly pack up the hosts DNA as opposed to their own. Thus, this can lead to the transfer of any piece of the bacterial genome.

Specialised transduction occurs when the phage packages DNA flanking the phage attachment site, which is then excised along with the phage DNA and transferred. As phages are preferential to the site of their attachment in the bacterial genome, this is not random³¹.

Lateral transduction is a relatively recent discovery and differs from the other forms of transduction, in that it does not seem to be result of erroneous behaviour of the phage. Here, phages delay the normal excision step in their life-cycle to a much later stage. This allows the phage genetic material responsible for packaging the genome to be expressed within the bacterium, initiating DNA packaging *in situ*. Thus, a large amount of bacterial chromosomal DNA can be packaged before phage excision, allowing much larger amounts of genetic material to be transferred to the environment outside of the bacterium (increasing frequency of transfer at least 1000-fold)^{31,32}.

1.1.4 What is being done to combat resistance?

Two main approaches can be taken towards killing drug-resistant bacteria: developing new antibiotics that work through different mechanisms or inhibiting the mechanisms of resistance.

Developing new antibiotics may prove much more difficult now, as many of the available effective simple structures have already been discovered and developed³³. Thus, discovering effective drugs with new modes of action is both more costly and time-consuming. This, in part, explains the lull in new antibiotics coming to market since the 1980s³⁴.

Additionally, the rate of the emergence of resistance mechanisms is rapid. This makes it difficult to produce new drugs fast enough to overcome resistance and gain the upper hand³⁵. This is not helped by the slow pace of drug development and the reluctance of large pharmaceutical companies to dedicate vast amounts of time and money to the task.

A perhaps more beneficial method of combatting resistance may be to develop drugs that will inhibit bacterial methods of inhibition, to be used alongside traditional antibiotics³⁶. For sensible design of such inhibitors, we must understand the mechanisms of antibiotic activity and the mechanisms of resistance in bacteria.

1.2 The history and current state of antibiotics

Since their discovery antibiotics, compounds that are able to destroy bacteria, have reduced the mortality of countries with access to them by a significant amount. In England, deaths due to infectious diseases fell from 25% to less than 1% from 1900 to 1945³⁷. Whilst this was in no small part due to better practices in general, the contribution of commercial antibiotics since 1942 (the year of the introduction of penicillin)³⁸ cannot be understated.

1.2.1 The 'golden-age' of antibiotic discovery

The 1900s brought about with them a great acceleration in medicinal chemistry. When we think of the first antibiotics, penicillin is often the first thing that comes to mind. However, the sulfa drugs were in fact introduced before penicillin, after the discovery of a sulphonamide by the name of Prontosil by Klarer and Mietzsch in 1932, along with its exhibition of antibacterial activity by Domagk in 1935³⁹. This drug was quickly available for clinical use and became widely successful. It was used to effectively treat patients in a London hospital and one of the sons of former president Franklin Delano Roosevelt of *Streptococcal septicaemia* infections, amongst other examples^{40,41}.

Prontosil was in fact a precursor to the active drug moiety (a prodrug), which was sulphanilamide, and showed no *in vitro* activity but did show *in vivo* activity. Sulphanilamide is metabolised from Prontosil through reduction of the central azoic bond, yielding the active form (*Fig. 5*)⁴².

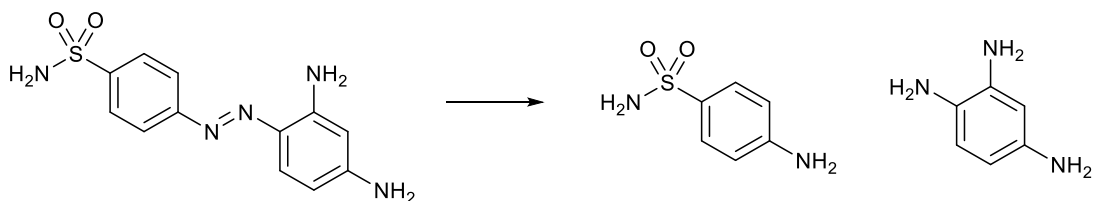


Figure 5. The structure of Prontosil, the first sulphonamide drug made available to the clinic for the treatment of bacterial infections, and the two molecules it is reduced to in vivo, sulphanilamide and 1,2,4-triaminobenzene. Sulphanilamide is the molecule responsible for antibacterial effects⁴².

The sulfa drugs are not as widely reputed as penicillin, despite being the first antibiotic introduced to the clinic. This can most likely be attributed to the fact that sulfa drugs have fallen out of general use nowadays, due to the development of drugs with fewer potential adverse effects and the rapidly developed resistance to sulfa drugs by bacteria^{43,44}.

Penicillin, the first of the most-well known class of antibiotics, was first recognised for its antibacterial activity in 1929 by Fleming⁴⁵ and its potential as a chemotherapeutic agent was investigated at Oxford by Florey in the early 1940s^{46,47}.

The introduction of penicillin led to much further scientific inquiry into other compounds that could destroy bacteria, leading to an antibiotic 'golden-age'. The exact years that this golden age covers are often cited to be 1940 - 1960, but true stagnation in discovery didn't truly occur until 1987, with the discovery of a class of acidic peptide antibiotics⁴⁸ (this would lead to the approval of daptomycin in 2003)⁴⁹.

During this 'golden-age', many antibiotics were discovered from natural sources, beginning in 1944 with streptomycin being obtained from the soil bacterium *Streptomyces griseus*. This resulted in further investigation of soil bacteria for these compounds, giving us aminoglycoside, chloramphenicol, tetracycline and macrolide in the 1950s⁵⁰.

Not all of the antibiotics in this era were isolated from soil bacteria; nalidixic acid, a synthetic quinolone antibiotic, was created in 1962⁵¹. However, a large proportion of effort in the area of antibiotic research has focused upon modifying existing scaffolds found as natural products for increased effectiveness, as opposed to finding new ones. Whilst this is an important endeavour, and can in some cases counter resistance mechanisms (e.g.

second generation antibiotic cefuroxime countering resistance to first generation antibiotic cephalotin)⁵², this does not result in producing antibiotics with novel modes of action (*Fig. 6*).

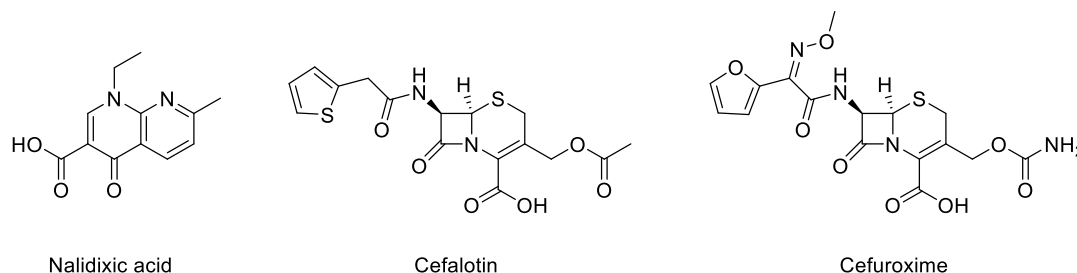


Figure 6. The structures of antibiotics nalidixic acid, cefalotin and cefuroxime.

One major obstacle that has appeared since this era is that many of the antibiotics that are amenable to discovery, isolation and analysis have been found. Many antibiotics of this era were found through screening of natural products solely for their inhibition of growth of bacterial organisms, whilst their mechanism of action was disregarded. This led to rapid discovery and rediscovery, but eventually led to a decline in novel findings. To fight against this, screening methods were devised to identify compounds and ascertain their modes of action, such as inhibiting peptidoglycan biosynthesis. These could then be tested for their similarity to past inhibitors and hits could be more fastidiously selected for based on novelty. This would evolve into screens for specific enzyme inhibitors, a targeted approach. Whilst this worked well for a time, it is time-intensive, inefficient and eventually led to the screens relying on already existing chemical libraries, partly due to the unsuitability of crude fermentation broths for these screens. These chemical libraries proved to be a less productive source and ultimately led to scientific commercial enterprises abandoning these efforts in favour of more profitable endeavours⁵³.

Since this time, discovery has happened at a much slower rate (*Fig. 7*). Whilst we are not on the verge of returning to pre-antibiotic risks of infection yet, if scientific research in this area does not outpace the evolution of bacterial resistance mechanisms then it is only a matter of time.

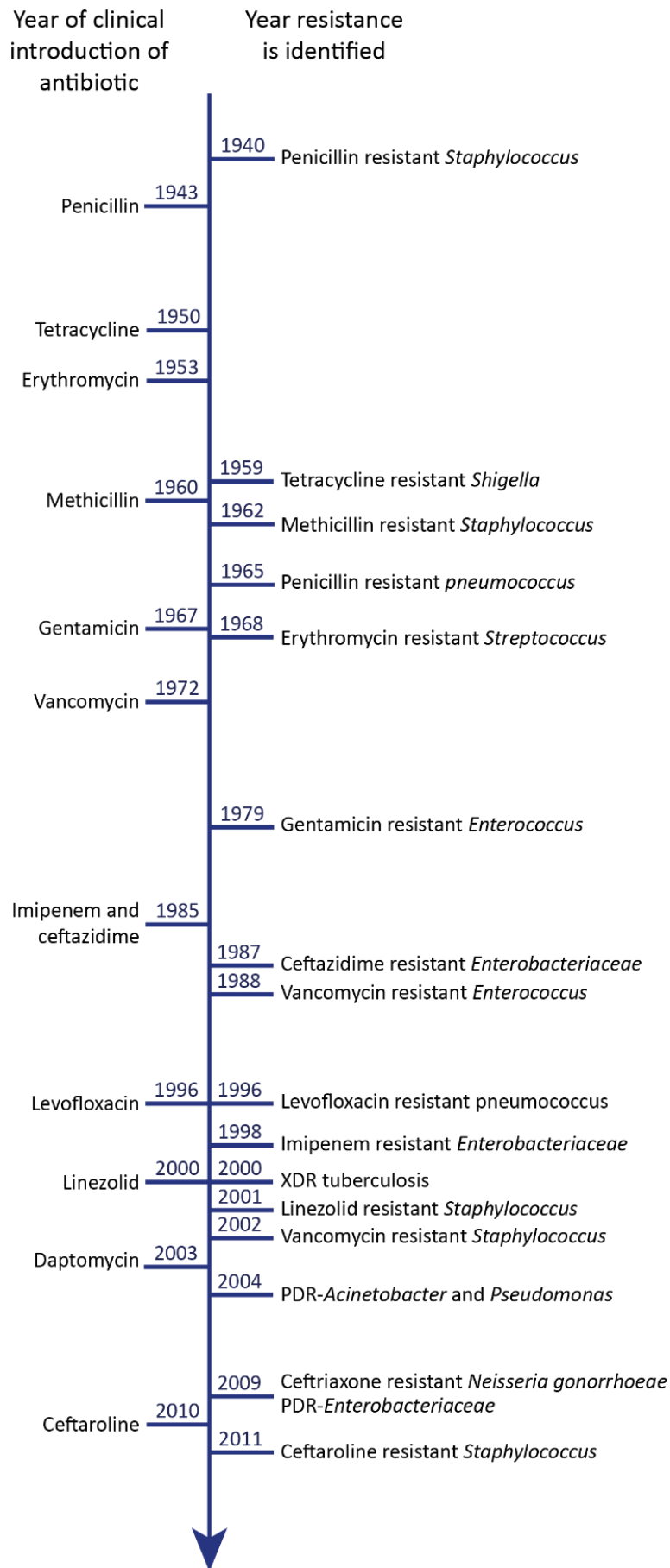


Figure 7. A timeline of antibiotic discovery and the discovery of bacterial resistance to antibiotics. Adapted from a CDC report (2013)⁵⁴.

1.2.2 The genomic revolution and why it did not help

With the advent of the sequencing of the first complete bacterial genome in 1995, drug companies took a new approach to developing new antibiotics. Given the information now available a genomics-derived target-based approach was favoured in screens, to find antibacterial molecules with novel modes of action. However, as a 2007 GlaxoSmithKline (GSK) paper shows us, this did not yield success as expected⁵⁵.

In the six years since the sequencing of a complete bacterial genome, GSK ran sixty seven high-throughput screening (HTS) campaigns on antibacterial targets against their in house compound collection (ranging from 260,000 – 530,000 compounds). Of this, only sixteen screens gave hits and only five of these hits evolved into leads. This was between four and five times less successful than in GSK's other therapeutic areas over the same period. As such, it was viewed as being financially untenable to continue this research in such a manner⁵⁵.

An analysis of these campaigns attributed the lack of success to a number of factors, such as the variation in homology of a target identified *via* genomic analysis across species introducing difficulties in translation of activity throughout different species of bacteria⁵⁵.

A major factor in the low yield of novel antibiotics was due to the chemical diversity of compounds present in the libraries of pharmaceutical companies. Such libraries tend to be heavily weighted towards molecules that follow Lipinski's 'rule of five'⁵⁶, whereas most known antibacterial molecules do not strictly adhere to these rules. As such, it was deemed that efforts should be more focussed on specific antibacterial libraries versus the larger more general libraries usually used for HTS campaigns. Additionally, novel compound classes needed to be found to further explore chemical space, perhaps leading to the discovery of novel antibacterial mechanisms⁵⁵.

1.2.3 An overview of recent trends in antibiotic research

There have been thirty-eight new antibiotics released to market worldwide since the year 2000. Of these, five were the first in their class⁵⁷. The release of these new drugs has been accelerated by worldwide efforts and programs,

such as the U.S Food and Drug Administration Generating Antibiotic Incentives Now (GAIN) Act⁵⁸ and the Global Antibiotic Research & Development Partnership (GARDP)⁵⁹. Unfortunately despite these international efforts, private investment in antibiotics has continued to decline⁶⁰.

It is not all despondent however; between 2013 and 2019 deaths in the U.S. from antibiotic-resistant infections dropped⁶¹. But this is still not enough to deem the current pace of discovery as sufficient, as noted by the WHO in a 2019 antibiotic clinical development report, “The clinical pipeline remains insufficient to tackle the challenge of increasing emergence and spread of antimicrobial resistance.”⁶⁰

This same report noted that since 2017 eight new antibiotics have been approved, but only one is of a new class. In addition to this, none were viable to treat carbapenem-resistant *Acinetobacter baumannii* and *Pseudomonas aeruginosa*. As such, these eight are noted as being of limited clinical benefit⁶⁰.

An accompanying report focusing on antibiotic preclinical development of agents to act against WHO priority pathogens *Mycobacterium tuberculosis* and *Clostridioides difficile* predicted that of two hundred and fifty two agents being developed, approximately two to five direct-acting small molecules and one non-traditional product may make it to market in the next decade. Whilst preclinical approaches are seen as being more innovative, there is also an increased failure rate versus proven pathways⁶².

From these combined reports we can conclude that current efforts may not be able to stem the tide of antibacterial resistance and that more must be done. Of particular concern is the disparity between recently approved antibiotics and the WHO priority pathogens list.

1.2.4 The rise of resistance

Almost as soon as antibiotics went into widespread use, resistance became a known issue. Penicillin resistant *Staphylococcus aureus* emerged in London hospitals as early as the 1940s⁶³. This amazing adaptability of bacteria has allowed them to develop resistance to any antibiotics shortly after introduction.

Since then antibiotic resistance has been constantly accelerating due to multiple factors including: inappropriately prescribed antibiotics in humans, antibiotics applied as pesticides to fight crop disease, antibiotics used in the feed of animals⁶¹, and increasingly frequent cases of HGT⁶⁴. Greater education can aid the fight against rising resistance, but it is naïve to believe this will happen quickly.

Antibiotic resistance can occur not only in the bodies of humans and animals, but in the environment. In 2013, an estimated 53,800 tons of waste of thirty six common antibiotics entered the environment after wastewater treatment in China. These predicted environmental concentrations were found to correlate to resistance rates in hospitals⁶⁵. This correlation is due to antibiotic resistance genes that are left in the environment through many avenues, such as human waste and industrial effluents, and are able to transfer their genes to other bacteria⁶⁶. Given this level of use, it is clear that antibiotic resistance is bound to further rise and it will be in the hands of scientists to develop new ways to circumvent this resistance.

1.3 β -lactam antibiotics and β -lactamases

1.3.1 β -lactam antibiotics

The most widely recognised antibacterial compounds are the β -lactam antibiotics. These kill bacteria by stopping peptidoglycan synthesis through inhibition of PBPs. Such antibiotics include the penicillins, cephalosporins, carbapenems and monobactams. This inhibition results in the cell wall becoming progressively thinner until it eventually bursts, killing the bacteria. As human cells do not feature this peptidoglycan cell wall, they are not targeted by β -lactams.

Penicillins contain a β -lactam ring that mimics a D-Ala-D-Ala residue within the growing peptidoglycan chain. This is the target of DD-transpeptidase, a PBP that is essential for cell wall biosynthesis. When DD-transpeptidase reacts with penicillin, the penicillin molecule covalently attaches to the DD-transpeptidase active site, rendering it inactive and thus unable to participate in cell wall biosynthesis (*Fig. 8*)⁶⁷.

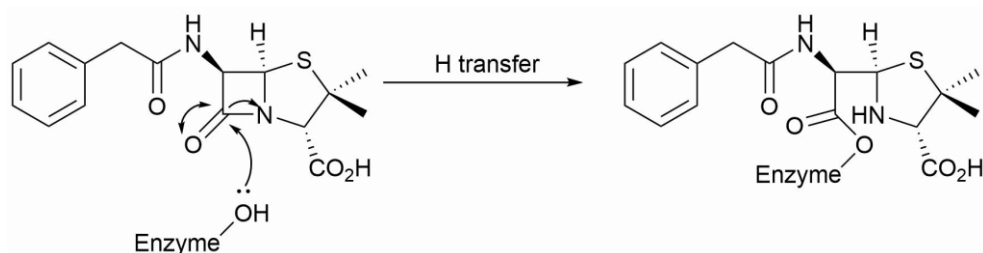


Figure 8. The mode of action of benzyl penicillin. When benzyl penicillin reacts with a PBP, the PBP attacks the carbonyl of benzyl penicillin via a serine residue in the enzyme active site. This forms a covalent bond between the enzyme and penicillin molecule, rendering the serine residue that is involved in catalytic function unusable and thus renders the enzyme inactive⁶⁸.

There are multiple classes of PBPs, with the biggest distinction depending on the structure and catalytic activity of the N-terminal domain. In class A PBPs the N-terminal domain catalyses the elongation of non-crosslinked glycan chains, whereas in class B PBPs the N-terminal domain interacts with other proteins involved in the cell cycle. In both cases, the C-terminal domain (the penicillin binding domain) catalyses the peptide cross-linking of two adjacent glycan chains⁶⁹. Hence, both classes are inhibited by β -lactam antibiotics.

1.3.2 β -lactamase enzymes

β -lactam antibiotics are susceptible to inactivation by a class of enzymes known as β -lactamases. These enzymes confer resistance to many drugs, from traditional ones like penicillin to more recent ones such as carbapenems. These drugs feature a β -lactam ring that is essential to their function, and it is this ring that the β -lactamases break down (Fig. 9).

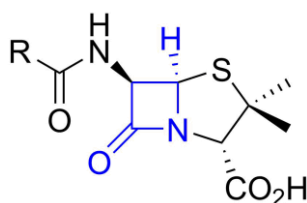


Figure 9. The penicillin core structure, with the β -lactam ring highlighted in blue.

β -lactamases seem to have evolved from PBPs. This is supported by both sequence-based analysis and structural evidence. Why evolution resulted in different forms can be explained by the paths occurring at different points and according to different environmental pressures⁷⁰.

The β -lactam family consists of serine- β -lactamases (SBLs) and metallo- β -lactamases (MBLs). SBLs use a serine residue to facilitate hydrolysis of the β -lactam ring, whilst MBLs utilise zinc ions and a bound hydroxide ion to do

this^{71,72}. MBLs have also evolved to use other available metals, such as cobalt, to overcome zinc scarcity⁷³.

Due to the mechanistic differences between SBLs and MBLs, drugs that affect one may not work on the other. For example, Avibactam, an effective inhibitor of SBLs that is now commonly used in combination therapies to tackle SBL-mediated antibiotic resistance, is ineffective against MBLs⁷⁴. MBLs catalyse the hydrolysis of Avibactam, albeit inefficiently, rendering it useless against bacteria possessing these enzymes. This is thought to occur *via* the nucleophilic attack of the Avibactam's cyclic urea group, followed by decarboxylation (*Fig. 10*)⁷⁵.

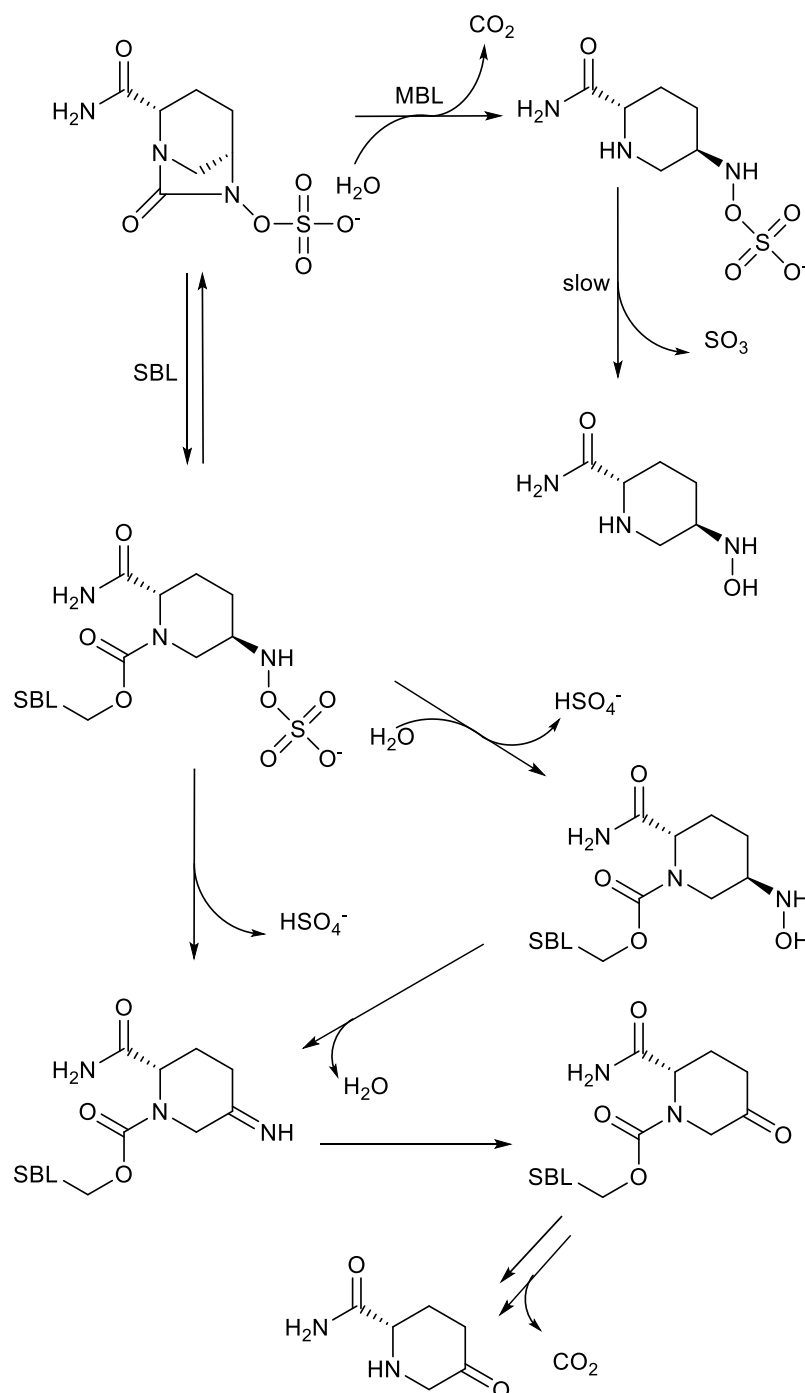


Figure 10. The mechanisms by which Avibactam reacts with MBLs and SBLs. Due to the hydrolysis of Avibactam by MBLs, this makes the drug ineffective for their inhibition. SBLs however are inhibited by Avibactam as they are rendered inactive through a more efficient mechanism⁷⁵.

Under the Ambler classification scheme, the β -lactamases are classified as being type A, B, C or D. These can be distinguished sequence similarity, particularly through the amino acids present in the enzyme active site. Type A, C and D feature a serine residue in the active site (so are SBLs), whilst type B β -lactamases use metal ions (so are MBLs)⁷⁶.

The Ambler system remains the most commonly accepted method of classification, although it has been subject to criticism as it relies solely on sequence homology. An alternative model, The Bush-Jacoby system, classifies the β -lactamases according to substrate hydrolysis profiles and inhibitor profile⁷⁷. This may be a more clinically useful system, but due to the cost of gaining experimental data for every enzyme of a large protein family, it is not entirely pragmatic. Thus, we shall be using the Ambler classification.

1.3.2.1 Serine- β -lactamases

All three classes of SBLs feature similar tertiary structures, whilst the differences in their primary structures and catalytic mechanisms explains their separation⁷⁸. Their structural similarity suggests a common ancestor between the classes, which later diverged⁷⁹. As such, they all share a conserved variant Ser-Xaa-Xaa-Lys motif across all classes, and with their PBP ancestors⁷⁰.

The key feature of SBLs is, of course, the serine residue that is instrumental in the catalytic mechanism. This serine acts as a nucleophile to hydrolyse β -lactams. The serine residue attacks the carbonyl carbon of the ring, generating an acylenzyme intermediate (this occurs *via* a tetrahedral oxyanion transition state). The acylenzyme is then deacylated by a water molecule which acts as a base, completing the catalytic mechanism and resulting in the release of the deactivated β -lactam⁸⁰.

1.3.2.1.1 Class A

Class A represents the largest class of β -lactamases. This class has a wide spectrum of activity. It includes many prolific and well-known enzymes, such as TEM (the first plasmid-borne β -lactamase discovered in Gram-negative bacteria) and KPC (*K. pneumoniae* carbapenemase). Many of the subtypes have been able to spread through HGT by virtue of being plasmid borne. They are also noted as being able to easily expand their activity towards new substrates through point mutations⁸⁰.

Many extended-spectrum β -lactamases (ESBLs) belong to class A. Notably, many are able to hydrolyse penicillins and cephalosporins, such as CTX-M-type enzymes, which are the most widely spread ESBLs. Others, such as KPC-type enzymes, are able to hydrolyse carbapenemases⁸¹.

Whilst the class A β -lactamases are the most widely covered, their exact acylation mechanism is still a source of contention. The two main mechanisms differ in which conserved residue acts as a base, deprotonating the active serine residue and enabling its attack of the carbonyl carbon of the β -lactam ring (*Fig. 11*). Lys73 and Glu166 (both part of the aforementioned SBL Ser-Xaa-Xaa-Lys motif) are suggested, and both suggestions are supported by various crystallographic, computational and biochemical studies⁸⁰.

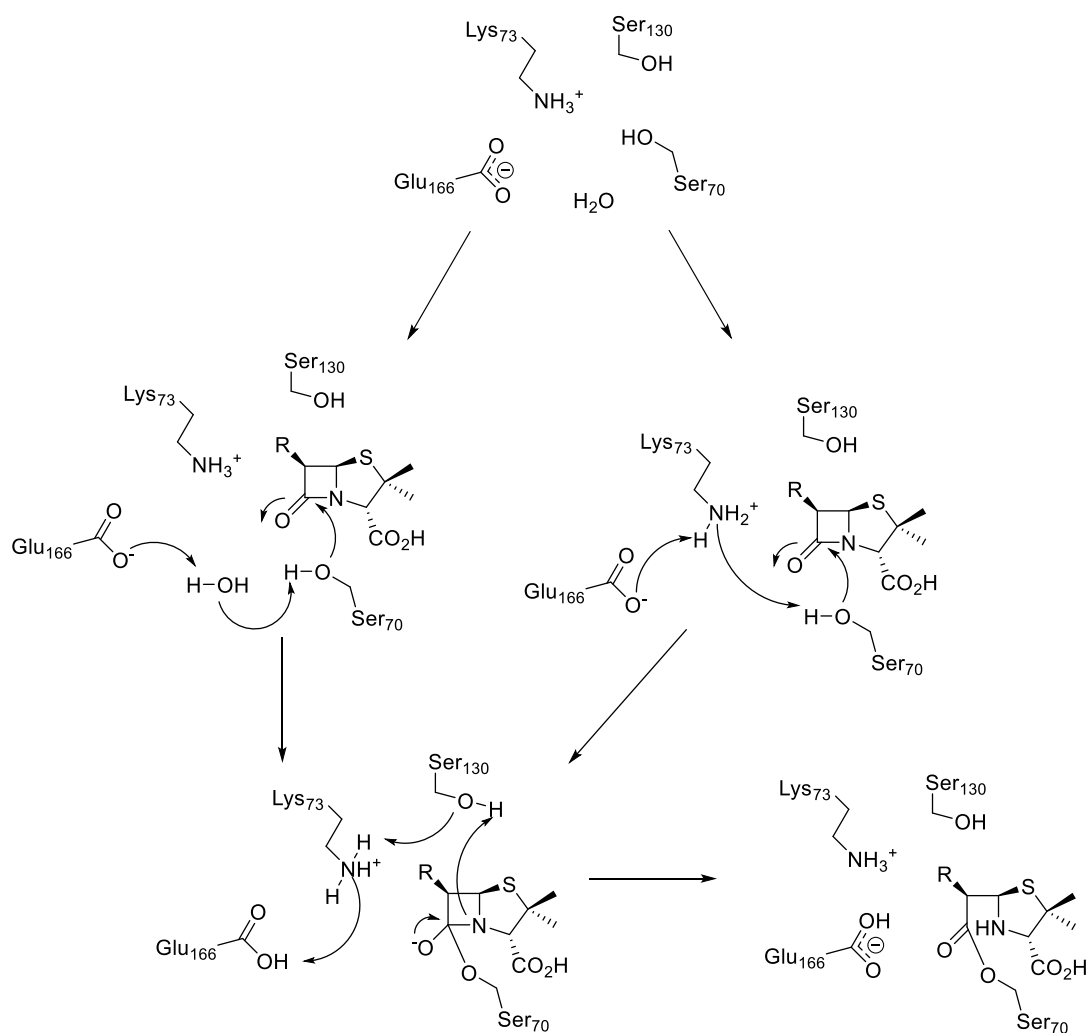


Figure 11. Two alternative acylation mechanisms for class A SBLs. (Left) Ser₇₀ is activated by Glu₁₆₆ via a water molecule. (Right) Ser₇₀ is activated by Glu₁₆₆ via Lys₇₃⁸⁰.

The degradation of carbapenemases by class A enzymes, most notably KPC, is of high clinical relevance due to their global distribution. These enzymes seem to require very specific spatial requirements for their catalytic activity against carbapenemases. In particular, a balance between needing to direct the carbapenem 6 α -hydroxyethyl substituent away from the nucleophilic water base and to hold the acylenzyme carbonyl within the oxyanion site^{80,81}.

1.3.2.1.2 Class C

Class C β -lactamases also are widely distributed. The first β -lactamase to be identified, in *E. coli*, is a class C enzyme. They are common in the chromosomes of Gram-negative species. In fact, many Gram-negative species carry the chromosomal genes encoding class C enzymes, *ampC*, but these are often not expressed in normal conditions. Instead, expression can be induced by exposure to some β -lactams⁸¹.

The mechanism of class C enzymes is less well studied, and thus less well understood, than for class A enzymes. Lys67 and Tyr150 are seen as being instrumental residues in the acylation step, as recognised through computational simulations, but exactly how is still up for debate. For the deacylation step, both a substrate-assisted and a conjugate-base mechanism are seen as being reasonable, but it is not clear which is correct (*Fig. 12*)⁸⁰.

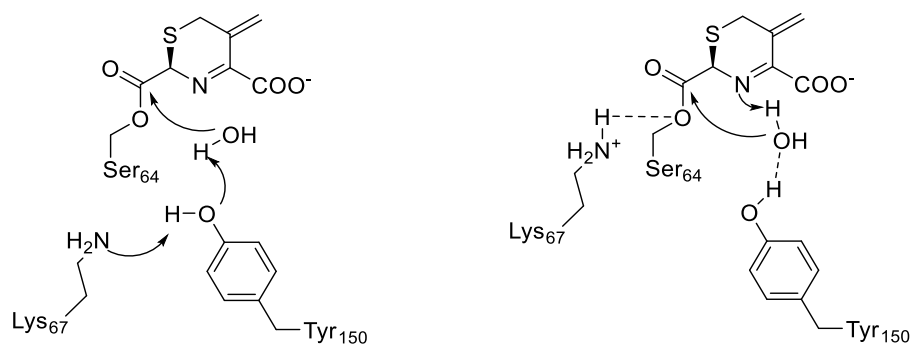


Figure 12. Proposed diacylation mechanisms of class C SBLs. (Left) Conjugate-base mechanism. (Right) Substrate-activated mechanism. It is unclear which mechanism is a more true representation⁸⁰.

1.3.2.1.3 Class D

Class D enzymes, notably the OXA enzymes, are structurally dissimilar to their A and C counterparts. So much so, that the amino acid similarities between class D and A or C are less than 20%⁸¹.

The OXA class is extremely diverse and relatively poorly understood. Enzymes in this class have exhibited activity against penicillins, cephalosporins and carbapenems and have very different sensitivities to inhibitors.

The mechanism of this class is thought to be dependent on a carboxylated lysine (the counterpart to Lys73 in class A β -lactamases) in both the acylation

and deacylation steps. Though initially seen as surprising (the carboxylation is a reversible reaction with carbon dioxide and had only previously been seen of lysine residues in protein metal binding centres), it has since been supported by structural work, biochemical studies and computational simulations⁸⁰.

1.3.2.3 Metallo- β -lactamases

Enzymes that use metals to perform their functions, metalloenzymes, make up over thirty percent of known enzymes. Despite this, less than five percent of small molecule β -lactamase inhibitor drugs target a metalloenzyme⁸². This clear gap in drug discovery presents an exciting opportunity for innovation as well as potentially addressing unmet clinical needs.

Metalloenzymes are often selective and active catalysts that are able to work in mild conditions. Due to the necessity of this behaviour, nature has found ingenious ways to utilise ordinarily toxic metal elements for the efficient catalysis of essential processes⁸³.

Despite considerable research into metalloenzymes, the details relating to the selection of metals that are incorporated for biological catalysis is still poorly understood^{83,84}. However, the majority of metalloenzymes use commonly found metals such as zinc, iron and copper.

Zinc is the second most common metal in biology, after iron. Due to the zinc ions (Zn^{2+}) filled d^{10} orbital, it does not participate in redox reactions and instead acts as a Lewis acid. Due to this inactivity in redox reactions, Zn^{2+} is inherently stable in complex biological media; due to its abundance and ability to act as a Lewis acid this explains its commonality and usefulness throughout metalloenzymes⁸⁵.

The B class of β -lactamases are metalloenzymes: metallo- β -lactamases. These contain one or two zinc metal ions within their active site to facilitate their catalytic action. Structural and sequence comparisons reveal that this class is evolutionarily distinct from and A, C and D classes, which are thought to have evolved from transpeptidases. It has been proposed that instead, MBLs evolved due to an ancient gene duplication event, whereby errors in DNA replication and repair machinations lead to a favourable change in the organism⁷⁰.

MBLs have spread across the globe, as seen by the identification of MBL genes in clinical isolates from countries such as China, India and the UK^{86–88}. Whole genome sequencing of these isolates has shown evolutionary divergence before their appearance in the hospitals they were gathered from, revealing that they arrived from various external sources.

Despite considerable research into inhibiting β -lactamases, currently there are very few inhibitors of MBLs available for clinical use⁵⁷. Due to the increasing prevalence of MBL containing bacteria this poses a pressing medical need. As noted by the WHO in their aforementioned 2019 report, “More than 40% of the pipeline targeting WHO priority pathogens consists of additional β -lactam and β -lactamase inhibitor (BLI) combinations, with a major gap in activity against metallo- β -lactamase producers.”⁶⁰

The MBLs belong to a superfamily of metalloproteins, the metallo-hydrolase/oxidoreductase superfamily in the Structural Classification of Proteins database⁸⁹. Despite often low sequence similarity between members, functional similarities in this family exist through their active site (usually containing two Zn^{2+} ions), which activates a water molecule, enabling the nucleophilic attack of a substrate and the stabilization of a transition state. Within this superfamily catalytic landscapes show significant overlap and directed evolution studies have shown complete switching of catalytic activities is possible. Hence, the nuanced nature of specific catalytic activity appears to stem from the amino acids present within the active site⁹⁰.

MBLs feature a characteristic $\alpha\beta\alpha$ -fold, which consists of two β -sheets surrounded by five solvent exposed α -helices. The N- and C-terminal domains, each featuring a β -strand and two α -helices, can be superimposed upon each other when rotated around a central axis. The active site of the molecule, where the Zn ions lie, is located on the external edge of the $\beta\beta$ sandwich⁹¹.

Whilst this $\alpha\beta\alpha$ -fold was first found in MBLs⁹², it has since been found to be a common structural motif throughout human enzymes as well, involved in a number of biochemical processes⁹³. As such, design of molecules to inhibit this particular moiety must be specific and selective for the target, in order to avoid toxicity issues.

There are three subclasses of MBLs: B1, B2 and B3⁹⁴. These are determined *via* their primary amino acid sequence homology⁹⁵, which in turn distinguishes between their structural characteristics and behaviour of the active sites.

All three types of MBL attack the β -lactam ring through use of a bound hydroxide ion (*Fig. 13*). However, the zinc-binding environment for this hydroxide varies between the MBL subclasses. In general, B2 have mono-zinc active sites, whilst B1 and B3 have di-zinc active sites, which are differentiated as Zn1 or Zn2⁹⁴.

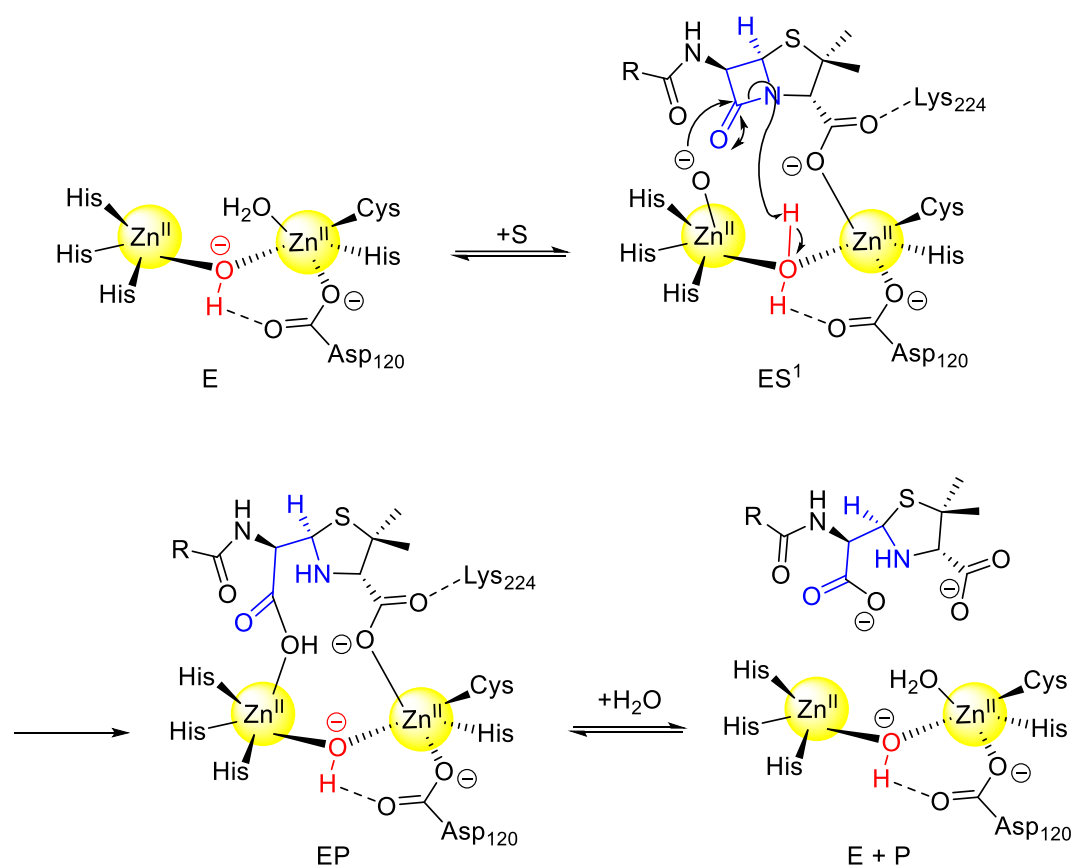


Figure 13. A proposed mechanism of penicillin degradation by a B1 metallo- β -lactamase. When the substrate (S) encounters the enzyme (E) the carboxylic acid of S forms a bond with the Zn2 metal centre. Then, a bound water molecule at Zn1 attacks the carbonyl carbon of the β -lactam ring of S, breaking the amide bond (ES¹). The inactivated antibiotic (P) detaches from E, which is then free to catalyse the degradation of further molecules of S⁹⁶.

B2 MBLs are active in their mono-zinc form; this zinc ion is located in the site of the Zn2 ion in B1 and B3 MBLs. If a second zinc ion is added to the Zn1 site of a B2 MBL then this inactivates it, due to the closing of a regulatory loop (e.g. Gly232-Asn233 in CphA) near to the active site⁹⁷. B2 MBLs also generally share the same ligand residues around the Zn2 ion as the B1 MBLs:

Asp, Cys and His (Fig. 14)^{95,96}. B2 MBLs preferentially degrade carbapenems, unlike B1 and B3 MBLs which have broader substrate profiles^{98,99}.

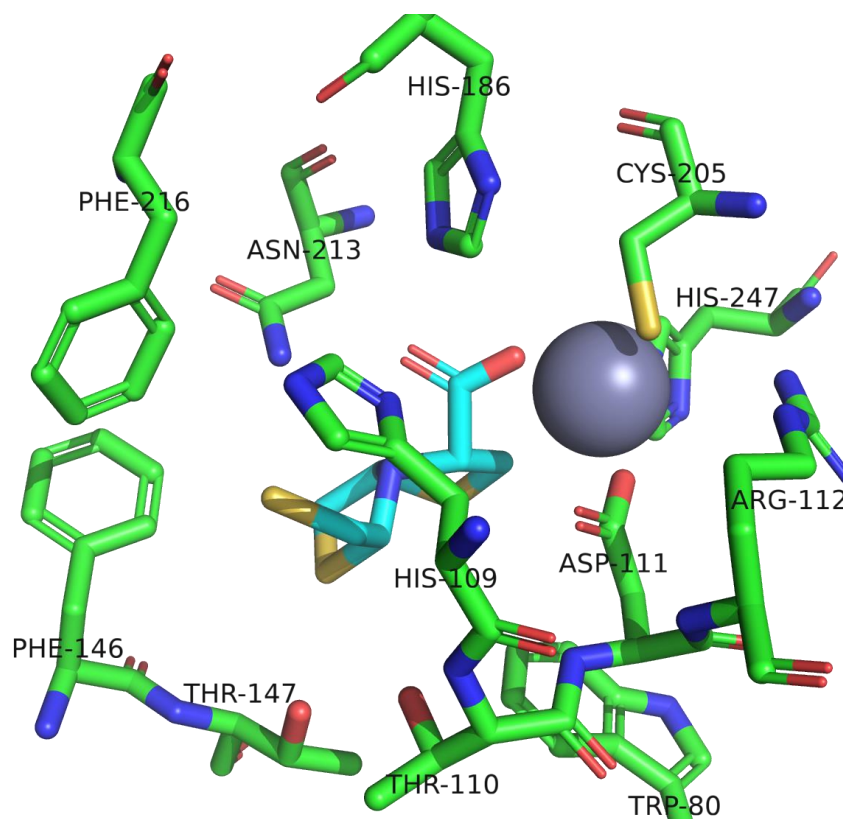


Figure 14. A bisthiazolidine inhibitor (blue) coordinating to the zinc metal centre (grey sphere) in *Sfh-1* (PDB ID: 5EW0)¹⁰⁰, a mono-zinc B2 MBL. We can also see the Asp, Cys and His residues bound to the zinc metal centre here.

B3 MBLs are generally active in the di-zinc form and have broad substrate profiles^{101–106}. They differ from the B1 and B2 MBLs by the residues in the Zn2 site, which are usually Asp, His, His, rather than Asp, Cys, His. The residues around the Zn1 site are His, His, His but there are exceptions to this (e.g. in the GOB-1 B3 MBL it is Gln, His, His)¹⁰⁵. B3 enzymes feature the only known example of a tetrameric MBL, which is L1¹⁰¹.

B1 MBLs are active in both mono- and di-zinc forms. Whilst the ion at the Zn2 site is essential for catalytic function, the ion at the Zn1 site lowers the activation barrier by stabilising the negative charge created upon nucleophilic attack of the β -lactam ring by water¹⁰⁷.

The N-terminal domain of B1 MBLs features a flexible loop which aids in substrate binding when the substrates contain a hydrophobic side-chain. This loop blocks molecules in the active site through interaction of the hydrophobic side-chain with a Trp64 residue. This loop also interacts with inhibitors (other

than carbapenems). If this loop is removed, then enzymatic activity is greatly reduced. This feature is not conserved in B2 and B3 MBLs⁹¹.

1.3.2.4 IMP-1, VIM-2 and NDM-1

B1 MBLs are the most clinically relevant subclass, containing the IMP-, VIM- and NDM-type enzymes⁹⁴. The clinical relevance of these is due to their generally broad substrate profiles and propensity for spreading to other bacteria, being plasmid encoded *via* horizontal gene transfer, therefore accelerating the rise of resistance¹⁰⁸⁻¹¹¹. As such, this subclass has rapidly spread across the globe since their discovery (*Fig. 15*)

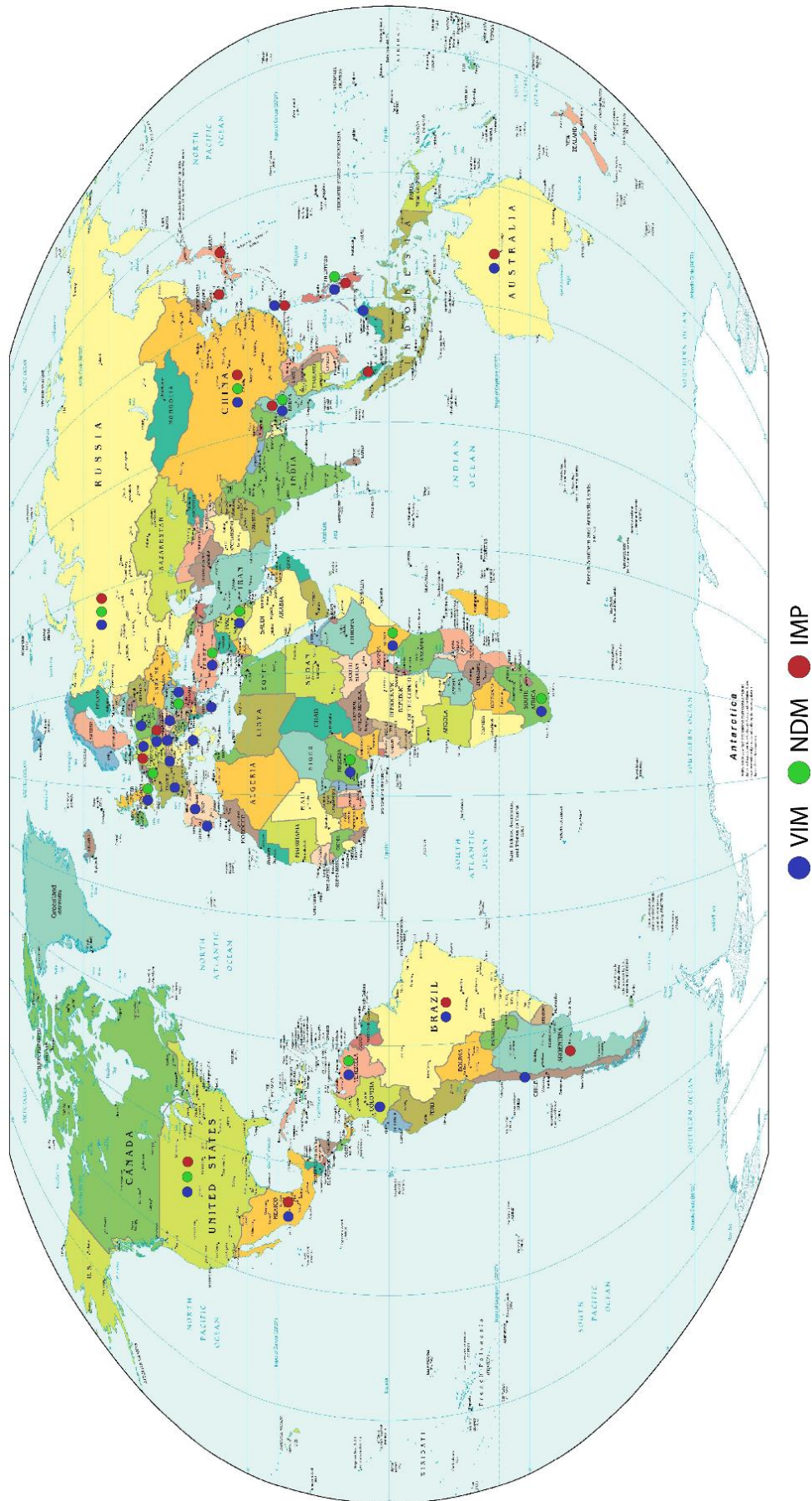


Figure 15. The distribution of B1 metallo-β-lactamase-positive Enterobacteriaceae and *P. aeruginosa* collected from 2012 to 2014. Adapted from Kazmierczak et al.¹¹¹

1.3.2.4.1 IMP-1

IMP-1 was first discovered in Japan in 1983¹¹². It spread throughout Asia and was molecularly characterised in 1994¹¹³.

It was first identified in a patient in Europe in 1997, from a multidrug resistant strain of *Acinetobacter baumannii*. The strain carried the encoding *bla*_{IMP-1} gene and showed resistance to fluoroquinolones, amikacin, tobramycin, gentamicin, fosfomicin, trimethoprim/sulfamethoxazole, piperacillin, piperacillin/tazobactam, ticarcillin/clavulanate, aztreonam, ceftazidime, cefepime, imipenem and meropenem. The only antibiotic it did show susceptibility to was polymyxin B. A crude extract showed inhibition by EDTA. Previously this variant had only been seen in the China, South Korea & Japan¹⁰⁸.

As of 2016, IMP-1 variants had appeared on all continents (other than Antarctica), and are the predominant MBL in Japan and south-east Asia¹¹⁴.

1.3.2.4.2 VIM-2

VIM-2 was identified in the year 2000, in Marseilles, France. Further to this, it has appeared in Japan, Spain, Belarus, Kazakhstan, Russia, Egypt, Columbia and Tanzania, amongst elsewhere, indicating a truly global spread^{115–120}. Having 90% sequence similarity with VIM-1, VIM-2 was found only 300 km from Verona, Italy, where VIM-1 was first discovered¹¹⁰.

Upon its discovery in Marseilles, VIM-2 showed resistance to most ureidopenicillins, ureidopenicillins- β -lactamase inhibitors, narrow-spectrum cephalosporins, cefepime, ceftazidime, imipenem but showed full susceptibility to aztreonam. The COL-1 *P. aeruginosa* bacteria that the isolate came from also showed resistance to kanamycin, tobramycin, streptomycin, tetracycline and chloramphenicol, but showed moderate susceptibility to fluoroquinolones and rifampin, and full susceptibility to fosfomicin. Like other MBLs, it showed inhibition by EDTA¹¹⁰.

1.3.2.4.3 NDM-1

A more recent discovery than IMP-1 and VIM-2, NDM-1 was identified in 2009 in a Swedish patient of Indian origin, who had recently travelled to New Delhi,

India¹²¹. NDM-1 was next found in the UK, and further to that the *bla*_{NDM-1} gene has spread across the globe, with NDM variants seen on all continents other than Antarctica¹²².

NDM-1 is able to hydrolyse all β -lactams, including carbapenems, other than aztreonam¹²². It shows moderate susceptibility to cefepime and ciprofloxacin, as well as full susceptibility to colistin and tiglecyclin¹²³. As expected for an MBL, it was inhibited by EDTA¹²¹.

NDM-1 is unique compared to other clinically relevant MBLs, in that it is a lipoprotein located at the outer membrane of Gram-negative bacteria, as opposed to being a soluble periplasmic enzyme (as is true for the other clinically relevant MBLs). This location provides several evolutionary advantages: the stabilisation of the enzyme under conditions of metal starvation that occur at infection sites (which also allows it to more easily confer resistance under limited metal availability) and providing a mechanism to disseminate into the bacterium's environment through OMVs¹²⁴. Due to the difference in cellular location of most MBLs, they are not frequently found in OMVs. However, due to the outer-membrane location of NDM-1, it is easily able to be secreted into the environment through this mechanism, enhancing its ability to spread through HGT (as well as providing additional resistance to other bacteria in the environment)¹²⁵.

1.3.3 Inhibitors of β -lactamases

Almost since the inception of β -lactam drugs in the clinic, resistance has been seen. In Gram-positive bacteria this was first found to be due to enzymatic hydrolysis of the molecules by penicillinases¹²⁶. Later on however, decreased PBP affinity for β -lactams become the more clinically relevant resistant mechanism¹²⁷.

For Gram-negative bacteria, β -lactamases have remained the primary cause of antibiotic resistance. This has led to the discovery and development of β -lactamase inhibitors (BLIs), to enable us to continue using life-saving antibiotics. The most famous and first of these is clavulanic acid, found as an inhibitor for TEM-1. What was learnt from examining this inhibition mechanism has since been applied to developing a wealth of β -lactamase inhibitors⁸¹.

1.3.3.1 Serine- β -lactamase inhibitors

SBLs all feature a nucleophilic Ser residue as their primary moiety for the breakdown of β -lactam antibiotics. Blocking this residue through preferential binding and therefore preventing the enzymes catalytic activity towards co-administered antibiotics is the basis of inhibitor design.

1.3.3.1.1 Clavulanic acid and its analogues

Clavulanic acid and its mechanistically similar inhibitors, such as sulbactam and tazobactam, are 'suicide' inhibitors, meaning they are destroyed in the process of their action⁸¹. They are structurally related to the β -lactams they are there to protect, but as part of their inhibitory mechanism they block the catalytic Ser residue, rendering the enzyme inactive.

These inhibitors acylate the nucleophilic serine residue as happens in the catalysis of β -lactams, through the carbonyl on their β -lactam ring. However, after this step their mechanism differs to that of the β -lactam antibiotics and leads to either irreversible or transient inhibition, through multiple mechanisms (Fig. 16)¹²⁸.

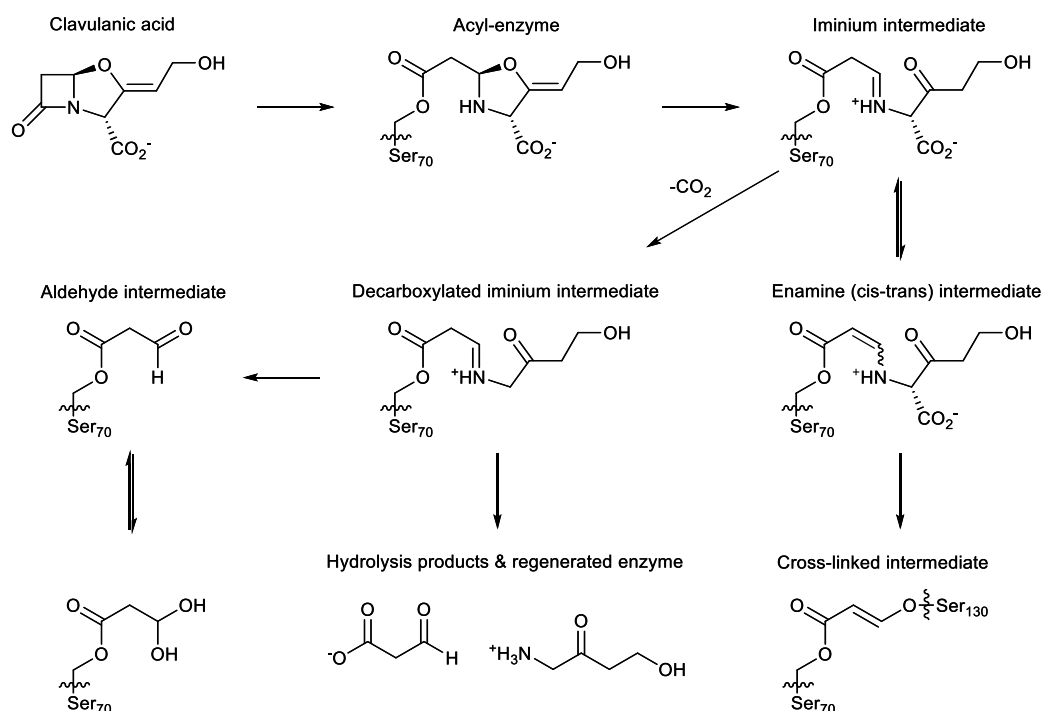


Figure 16. A proposed mechanism for the inactivation of class A β -lactamases by clavulanic acid¹²⁸.

Modifications of traditional β -lactam scaffolds has provided some inhibitors capable of MBL inhibition. Cefiderocol is a β -lactam based β -lactamase

inhibitor that has shown stability to all classes of SBLs and has shown activity versus class B β -lactamases (Fig. 17). Additionally, cefiderocol has antibiotic activity of its own through binding to a number of PBPs. The mechanism of cefiderocol is yet to be elucidated, but it is thought to be through inherent resistance to hydrolysis^{129,130}.

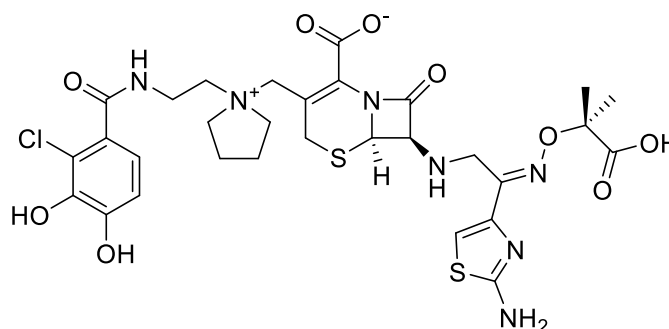


Figure 17. The structure of cefiderocol, a β -lactam based β -lactamase inhibitor that has shown stability to all classes of SBLs and has shown activity versus class B β -lactamases.

Unfortunately, the activity of the majority of these BLIs is restricted to a limited amount of class A SBLs and so further inhibitors have been designed.

1.3.3.1.2 Avibactam

Avibactam is a non- β -lactam inhibitor. It is able to inhibit both class A and class C SBLs (including some class A ESBLs that are not inhibited by clavulanic acid and its analogues, such as KPC and CTX-M variant enzymes). It is a bridged diazabicyclo[3.2.1]octanone and follows a different mechanism of action than the β -lactam inhibitors⁸¹.

Avibactam forms a covalent bond with the enzyme, through acylation of a carbonyl. However this is reversible, and subsequent deacylation results in the regeneration of the intact avibactam molecule and the enzyme. This means that the avibactam molecule is then free to re-acylate with the enzyme, resulting in consistent inhibition of catalytic activity (Fig. 10)¹³¹.

1.3.3.1.3 Aztreonam and Syn 2190

Aztreonam belongs to a class of monobactam inhibitors. Aztreonam interacts with many PBPs, but also resists hydrolysis by many clinically relevant SBLs.

It has low substrate affinity to class A enzymes TEM-1, -2 and SHV-1, and class D enzyme OXA-2¹³².

However, when aztreonam interacts with class C enzymes it forms a stable acyl-enzyme which is only very slowly hydrolysed. By utilizing the crystal structures of aztreonam interacting with these catalysts, further inhibitors have been designed with greater specificity for certain substrates. Monobactam Syn 2190 was designed based on Aztreonam (Fig. 18). When administered in combination with cefotetan, it showed 100% specificity and 91% sensitivity for ESBL AmpC producing *Klebsiella pneumoniae*¹³³.

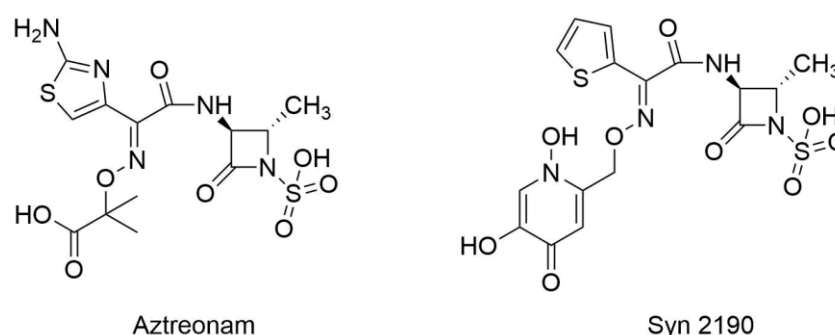


Figure 18. Aztreonam and Syn 2190. Syn 2190 was designed based on observations of the formation of an acyl-enzyme complex when Aztreonam interacts with class C β -lactamases¹³⁴.

1.3.3.1.4 Vaborbactam

Vaborbactam (Fig. 19) is a non- β -lactam inhibitor based on a cyclic boronic acid pharmacophore. The compound is able to inhibit clinically relevant class A and class C β -lactamases, such as KPC, CTX-M, MIR and FOX variants. It is able to restore the activity of meropenem, and other β -lactam antibiotics, in *Enterobacteriaceae*¹³⁵.

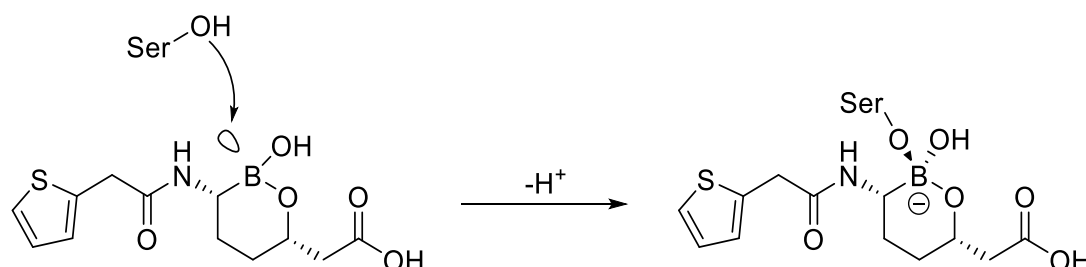


Figure 19. The structure of the antibiotic vaborbactam and its conversion from an sp^2 form to an sp^3 form when a covalent adduct forms with a nucleophilic Ser residue. The sp^3 form mimics the tetrahedral transition state that occurs during the β -lactam acylation/deacylation pathways.

As boron has an empty p-orbital, it is an effective electrophile as it can form dative covalent bonds with a nucleophilic Ser residue, as lies in the active site of SBLs. This covalent adduct that is formed mimics the tetrahedral transition state that occurs during the β -lactam acylation/deacylation pathways. This is a reversible reaction with vaborbactam, as the key boronate cyclic ring is reformed after hydrolysis. As such, it is then able to react again with the enzyme, effectively consistently blocking the active site in the enzymes so co-administered antibiotics are able to bind with PBPs^{136,137}.

To observe the method of binding to β -lactamases, Hecker *et al.* crystallised the complex vaborbactam forms with class A CTX-M-15 and class C AmpC enzymes. In both, the catalytic serine residue was seen to form a covalent bond with the boron atom of the inhibitor. The amide moiety present in vaborbactam was seen to form extensive coordination with backbone residues, as was the carboxylate. The inhibitor did show largely different conformations though, with interactions with the oxyanion pocket of the enzymes differing. However, this ability to have different conformations whilst retaining inhibitory activity is thought to be responsible for its ability to inhibit different classes of enzymes¹³⁸.

1.3.3.1.5 Taniborbactam

Additional research into cyclic boronates has led to the development of taniborbactam (*Fig. 20*). Taniborbactam is capable of inhibiting both SBLs and MBLs. Crystallographic studies with CTX-M-15 showed the active site serine molecule covalently bound to the boron atom, whilst the amide moiety provided hydrogen bond contacts with the Ser237 backbone carbonyl, Asn132 and Asn104. Additionally, the carboxylate moiety formed hydrogen bonds with Thr235 and Ser237. Further to this, the cyclohexyl group occupied the same space as the aryl group of several penicillins and cephalosporins. This mode of binding shares many similarities as were seen by Cahill *et al.* in crystallographic studies of CTX-15-M with other cycloboronates^{139,140}. Taniborbactam co-dosed with cefepime is now in stage 3 clinical trials for the treatment of complicated urinary tract infections, including those where NDM and VIM MBLs are present^{141,142}.

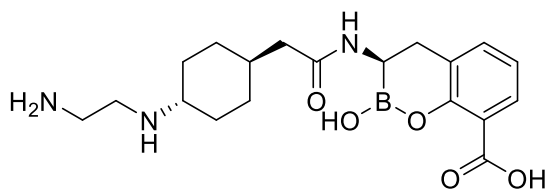


Figure 20. The structure of the antibiotic taniborbactam.

1.3.3.2 Metallo- β -lactamase inhibitors

MBLs differ in structure to their SBL cousins, most notably through the action of their catalytic mechanism. Whilst SBLs utilise a nucleophilic Ser residue for this action, MBLs utilise a nucleophilic water which is held by the active site Zn ions, rather than being covalently bound to the enzyme. For this reason, inhibitors for SBLs will generally not work with MBLs. As such, inhibitors have had to be designed with this difference in mechanism in mind.

Inhibitors of MBLs broadly fall into three different categories, based upon their action: (i) allosteric inhibitors; (ii) covalent bond forming inhibitors; (iii) metal-ion binding inhibitors. In addition to these, there are also some inhibitors with mechanisms that are uncharacterised¹⁴³.

1.3.3.2.1 (i) Allosteric inhibitors

Allosteric inhibitors act through binding to a site separate to that of the active site in an enzyme, which nevertheless inhibits the catalytic activity. How this exactly operates can vary greatly between species.

A DNA aptamer (10-mer) was discovered to be an uncompetitive inhibitor of BclI. Enzyme kinetic studies first indicated this allosteric activity, which was further supported by crystallographic studies and then confirmed *via* NMR titration experiments. These NMR experiments showed reduction in the chemical shifts of residues not in the active site upon addition of the DNA aptamer and mutation studies provided further evidence of this being the site of binding¹⁴⁴.

Carnosic acid (*Fig. 21*) has also been shown to inhibit an MBL, NDM-1, by restoring the activity of meropenem through an allosteric mechanism. Yang *et al.* provided evidence for this allosteric binding through a combination of molecular docking and molecular dynamics simulation. These findings were further reinforced *via* fluorescence quenching and enzyme inhibition assay

experiments, indicating that residues Phe46, Tyr64, Leu65, Asp66 and Thr94 are allosteric sites of NDM-1¹⁴⁵.

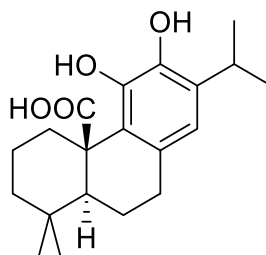


Figure 21. The structure of carnosic acid. This compound is suspected of possible inhibitory activity in NDM-1 via an allosteric site.

Allosteric inhibitors provide an interesting solution for problems associated with producing selective MBL inhibitors. As there is no metal binding involved in the action of these inhibitors, the danger of toxicity due to metal binding of critical enzymes in humans (e.g. histone deacetylases) is reduced.

On the other hand, due to the poor sequence similarity between MBLs the design of these types of inhibitors is hindered. It will be difficult to find allosteric sites that exist throughout different MBLs, and so designing a more general allosteric inhibitor would be perhaps impossible.

1.3.3.2.2 (ii) Covalent bond forming inhibitors

A major challenge in the development of inhibitors for MBLs is the lack of covalent bond formation throughout the transition state of the catalytic mechanism. This is a major cause of SBL inhibitors being useless for MBL inhibition.

However, covalent inhibitors can be designed to target key residues within the active site that are not directly involved in the catalytic mechanism. Kurosaki *et al.* designed an irreversible inhibitor of IMP-1 with this in mind. Through a thiol moiety the molecule was held between the active site Zn ions, enabling a leaving group to be displaced through nucleophilic attack of a carbonyl by the amino functionality in the Lys224 sidechain (this residue is conserved through many B1 MBLs), forming an amide bond. This site of binding was confirmed through X-ray crystallography¹⁴⁶.

Unfortunately, these types of MBL inhibitors must be reactive for their mechanism to work. This carries risks of non-selectivity and therefore toxicity¹⁴³.

1.3.3.2.3 (iii) Metal-ion binding inhibitors

Inhibition through metal-ion binding is the most common type of inhibitor design of class B β -lactamases¹⁴³. A wealth of compounds have been designed with this goal in mind, and many have been successful in stopping the enzymatic activity of their targets. Designing these inhibitors to be selective however, therefore avoiding toxicity issues, may be the biggest challenge.

The first metal-ion binding inhibitor of MBLs was in fact found alongside the first report of an MBL. EDTA was used to suggest the existence of a metal in the active site of a β -lactamase from *Bacillus cereus*. Addition of EDTA to this enzyme showed inhibition of cephalosporinase activity¹⁴⁷.

Whilst a cyclic boronic acid inhibitor, vaborbactam, is available for SBLs, it does not inhibit MBLs. However, further development has identified cyclic boronate inhibitors for both SBLs and MBLs. Brem *et al.* has shown a molecule (Fig. 22) to be a promising candidate⁷¹.

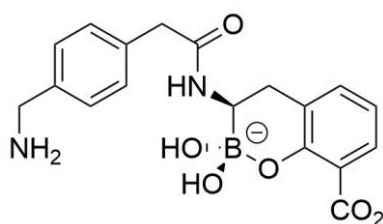


Figure 22. A cyclic boronate capable of inhibiting MBLs, designed by Brem *et al.*⁷¹

The compound binds to the zinc metal centre *via* its oxygen atoms in the boronate moiety. The hydroxyl groups bind to the primary zinc centre, whilst the adjacent ether oxygen and the carbonyl oxygen of the carboxylic acid group coordinates to the secondary zinc centre. The key to its activity is the mimicry of the tetrahedral transition state that occurs during β -lactam hydrolysis. The hydroxyl oxygen of the carboxylic acid group also participates in binding; this coordinates to a nucleophilic side chain in the active site (*i.e.* Lys₂₂₄ in BcII and NDM-1, Arg₂₂₈ in the VIM family) (Fig. 23). The ring structures of the molecule are well positioned to make favourable hydrophobic

interactions with conserved Trp₈₇ and Phe₆₁ residues (as shown with BclI and VIM-2). Additional to this, the amide group and adjacent side chain are well-positioned to form additional interactions with other residues within the binding pocket⁷¹. This work has contributed to the development of the aforementioned taniborbactam.

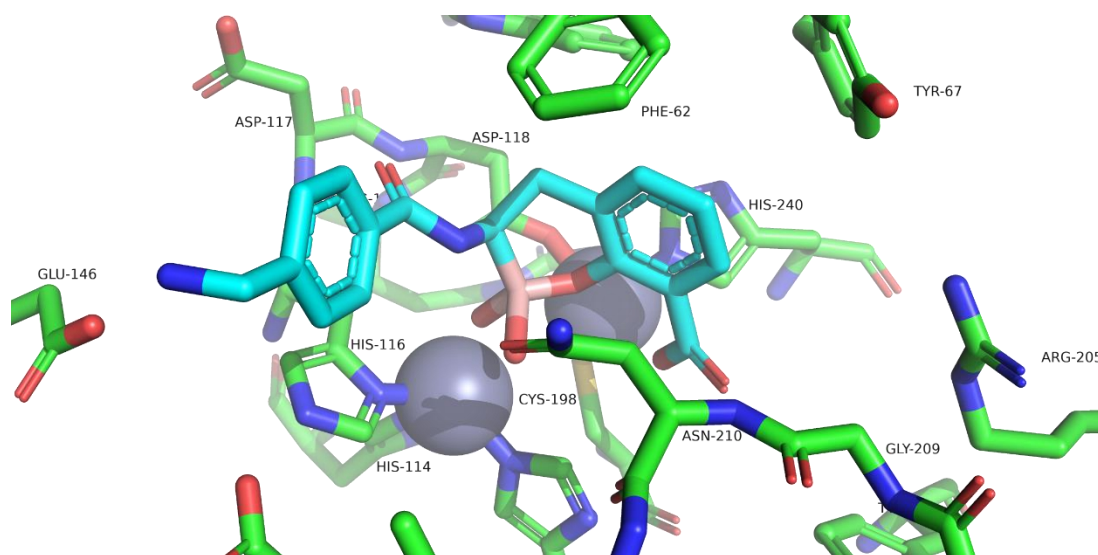


Figure 23. Cyclic boronate bound to VIM-2 MBL (PDB ID: 5FQC). The zinc binding sites in the active site of the MBL bind to the oxygens adjacent to the boronate core in VIM-2, in a tetrahedral conformation. There is also binding with some of the residues in the core, such as the terminal primary amine moiety binding with Glu146.

The aforementioned cyclic boronate taniborbactam has also been shown to be active in MBLs. Crystallographic studies performed by Krajnc *et al.* showed multiple modes of structure throughout the inhibition. In addition to previously seen bicyclic sp^2 and sp^3 forms⁷¹, an unexpected tricyclic sp^3 binding conformation with NDM-1 was observed, showing the incredible flexibility of the inhibitory states of these molecules (Fig. 24). The gravity of this observation is further compounded as it is the mimicry of the tetrahedral transition state of β -lactam hydrolysis that is key to the inhibitory effects. Interestingly, the L3 loop which is thought to be important in binding showed little importance in stabilizing Taniborbactam¹⁴⁸. The sidechain aids stabilization of binding through favourable interactions with negatively charged residues (e.g. Glu149 in VIM-2 and NDM-1)¹⁴⁰.

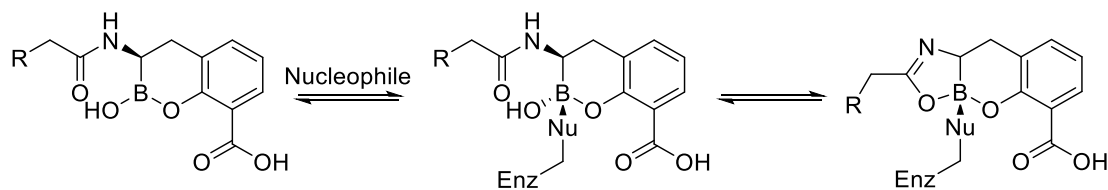


Figure 24. The three conformational structures of taniborbactam. When unbound to an enzyme, taniborbactam shows an sp^2 structure. When bound to an enzymes it displays an sp^3 structure, which can be tetrahedral or bicyclic¹⁴⁸.

Captopril is a thiol containing molecule designed for inhibition of angiotensin-converting enzymes (ACE). It was later found to bind to MBLs, and crystal structures of it bound to IMP-1, BcII and VIM-2 showed this to be through the thiol(ate) binding to the Zn^{2+} metal centres. Stronger inhibition was consistently observed when the captopril carboxylate was bound to the conserved Lys/Arg224 residue. Additionally, differing inhibition was shown between the L- and D- stereoisomers, due to electrostatic interactions with sidechain residues¹⁴⁹.

Due to the propensity of thiols for metal binding, further inhibitors have been designed based on them. Cain *et al.* utilised *in silico* design to guide the synthesis of a small library of thiol-based inhibitors. These showed potent inhibition of B1 MBLs including NDM-1, IMP-1 and VIM-2. Additionally, these thiol inhibitors showed selectivity for bacterial MBL enzymes versus human MBL fold nucleases. Restoration of meropenem activity was shown in both NDM-1 producing *K. pneumoniae* and *E. coli*¹⁵⁰.

Crystallization of this thiol with VIM-2 showed the thiol moiety binding between the zinc metal centres in the active site, displacing the bound nucleophilic water molecule (Fig. 25). This agrees with modes of binding seen in other studies^{146,151}. The carboxylate moiety showed unexpected binding with Arg119 through a water molecule, rather than the expected binding with Arg228¹⁵⁰.

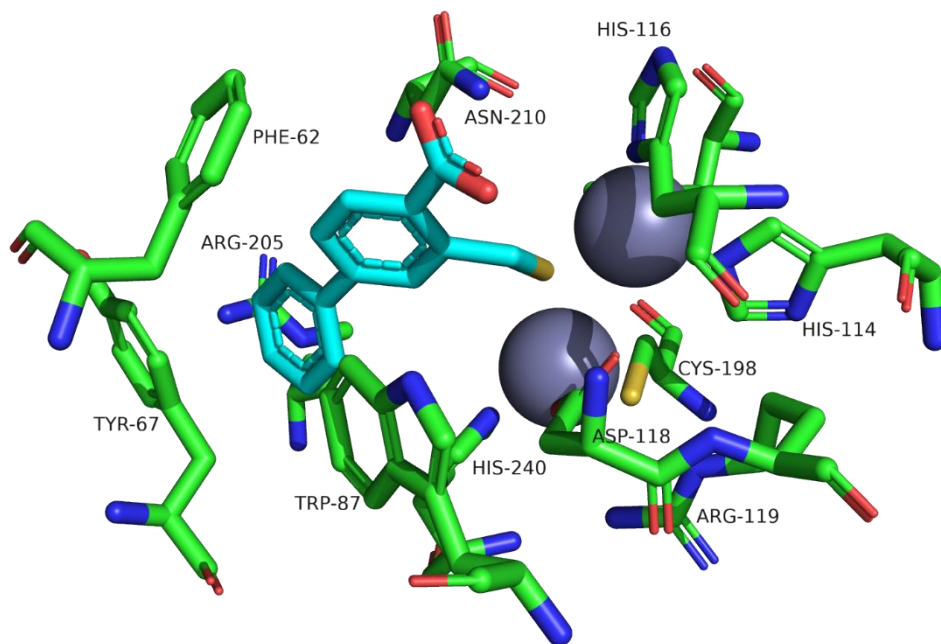


Figure 25. Thiol bound to VIM-2 MBL (PDB ID: 5K48). The thiol moiety binds directly between the zinc metal centres, displacing the bound hydroxide ion and therefore inhibiting the enzymes activity.

Chapter 2

Design, docking & synthesis of metallo- β -lactamase inhibitors

2.1 Cyclic boronates

2.1.1 Introduction

Cyclic boronates are compounds that act as inhibitors of B1 MBLs. Their effectiveness as MBL inhibitors was shown through previous work in the Fishwick and Schofield groups, published in Brem *et al.*⁷¹, which demonstrated the structural basis of inhibition.

Interestingly, these compounds had a different structure than was expected from their synthetic design, revealed *via* the obtained crystal structure. The compounds were designed as boronic acid inhibitors, which showed promising docking scores and poses *via* Schrödinger's docking software Glide, but when crystal structures were obtained the active compound was found to feature a cyclic boronate moiety (**3**) as opposed to the expected boronic acid (**1**). The conversion from boronic acid to cyclic boronate happens spontaneously through nucleophilic attack of the boron atom by the phenolic moiety¹⁵². The exact mechanism by which this occurs has not been fully investigated, although it likely involves attack of the boron atom *via* its empty p-orbital, followed by ejection of a hydroxide group, neutralising the negatively charged boron (*Fig. 26*).

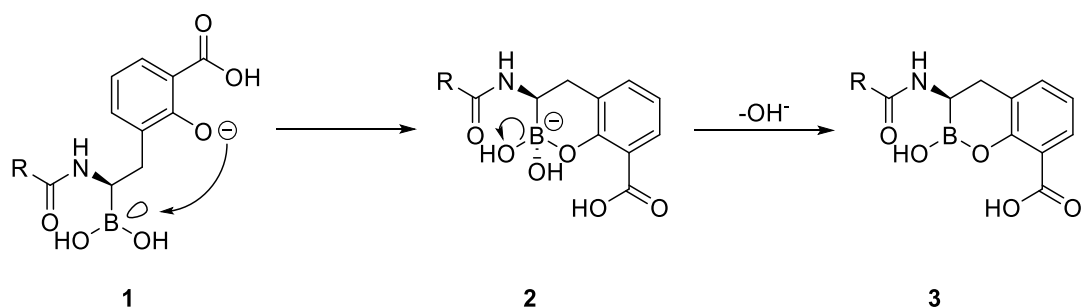


Figure 26. The phenolic moiety (as the phenoxide ion) of the boronic acid 2.1 attacks the boron atom through its empty p-orbital, causing the molecule to cyclise, giving 2.2. Hydroxide is then ejected to neutralise the boron atom, resulting in the cyclic boronate structure (2.3).

Cyclic boronates with an aromatic side-chain positioned analogously to the 6 β /7 β side chains of the penicillins and cephalosporins were shown to inhibit many B1 MBLs such as IMP-1, VIM-2 and NDM-1 through *in vitro* assays. Further to this, inhibition was also shown in class A and D SBLs, as well as some PBPs. *In vitro* testing with antibiotic resistant forms of *K. pneumoniae* and *E. coli* revealed that these compounds were able to restore the susceptibility of the bacteria to antibiotics when co-dosed with Meropenem, further underlining the potential of these compounds in the treatment of bacterial infection¹⁵².

Crystal structures of cyclic boronates in BclI and VIM-2 MBLs showed that the mode of action of inhibition is *via* a tetrahedral binding mode, whereby the two hydroxyl groups attached to the boron atom are bound to Zn1 and the boronic ether oxygen and carboxylic acid carbonyl are bound to Zn2. There are additional interactions between a boronic acid hydroxy group and Asn233 and the carboxylate of the inhibitor with Lys224/Arg228 in VIM-2. This tetrahedral intermediate state would appear to mimic a transitional state of β -lactam hydrolysis, which may explain the potency of these inhibitors (Fig. 27)⁷¹.

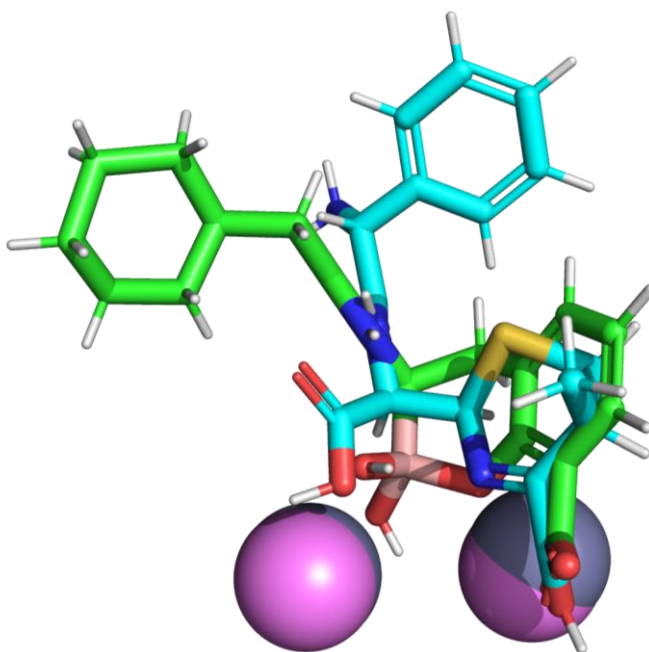
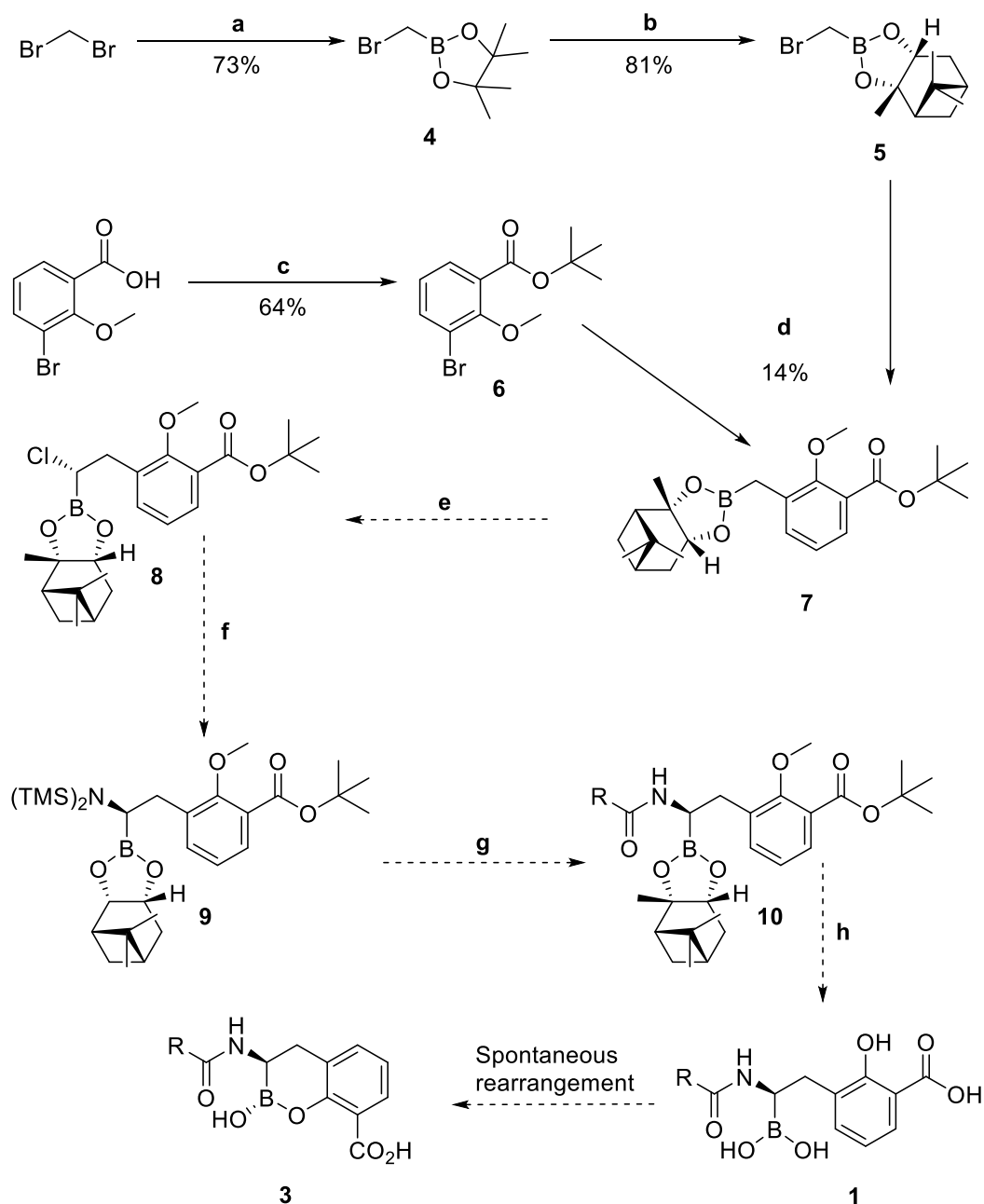


Figure 27. Hydrolysed cefuroxime (cyan) complexed with NDM-1 (PDB ID: 4RL2) overlaid with taniborbactam (green) complexed with NDM-1 (PDB ID: 6RMF). A tetrahedral centre between the zinc atoms can be seen in both structures (at the boron centre in the green structure, and adjacent to the carboxylic acid residue in the cyan structure).

In light of this prior success, early in the present project, it was proposed to design further cyclic boronate inhibitors (**2.3**) with improved potency *via* alteration of the 'R' group attached through the amide bond. The ultimate goal here was to fine-tune the side-chain interactions of the inhibitor and protein residues, in terms of increased selectivity and potency in the presence of the MBL target enzymes. It was hoped that this would provide further validation of the cyclic boronate core as a 'tuneable' metalloenzyme inhibiting moiety.

2.1.2 Synthesis of cyclic boronate MBL inhibitors

In light of the synthetic route already established for cyclic boronates by Cain (*Scheme 1*), it was decided that structure-based design using computational methods could be left to a later stage of the project¹⁵². Therefore synthesis of the boronic acid 'core' structure was started (*Scheme 1*) before the ultimate target molecules were designed.



Scheme 1. Original cyclic boronate synthesis, as designed by Cain¹⁵². a) i) *n*-BuLi, B(OiPr)₃, THF, -100 °C to RT, 5 hrs, ii) CH₃SO₃H, 0 °C, 1 hrs, iii) Pinacol, RT, 16 hrs; b) (+)-Pinanediol, THF, RT, 16 hrs; c) i) Oxalyl chloride, cat. DMF, DCM, RT, 1 hrs ii) *t*-BuOH, 70 °C, 16 hrs; d) *n*-BuLi, THF, -100 °C, 3 hrs; e) i) LDA, DCM, THF, -100 °C, 30 min, ii) ZnCl₂, THF, -100 °C to RT, 16 hrs; f) LiHMDS, THF, -100 °C to RT, 16 hrs; g) i) MeOH, THF, RT, 2 hrs ii) RCO₂H, HATU, Et₃N, -20 °C to RT, 16 hrs; h) BBr₃, DCM, -78 °C, 3 hrs.

The first step, conversion of dibromomethane to the boronic pinacol ester (4) proceeded as expected. This step was accomplished at -100 °C using a methanol and liquid nitrogen bath, by a lithium-halogen exchange reaction using *n*-butyllithium. The reaction was then allowed to reach room temperature and thus reacted with triisopropyl borate, forming diisopropyl bromomethylboronate *in situ*. The solution was then cooled to 0 °C and

acidified with methanesulfonic acid. After stirring for an hour pinacol was added and the subsequent reaction produced molecule **4** as a colourless solid. Initial attempts at purification of this compound were made by using normal-phase column chromatography, followed by distillation under reduced pressure. However, the final product could not be obtained pure *via* this method. Later attempts at purification used solely distillation under reduced pressure and gave the product as a colourless oil. Analysis of this oil using ¹H NMR, indicated the presence of only small amounts of impurities, and this material was considered of sufficient purity for direct use in subsequent reactions. Interestingly, increasing the scale of this reaction significantly increased the yield of the products (by up to 25% when increasing the scale from 5 mmol to 50 mmol).

The next reaction in this sequence was a simple substitution, creating the (+)-pinanediol ester (**5**) in place of the pinacol ester (**4**). Installation of the (+)-pinanediol ester was required in order to produce the desired stereochemistry at a later step in the route. The (+)-pinanediol group was introduced by stirring (1*S*,2*S*,3*R*,5*S*)-(+)-pinanediol at RT with **4** in THF and subsequent purification using normal-phase flash column chromatography afforded the pure product **5**. By reducing the amount of solvent used in the reaction mixture the yield was increased from 25% to 81% over the course of synthesis.

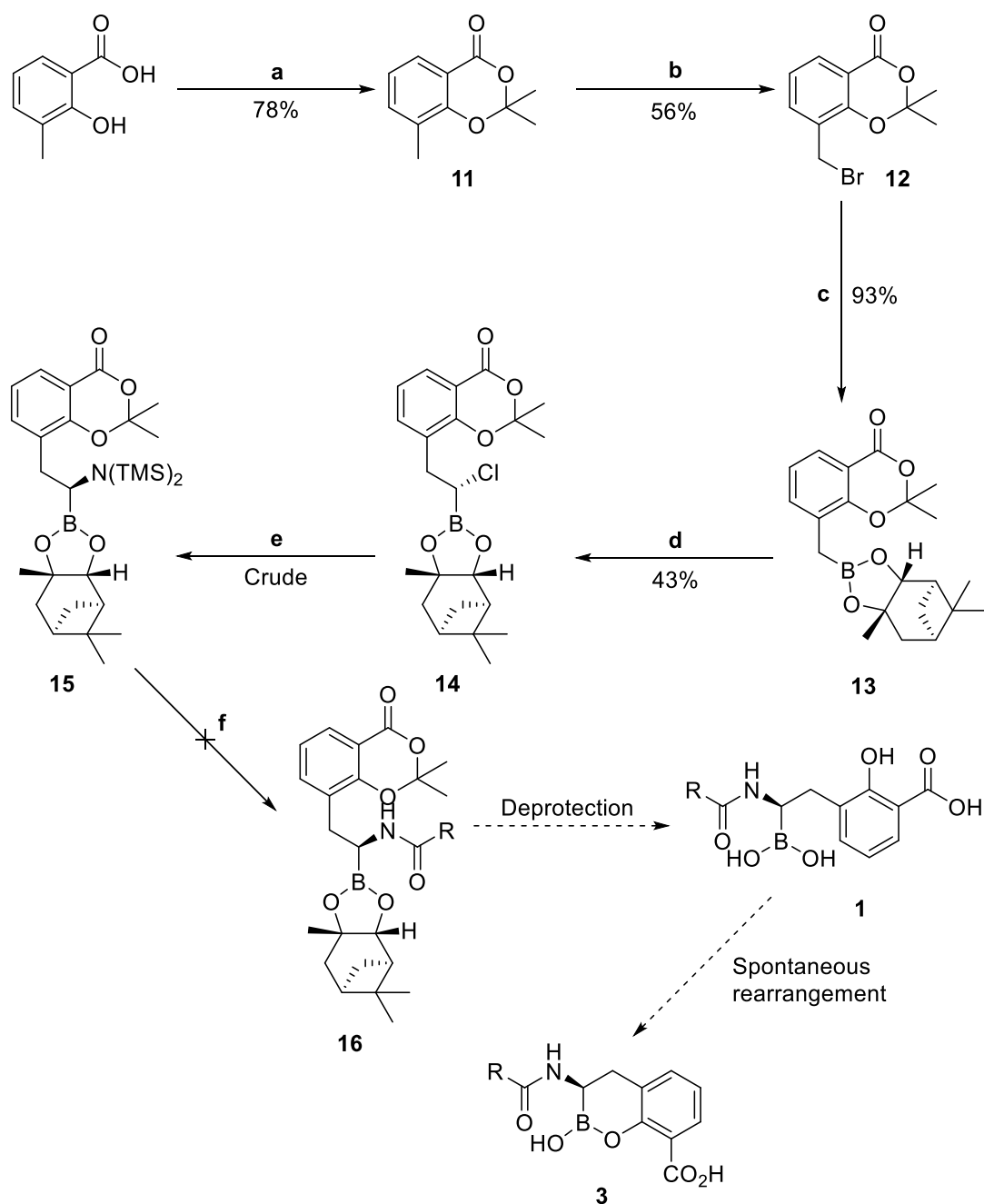
At the other starting point of this convergent synthetic route, 3-bromo-2-methoxy benzoic acid was esterified using *tert*-butanol to give **6**. Purification was achieved *via* normal-phase flash column chromatography. Yields from this step were generally around 50%.

At this point the synthesis converged and the two compounds, **5** and **6**, were combined. This was achieved through a lithium-halogen exchange reaction using *n*-butyllithium and **6** at -100 °C. Compound **5** was then added to the reaction mixture at -100 °C and the reaction was stirred, being allowed to reach RT. Yields for this reaction were generally poor however, being around 10 - 12%. This was partly attributed to homocoupling of **6** versus the desired S_N2 product.

Due to the low yields seen in this step, it was decided to attempt a Negishi cross-coupling, as found in a patent which claimed yields of 83%¹⁵³. Zinc

powder and **5** were placed in a nitrogen flushed flask and anhydrous THF was added, followed by 1 M DIBAL-H solution. This was stirred at 50 °C for 1 hr and then added dropwise into a mixture of palladium tributylphosphate and **6** in anhydrous THF at RT, which was stirred for a further hour. Whilst this did produce a product of the correct mass following analysis of the crude reaction mixture using LC-MS, it was not possible to isolate this material.

Whilst the desired product had been produced *via* the lithium exchange reaction, continuing on this course with such low yields at an early stage seemed untenable. Despite previous reports by Cain *et al.* which had produced intermediate **7** in a good yield (76%), this work was unable to repeat this reaction at the same scale and yield. Thus, a new synthetic route was devised to overcome these challenges (*Scheme 2*).



Scheme 2. A new scheme towards the desired cyclic boronate inhibitor, designed to overcome synthetic challenges met in the original route. (a) TFA, TFAA, toluene, acetone, 0°C to RT. (b) NBS, AIBN, MeCN, 80°C. (c) Bis[*(+)*-pinanediolato]diboron, KOAc, Pd(*dppf*)Cl₂, 1,4-dioxane, 95°C. (d) i) LDA, DCM, THF, -100°C, 30 min. ii) ZnCl₂, THF, -100°C to RT, 16 hr. (e) LiHMDS, THF, -100°C to RT, 16 hr. (f) i) MeOH, THF, RT, 2 hr. ii) RCO₂H, HATU, Et₃N, -20°C to RT, 16 hr.

The first step of this synthesis proved simpler and more successful than that of the previous route. Thus, addition of TFAA to a solution of 3-methyl salicylic acid in TFA produced **11**. This was obtained as a translucent brown oil which spontaneously crystallised into large, clear rectangular crystals. Presumably, this reaction proceeds *via* attack of acetone *via* the phenolic moiety, followed

by attack of the carboxylic acid carbonyl through the alcohol on the newly installed hemiacetal group (Fig. 28). This reaction was generally high yielding, but this did drop off as scale was increased from 78% at 6.57 mmol scale to 13% at 131.4 mmol scale. In light of this, the reaction was generally performed at around a 40 mmol scale, which gave yields of around 60%, this being an acceptable balance between scale and yield.

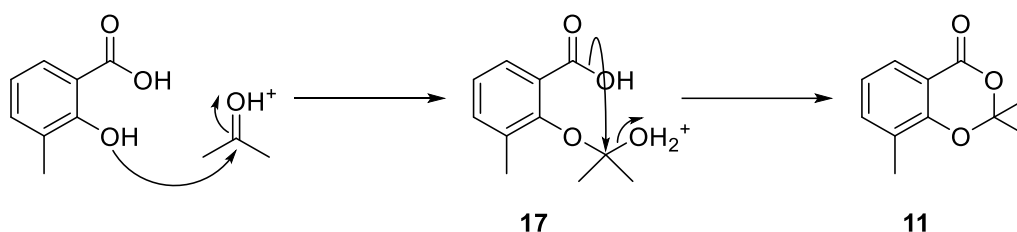


Figure 28. Formation of the acetonide via a hemiacetal intermediate.

Next, molecule **11** was brominated using *N*-bromosuccinimide and benzoyl peroxide, giving molecule **12** as colourless plates following recrystallisation from ethanol. This reaction generally gave yields of around 50%.

In the next step, a Suzuki cross-coupling of **12** and bis[(+)-pinanediolato]diboron was completed to install the boronic (+)-pinanediolato moiety. Compound **12**, bis[(+)-pinanediolato]diboron and potassium hydroxide were dissolved in 1,4-dioxane and the solution was degassed with nitrogen. This was then added to a nitrogen-flushed flask containing bis(diphenylphosphino)ferrocene dichloropalladium (II) and this solution was degassed further. The mixture was then heated to 95 °C and stirred for a day under nitrogen. When the reaction was complete (as judged *via* TLC), ethyl acetate was added and the solids were removed, then the solution was concentrated and purified *via* automated normal-phase flash column chromatography, affording **13** as a clear oil. This first attempt achieved a yield of 64%, far higher than was seen when completing this synthesis *via* the aforementioned convergent route. This yield was further optimised *via* increasing the amount of base used from two equivalents to four equivalents, therefore accelerating the transmetalation step in the reaction cycle, to a best performance of 93%.

The next step of the synthesis was a Matteson homologation, using DCM as a reagent to install a chloroalkyl group between the boron and adjacent

methylene group, resulting in an enantiomerically pure product (*S*-absolute stereochemistry)¹⁵⁴. The Matteson homologation presumably occurs *via* attack of the boron atom by a deprotonated DCM ion, which forms a dative bond through boron's empty p-orbital. Zinc chloride is added to stabilise this transitional state through interactions with a chlorine atom of the deprotonated DCM moiety and an oxygen of the boronate (*Fig. 29*). The zinc chloride stabilisation is where stereoselectivity arises in this step, as conformation **19** is disfavoured through clashing chlorine atoms, whereas **18** is sterically favoured¹⁵⁵. Following this, the alkyl group adjacent to the boron atom attacks the carbon of the deprotonated DCM group, with a chlorine ion acting as a leaving group. This gave an enantiomerically pure product with a chloromethylene group added into the carbon chain¹⁵⁶.

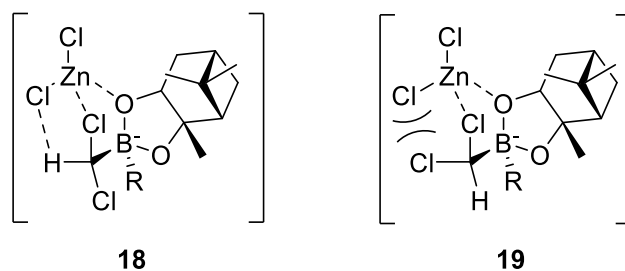


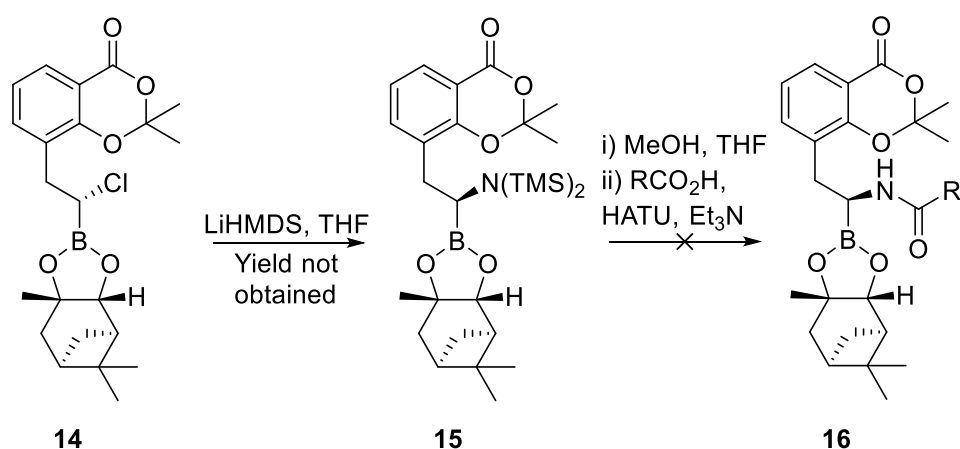
Figure 29. Favoured (18, left) and disfavoured (19, right) transitional states of the Matteson homologation¹⁵⁵. The steric clash between the chlorine atoms in the disfavoured transition state results in the enantiomeric purity of the reaction.

Initially, this Matteson homologation was attempted as previously described¹⁵². This involved the *in situ* generation of lithium diisopropylamide, which was then added to **13** and DCM at -100 °C. Zinc chloride solution was added to the reaction mixture which was then left to stir overnight, being allowed to reach room temperature. Unfortunately despite many attempts this step proved unsuccessful using these published conditions.

A modified synthetic step was then performed, upon guidance from collaborators in the Schofield group¹⁵⁷. Here, DCM was placed in anhydrous THF under argon and 2.5 M *n*-butyllithium was added slowly dropwise at -100 °C. The resulting solution was left to stir for an hour, being maintained at -100 °C, where a white turbid solid was seen to form. If the reaction mixture stayed clear or any black colouration was seen in the reaction mixture at this point it was disposed of and the step was restarted. A solution of intermediate **13** in

dry THF was then added slowly dropwise to the reaction mixture at $-100\text{ }^{\circ}\text{C}$, stirred for a further 30 mins, and then the zinc chloride solution was added in one portion dropwise. The reaction mixture was then left to stir overnight, being allowed to reach room temperature. The following day the reaction mixture was worked up and purified *via* automated normal-phase flash column chromatography, giving **14** as a pale yellow oil. Unfortunately it was not possible to completely purify this product; some of **13** always remained, as seen by ^1H NMR. However, this could be removed after the next reaction step. A yield of approximately 43% (calculated using purity analysis *via* ^1H NMR) was attained at this step.

The next step of the synthetic route involved formation of disilazide **15** *via* an $\text{S}_{\text{N}}2$ displacement of the chlorine atom in **14** with an amine. The crude product of this reaction was too unstable to store for any length of time. Thus the next step to create **16**, an amide coupling, was immediately carried out with crude **14**. Unfortunately the amide coupling was unsuccessful and this synthetic route was halted here (*Scheme 3*).



Scheme 3. The conversion of 14 to 15 was successful, but the following amide coupling to create 16 was not. The synthetic route was not continued past this point.

Whilst this route was ultimately unsuccessful, useful synthetic optimisations were made along the way. Further explorations of structures of this class of inhibitors and their activity in MBLs has been published by our collaborators in Parkova *et al.*¹⁵⁸

2.2 Thiol-based MBL inhibitors

2.2.1 Introduction

Due to the strong metal coordinating ability of sulphur, thiol-containing compounds have been investigated as MBL inhibitors for over twenty years, such as thiomandelic acid (**20**), mercaptocarboxylic acids (**21**) and thioesters (**22**) (Fig. 30)^{159–161}.

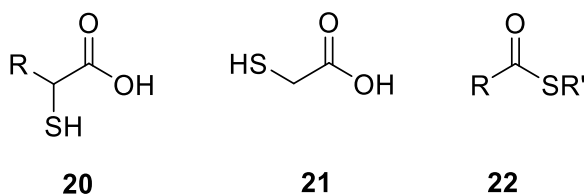


Figure 30. From left to right, general structures of thiomandelic acids (**20**), mercaptocarboxylic acids (**21**) and thioesters (**22**).

Captopril is a thiol-based ACE inhibitor. ACE contains a single zinc ion at its active site, and so captopril's activity in this enzyme was hypothesised to translate to MBLs. Captopril was shown to inhibit B1 MBLs by Heinz *et al.* in 2003, and since then has undergone significant further investigation, showing inhibition against the clinically relevant IMP-1 and NDM-1 MBL subtypes^{162–164}.

Brem *et al.* investigated the structural basis of MBL inhibition by all four captopril isomers (Fig. 31). This work showed all four isomers to be inhibitors of clinically relevant B1 MBLs. D-Captopril (**25**) showed the greatest inhibition of BcII, IMP-1, VIM-2, SPM-1 and NDM-1, giving insight into the optimum binding mode for B1 MBL inhibitors. All captopril isomers inhibited their B1 MBL targets through the binding of the thiol moiety between the zinc ions in the active sites, therefore displacing the bound hydroxide ion and causing inhibition of the enzyme⁷¹.

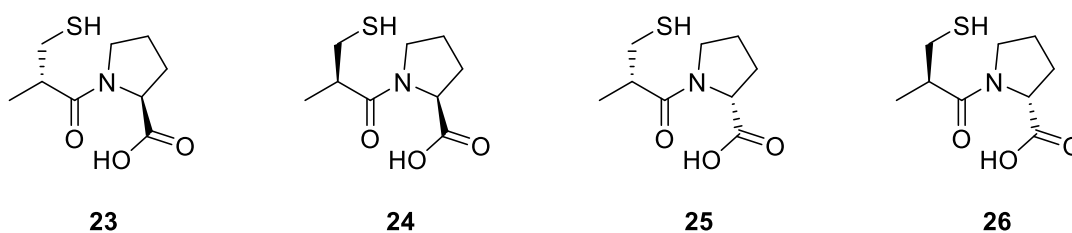


Figure 31. The four captopril isomers. From left to right: L-captopril, epi-L-captopril, D-captopril, epi-D-captopril.

Cain *et al.* went on to use an *in silico* fragment-based approach to design and produce specific MBL inhibitors. Through the use of the SPROUT molecular design program, whereby fragments are docked into targeted regions in the crystal structure and linked together to create potential ligands, a series of thiol-based compounds were designed to be B1 MBL inhibitors^{165,166}. The first of these compounds was designed to place the thiol moiety between the active site zinc atoms, displacing the catalytically essential hydroxide ion, with additional interactions forming between a carboxylate moiety with a Lys211 and the Zn2 ion. Additionally, an aryl ring was included to form edge to face aryl interactions with Trp93¹⁵⁰.

Crystallographic investigation of the inhibitor was carried out using the crystal structure of VIM-2. Whilst the sulphur-zinc bond in the active site was as predicted, there were some marked differences from the docking model predictions. One of these was interaction of a carboxylic acid unit within the inhibitor, with the Asp117 residue through a water molecule. This carboxyl had been predicted to interact with Arg205 (equivalent to Lys211 in NDM-1). In fact, whilst the Arg205 residue is normally found near the active site, the crystallographic studies had revealed that this residue had relocated upon binding of the inhibitor to the enzyme. Additionally, face-to-face π -stacking interactions were found between the terminal phenyl group of the inhibitor and Tyr67 (Fig. 32).

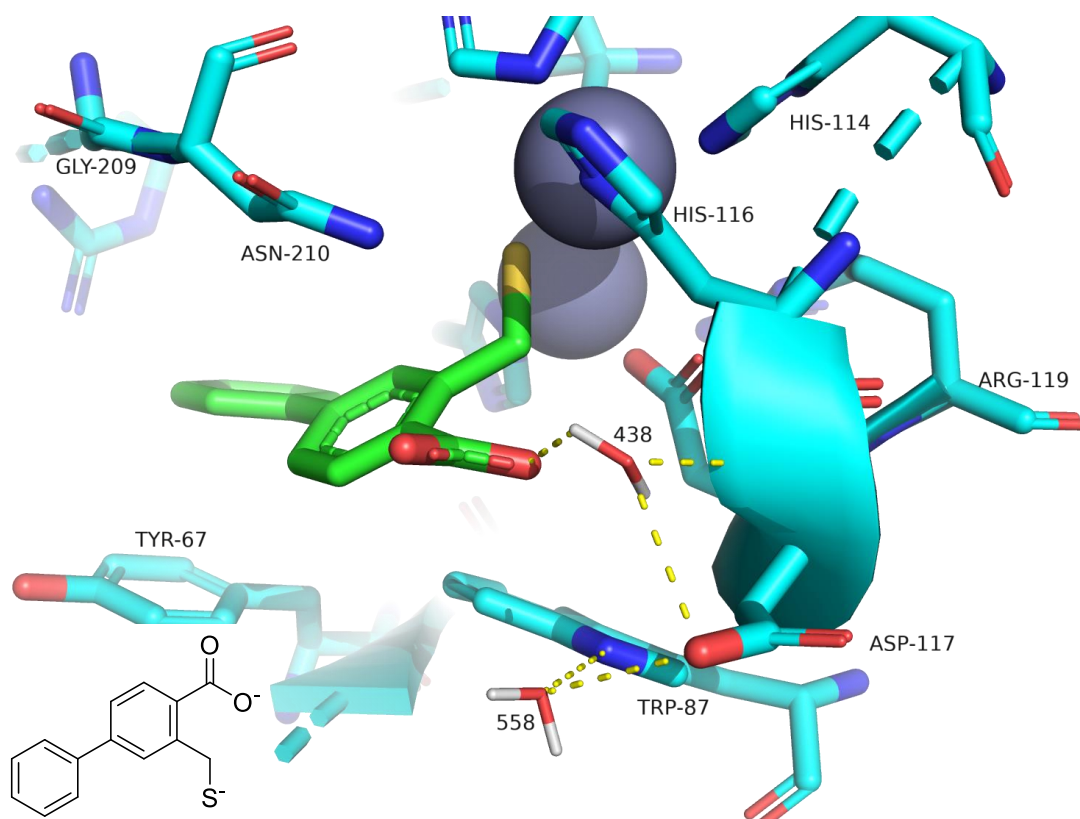


Figure 32. A crystal structure of a thiol-based inhibitor (the structure of which is shown in the bottom left corner) in VIM-2 (PDB ID: 5K48). Interactions between the carboxyl group and Asp117 through a water molecule 438 can be seen. There are face to face π -stacking interactions between the phenyl group and Tyr67. Arg205 has moved to accommodate the inhibitor. (Note: due to resolution constraints of crystallography the water molecules orientation is not preserved and so the water molecules presented here are unaligned. This may not represent their true orientation).

These compounds showed sub-micromolar potency against NDM-1, VIM-2 and IMP-1 in enzymatic assays, comparable to captopril. Interestingly, replacing the aryl ring within the inhibitor with a bromine atom destroyed inhibition of NDM-1, yet it was retained in VIM-2 and IMP-1. This difference in binding of the inhibitor between the two enzymes may be explained due to the active site differences between NDM-1 and VIM-2 or the removal of water molecules from the NDM-1 crystal structure to simplify docking calculations.

To further investigate the clinical potential of these compounds to re-establish antibiotic susceptibility within resistant bacteria, *in vitro* testing was carried out, involving co-dosing the inhibitor alongside meropenem in NDM-1 producing *K. pneumoniae* and *E. coli* respectively. These assays revealed these MBL inhibitors increase activity of the meropenem against these bacteria, lowering the MIC from >128 $\mu\text{g/ml}$ to a minimum of 8 $\mu\text{g/ml}$ and 16 $\mu\text{g/ml}$, respectively.

In light of these promising results it was proposed in the present project that further development of these compounds could extend their activity. In particular, it was reasoned that incorporation of additional moieties within these thiol-based inhibitors that could make additional contacts to amino acid residues within the enzyme, such as Tyr67 and Arg205 in VIM-2, could lead to increased efficacy of these MBL inhibitors (*Fig. 33*).

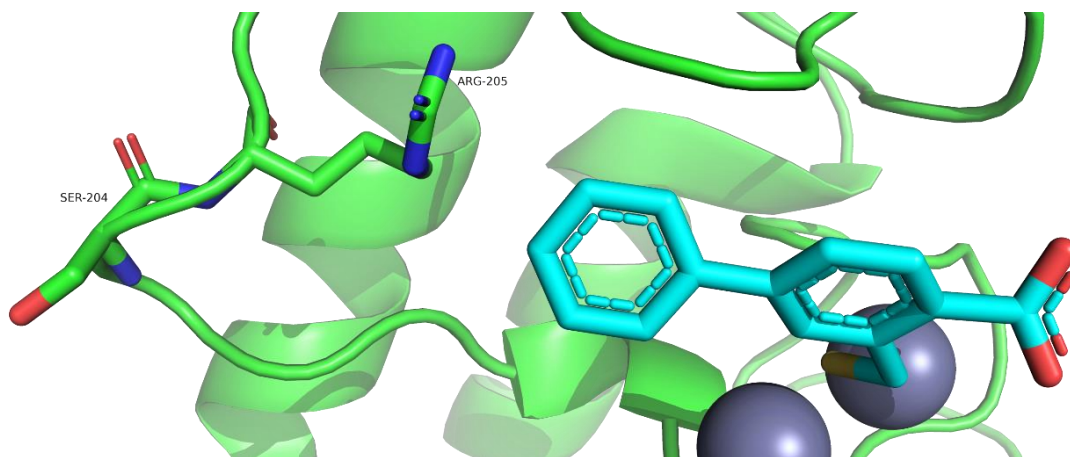


Figure 33. Residues in the binding pocket of VIM-2 (PDB ID: 5K48) such as Arg205 were targeted when designing further inhibitors of the thiol-based series.

The structures of the proposed designed inhibitors was also influenced by the use of eNTRY rules for Gram-negative penetration and accumulation proposed by Richter *et al.*¹⁶⁷ These rules state that to improve the likelihood of accumulation in Gram-negative bacteria compounds should be designed to contain a non-sterically encumbered ionisable nitrogen (primary amines being best), have low three-dimensionality (globularity less than or equal to 0.25) and be relatively rigid (number of rotatable bonds less than or equal to 5). These rules were all considered when designing new thiol-based inhibitors.

2.2.2 Computational docking of thiol-based MBL inhibitors

2.2.2.1 Optimisation of thiol-based MBL inhibitor binding utilising computational methods

Advances in computational models, based on real-world empirical evidence, have led to the development of sophisticated pieces of software intended to complement traditional drug design efforts¹⁶⁸. These programs are able to in-part replicate the energies and interactions present in protein-substrate

binding, therefore allowing one to predict how well compounds may bind to a given site.

X-ray crystal structures of proteins are the most common starting point for computational ligand design. For a crystal structure to be useful for computational docking of putative ligands, it must fulfil certain requirements: a suitable resolution (typically 2.5 Å or better); a good correlation between the model and experimental data which (known as R factor, below 28% is acceptable); low coordinate error (typically measured as a function of R factors and lying at 0.2 – 0.3 Å); consistent temperature factors (those of atoms in the chosen region should be no higher than the average of that of the protein as a whole); and chemical “correctness” (bond lengths should be within 0.015 Å and bond angles should be within 3 ° of what is ideal)¹⁶⁹.

If a crystal structure of the target protein is not available, then a homology model can be built using close protein analogues, and this can be used to perform the docking operations. A homology model analyses structurally similar and phenologically related protein crystal structures and then generates the target crystal structure based on this data¹⁷⁰. Due to global web-based resources, such as the protein data bank (PDB) and SWISS-MODEL, many crystal structures are freely available and the tools needed for homology modelling are open for use.

2.2.2.2 Structure-based drug design

Structure-based drug design utilises available structural models of proteins for the design of effective inhibitors¹⁷¹. These are typically from X-ray crystal structures, but homology models are acceptable in cases where these are not available. Cryo-EM structures are also becoming more commonly used as the technique becomes more widespread; this technique is applicable to some proteins that are difficult to crystallise and therefore unsuitable for X-ray crystallography¹⁷². Molecular modelling software is used to generate the electronic and spatial properties of the receptor target, identifying sites of potential binding. This process uses properties such as electrostatics, hydrophobic effects, hydrogen bonding and key binding residues to map the three dimensional site of the protein. Once the protein structure has been computationally analysed, it can be used to dock computationally designed

compounds in order to try to predict if binding between the small molecule and protein is favourable. A scoring system based on force fields from empirical data is then used to estimate binding and the binding poses can then be viewed. Analysis of the given binding poses can be used for further elaboration of the compounds, to enable them to make further favourable contacts with the target sites and therefore to increase their binding affinities. Selected molecules can then be synthesised in the laboratory for biological testing¹⁷³.

Docking of molecules into the active or allosteric sites of proteins *via* computational modelling can involve the altering of numerous simulated electronic and steric parameters. It is useful if these parameters can be tuned to agree with crystallographic observations, such as the observed binding poses of ligands. Further to this, if possible (that is, if the biological data is available) it is useful to compare and assess the scoring of the computational modelling against enzymatic assays. The comparison of different modelling runs varying different parameters can then be performed, with the analysis of results revealing the most suitable parameters to give the likely most true-to-life output. These parameters can then be used when docking newly designed compounds.

2.2.2.3 Schrödinger Glide docking software

Schrödinger Glide¹⁷⁴ (to be referred to as Glide from hereon) is a docking program that uses a range of calculations to predict the binding potential of compounds into target protein sites (*Fig. 34*).

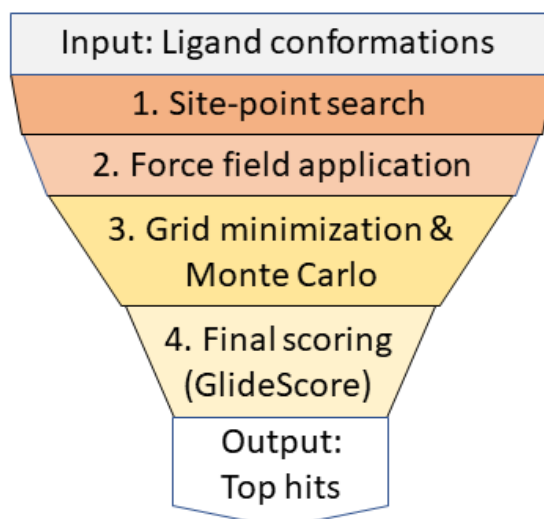


Figure 34. A diagram of the Glide docking “funnel” illustrating the process that docking within Glide operates by. Prepared (i.e. minimised) ligands are input into a preprocessed grid created from the protein target to begin the docking, which progresses as thus: 1. Site-point search, minima in the ligand torsion-angle space are exhaustively calculated over the entire phase space available to the ligand; 2. The ligands are minimised in the field of the receptor using an energy function (in our runs, this will be the OPLS3e force field¹⁷⁵); 3. The lowest energy poses are then subjected to a Monte Carlo procedure; 4. The poses are scored according to the GlideScore function. This results in an output of the highest scoring poses as the top hits.

First, the grid, the defined spatial coordinates of the protein that the docking will be performed within, is set within the site of the protein where the compounds are targeted towards (*i.e.* an active and/or allosteric site). A series of filters process the site *via* a set of forcefields, progressively creating a more accurate scoring of interactions (*e.g.* electronics, sterics, *etc.*) within the site. This is done at a preprocessing stage, so only needs to be done once for each receptor, therefore decreasing computational load.

Second, the designed ligands are prepared *via* ligand preparation (referred to as “LigPrep”). This produces a set of conformations from analysing minima in the ligand torsion-angle space. This method does use approximations and truncations to aid computational speed. By pre-preparing the ligands the region of phase space, the space in which all possible states of a system are represented, over which energy and gradient evaluations occurs in docking is dramatically decreased, further reducing computational load whilst retaining accuracy.

The ligands are then minimised in the field of the receptor using a molecular mechanics energy function and a distance-dependent dielectric model. Once this is completed the lowest energy poses undergo Monte Carlo simulations to examine nearby torsional minima, correcting the poses and angles.

The scoring function of the poses within the receptor site is then used to estimate binding energies to give a GlideScore. This is a modification of an empirically based function (ChemScore¹⁷⁶) that takes into account lipophilic ligand-atom/receptor-atom pairs, hydrogen bonding interactions, metal-ion interactions, Coulomb and Van der Waal interaction energies, and solvent effects¹⁷⁷.

Glide gives two options for scoring, SP (standard precision) and XP (extra precision). Both of these give results in units of kcal/mol. SP glide is a “softer” function that is computationally less intense and is appropriate for the screening of databases, with the aim of removing false negatives from the dataset. XP glide is a “harder” function which aims at minimising false positives by exacting large penalties upon features that violate established physical chemistry principles. This is a more computationally intense method so is more suited for limited numbers of ligands¹⁷⁸.

One major restriction with Glide docking is that it treats the receptor as a rigid structure, whereas in reality proteins are flexible and have many degrees of freedom. Glide SP and XP functions do in part account for this flexibility *via* scaling of the Van der Waal radii of non-polar protein and/or ligand atoms, but this is often insufficient to account for the dynamic nature of protein conformational changes. To better account for this, induced-fit docking (IFD) can be performed. Within the Schrödinger Maestro suite, this is done *via* Glide combined with protein structure prediction (Prime) techniques. The iterative coupling of these two techniques account for flexibility in both the ligand and the receptor, albeit at greatly increased computational load. This works *via* a first round of docking the ligands into a rigid receptor with a softened energy function, followed by a minimisation of the ligand/protein complex. Ligand docking is then repeated within the refined protein structures with a harder energy function and finally a scoring function ranks the complexes, accounting for receptor-ligand interaction energy, strain and solvation energies. IFD is

generally unsuitable for large numbers of compounds due to the computational cost involved, but is sometimes necessary for more accurate scoring, especially when the only crystal structures available feature structurally different ligands from those that are to be docked¹⁷⁹.

It should be noted that over the course of this project, the OPLS4 force-field was introduced to Maestro. This improved force-field is of particular relevance to this work as it improves the accuracy of sulphur interactions¹⁸⁰. The work presented here used the older OPLS3e force-field; it will be made clear in later sections when the OPLS4 force-field has been used.

2.2.2.4 Glide docking of previously assayed MBL inhibitors in VIM-2

Glide was used to dock a series of previously reported thiol-based inhibitors (*Table 1*)¹⁵⁰. Docking in VIM-2 (PDB ID: 5K48) was carried out using these compounds as a training set and GlideScore was compared to IC₅₀ results.

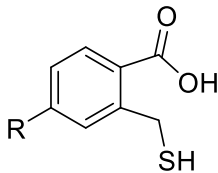
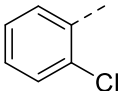
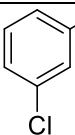
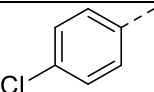
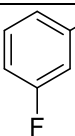
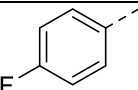
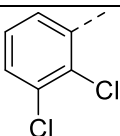
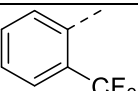
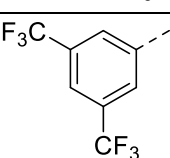
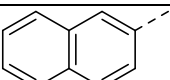
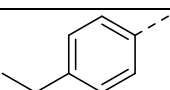
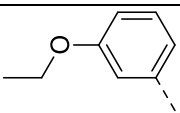
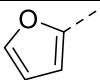
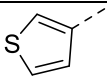
Compound number	Compound R-group structure	IC ₅₀ VIM-2 (μM)	Error (μM)
			
27		0.23	0.04
28		0.18	0.09
29		0.07	0.05
30		0.10	0.03
31		0.20	0.06
32		0.23	0.03
33		0.04	0.03
34		0.15	0.08
35		0.45	0.07
36		0.07	0.03
37		0.10	0.03
38		0.18	0.16
39		0.36	0.02
40		0.17	0.12

Table 1. Previously synthesised MBL inhibitor molecules from the Fishwick group with associated IC₅₀ data, tested via the metallo-β-lactamase assay described on page 106¹⁵⁰.

The above compounds were constructed in Maestro and LigPrep was used to generate the most likely conformation of each, with Epik metal binding states applied. This gave thirty compounds; fifteen containing a thiol and fifteen with a deprotonated thiol (thiolate anion). The deprotonated versions were used for docking, as these likely represent the metal binding states at the sulphur moieties of the inhibitors.

Crystal structure 5K48¹⁵⁰ was prepared *via* Protein Preparation in Maestro. Receptor grids were generated with metal constraints created on both active site zinc atoms. Multiple grids were generated for 5K48 to investigate the effect of including waters thought to be involved in the binding of the ligand through investigation of the crystal structure. Docking was performed both for waters left positionally unchanged from their default orientation in the downloaded crystal structure (therefore computationally orientated) and when manually orientated according to what was thought to be a sensible orientation based on surrounding polar residues.

For protein VIM-2 (PDB ID: 5K48), fourteen docking runs were performed. All docking runs used XP scoring. In all cases when metal constraints were applied to the docking, it was specified that both metal constraints to bind to a deprotonated thiol moiety. IFD docking was not used as a good quality crystal structure using a related ligand (**27**) was available.

In order to investigate the possible correlation between observed and predicted binding affinities, the results of the docking runs were plotted against the pIC₅₀ values. The coefficient of determination (R^2) and Kendall's rank correlation coefficient (τ) were calculated¹⁸¹ (*Table 2*).

Run no.	Settings description	R ²	τ
Glide 1	No metal constraints applied, no binding waters included	0.549	-0.596
Glide 2	Metal constraints applied, no binding waters included	0.527	-0.573
Glide 3	No metal constraints applied, waters 438 and 558 included	0.546	-0.528
Glide 4	No metal constraints applied, water 438 included	0.607	-0.618
Glide 5	No metal constraints applied, water 558 included	0.478	-0.551
Glide 6	Metal constraints applied, waters 438 and 558 included	0.537	-0.573
Glide 7	Metal constraints applied, water 438 included	0.533	-0.596
Glide 8	Metal constraints applied, water 558 included	0.639	-0.641
Glide 9	No metal constraints applied, waters 438 and 558 included and manually orientated	0.145	-0.348
Glide 10	No metal constraints applied, water 438 included and manually orientated	0.512	-0.483
Glide 11	No metal constraints applied, water 558 included and manually orientated	0.408	-0.461
Glide 12	Metal constraints applied, waters 438 and 558 included and manually orientated	0.495	-0.528
Glide 13	Metal constraints applied, water 438 included and manually orientated	0.492	-0.551
Glide 14	Metal constraints applied, water 558 included and manually orientated	0.542	-0.551

Table 2. A summary of Glide runs using a training set docked using different settings. The R² and τ values are listed alongside.

It is difficult to draw any solid conclusions about the best settings to use here, as changes in the similarity of the docking results with the pIC₅₀ values do not appear to strongly follow any trends.

One surprising result is the poor R² and τ values for Glide 9, which are significantly poorer than is seen in other runs. This suggests that manually

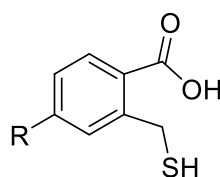
orientating the waters according to their estimated orientations with respect to nearby residues has created an unfavourable environment for the ligands. This is supported by the consistently lower values of both R^2 and τ of the results including the manually orientated waters versus those where the waters are included but not manually orientated.

Applying metal constraints does not show any telling trends, both with regards to the R^2 and τ values. Where it does consistently improve scores is using the runs with the manually orientated waters; this could be explained by the metal constraints improving the overall environment energies around the metal centre, countering the manually orientated waters.

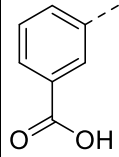
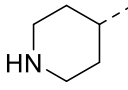
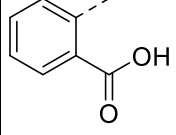
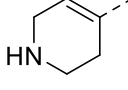
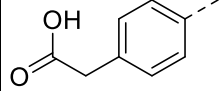
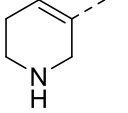
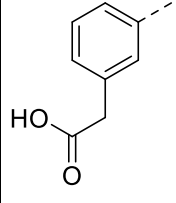
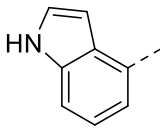
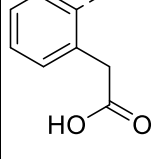
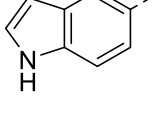
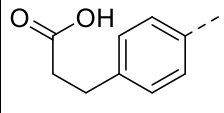
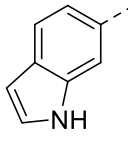
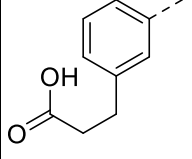
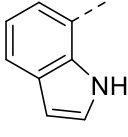
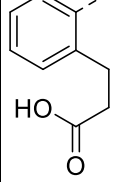
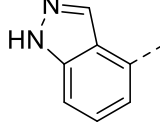
For both R^2 and τ , Glide 8 shows the values indicating the best fit of the computational data to the biological data. The Glide 8 R^2 value is 0.639, whilst the τ value is -0.641. These were the settings used for Glide docking runs of novel compounds.

2.2.2.5 Analysis of poses of novel ligands in Maestro Glide

Compound structure:



Compound no.	R-group structure	GlideS core (-)	Compound no.	R-group structure	GlideS core (-)
41		9.280	61		8.073
42		8.278	62		8.437
43		8.738	63		8.554
44		8.729	64		8.635
45		8.660	65		8.269
46		8.973	66		8.172
47		9.937	67		8.291

48		8.241	68		7.924
49		9.478	69		7.652
50		10.126	70		8.051
51		10.492	71		8.980
52		8.392	72		8.878
53		9.781	73		8.702
54		10.754	74		8.887
55		8.434	75		8.571

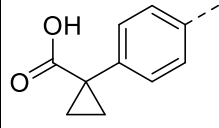
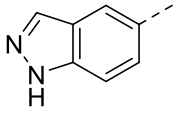
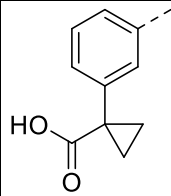
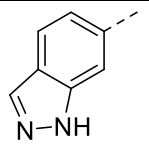
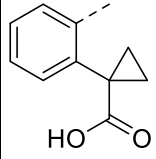
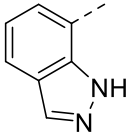
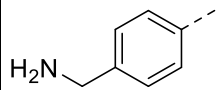
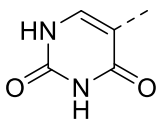
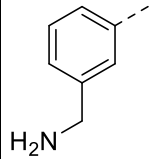
56		9.493	76		8.680
57		8.353	77		8.595
58		9.957	78		8.825
59		7.607	79		8.467
60		8.509			

Table 3. Designed thiol-based MBL inhibitor compounds docked with Maestro Glide.

A total of thirty nine compounds were designed and docked within Maestro Glide. They were constructed with various criteria in mind: incorporation of a terminal polar residue *via* incorporation of the 'R' group, interactions of the 'R' group with side-chain residues in or near the active site, availability of the desired 'R' group as a boronic acid, possibility of structure-activity-relationship investigation of the 'R' group, and satisfaction of the aforementioned eNTRY rules. These criteria were not always completely fulfilled, but were always used as a guide.

From the scores (*Table 3*), some general trends were observed. The highest scoring compounds generally have a terminal carboxylic acid group on the sidechain. Amongst the top scoring of these (-10.754, **54**), the carboxylate group is predicted to interact with the Arg205 residue and the aromatic ring of

the inhibitor is predicted to form π -stacking interactions with His240 in the protein active site (Fig. 35).

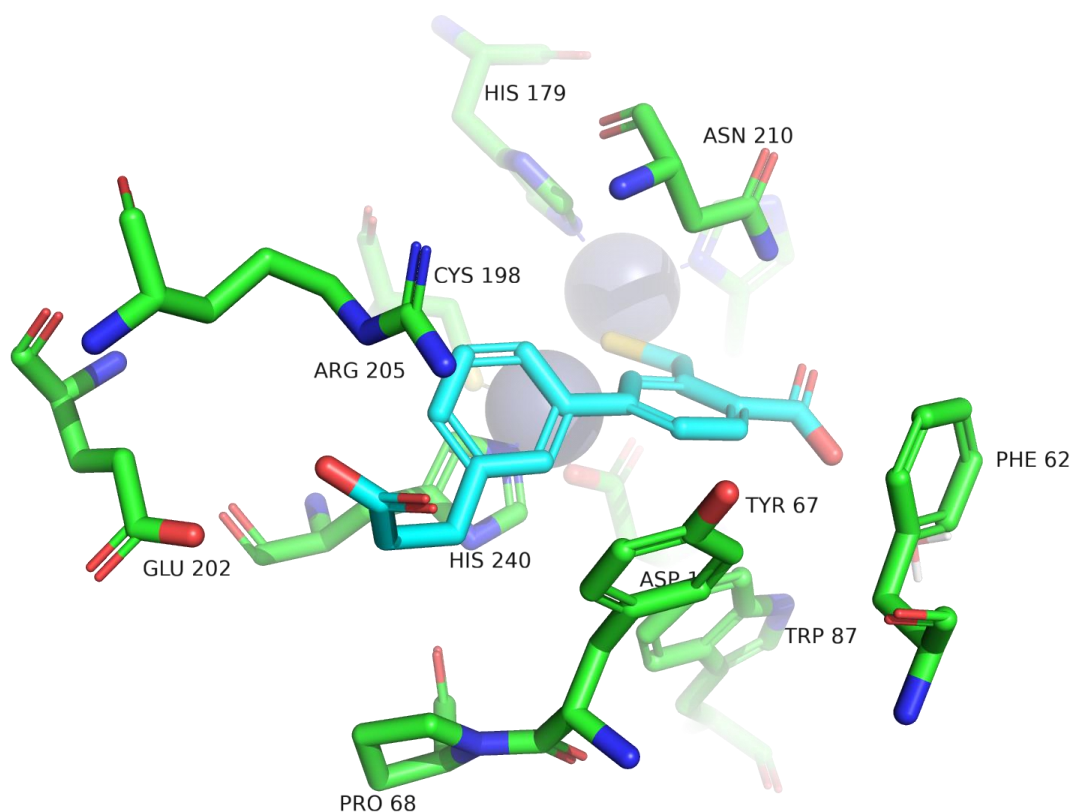


Figure 35. Docking of compound **54** with the 5K48 prepared grid in Maestro. The terminal carboxylic acid of the R-group interacts with the Arg205 residue, whilst the aromatic ring of the R-group forms π -stacking interactions with His240.

The next highest scoring that does not feature a carboxylic acid in the R-group is an alcohol (-9.280, **41**), which interacts with the Ser204 residue through the alcohol hydrogen, and with the Arg205 residue through the alcohol oxygen.

After this, the next highest scoring compound features an indole in its R-group (-8.980, **71**), which forms π -stacking interactions with His240; this is mirrored in the slightly lower scoring indole and imidazole containing compounds, which all score well.

The phenolic compounds also score highly, with the highest scoring (-8.973, **46**) interacting with the Asn210 backbone amide nitrogen; this behaviour is mirrored in the best scoring aniline containing compound (-8.635, **64**).

The best scoring benzylamine containing compound (-8.509, **60**) interacts with Glu202, but these are low scoring overall.

The uracil containing compound (-8.467, **79**) is predicted to interact with Arg205 and the Gly209 backbone amide nitrogen through its carbonyl atoms, and forms π -stacking interactions with His240.

All of the compounds containing a single nitrogen atom in the ring score badly; those that are aromatic form π -stacking interactions with His240, whilst the non-aromatics form interactions with Arg205.

The lowest scoring compound (-7.607, **59**), featuring a *para*-benzylamine, forms interactions with Tyr67, but apart from this weak interaction with a distant residue no other favourable interactions could be seen.

2.2.2.6 GOLD docking of previously assayed MBL inhibitors in VIM-2

GOLD (Genetic Optimisation for Ligand Docking) is a docking software distributed by CCDC (The Cambridge Crystallographic Data Centre). Whilst most docking software treats the protein structure as rigid by default when calculating binding energies, GOLD differs by allowing partial flexibility of the protein structure in its algorithm^{182,183}.

GOLD works *via* a genetic algorithm that is inspired by the process of evolution. It does this through manipulation of data-structures termed chromosomes each encode a possible ligand-receptor interaction (a solution) to the docking problem and are assigned a merit-based fitness score, which is dependent upon the combination of the number and strength of hydrogen bonds and the van der Waals energy of the bound complex. Firstly, a randomly generated population of chromosomes is created and the genetic algorithm repeatedly applies two operators, crossover and mutation. Crossover combines chromosomes, whilst mutation modifies them *via* random perturbations. This outputs modified chromosomes which replace the inputs if they are of greater fitness. After repeated rounds of this process, the final output should move towards that which is optimum and thus show the most likely binding modes of the ligand within the receptor¹⁸⁴. This process allows for partial ligand flexibility around the ligand cavity by applying the genetic algorithm to these residues as well as the ligand itself¹⁸².

The GoldScore that is given as the final output of ligand docking is based upon a number of factors, such as: H-bonding energy, van der Waals energy, metal interaction and ligand torsion strain. It differs from ChemScore mainly by not

incorporating a term, dG , representing the total free energy change that occurs on ligand binding¹⁸⁵.

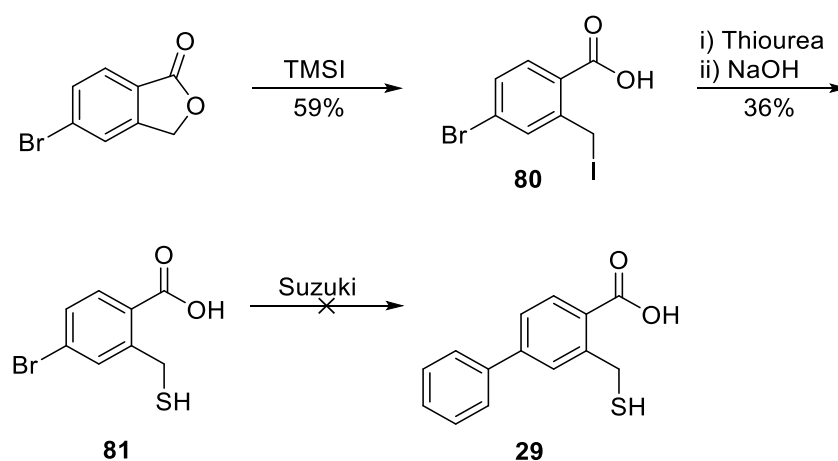
One run was performed within GOLD using the 5K48 crystal structure and ligands **27** – **40**. All protein preparation was done within the GOLD Wizard within the Hermes GUI, using settings that best mirrored what was used in Run 1 in the Maestro docking runs. The prepared ligands were imported from Maestro.

The results were plotted against the pIC_{50} values of the compounds, as for the Glide runs. R^2 was 0.155 and τ was 0.348. Given the poor performance of docking in GOLD compared to Glide (comparing runs with equivalent settings, those being no metal constraints and no waters included), it was decided not to continue with docking in GOLD.

2.2.3 Synthesis of thiol-based MBL inhibitors

Having used a simple docking approach to investigate the potential of substituted analogues of the previously reported thiol-based inhibitors to show enhanced binding to MBLs, it was decided to prepare examples of these molecules in order to investigate the predictions from the modelling studies.

The synthesis of this series of thiol-based inhibitors began by remaking the simplest of thiol-based inhibitors previously synthesised by the Fishwick group, 3-(sulfanylmethyl)-[1,1'-biphenyl]-4-carboxylic acid (**82**)¹⁵² (Scheme 4). This was done to establish the viability of late-stage functionalisation in the route through modifying the order of the steps.



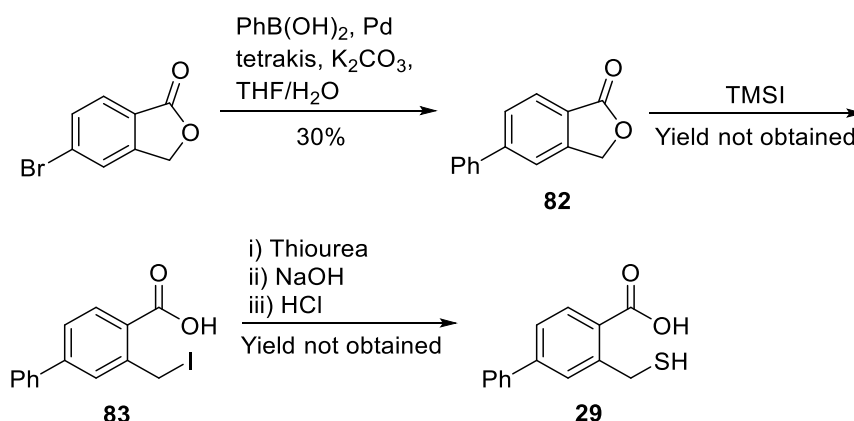
Scheme 4. The first synthesised analogue of the thiol series, based upon the approach described by Cain¹⁵².

The first step consisted of ring opening of 3-bromophthalide with iodotrimethylsilane. Upon completion the reaction was quenched with water and the precipitate collected *via* vacuum filtration. This crude product **80** was used in the next step without further purification, due to its instability.

Next, the thiol moiety was installed. Thiourea was dissolved in THF and stirred under reflux. Once the thiourea had completely dissolved, the compound **80** was added and the resulting solution was stirred at reflux overnight. Following this, the solvent was removed *in vacuo* and the solid residue was re-dissolved in aqueous 50% sodium hydroxide solution. This was then stirred at reflux for 2 hrs. After being allowed to cool this was acidified to cause the product **81** to precipitate out, which was collected and dried. A yield of 36% was achieved during this step.

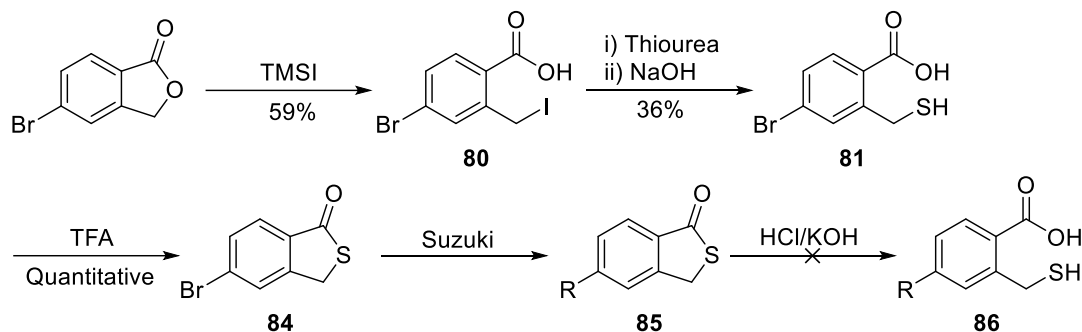
The next attempted step was a Suzuki reaction to install the phenyl group. Whilst sulphur is known to poison palladium catalysts in these types of reactions¹⁸⁶, it was thought that it might be possible to prepare a small amount of product before complete deactivation of the catalyst. As this was the final step of the synthesis this would be acceptable, as it would easily enable late stage derivatisation and only a small amount of the product would be needed for assays. Unfortunately this hypothesis proved invalid and no product was obtained from these efforts.

To confirm that the issue was due to catalyst poisoning *via* coordination of the thiol moiety, and not due to any other factors such as reagent quality, 3-(sulfanylmethyl)-[1,1'-biphenyl]-4-carboxylic acid (**27**) was synthesised as described by Cain¹⁵² (*Scheme 5*). This proceeded without issue and the desired final product was obtained.



Scheme 5. The synthesis of 3-(sulfanylmethyl)-[1,1'-biphenyl]-4-carboxylic acid, as described by Cain.

As the original route could not be completed due to the unsuccessful Suzuki reaction step, the desire for a late-stage diversification point was pursued from using an alternative approach. Since the Suzuki reaction was successful using 2-bromophthalide, it was posited that formation of the corresponding thiolactone (**84**) would enable the Suzuki reaction with the desired aryl substituent (**85**) and then a simple ring opening *via* hydrolysis would yield the final product (**86**) (Scheme 6).



Scheme 6. The planned synthetic route, utilising a late-stage diversification strategy.

The synthesis of **84** from **81** was simple and gave quantitative yields. The reactant was stirred in neat trifluoroacetic acid at 75 °C and the excess solvent was removed *in vacuo*. The product required no further purification.

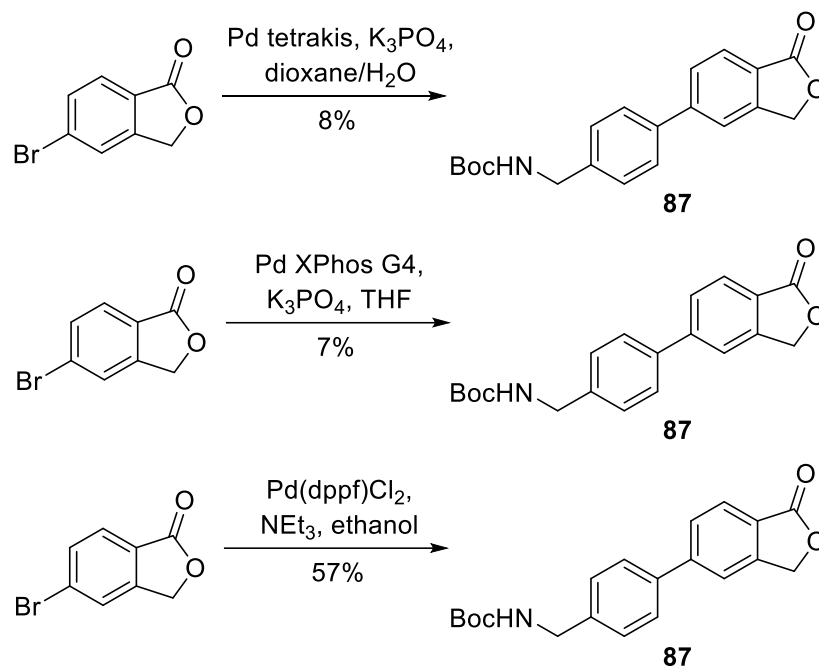
The reopening of the thiolactone ring in compound **84** was then attempted. Thus, compound **84** was stirred in aqueous hydrochloric acid solution at 100 °C overnight. Once cooled the reaction mixture was washed with ethyl acetate, removing the starting material. Extraneous effort was then put into removing all solvent from the product, *via in vacuo* methods and vacuum desiccation. Once these steps had been taken the solid that remained was

examined *via* bromocresol stain, which gave a positive response for the presence of an acid. On the basis of this stain and previous TLC during the reaction and work-up it was believed the ring opening was successful.

Alongside this work, Suzuki reactions were being done with the 5-bromophthalide substrate, for the dual purposes of honing reaction conditions for Suzuki reactions with **84** and to aid in developing a redundant synthetic route that could be used as a contingency plan if the current route was not successful.

The focus of these Suzuki reactions was to install an aryl group with a terminal amine moiety. This was chosen due to it fulfilling two criteria: side-chain interactions of the terminal amine moiety with Tyr67, and satisfying eNTRy rules. The final compound that would be produced through this synthetic route did in fact have the lowest docking score amongst the docked designed compounds, but it was decided that the data gained from it would be useful regardless of this (for both examining cellular accumulation and validation of the docking model). This led to 4-*N*-*boc*-aminomethylphenyl boronic acid being the first choice of reactant for the Suzuki reaction.

Initial Suzuki reaction attempts were successful, albeit low yielding. Using tetrakis(triphenylphosphine)palladium with potassium phosphate in dioxane and water led to only an 8% yield. The reaction was then attempted using palladium XPhos G4 catalyst in THF solvent, but this gave a similar yield of 7%. This Suzuki reaction using palladium XPhos G4 was also attempted in a microwave but no product formation was seen. Fortunately, conditions for a similar substrate were found in a patent¹⁸⁷. This reaction used bis(triphenylphosphine)palladium dichloride in ethanol with triethylamine used as the base. This was far more successful than previous attempts, achieving a yield of 57% (*Scheme 7*).



Scheme 7. Reaction conditions used to find effective Suzuki conditions for coupling aryl boronic acids featuring a terminal polar moiety and 5-bromophthalide.

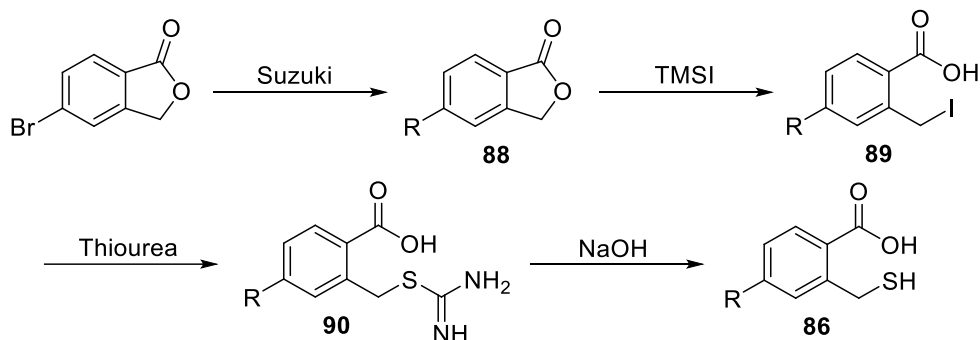
These conditions were also found to be favourable when using 4-aminomethylphenyl boronic acid. Whilst this Suzuki coupling was generally more successful in all runs, seeing a yield of 20% when using palladium XPhos G4, it was further improved by the newly found conditions to 47%.

Suzuki reactions were attempted using **84**. Initial attempts, which were carried out before finding the improved conditions, were completely unsuccessful with palladium tetrakis catalyst and either of the aforementioned coupling reagents. Much better success was found with the improved conditions, achieving a yield of 41% with 4-aminomethylphenyl boronic acid and 71% with 4-*N*-Boc-aminomethylphenyl boronic acid.

Following this, ring opening of the thiolactone **87** was attempted. Unfortunately despite the earlier success of a thiolactone ring opening reaction, these attempts were unsuccessful. Opening of the thiolactone ring was attempted multiple times, with aqueous hydrochloric acid solution, aqueous sodium hydroxide solution and under dry conditions using lithium hydroxide as a base, but only starting material and unidentifiable products were ever recovered.

Therefore an alternative synthetic route to the desired functionalised thiol inhibitors was investigated. This route had been partially developed for

redundancy in case of previous attempts being unsuccessful (*Scheme 8*). Diversification using this route came at the first step, hence why this was less preferable *versus* other previously attempted routes that featured diversification at later stages, but this route was proven to work as it had shown in the synthesis of **29**.



Scheme 8. The alternate synthetic route, following that proven to work previously in Cain¹⁵².

35 and **39** had both been previously synthesised (*Fig. 36*). It was decided to proceed with the route using only the non-protected compound, as the Boc group would have been cleaved in the next step regardless (ring opening of the lactone with iodotrimethylsilane, which also removes Boc groups) and it was judged to be wise to not introduce another variable into the reaction.

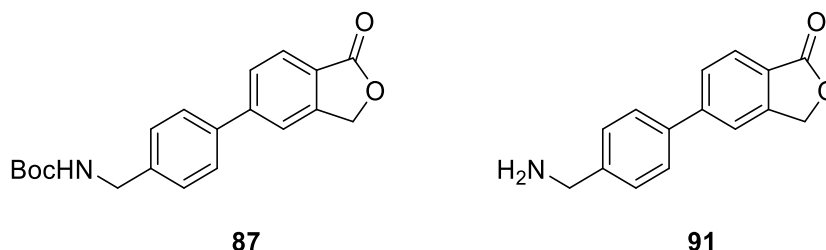


*Figure 36. Previously synthesised compounds featuring a terminal amine residue. Compound **39** was carried forward for further synthesis as the next step of the reaction would remove the Boc group of **35** anyway, and so a simpler approach was preferred.*

Unfortunately despite multiple attempts the ring opening of the lactone with iodotrimethylsilane was not successful. This ring opening normally occurs *via* silylation of the ester bond. The soft base that is the iodine ion then attacks the carbon adjacent to the non-carbonyl oxygen and the CO bond is cleaved. Upon aqueous work-up, the resulting silyl ether is then converted to the carboxylic acid (*Fig. 37*)¹⁸⁸. Unfortunately in the present attempts, the terminal amine moiety seemed to interrupt this process, but exactly how it did so is

unclear. It was first thought that the nucleophilic amine was becoming silylated, therefore causing the ester target to not be as labile to cleaving by the iodine atom. However the product of this was never seen *via* analytical methods. To investigate this further, 3 equivalents of iodotrimethylsilane were used in the reaction so if the suspected reaction was happening there would still be enough reagent to ensure the ring opening proceeded as intended, but unfortunately this was unsuccessful too.

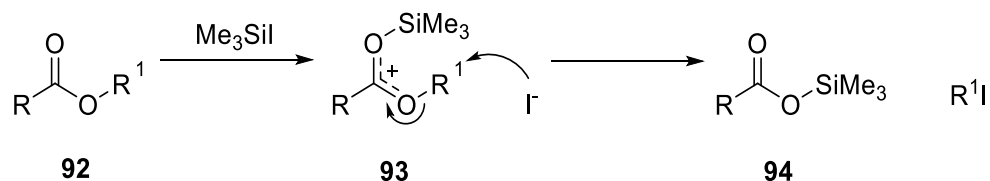
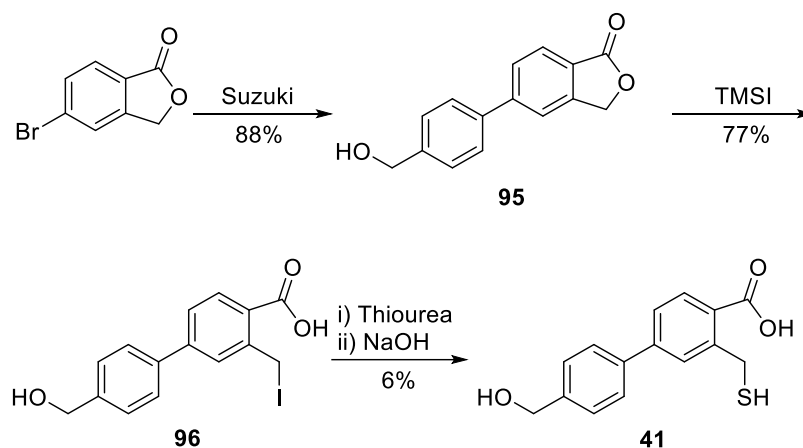


Figure 37. The mechanism of ester cleavage by iodotrimethylsilane.

Due to the continual difficulties with the synthesis of a thiol-based inhibitor featuring a terminal amine, another final product target was investigated. That containing a terminal *para*-hydroxymethyl group (**41**) scored far better than the amine in the docking runs, by virtue of interactions with Arg205. Unfortunately, this molecule did not satisfy all eNTRY rules that were aimed for, given that the target molecule did not contain an ionisable amine, but at this point it was seen as prudent to make this compromise (*Scheme 9*).



Scheme 9. The planned reaction scheme to create final compound **2.47**

The initial Suzuki reaction to attach the desired R group to 5-bromophthalide, producing **95**, was attempted with the optimised conditions described previously, and gave an excellent yield of 88%. This reaction was also

attempted using the thiolactone and was successful, albeit only giving the product in a yield of 13%, however this was not carried any further forward.

The lactone ring opening of **95** with iodotrimethylsilane was successful in this case, giving compound **96** in a respectable top yield of 77%.

This product was carried forward to the final step of the sequence, first an S_N2 with thiourea and then hydrolysis to give the desired final product **41**. This reaction was extremely poorly yielding, and it proved difficult to produce enough product for analysis, but eventually 15 mg of product, a yield of 6%, was obtained.

It is important to note that the analysis of **41** has not unequivocally confirmed its successful synthesis. Curiously, whilst the ¹H and ¹³C NMRs, including 2D spectra, were consistent with the desired compound structure, the HRMS analysis of this product disagreed with these data. The required negative ion mass is 273.0591 whilst the mass found is 271.0609. Without further investigation it has not been possible to reconcile this difference. Additionally the IR spectrum features all relevant peaks except that those of an SH group at 2540 – 2600 cm⁻¹, as this is generally a weak stretch and in this case is obscured by other stronger signals. It was intended to send a small amount of the compound for elemental analysis, but unfortunately due to the small amount produced after submission for assays there was not enough compound remaining to do this. Therefore whilst the data for this compound somewhat supports its successful synthesis, this must be met with a reasonable amount of uncertainty. It is also relevant that the compounds prior in the synthetic route do appear to have been successfully synthesised based on analytical evidence.

Following this, the synthesis of further terminal hydroxide bearing compounds was attempted, altering the position of the group on the biaryl ring from the *para* position to the *meta* and *ortho* positions (*Fig. 38*). In both cases the Suzuki reaction was successful and gave the desired products in acceptable yields. Unfortunately the iodotrimethylsilane step was not compatible with the *meta*-hydroxyl variant, and the thiol installation step was unsuccessful with the *para*-hydroxyl variant.

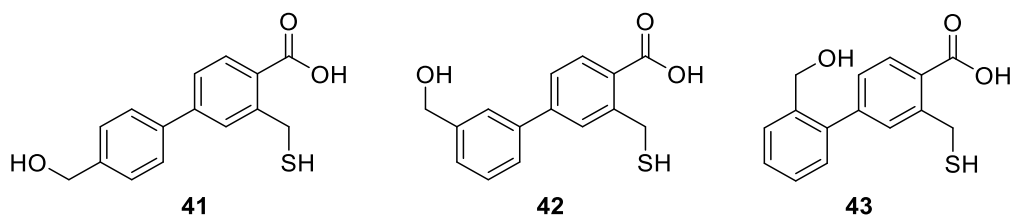
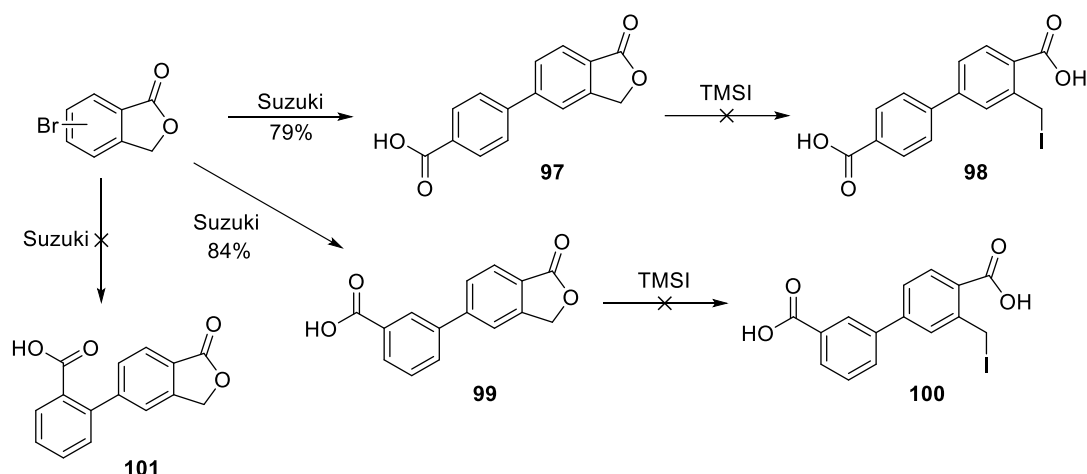


Figure 38. The successfully synthesised thiol-based inhibitor (left), and its two unsuccessful analogues.

The next attempted synthesis of thiol inhibitor-based analogues involved compounds with carboxylic acid units in the *ortho*, *meta* or *para* positions respectively of the aryl ring, as these were also high scoring compounds within the docking runs, with inexpensive boronic acids required for the synthesis (Scheme 10). The Suzuki reactions were successful for the *para* and *meta* versions, with admirable yields of 79% and 84% respectively, but not the *ortho* version.

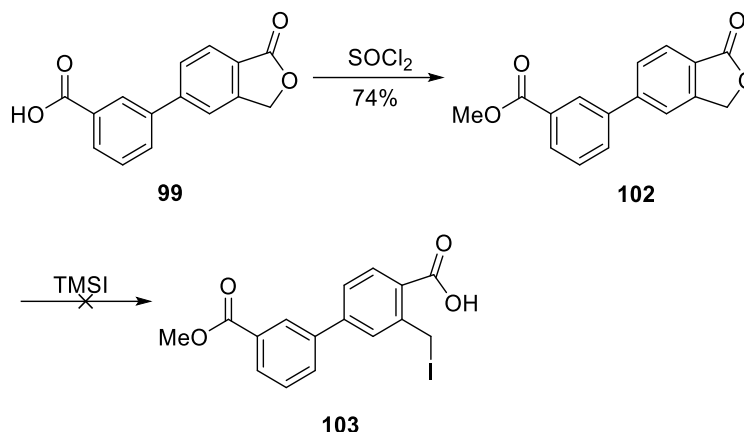


Scheme 10. Synthetic attempts at forming thiols with terminal carboxylic acids. The *ortho*-version was unable to be formed by Suzuki reaction. The *para*- and *meta*-version failed at the ring-opening reaction.

97 and **99** were taken forward to the iodotrimethylsilane ring opening step, but this was unsuccessful in both cases.

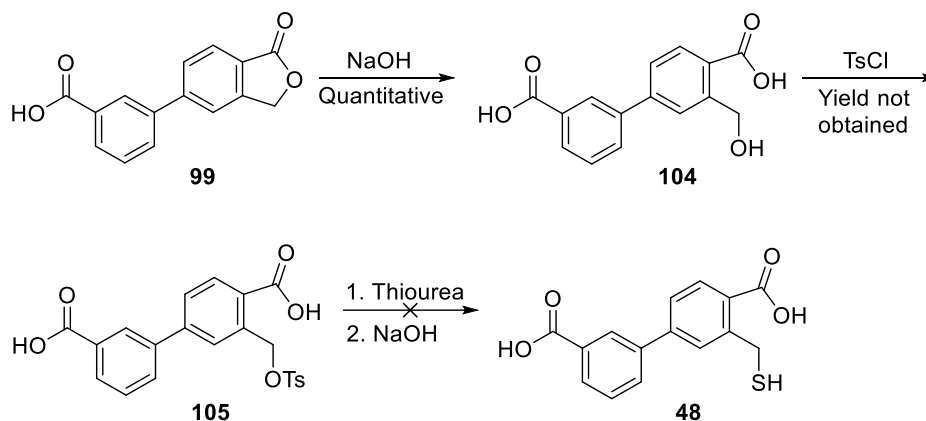
As the installed carboxylic acid moiety was the commonality here it was suspected that this was the cause of issues in synthesis and so **99** was then successfully methylated using thionyl chloride and methanol. Whilst that was introducing an ester that may be changed to the carboxylic acid by iodotrimethylsilane, it was decided that if only one equivalent of iodotrimethylsilane was used in the reaction then the lactone would more likely

be opened preferentially due to the strain of the 5-membered ring (*Scheme 11*). This hypothesis also proved invalid.



*Scheme 11. Protection of the terminal carboxylic acid on **99** and then subsequent ring-opening with TMSI was unsuccessful.*

With the repeated issues due to the ring opening a new method of accomplishing the synthesis was sought out. A basic hydrolysis of the ester followed by tosylation of the created alcohol and subsequent substitution with thiourea followed by hydrolysis was seen to be a reasonable route to attempt (*Scheme 12*).

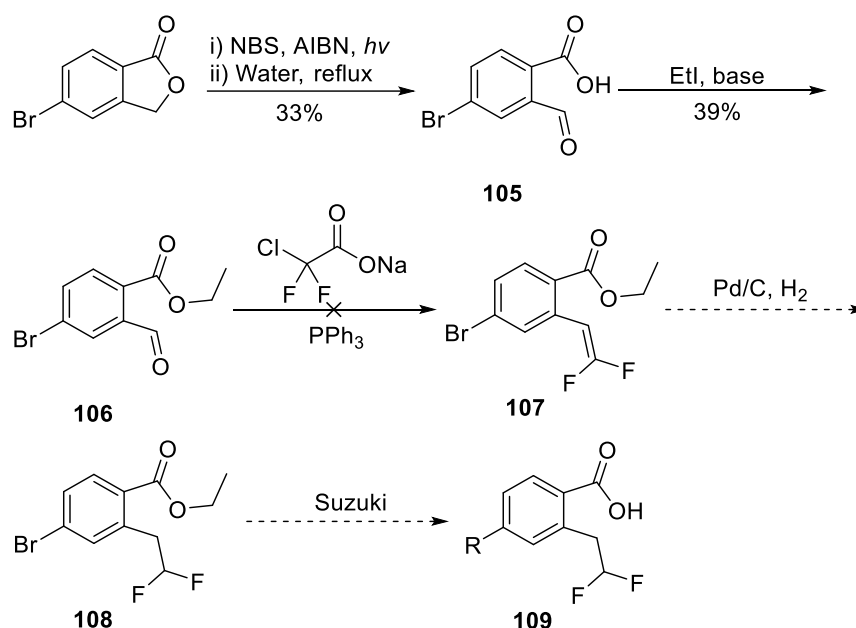


Scheme 12. Creation of the desired thiol final products via a different route, that of tosyl substitution, was also unsuccessful.

The hydrolysis of **99** to create **104** was successful, as was the following tosylation. However the final thiourea substitution and hydrolysis failed. This marked the end of the attempts to create this series.

The one final compound in the thiol series that was synthesised, 4'-(hydroxymethyl)-3-(sulfanylmethyl)-[1,1'-biphenyl]-4-carboxylic acid (**41**), was sent for testing in clinically relevant MBLs.

One other synthetic attempt of note was to install a bioisosteric analogue of thiol groups, a difluoromethyl group (*Scheme 13*). Here, it was reasoned that the proton of the difluoromethyl moiety would be removed at the active site of the enzyme, much as it is in thiols, and the group would bind in the same position, displacing the catalytically essential hydroxide.



Scheme 13. The planned synthesis of a bioisosteric difluoromethyl version of the thiol series.

The first step involved the ring opening of 5-bromophthalide *via* bromination of the ring, followed by hydrolysis to the aldehyde. This was successful, although the product was not completely purified, giving 4-bromo-2-formylbenzoic acid. This compound was subsequently esterified at the carboxylic acid moiety with iodoethane.

Following this, a procedure for installation of a difluoroalkene found in a patent was followed¹⁸⁹. This reaction is thought to occur in a Wittig-like fashion *via* the generation of a difluorocarbene group *in situ* from sodium chlorodifluoroacetate, releasing carbon dioxide and sodium chloride. This difluorocarbene then reacts with triphenylphosphine to form difluoromethylene phosphonium ylide. This very reactive ylide intermediate then attacks the aldehyde to give **107** as the product (*Fig. 39*)¹⁹⁰. However despite multiple

attempts this approach was unsuccessful. Whilst there were other ideas for installation of a difluoromethyl group they were not attempted, as it was decided it would be prudent to focus on other endeavours.

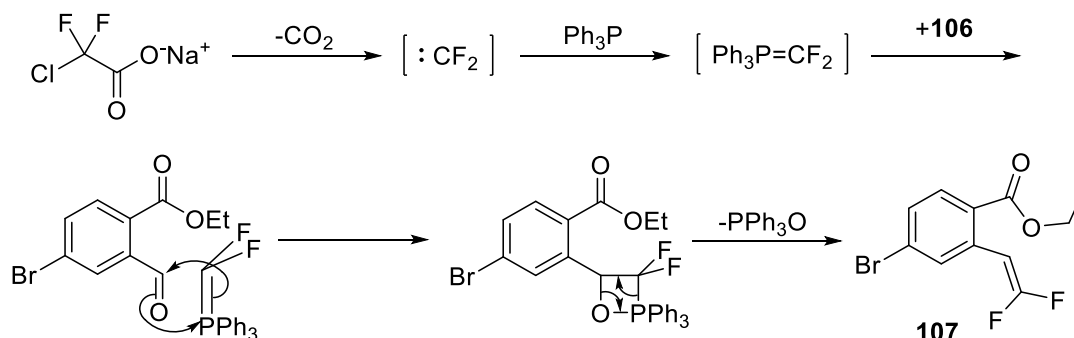


Figure 39. The mechanism of installation of a difluoro containing moiety.

However, two compounds featuring a similar moiety to a difluoromethyl, a difluoromethoxy group, were purchased and tested in the second round assay (Fig. 40).

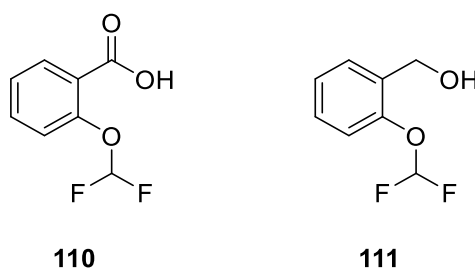


Figure 40. These two compounds were purchased and sent for testing in MBLs, to see whether the difluoromethoxy group would display inhibition.

2.3 Dithiocarboxylates

2.3.1 Introduction

Dithiocarboxylic acids have been known since 1866, when dithiobenzoic acid was discovered by Fleischer as a by-product found during the synthesis of thiophenol¹⁹¹. Despite its early discovery and its similarity to carboxylic acids, an important and widespread group in medicinal chemistry and life, dithiocarboxylic acids have been almost completely unexplored as a functional group in MBL inhibitors. This can be in part attributed to the often strong and unpleasant odour of sulphur containing compounds, as well as the instability and difficulty in handling of dithiocarboxylic acids¹⁹².

(It is important to note that “dithiocarboxylic acids” also refers to another class of compounds that have been tested against NDM-1, showing improved MICs in clinical *Enterobacteriaceae* isolates when co-dosed with Meropenem. These compounds in fact contain two thiol acids (C(O)SH), rather than a singular dithiocarboxylic acid group (C(S)SH)) (Fig. 41)¹⁹³.

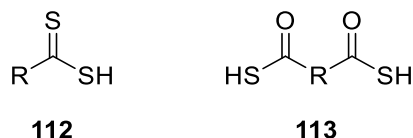


Figure 41. The dithiocarboxylic acid moiety (**112**) that this thesis refers to. Another class of compounds that have also been referred to as dithiocarboxylic acids is also shown (**113**).

To attempt to remedy stability issues, these dithiocarboxylic acids can be transformed into dithiocarboxylates, their salt or ester forms. As alkali metal salts the compounds show high stability in the solid states at room temperature¹⁹⁴. If left in their non-salt forms, there is a tendency for the compounds to form disulphides, thiol acids or oligomers¹⁹².

Interestingly, Grote *et al.* found that aryl dithiocarboxylic acids with substituents in the *ortho* and *para* positions around a phenyl ring were inherently more stable in their free forms and so were able to be isolated and analysed, whereas smaller dithiocarboxylic acids, including dithiobenzoic acid, were not.

Another problem that can occur when synthesising these compounds is the formation of a dianion when there is an α -hydrogen available. This can cause double deprotonation of the group, therefore resulting in another byproduct (Fig. 42)¹⁹². Thus, synthesis of aryl dithiocarboxylic acids can be less problematic as this cannot happen without an α -hydrogen present.

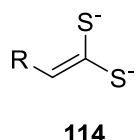


Figure 42. Double deprotonation of the dithiocarboxylate group can occur if there is an available α -hydrogen. This cannot occur in aryl dithiocarboxylic acids, so these have been seen to be more stable.

The pKa of these acids is much lower than that of their oxygen counterparts, for example, the pKa of the simplest aryl dithiocarboxylic acid, dithiobenzoic

acid, is 1.92¹⁹⁵. This can be attributed to the addition shell of electrons that sulphur possesses in comparison to oxygen.

It has been noted before that these compounds may be useful in therapeutics, as they have shown antifungal activity that can perhaps be attributed to their chelating properties¹⁹⁶. The chelating activity of these compounds with Zn^{II} has been shown in other inorganic studies¹⁹⁷.

For the present investigations involving the establishment of a 'toolbox' of Zn-coordinating moieties that could be used to create inhibitors of MBLs, it was therefore attractive to explore the potential of dithiocarboxylate-based MBL inhibitors. Lending further support to this proposal is the recent report of dithiocarbamate containing inhibitors against MBLs. Thus, Zhang *et al.* showed sodium 1,4,7-triazonane-1,4,7-tris(carboxylodithioate) (**115**, Fig. 43) restored meropenem activity against NDM-1 in *in vitro* assays. Furthermore, these compounds were tested in resistance gene *bla*_{NDM-1} carrying *Escherichia coli*, *Citrobacter freundii*, *Proteus mirabilis* and *Klebsiella pneumonia* and showed restoration of meropenem activity, with low toxicity against mammalian cells¹⁹⁸. Zhang *et al.* later extended this work to show the activity of non-cyclic compounds featuring the dithiocarbamate moiety and also showed this activity in bacteria containing *bla*_{IMP-4} genes¹⁹⁹. Dithiocarbamate activity has been further extended and shown in multiple MBLs by Ge *et al.*²⁰⁰

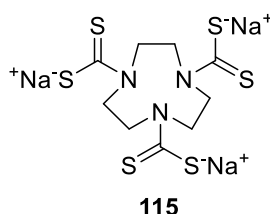
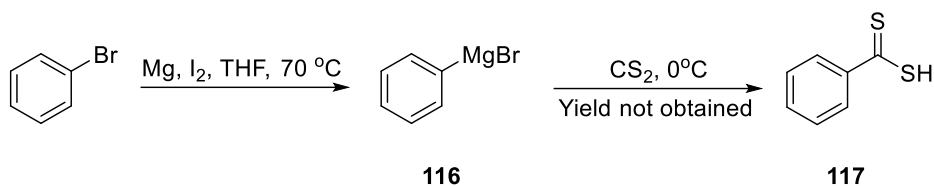


Figure 43. The structure of sodium 1,4,7-triazonane-1,4,7-tris(carboxylodithioate).

2.3.2 Synthesis of dithiocarboxylate-based MBL inhibitors

In order to establish the best approach for synthesising dithiocarboxylates it was decided to prepare the simplest aryl dithiocarboxylate, dithiobenzoic acid (Scheme 14). The synthetic steps were based upon those described by Kumar *et al.*; it is notable however that these reports referred to only the generation

of the dithiocarboxylate group *in situ*, which was then used immediately without isolation²⁰¹.



Scheme 14. The synthetic route towards dithiobenzoic acid, the simplest aryl dithiocarboxylate and the first target product of this series.

Problems were encountered with producing compound **117**, notably that it broke down upon purification *via* normal-phase or reverse-phase flash column chromatography. Thus, it was decided to attempt to isolate the product *via* acid-base work ups. This seemed successful at first, but **117** was inherently unstable and so was unable to be isolated before breaking down.

It was thought that perhaps salting the dithiocarboxylate moiety may lend it additional stability. The next attempt followed the same synthetic steps as had previously been attempted, but then once the dithiocarboxylate **117** was generated it was purified *via* work-up and immediately put into a suspension of sodium hydride in dry toluene at 0 °C and stirred for 3 hours, being allowed to reach room temperature. This reaction was successful and aided purification, as the salt precipitated out of the toluene and the compound could then be collected *via* vacuum filtration as an orange salt. Less than one equivalent of sodium hydride was used in the reaction to ensure that there was none remaining in the product. This reaction achieved an acceptable yield of 24%.

The product was confirmed using ¹H & ¹³C NMR, and by negative HRMS. The ¹³C NMR featured an interesting and useful analytical feature of the dithiocarboxylate salt. Initially the carbon signal of the dithiocarboxylate group could not be seen. Other analysis indicated that the product was correct, and so a wide-field NMR was requested to extend the visible range of the spectrum. This showed a signal at 257.1 ppm. 2D HMBC NMR proved this to belong to the dithiocarboxylate salt carbon, and this was established as a valuable diagnostic peak for these compounds (*Fig. 44*).

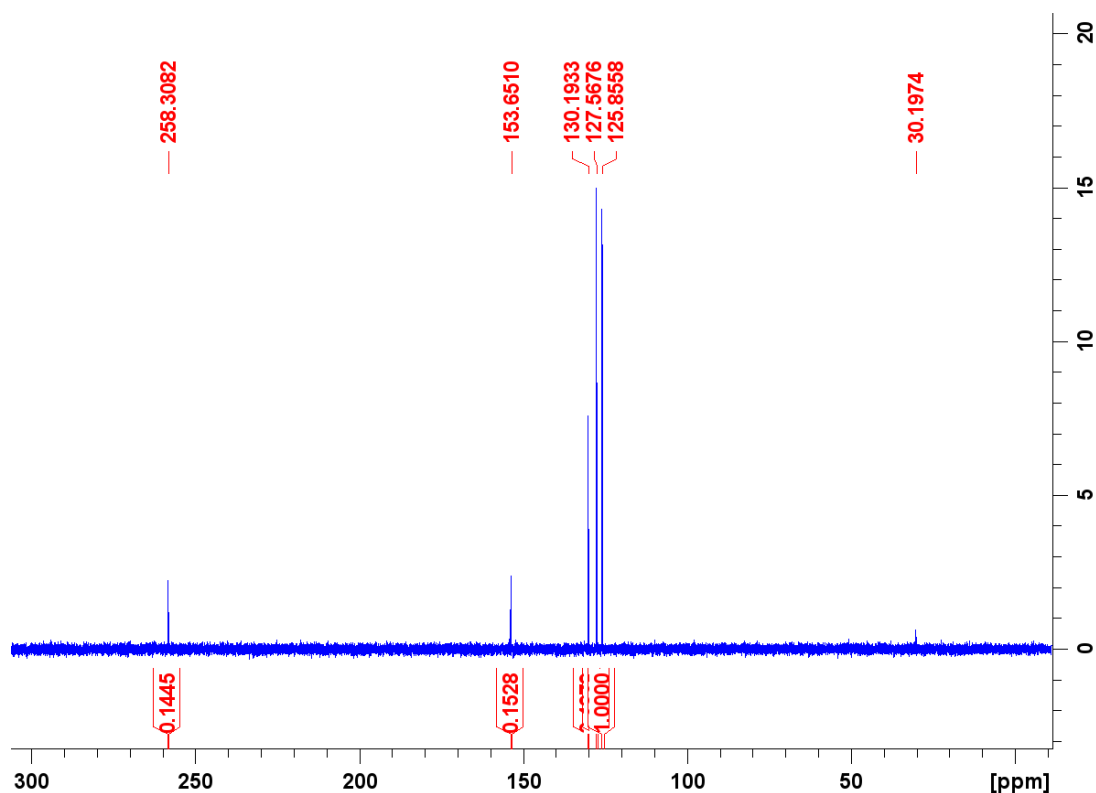
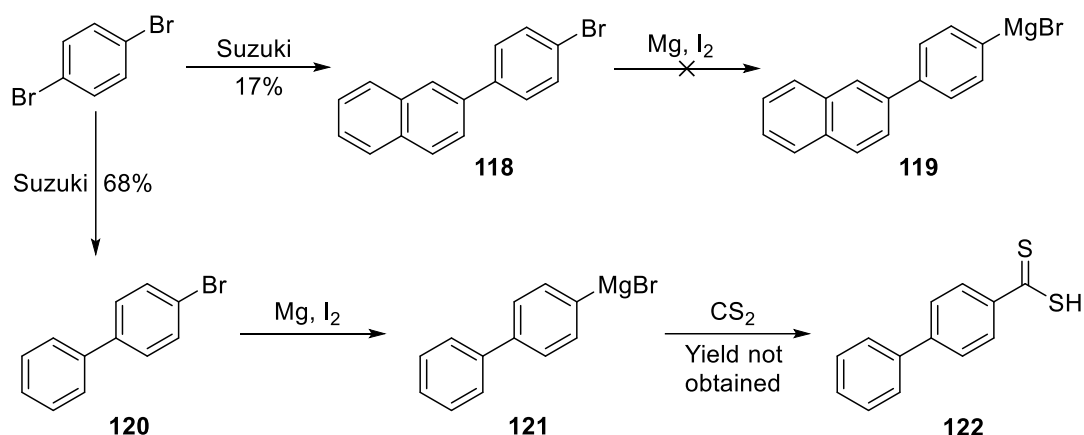


Figure 44. A ^{13}C NMR for dithiobenzoic acid, displaying the characteristic dithiocarbonyl carbon peak at 258 ppm.

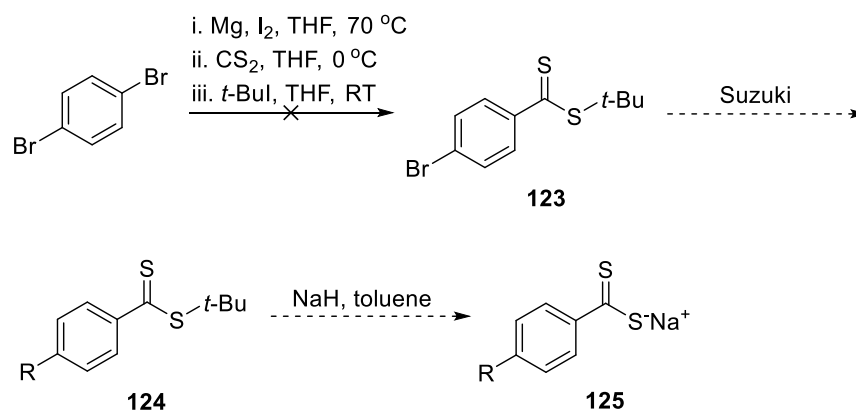
Encouraged by these results, more substrates were planned to be synthesised, to then be converted to Grignard reagents and then dithiocarboxylate salts. As these compounds had not been tested in MBLs before, docking was not carried out to decide what to make. Any data would be useful data, which could hopefully later be used for validation of any docking score trends. Thus, the group chemicals were searched for suitable substrates with which to transform into dithiocarboxylates.

Compounds **121** and **118** were successfully synthesised *via* Suzuki reactions of 1,4-dibromobenzene with either phenylboronic acid or 2-naphthylboronic acid, giving a 68% yield and 17% yield respectively. However, neither of these compounds were successfully converted to their dithiocarboxylate salts. For 4-bromobiphenyl this was due to the rapid degradation of the dithiocarboxylate group. For 2-(4-bromophenyl)naphthalene the Grignard generation appeared to be unsuccessful (*Scheme 15*).



Scheme 15. Attempted syntheses of two novel dithiocarboxylic acids. Grignard **119** failed to form. Dithiocarboxylate **122** rapidly degraded.

As an alternative route, *tert*-butyl protection of the dithiocarboxylate moiety was attempted, which could then be reacted on and subsequently deprotected and salted to create final products (Scheme 16). This was first attempted with sodium benzenecarbothioylsulfanide, *tert*-butyl iodide and *tert*-butanol but was unsuccessful, as the dithiocarboxylate group appeared to have broken down during the reaction. This was determined by the lack of a thiocarbonyl carbon signal *via* ^{13}C NMR.



Scheme 16. Planned synthetic route for installation of the dithiocarboxylate moiety, protection, diversification and salting to attain final products.

The next attempt at creating a protected dithiobenzoic carboxylate involved generating a Grignard reagent from 1,4-dibromobenzene, generation of the dithiocarboxylate group *in situ* and protection with *tert*-butyl iodide following acidic work-up. This was also unsuccessful.

This same reaction was attempted but this time with 1,3-dibromobenzene and with the addition of *tert*-butyl iodide prior to any form of work-up, which was

again unsuccessful. Making the dithiocarboxylate salt of 3-bromodithiobenzoic acid was also attempted, but this was, once again, unsuccessful.

Abandoning the idea of *tert*-butyl protection, directly turning halogenated compounds into Grignard reagents and then sodium dithiocarboxylate salts was returned to. This was attempted with 3-bromobiphenyl but no product was obtained due to rapid degradation. The salt was successfully produced but degraded by approximately 50% under nitrogen at room temperature in 1 day, giving it a half-life of roughly 24 hours, observed by ^1H NMR (Fig. 45).

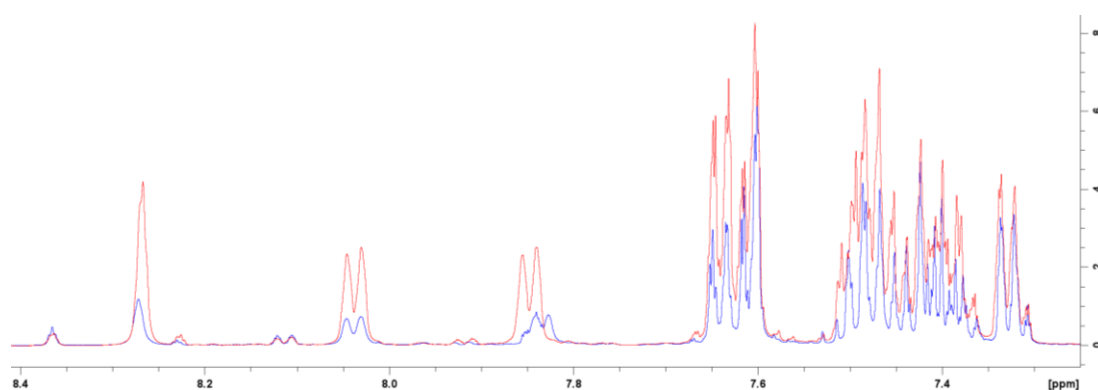
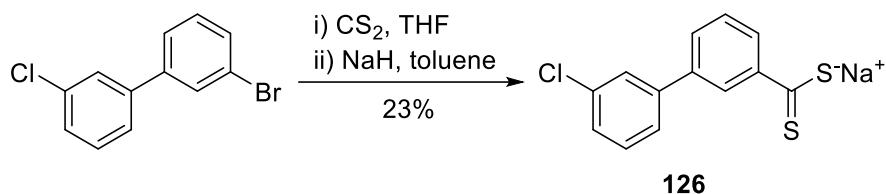


Figure 45. A section of the ^1H NMR of the dithiocarboxylate acid salt of 3-bromobiphenyl. 0 days is displayed in red and 1 days is displayed in blue. We can see the relative amount of compound has altered in 24 hours. By integrating common non-degraded peaks in the NMR we can measure that the product has degraded by approximately 50% over this time.

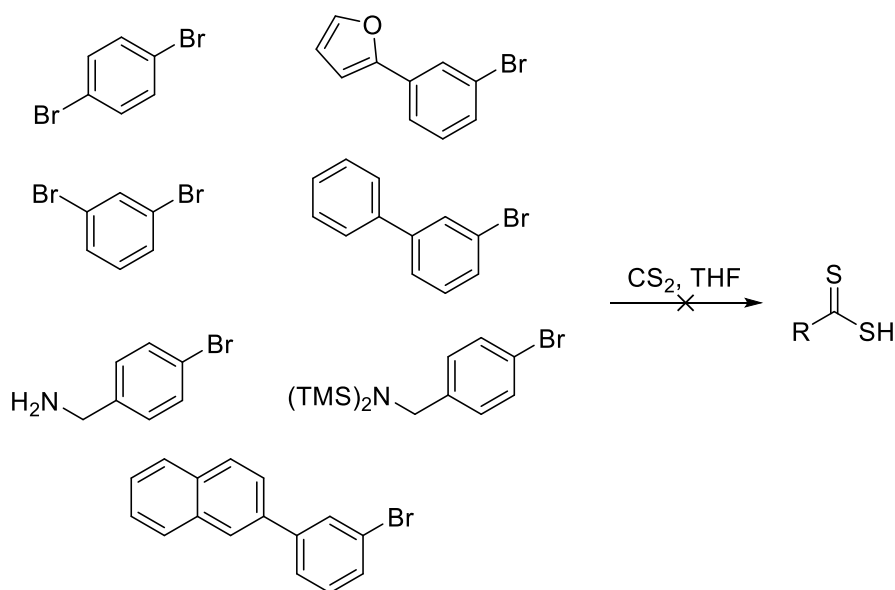
3-Bromo-3'-chlorobiphenyl was the next reagent used as a substrate for transformation into a dithiocarboxylate (Scheme 17). The dithiocarboxylate product was immediately purified *via* automated normal-phase flash column chromatography on silica deactivated with 0.1% triethylamine in DCM. The appropriate fractions were then collected and combined, then concentrated *in vacuo* in an RBF. Dry sodium hydride was added to this and the flask was then nitrogen flushed. Dry toluene was added and the reaction mixture was stirred over 72 hours, giving the product as a deep red solid in a yield of 23%. The product was confirmed *via* ^1H NMR, ^{13}C NMR and negative HRMS. 16 days after isolation the product was tested for purity *via* ^1H NMR and no degradation of the product was seen.



Scheme 17. The reactions of 3-Bromo-3'-chlorobiphenyl to sodium {3'-chloro-[1,1'-biphenyl]-3-carbothioyl}sulfanide

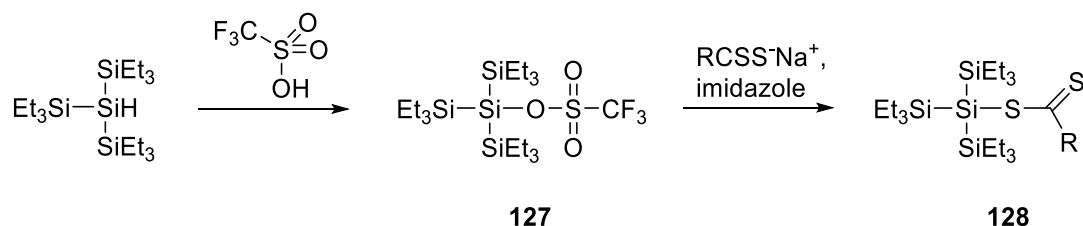
At this point compounds were assayed in B1 MBLs at the University of Oxford. The assays were conducted by Dr Karina Calvopina²⁰². Inhibition comparable to captopril of four B1 MBL subtypes was seen, validating the series as being worthy of further investigation. The results will be discussed in full in the following chapter.

There was then a series of unsuccessful attempts at forming stable dithiocarboxylates with the following brominated reagents (Scheme 18): 2-(3-bromophenyl)furan; 1,4-dibromobenzene; 1,3-dibromobenzene; 3-bromobiphenyl; 4-bromobenzylamine; 2-(3-bromophenyl)naphthalene; [(4-bromophenyl)methyl]bis(trimethylsilyl)amine. Evidently, this was not a robust synthesis. A further attempt of making sodium {[1,1'-biphenyl]-3-carbothioyl}sulfanide from 1,3-dibromobenzene was successful, albeit in a 3% yield.



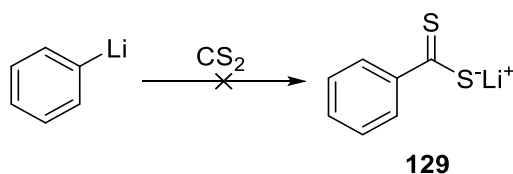
Scheme 18. Various brominated compounds that failed to be converted to their dithiocarboxylic acid analogues.

Due to the difficulties with synthesis other protection strategies were investigated. One promising avenue was a tris(triethylsilyl)silane protecting group, which has shown use before as a protecting group for carboxylic acids²⁰³. The synthetic steps to attaching this group were production of tris(triethylsilyl)triflate from tris(triethylsilyl)silane and triflic acid, followed by addition of the sodium dithiocarboxylate salt with imidazole (*Scheme 19*). Despite some possible product produced in the reaction the product was not obtained through multiple attempts. However, this may have been due to possible UV reactivity of the group, of which purification had been attempted *via* automated column chromatography measured *via* a UV trace. Whilst Tan *et al.* stated that 24 hours irradiation was required to fully deprotect the functionality, this concerned carboxylic acids, not the sulphur equivalent. Therefore the reaction was attempted again without purification using UV trace analysis, but this was again unsuccessful.



Scheme 19. The hypothesised protection of a dithiocarboxylic acid with a triethylsilyl group.

Another route of making dithiocarboxylate salts that was attempted was *via* aryl lithium reagents. If successful this would create insert the desired functional group and create the lithium salt in one synthetic step (*Scheme 20*). This was attempted with phenyllithium but was unsuccessful.



Scheme 20. The failed attempt at converting phenyl lithium to its dithiocarboxylate lithium salt analogue.

Thus, the only method of synthesis and isolation that had been successful was returned to, but this time with a further simplification: purchase of the Grignard reagents for use directly. Some of the failures seen could be directly attributed to unsuccessful generation of the Grignard, so removing this

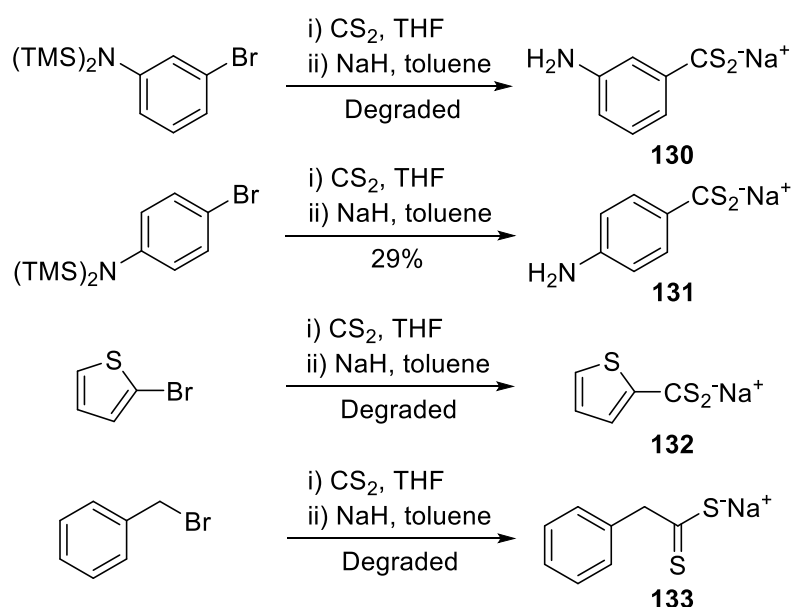
variable from the synthesis and enabling a two-step route (dithiocarboxylate generation then salting) seemed sensible.

The first attempt at this was with 3-[bis(trimethylsilyl)amino]phenyl magnesium chloride. Whilst the dithiocarboxylate group was installed successfully (as seen *via* LC-MS), the product degraded before isolation and purification were possible.

However, 4-[bis(trimethylsilyl)amino]phenyl magnesium bromide was successfully reacted and purified to give sodium (4-aminobenzenecarbothioyl)sulfanide in a respectable 29% yield. This reinforces the importance of electronics on the stability of these compounds, as highlighted by Grote *et al*¹⁹².

2-Thienyl magnesium bromide was successfully reacted too, but once again this compound quickly degraded, despite yielding a promising looking deep red solid initially.

Benzyl magnesium chloride was also successfully reacted, as seen by LC-MS, but this also quickly degraded (possibly due to double deprotonation as this compound featured an available α -hydrogen adjacent to the dithiocarboxylate moiety) (*Scheme 21*).



Scheme 21. Successful conversions of brominated reagents to their dithiocarboxylate sodium salt analogues.

Due to the synthetic difficulties encountered it was deemed prudent to purchase pre-made Grignard reagents that computational docking predicted to result in potent inhibitors once transformed to their dithiocarboxylate versions. Whilst it was not possible to effectively validate the docking results with only a limited amount of biological results and no obtained crystal structures, it was decided that it would be better to decide what compounds to next synthesise based on docking results regardless, since dithiocarboxylates had shown inhibition in MBL assays. A selection of Grignard reagents was filtered through computational docking, utilising KNIME workflow software to perform a virtual reaction on a Fluorochem Grignard catalogue. This converted the Grignard reagents into dithiocarboxylates using RDKit software nodes, and the resulting compounds were then docked into a prepared protein grid (PDB: 5K48) using the Maestro nodes within KNIME (*Fig. 46*)^{204,205}. The Glide docking here used the OPLS4 forcefield¹⁸⁰.

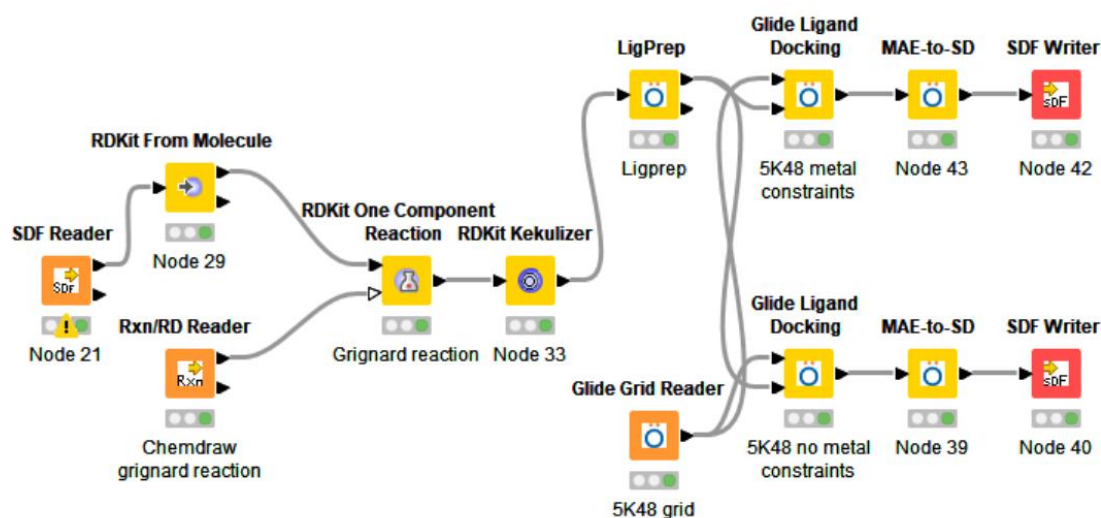


Figure 46. The workflow used for computational docking of a catalogue. The source file received from Fluorochem was inserted into the “SDF Reader” and the structures were then converted to an RDKit suitable format from SMILES by “RDKit From Molecule”. A reaction was designed in Chemdraw to convert Grignard moieties to dithiocarboxylate groups, in the “Rxn/RD Reader” node. This was the instruction for the “RDKit One Component Reaction” node, which had the prepared molecules to input. The results of this were put into “RDKit Kekulizer” to make them suitable for use in Maestro software nodes. The resultant prepared molecules were then prepared for docking via the “LigPrep” node. A preprepared grid was entered in the “Glide Grid Reader”. The two aforementioned nodes were then input into two “Glide Ligand Docking” nodes, one that specified metal constraints at the active site and one that didn’t, and the molecules were docked.

The results with metal constraints were selected after viewing the docked poses. The top results of this selection were chosen to be purchased based on multiple factors: docking score, observed pose, skeletal variance and price. A high docking score was desired as this should correlate to effective inhibitory activity within the target MBLs. The observed pose must appear reasonable for the compound to be selected; that is, it must dock the compound with the dithiocarboxylate moiety placed in a position to displace the hydroxide ion and otherwise appear reasonable in its interactions and spatial placement. Exploring skeletal variance was essential for these compounds due to the instability of the dithiocarboxylate group; making a variety of compounds with different skeletal structures increased the chances of finding a stable substrate from which to continue this series. On the basis of these criteria, five new target molecules were selected (*Fig. 47*).

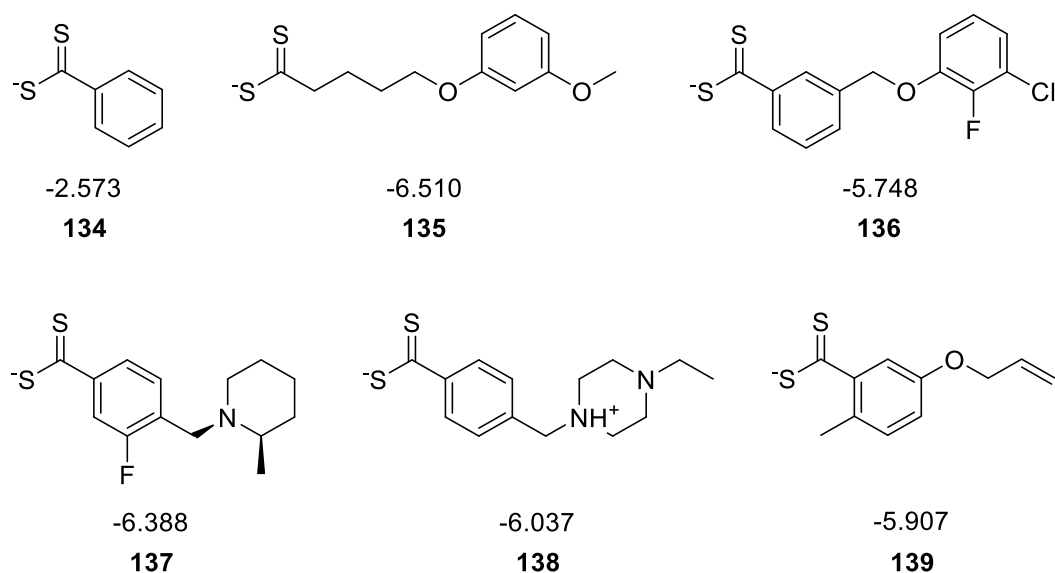
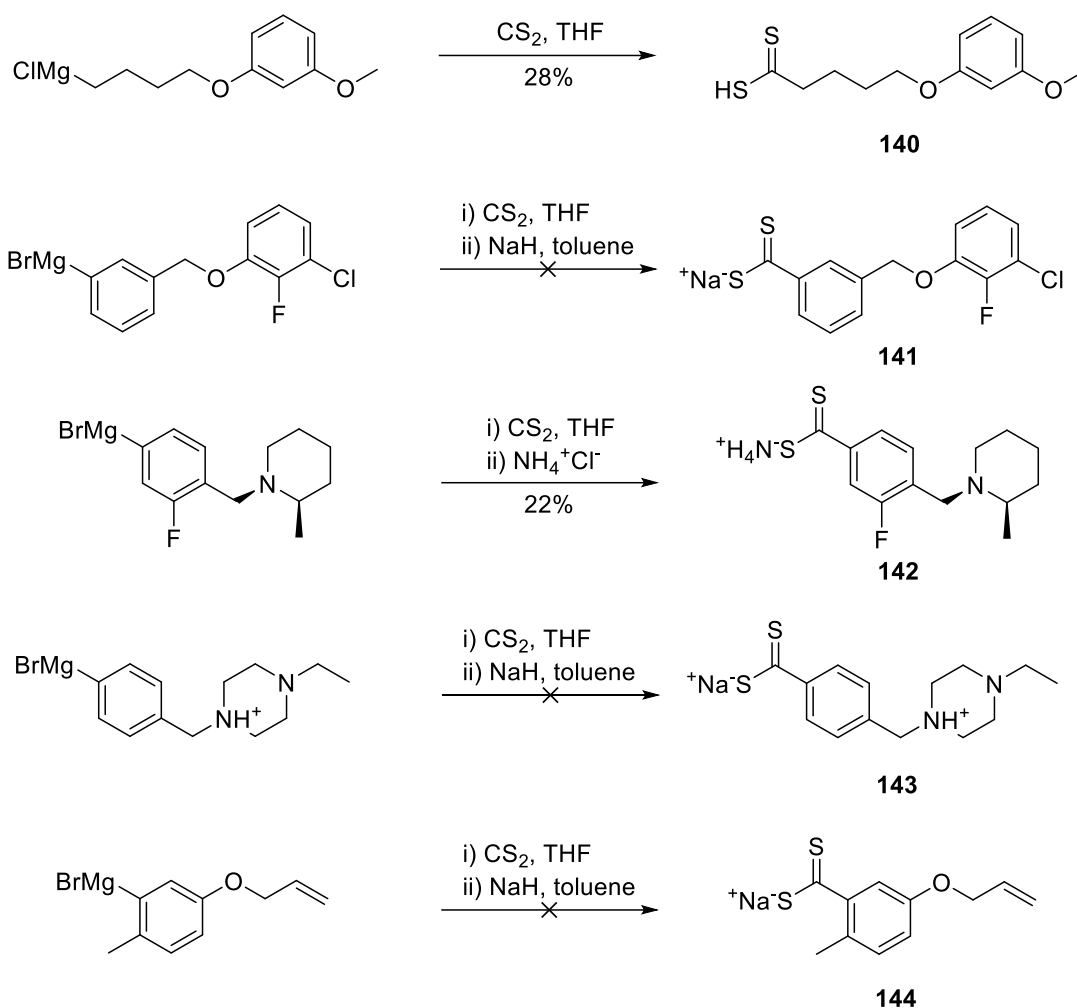


Figure 47. The docked forms of the chosen molecules for purchase along with their docking scores (XP GScore), after their planned chemical transformation. Phenyldithiocarboxylic acid is also included.

Using the previously established dithiocarboxylate salt transforming reaction, **135** was successfully synthesised. Unfortunately the syntheses of **136**, **138** and **139** were unsuccessful.

The synthesis was slightly altered for the creation of **137**, to form the ammonium salt as opposed to the sodium salt. Whilst creation of the sodium salt had previously failed, creation of the ammonium salt was successful, yielding the product as an off-white solid (*Scheme 22*).



Scheme 22. The attempted transformations of pre-made Grignard reagents to their dithiocarboxylate salt analogues.

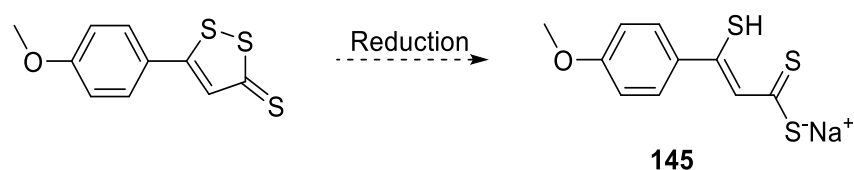
Successfully synthesised compounds were submitted for HPLC analysis and sent for IC₅₀ assay in B1 MBLs at the University of Oxford. Results are presented in the following chapter.

2.4 Anethole trithione

2.4.1 Docking & synthesis

Anethole trithione is an organosulphur compound used to treat dry mouth²⁰⁶. Based on the sulphur rich ring in its structure it was thought that it could be used to creating a new series of metal-binding inhibitors. Indeed, the trithione group itself appears in a number of compounds with potentially efficacious action on various diseases²⁰⁷.

It was decided that both anethole trithione itself would be tested, and also to attempt to open the trithione group and salt the resulting dithiocarboxylic acid moiety to produce **2.89** (*Scheme 23*).



*Scheme 23. The planned chemical transformation of anethole trithione to **145** (sodium [(Z)-3-(4-methoxyphenyl)-3-sulfanylprop-2-enethioyl]sulfanide).*

To investigate the reduction cyclic voltammetry was used to find the reduction potential, but this also gave no useful results. As such, this was abandoned.

However, anethole trithione itself was assayed in B1 MBLs at the University of Oxford, in order to observe if it showed any enzymatic activity itself.

Chapter 3

Metallo- β -lactamase inhibition assay results & discussion

3.1 Metallo- β -lactamase assay platform

The assay used to determine MBL inhibition was developed by van Berkel *et al.* and used by Cain in previous work by the Fishwick group^{152,208}. Van Berkel *et al.*, part of the Schofield group at the University of Oxford, developed this assay in response to the lack of an appropriate, efficient screening platform for multiple MBLs due to the scarcity of suitable detection substrates for these enzymes.

Previously used screening methods for β -lactamases used chromogenic cephalosporin-based substrates, such as CENTA (**146**)²⁰⁹ and nitrocefin (**147**)²¹⁰ (*Fig. 48*), but these compounds are difficult to produce, expensive and often suffer from poor substrate recognition by some MBLs, due to the diversity of sequence, structure and specificity of the enzymes. Thus the development of an inexpensive and robust substrate for MBL detection would be a boon to the research area.

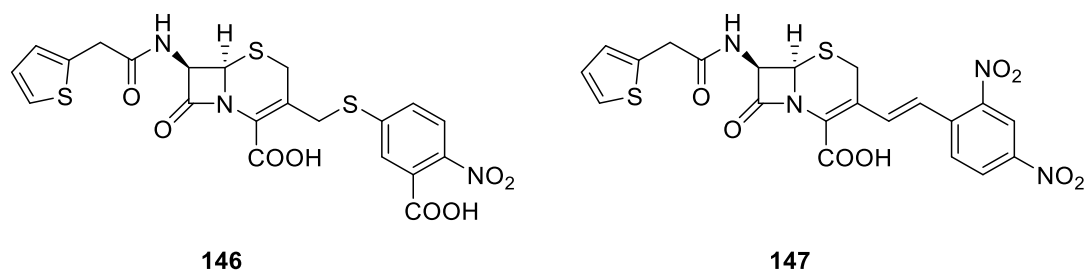


Figure 48. CENTA (146) and nitrocefin (147) are chromogenic cephalosporin-based substrates used for detection of β -lactamases.

The group noted that umbelliferone displays strong fluorescence when in its free form, whilst being almost entirely unfluorescent when covalently linked to an ether²¹¹. These properties made it an ideal candidate for the development of a fluorescence assay. The umbelliferone moiety was connected to cephalosporin *via* an ether bond. When introduced to a β -lactamase, the β -lactam ring is hydrolysed and umbelliferone is released, resulting in an increase in fluorescence (*Fig. 49*). This newly developed substrate was called FC5^{208,212}.

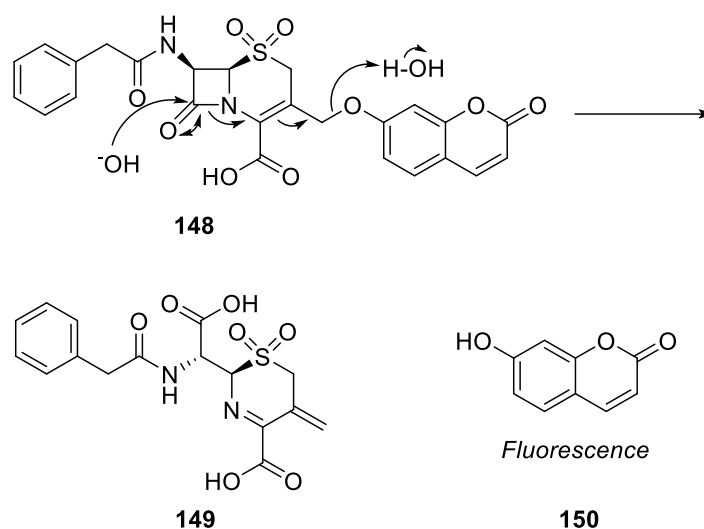


Figure 49. Newly developed fluorescence based screening substrate FC5 (**148**). When the β -lactam moiety is hydrolysed umbelliferone (**150**) is released, resulting in an increase in fluorescence.

FC5 displayed fantastic results as an assay substrate, being highly sensitive and therefore enabling enzyme concentrations of up to twenty times lower compared with previously used substrates with NDM-1. FC5 also displayed favourable results in VIM-2, IMP-1 and SPM-1 (SPM-1 is unusual in MBLs in that it displays structural features found in both B1 and B2 MBLs²¹³), performing equally as well or better than previously used substrates. In all cases FC5 allowed the use of low enzyme concentrations ($> 1\text{nM}$) and enabled the detecting of weak binding fragments or slow binding inhibitors²⁰⁸.

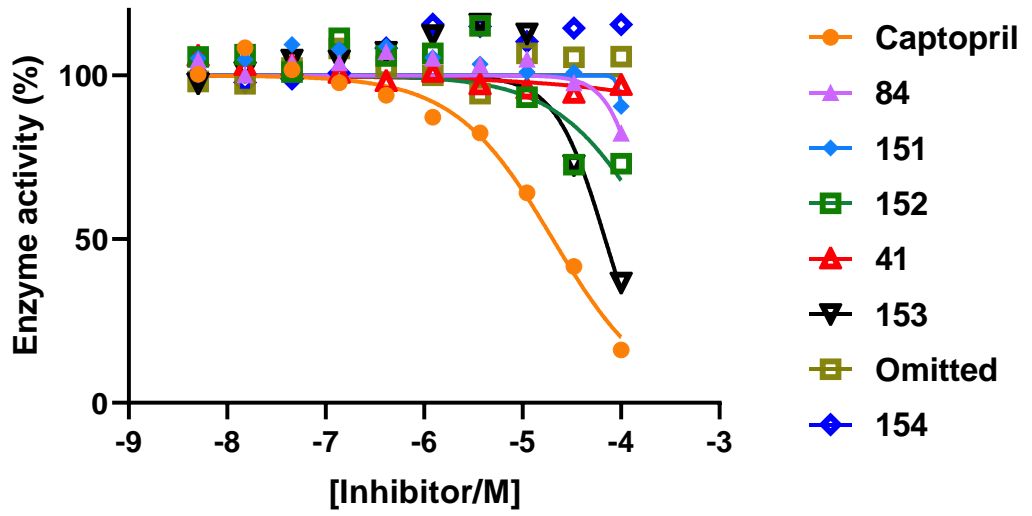
3.2 Biological results

A selection of eleven compounds of interest were sent to the Schofield group at Oxford University for IC_{50} assays in clinically relevant B1 MBLs: IMP-1, NDM-1, VIM-1 & VIM-2 (Fig. 50). These compounds were selected for the reasons outlined in the preceding chapter.

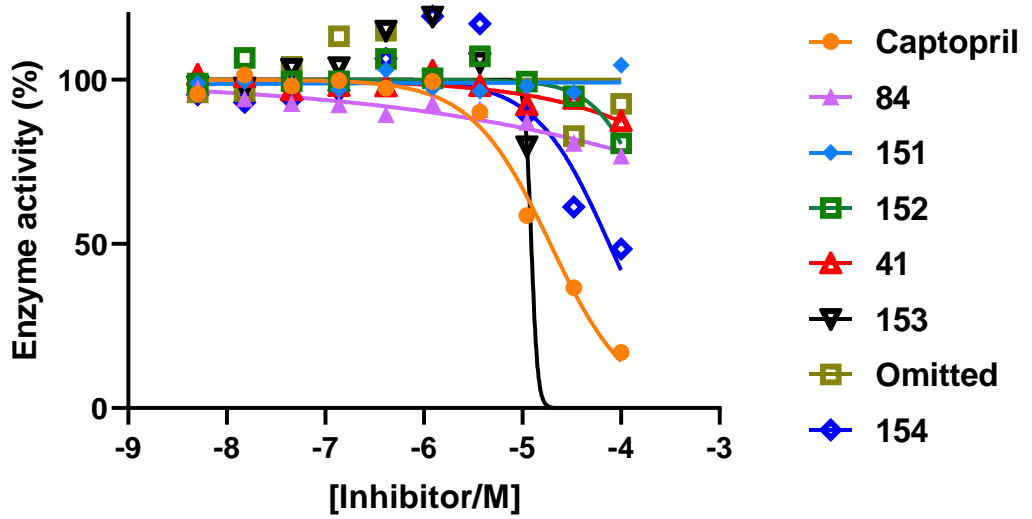
	pIC ₅₀ (μM)			
	VIM-1	NDM-1	VIM-2	IMP-1
Captopril	4.7	4.7	5.7	5.0
* 84	<4.0	<4.0	<4.0	<4.0
* 151	<4.0	<4.0	<4.0	<4.0
* 152	<4.0	<4.0	<4.0	<4.0
* 41	<4.0	<4.0	<4.0	<4.0
* 153	4.2	5.0	4.0	4.5
* Omitted	<4.0	<4.0	<4.0	<4.0
* 154	<4.0	4.1	<4.0	<4.0
* 126	4.4	5.3	4.3	4.8
* 155	<4.0	<4.0	<4.0	<4.0
* 110	<4.0	<4.0	<4.0	<4.0
* 111	<4.0	<4.0	<4.0	<4.0

Table 4. The results from the first set of compounds sent for assays in B1 MBLs. (*) Highest concentration tested 100 μM. Results for **Omitted** should be ignored due to an error in synthesis.

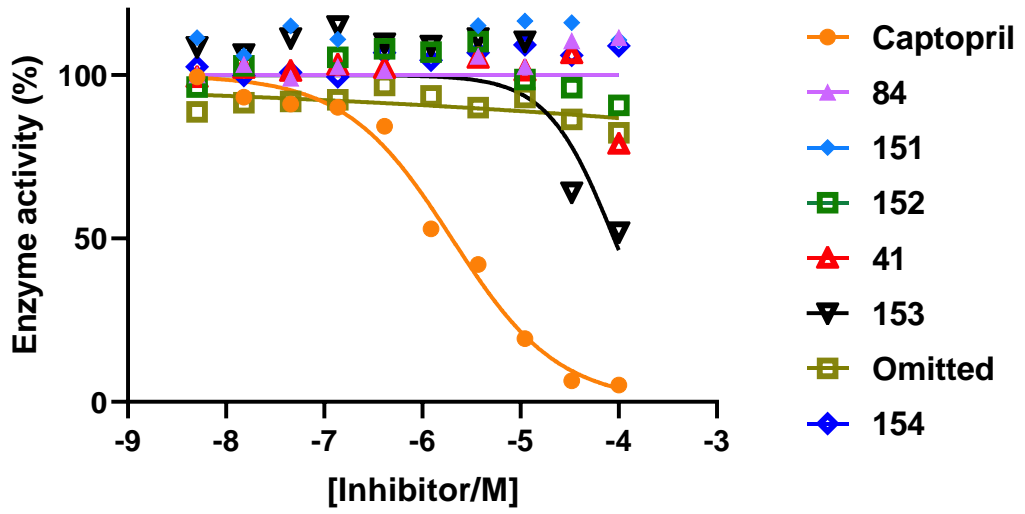
Dose response With VIM1/FC5



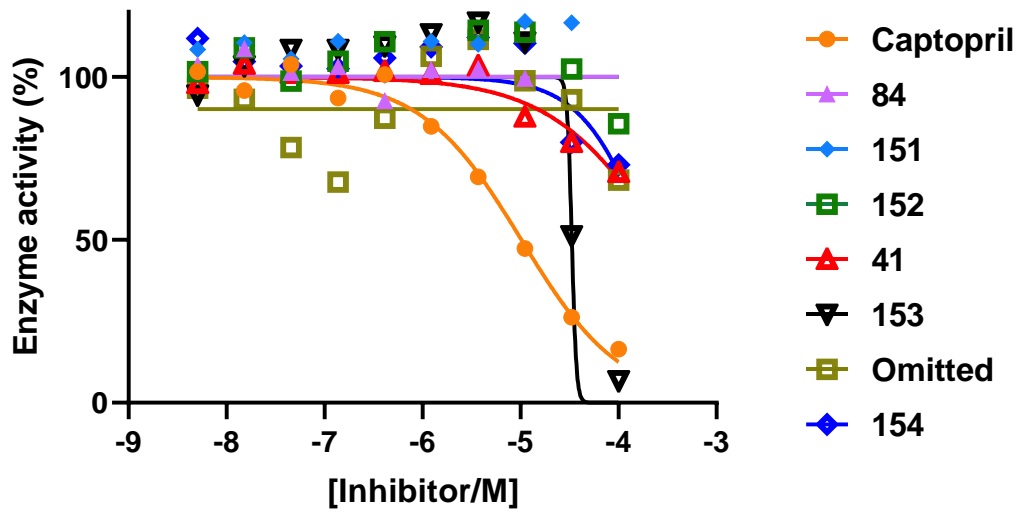
Dose Response With NDM1/FC5



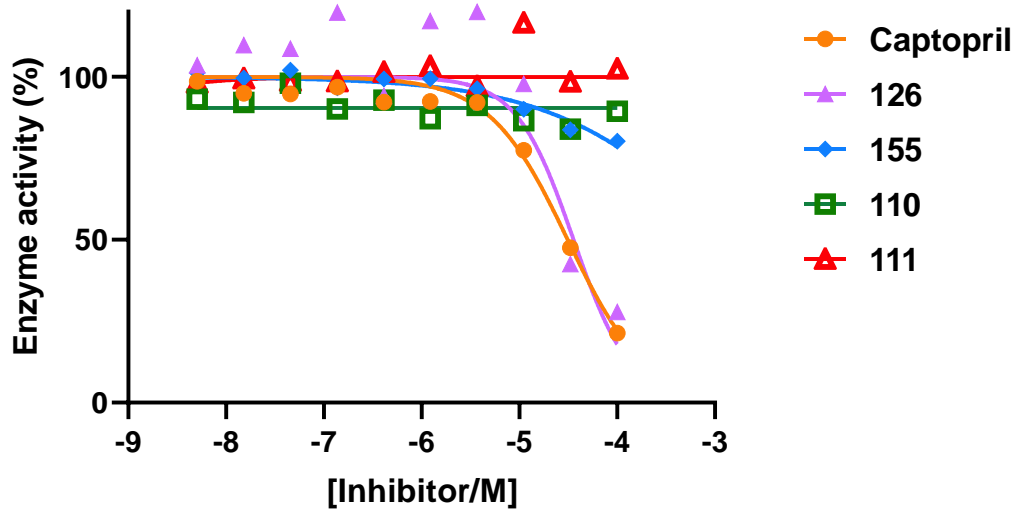
Dose-Response With VIM2/FC5



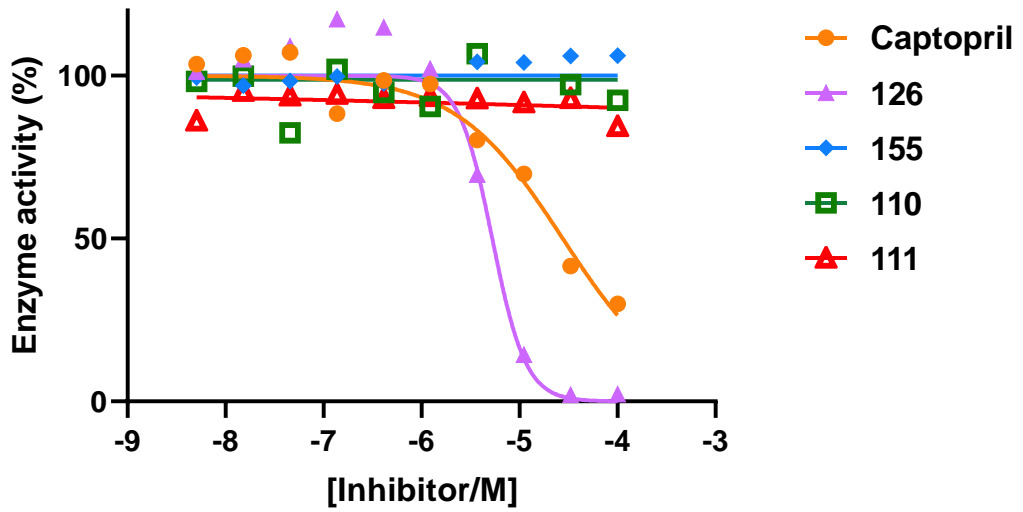
Dose-Response With IMP1/FC5



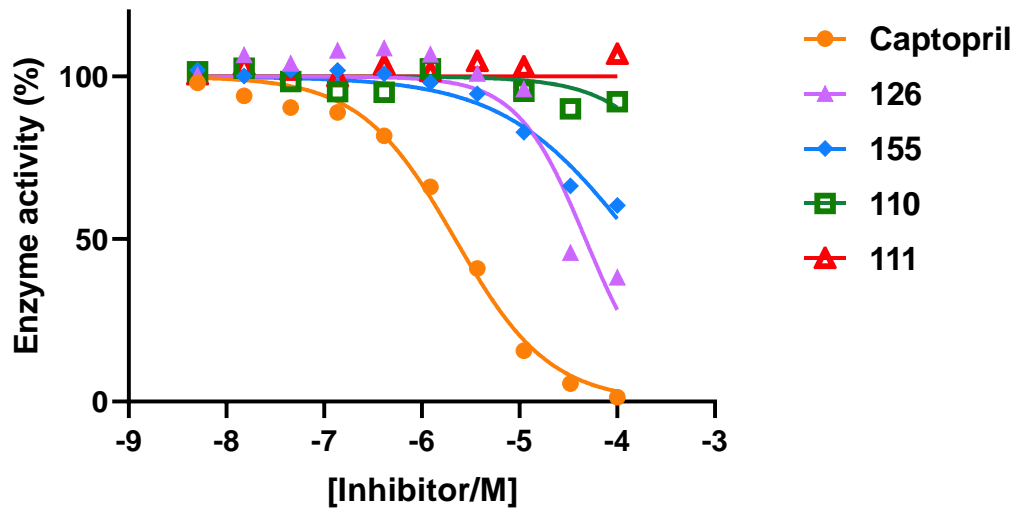
Dose response With VIM1/FC5



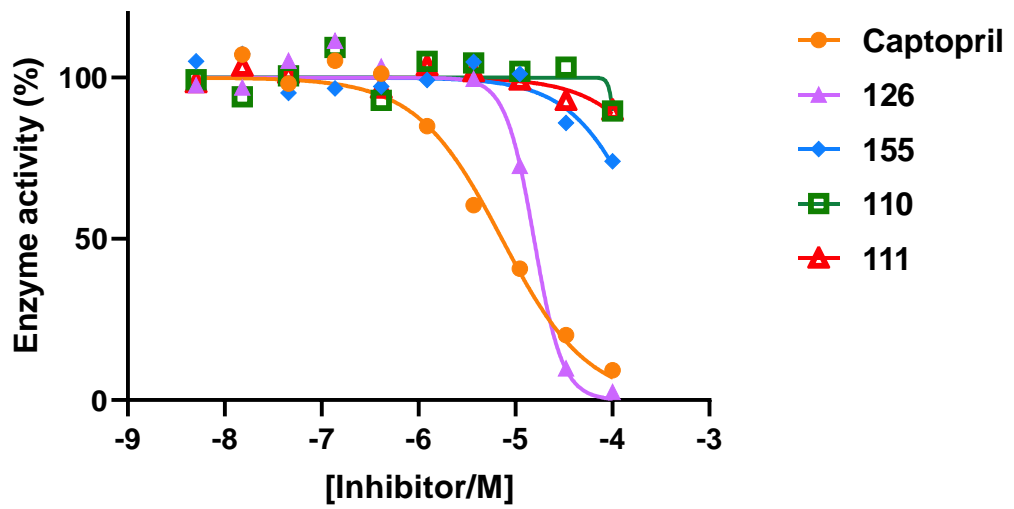
Dose Response With NDM1/FC5



Dose-Response With VIM2/FC5



Dose-Response With IMP1/FC5



Graphs 1-8. Response curves of compounds sent for testing in B1 MBLs, alongside captopril.

3.3 Analysis of metallo- β -lactamase enzyme assay results

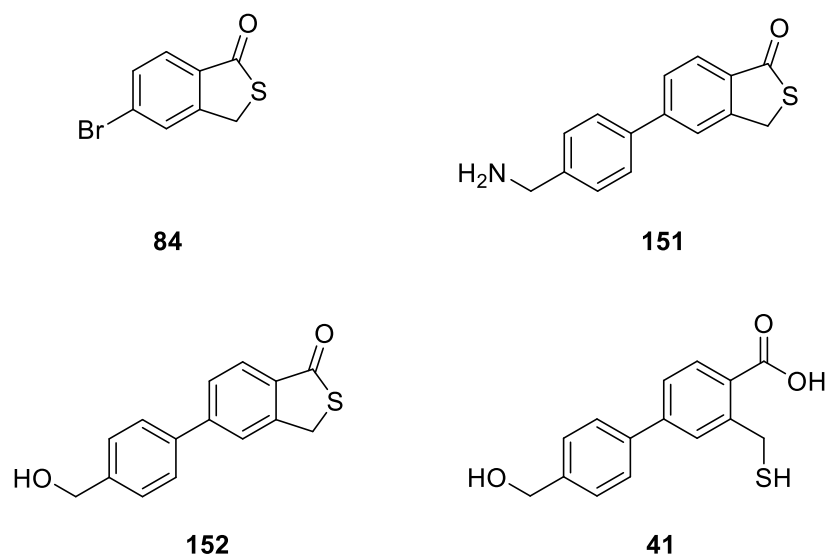


Figure 51. The structures of thiolactone compounds **84**, **151**, **152** and thiol compound **41**.

Compounds **84**, **151** and **152** (Fig. 51) were produced in the attempted synthesis of thiol-based compounds. These compounds were tested to examine the potential of thiolactones as MBL inhibitors, *via* a prodrug approach whereby the thiolactone is hydrolysed in the cell and the thiol can then bind to the active site of the enzyme (Fig. 52).

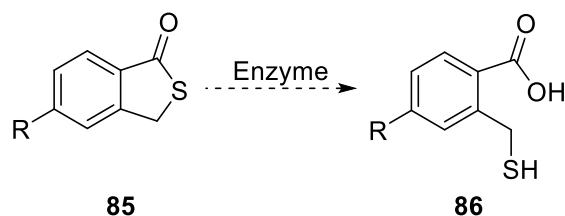


Figure 52. The proposed hydrolysis of **85** in MBL enzymes, to be harnessed as a prodrug approach for MBL inhibition.

Compound **84** showed no inhibition in VIM-2 and IMP-1. However, this molecule did exhibit slight inhibition at 100 μ M (~80% percent response) in VIM-1. In NDM-1 the percent response follows inhibitor concentration closely, but unfortunately is still very weak, with the same approximate percent response at 100 μ M.

Compound **151** showed no inhibition in any of the assays. This may be due to the terminal amine group causing the compound to coordinate elsewhere in the enzyme, resulting in no active site effects. Otherwise, it would be expected to have similar inhibition to the other thiolactones tested.

Compound **152** showed signs of weak inhibition in all tested enzymes at 100 μM . However, in no case was it significant enough to have an IC_{50} above 1mM.

These results agree with Cains previous findings¹⁵², suggesting that the thiolactones are not being hydrolysed by the enzymes, with hydrolysis happening either too slowly to be detected *via* the assay or not at all.

Compound **41** showed similar activity to the aforementioned compounds. No activity was seen in VIM-1, whilst very modest activity was seen in the other MBLs. This was a very disappointing result from a compound that had taken a lot of work to produce, and is not in line with docking predictions.

The similar activity of **152** may suggest that this compound cyclised into its thiolactone form in the time between the time of synthesis and analysis, and the time of assay. This would explain the difference in activity between this compound and those previously tested by Cain¹⁵².

It should also be noted that HPLC analysis at the time of assay revealed **41** to only be 75% pure. The degradation of the compound was previously implied following an earlier analysis of the material using ^1H NMR, but not quantified until the time of assay.

Once again it must be reiterated that the identification of **41** it not unequivocal. Resynthesis and another round of assay testing is required for validation of this negative results.

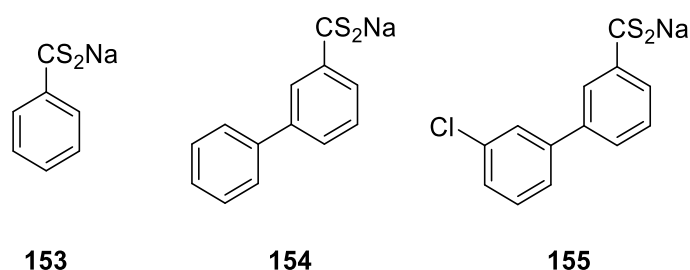


Figure 53. The structures of dithiocarboxylate salt compounds **153**, **154** and **155**.

The results of the biological assays for compound **153** (Fig. 53) were far more encouraging. In all MBL assays this compound showed inhibition generally between 10 - 50 μM . At 100 μM concentration the compound showed similar inhibitory values to that for captopril in all cases, with results in VIM-2 being markedly better. With this proven potency it was possible to justify further development of compounds featuring this moiety.

Some degradation of **153** was noted *via* HPLC at this point. Whilst the compound was thought to be almost entirely pure at the time of synthesis, when analysed by the time of assay it was revealed to have degraded to 86% purity.

Results for **154** in all tested MBLs were disappointing. The reason for these poorer than expected results were explained *via* the HPLC results. From the time of synthesis to the time of assay, the compound had significantly degraded, being only 42% pure at the time of assay. This can somewhat explain the poor assay results, as it is the dithiocarboxylate warhead moiety that is the likely point of degradation (this moiety being the common functionality and known as being unstable, as noted in literature¹⁹²). Nevertheless, reasonably significant inhibition was seen in NDM-1 whilst poor inhibition was seen in IMP-1 and no inhibition was seen in assays involving the VIM subtypes. This may suggest that the aryl group attached to the molecule causes selectivity between MBL subtypes to arise, as suggested by docking performed within the different MBL subtypes (*Fig. 54*).

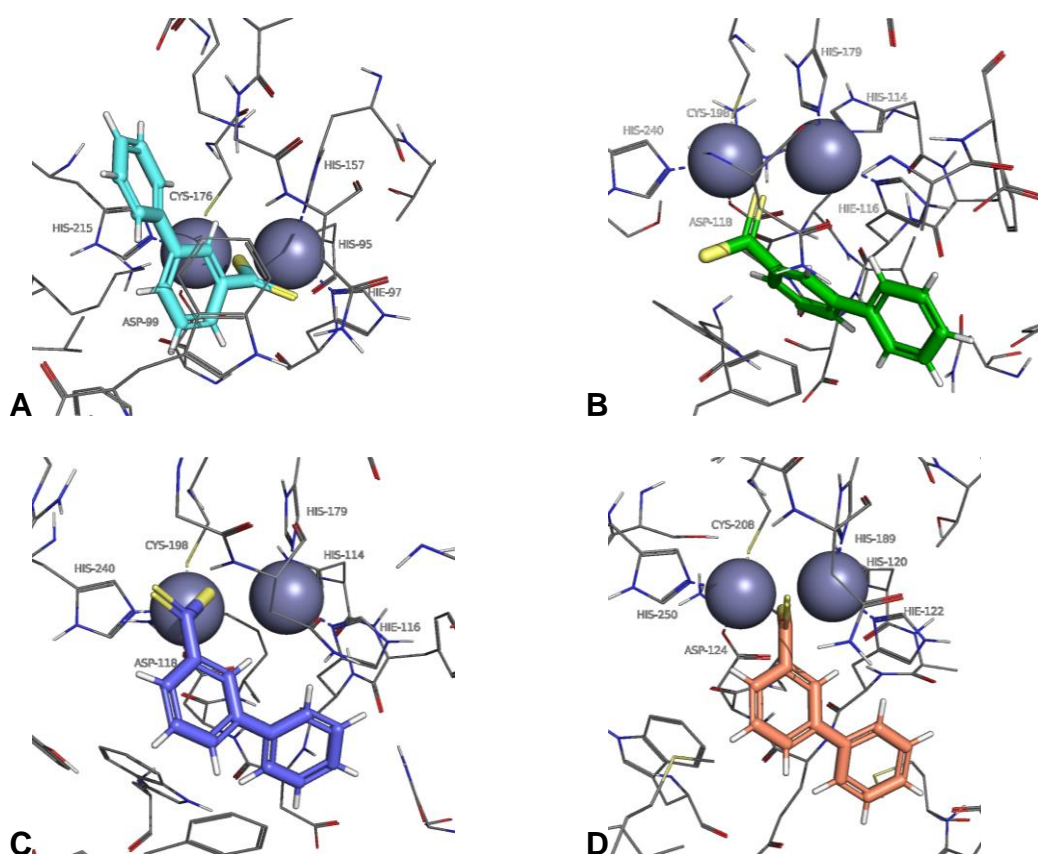


Figure 54. Poses of **154** displayed via docking analysis (**A** – IMP-1, **B** – VIM-1, **C** – VIM-2, **D** – NDM-1). All images are orientated similarly around the active site. The pose of **154** in IMP-1 is predicted to be markedly different but the poses in other tested subtypes are predicted to be somewhat similar.

Compound **126** showed very encouraging results in the tested MBL assays. However, the IC₅₀ results were slightly poorer than those seen for **153**. Once again, HPLCs revealed that the compound was not of the desired purity at the time of testing, due to degradation. At the time of assay the compound was only 60% pure. Under the assumption that the degradation compounds do not inhibit MBLs, then we can extrapolate the true potency of this compound being greater than that of **153**. However, more work investigating and identifying the breakdown products, and subsequent assays in MBLs thereof, would be required to confirm this hypothesis.

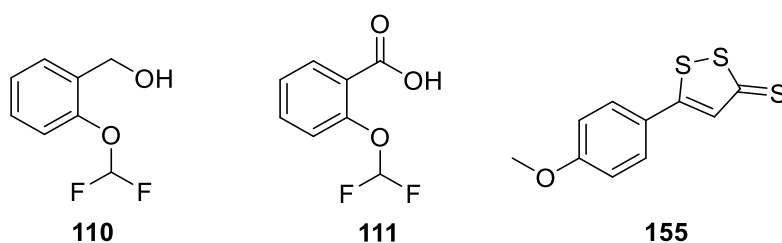
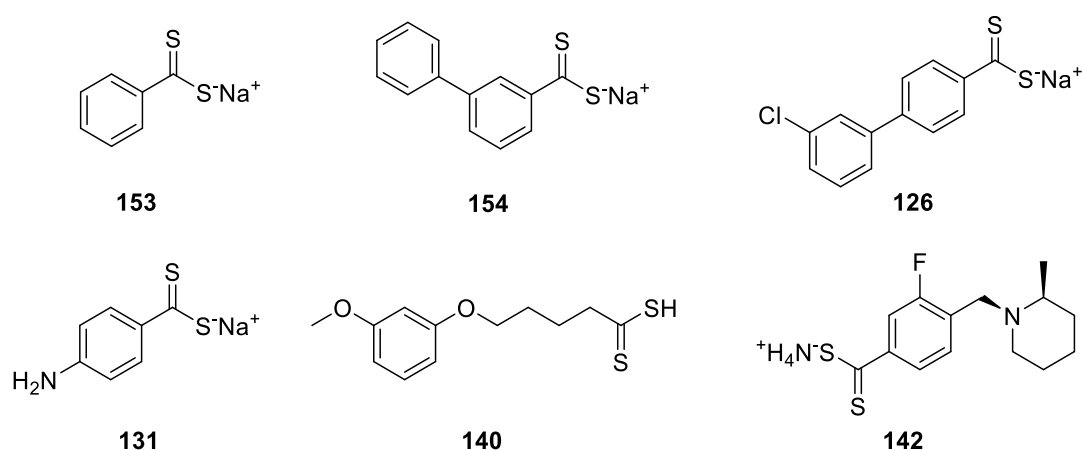


Figure 55. The structures of purchased compounds **110**, **111** and **150**.

Compounds **110** and **111** were purchased from commercially available sources as fragments to investigate whether the difluoromethoxy group could act as a inhibitor analogously as to how a thiol-based inhibitor would act. Modest inhibition was seen by **111** (shown on graphs 5, 6 & 8) whilst no inhibition was seen in the tested MBL subtypes with **110**. This suggests that the inhibition is due to the binding of the carboxylate moiety of **111**, rather than the difluoromethoxy group, as this is the only point of difference between the compounds.

Compound **155**, anethole trithione, showed no inhibition of any of the MBLs.

A second round of testing with the same assay panel was completed for a further selection of synthesised dithiocarboxylate containing compounds (*Fig. 55*). Skeletal variance between structures was desired to explore the stability of the dithiocarboxylate group on different substrates.

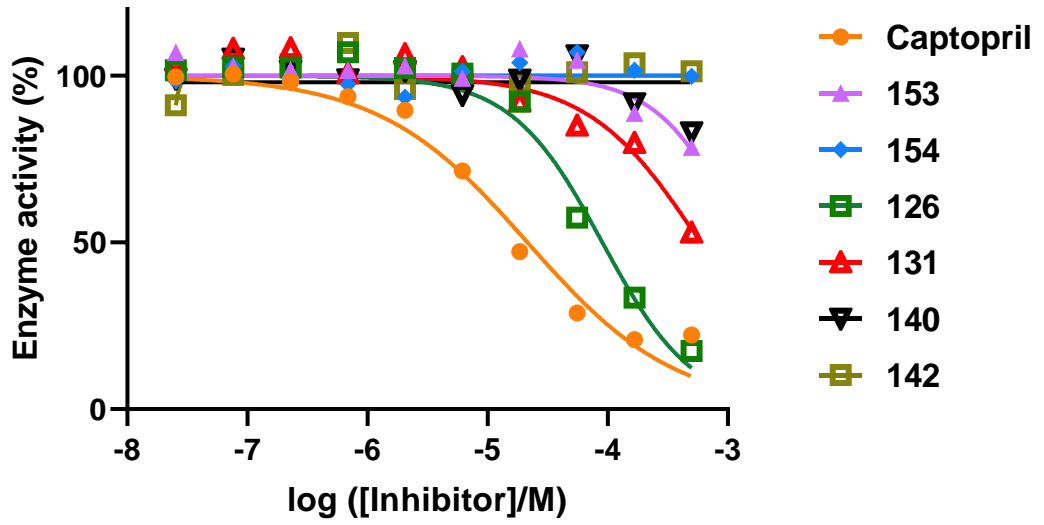


*Figure 56. The second round of compounds sent for testing against B1 MBLs. **153**, **154** and **126** were included for a second round of testing, to validate previous results.*

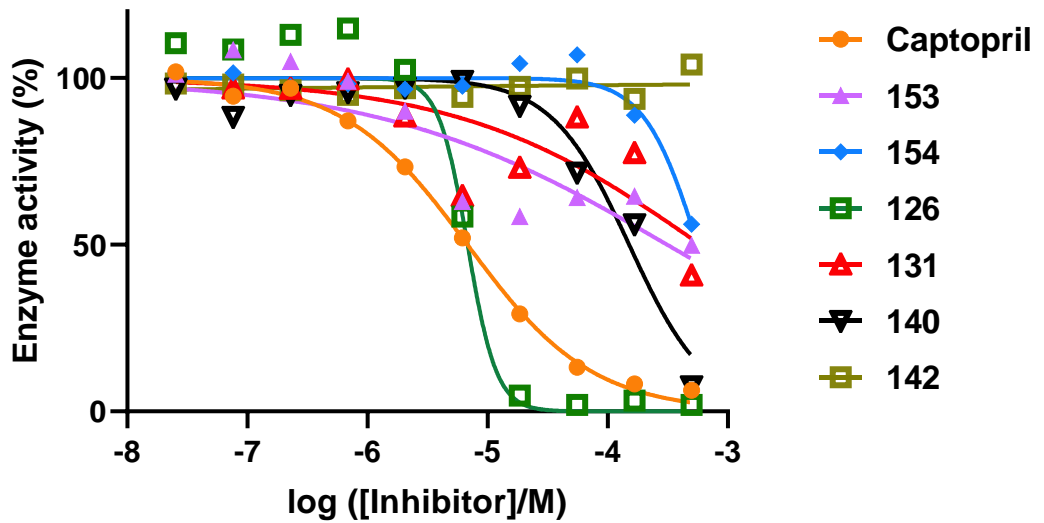
	pIC ₅₀ (μM)			
	VIM-1	NDM-1	VIM-2	IMP-1
Captopril	4.1	5.2	5.8	5.5
* 153	<3.3	<3.3	<3.3	ND
* 154	<3.3	<3.3	<3.3	4.1
* 126	4.0	5.2	3.9	5.1
* 131	<3.3	<3.3	<3.3	3.6
* 140	<3.3	3.8	<3.3	<3.3
* 142	<3.3	<3.3	<3.3	<3.3

Table 5. The enzymatic results from the second set of compounds sent for assays in B1 MBLs. () Highest concentration tested 5 mM.*

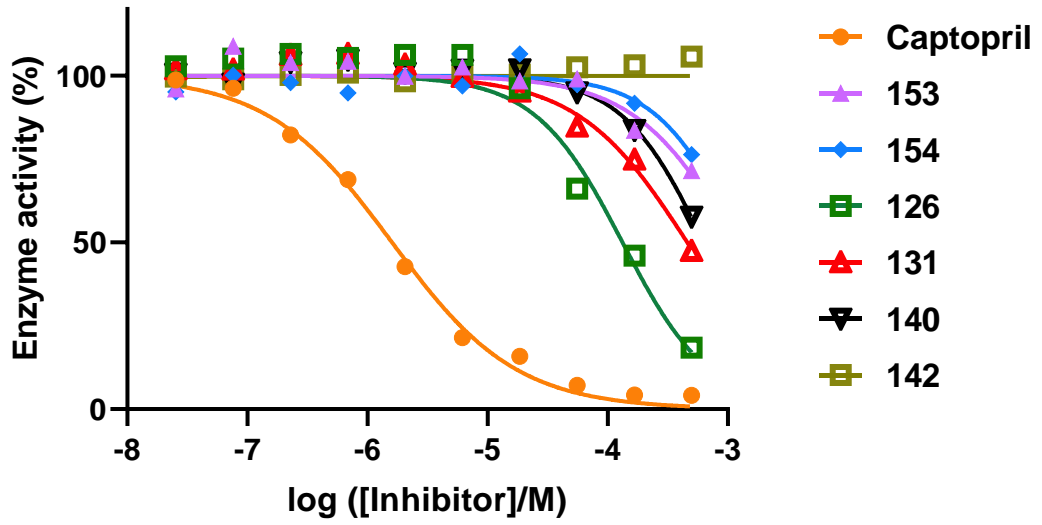
Dose Response with VIM1/FC5



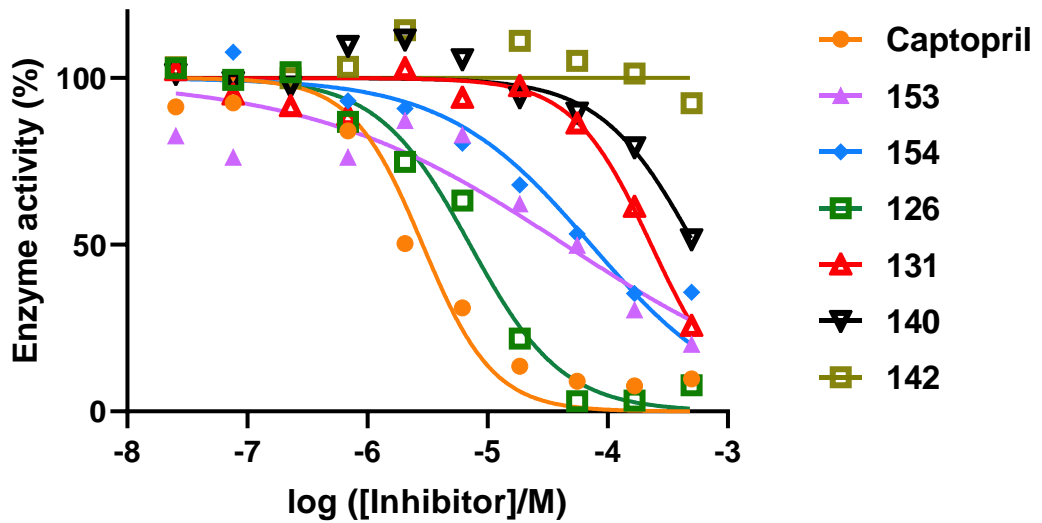
Dose response with NDM1/FC5



Dose response with VIM2/FC5



Dose response with IMP1/FC5



Graphs 9-12. Response curves of compounds sent for the second round of testing in B1 MBLs, alongside captopril.

Enzyme assay results for **153** in this second round of testing showed lower pIC₅₀ results than that of the first round testing results of **153**. However this was not unexpected, as HPLC results of the compound at the time of assay showed 53% purity (this is further explained in section 3.3). These results are still useful, as they indicate that the degradation products of dithiocarboxylates do not inhibit MBLs, as expected.

Compound **154** showed similar results to the first round of testing, only showing inhibition over the lower bound in a single B1 MBL subtype. Interesting, this time it showed inhibition of IMP-1, whereas previously inhibition of NDM-1 was shown in this enzyme assay. This means that the inhibition shown in both rounds of testing does not provide evidence of selectivity, as the level of inhibition in either case is too low to infer this and results are inconsistent.

Compound **126** showed good inhibition in all tested MBLs in this second round assay. It showed slightly improved results in NDM-1 and IMP-1 versus the VIM subtypes. The results also showed consistency with the first round of testing, in terms of potency and selectivity between MBL subtypes.

Compound **131** showed no inhibition which is most likely due to degradation, as discussed in the next section. The compound showed only 27% purity at the time of testing *via* HPLC.

Compound **140** showed slight inhibition of NDM-1. At the time of assay this compound had degraded (62% purity *via* HPLC), so it is reasonable to assume that the pure compound would show significantly better inhibition. Regardless, it was encouraging to see inhibition using a dithiocarboxylate moiety in its non-salted form, as all previously assayed dithiocarboxylates had been sent as a sodium salt.

Compound **142** showed no inhibition. Once again degradation of this compound was seen immediately prior to sending (34% purity *via* HPLC).

It should be noted that these compounds were not tested for 44 days since dispatch. Despite being stored at -80 °C they may have degraded further during this time.

3.3 Dithiocarboxylate degradation

Dithiocarboxylates are known to be unstable¹⁹². However, this appears to be significantly affected by the rest of the constituent molecule to which they are a feature of. In fact, they are liable to decompose through a variety of different methods, such as the formation of oligomers or degradation to thiocarboxylic acids. Grote *et al.* found a number of different degradation products that occurred almost immediately after synthesis, and even when the solutions were kept dilute. It was noted that the stability is dependent on the size of the stabilising organic group carrying the dithiocarboxylate unit. If the dithiocarboxylate moiety lies adjacent to an aryl ring, it also appears important to organise substituents around the ring *ortho* or *para* to the dithiocarboxylate group. It is possible that in this configuration the attached groups in the *ortho* positions may act as steric shield of the dithiocarboxylate group, protecting it from intermolecular attack. Whilst this data is useful and informative, it was also concluded that it is incomplete and more of these compounds must be synthesised and analysed to determine true nature of the stability of dithiocarboxylate containing compounds¹⁹².

Therefore stability studies in D₂O were conducted *via* ¹H NMR analysis of **153** (*Fig. 57*). After one month in D₂O, stored at RT in the dark, (red trace) there was only a minor change in purity from the compound at 0 days (green trace). However, after two months, once again kept at RT in the dark, (blue trace) the compound had significantly degraded. The degradation could be seen within the D₂O solution itself, which had changed from a translucent deep red solution to an opaque pink solution in this time. Evidently there is a point of acceleration of degradation with this compound in water. Hence, it should be stored under anhydrous conditions at all times.

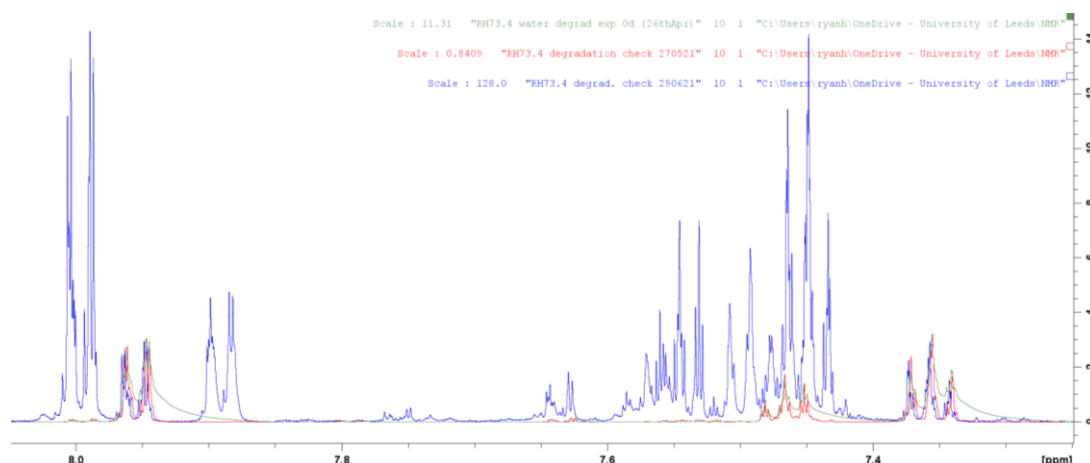


Figure 57. Overlaid ^1H NMR spectra of **153** in D_2O at 0 days (green), 1 month (red) and 2 months (blue). The spectra are normalised so that the **153** structure signal is approximately equivalent in all cases. The same ^1H NMR spectrometer was used at the same settings with the same sample in all cases.

However this result is somewhat encouraging for the use of these compounds as drugs. The stability of over a month in D_2O suggests that more stable substrates of these compounds can survive in water for extended periods of time; certainly enough time for activity in the body to occur and notably over the period of time that common antibiotics such as penicillins would be active in the body.

During the syntheses the degradation of many compounds was seen (Fig. 58), including: [1,1'-biphenyl]-4-carbodithioic acid (**122**), [1,1'-biphenyl]-3-carbodithioic acid (**156**), 3-aminobenzene-1-carbodithioic acid (**157**), thiophene-2-carbodithioic acid (**158**), 2-phenylethanedithioic acid (**159**); plus many others that degraded even before their analysis.

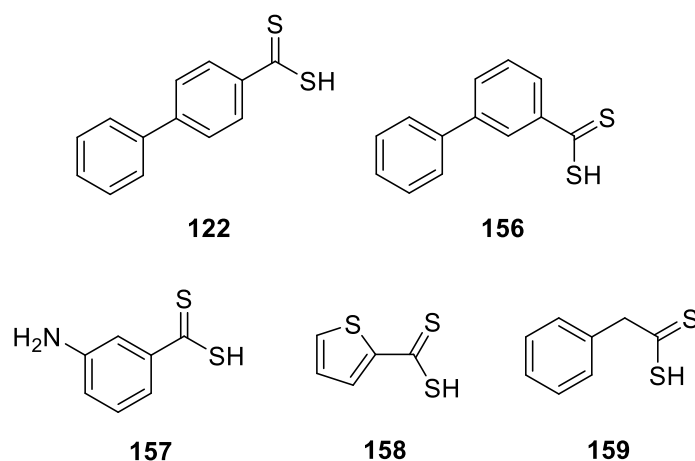


Figure 58. A selection of dithiocarboxylate containing compounds that rapidly degraded.

Some of these synthesised dithiocarboxylates degraded even in their sodium salt forms under nitrogen and kept in a freezer, suggesting that there may not be a reliable form of the dithiocarboxylate moiety for easy storage.

Compound **131** was seen to degrade immediately after synthesis. HPLC spectra of the compound showed a reduction in purity from 94% to 27% over thirteen days when kept under nitrogen at room temperature. Some of this degradation may have occurred when the sample was solvated for HPLC analysis. When **131** was later repurified *via* automated reverse phase flash column chromatography the products were all collected and submitted for NMR and LC-MS analysis.

The first compound to be collected from the column (fraction 2, where each fraction refers to an 18 mL test tube) was the desired product, showing the correct mass following analysis using LC-MS. Other compounds were collected in fractions following this, none of which showed the correct mass. This is logical, with the original desired compounds being expected to be collected from the column in 100% water, given the polar structure of **131**, and the degraded compounds that no longer contain an intact dithiocarboxylate moiety expected to be collected from the column at a lower water/acetonitrile ratio.

The other compounds to be collected from the column were at fractions 11 - 13, 14 - 17 and 18 - 19, as viewed on the Biotage column chromatogram UV trace. These were the only major fractions and so were the ones chosen for analysis. There was some overlap of the peaks on the UV trace which shows that some fractions will not be only a single product, they will be a mixture of products.

The LC-MS spectra of fractions 11 - 13 (Negative ion mass found 270.71-270.74) suggests the compound to be a dimer (**160**, formula $C_{14}H_{12}N_2O_2S$). This may be a dimer formed after degradation of the dithiocarboxylate to thiocarboxylate (Negative ion mass required 271.0547) (*Fig. 59*).

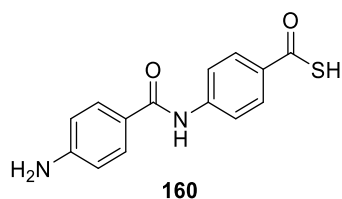


Figure 59. Suspected products of degradation of compound **131** from reverse-phase column chromatography fractions 11-13.

The LC-MS spectrum of fraction 14 (Negative ion mass found 286.77) suggest the compound to be a dimer formed when only one of the product molecules has degraded to a thiocarboxylate (**161**, formula $C_{14}H_{12}N_2OS_2$, Negative ion mass required 287.0318) (Fig. 60)

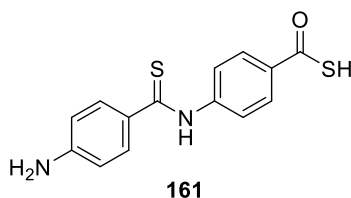


Figure 60. Suspected products of degradation of compound **131** from reverse-phase column chromatography fraction 14.

The LC-MS spectra of fractions 15 - 19 seems to consist of variety of oligomers formed from product and degraded product monomers (Fig. 61), of the following structure and expected masses (negative ion masses found are shown in brackets):

162, $C_{14}H_{12}N_2S_3$ negative ion mass required 303.01 (found 302.71-302.78);

163 $C_{21}H_{17}N_3O_2S_2$ negative ion mass required 406.07 (found 405.99-406.03);

164, $C_{21}H_{17}N_3OS_3$ negative ion mass required 422.05 (found 421.95);

165, $C_{21}H_{17}N_3S_4$ negative ion mass required 438.02 (found 438.88-438.89);

166, $C_{28}H_{22}N_4O_3S_2$ required negative ion mass 525.11 (found 525.15);

167, $C_{35}H_{27}N_5O_5S$ negative ion mass required 628.17 (found 629.04).

Analysis of further fractions and masses was discontinued here, as it seems clear that all constituents are products of oligomerisation after fraction 2.

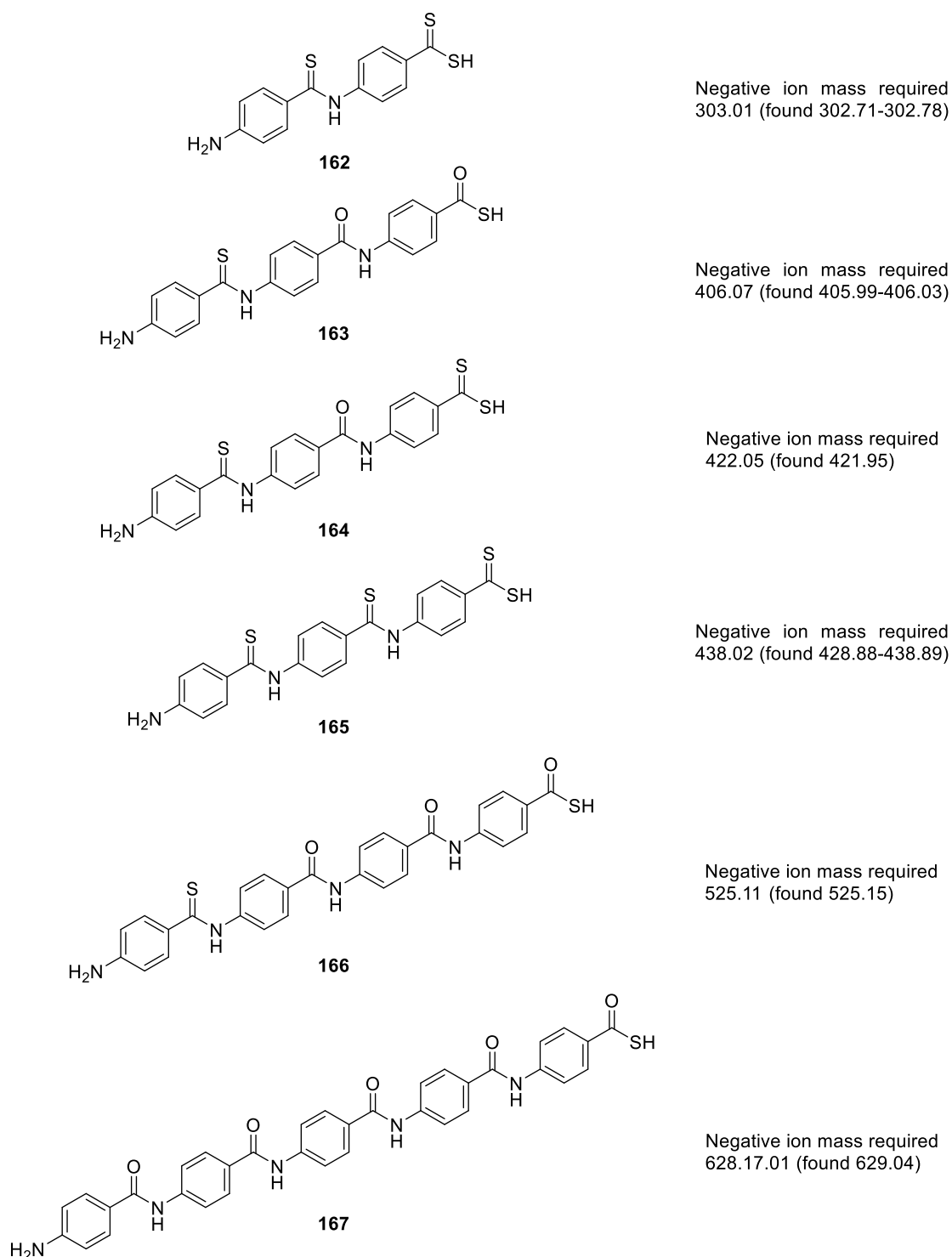


Figure 61. Suspected products of degradation of compound **131** from reverse-phase column chromatography fractions 15-19.

Due to the extremely similar proton environments of the different oligomers, the ^1H NMR spectra were not useful for structure determination. The proton NMR spectra did however all show characteristic symmetrical doublet peaks

as expected for the symmetrical phenyl ring structure of **131** oligomers, so this does lend some further evidence towards the hypothesised structures.

Because of the machine time required for wide-field ^{13}C NMR acquisition these were not obtained for the oligomers in order to determine whether the dithiocarbonyl carbon peak was present for these fractions.

Whilst these results may not be completely representative of all aryl dithiocarboxylate compounds, they do infer an explanation of the poor stability of these compounds: that the dithiocarbonyl carbon is highly susceptible to nucleophilic attack.

3.4 The mass difference problem

Throughout this work, with the exception of the work on the synthesis of cyclic boronates, sulphur has been a major feature of the compounds made. The design has been focused upon a sulphur containing warhead to be the primary moiety in the inhibition of the active site of the targeted metalloenzymes.

However in multiple compounds a discrepancy has appeared in HRMS analysis of these compounds. For three separate compounds, with unrelated synthetic routes, the mass that was found is approximately 2 ppm different from that which is expected (*Fig. 62*).

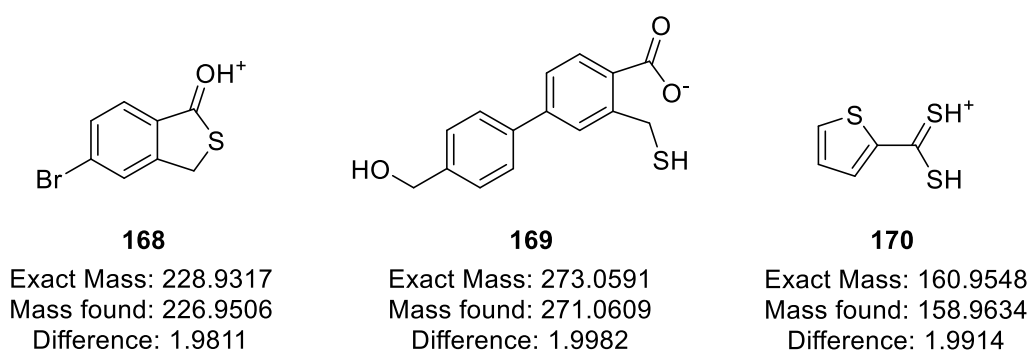


Figure 62. The three sulphur containing compounds displaying the mass discrepancy on the same HRMS machine, with their expected mass ions and the mass found. The difference between the mass needed and mass found is similar (< 0.02 ppm) in all cases.

Repeated attempts to obtain the expected mass ion *via* HRMS were unsuccessful. Thus far, it has not been possible to explain this discrepancy

despite attempts to reconcile the displayed masses with possible differences in structure, whilst maintaining coherence with other analytical results.

It has also not been possible to find other examples of this discrepancy within the literature. Therefore it seems appropriate to note this unexpected result in the synthesis of these compounds and to recommend further investigation of this in future work.

Chapter 4

Conclusions & Future Work

4.1 General conclusions

The research described in this thesis has involved an investigation into the potential of known metal-binding functionalities as to their viability in metalloenzyme-targeting drug design. It has also explored little known metal-binding moieties in an attempt to introduce them to the repertoire of “tools” that a medicinal chemist has available when designing novel metal-binding inhibitors.

For the purposes of this investigation the targets chosen were B1 MBLs, namely VIM-1, VIM-2, IMP-1 and NDM-1. These enzymes feature a dizinc active site and are all clinically relevant, making them appropriate choices. Another reason for this choice is access to a sensitive assay, which is essential for identification of weakly-binding fragments, as newly explored pharmacophores may be.

In silico design was used throughout to guide molecular design. Schrödinger Glide software is a powerful tool for predicting the potency of potential inhibitors and such methods are commonplace in modern drug design, owing to their ability to streamline and optimise the drug design pipeline when used effectively. KNIME was effectively used alongside Schrödinger software to enable the selection of desired structures from large libraries.

This work successfully extended the investigation of one class of previously identified inhibitor. It also identified a novel inhibitory moiety in MBLs, which showed comparable activity to a known inhibitor in all tested subtypes.

4.2 Thiol-based inhibitors

4.2.1 *In silico* design

Significant *in silico* design was used to develop thiol-based inhibitors designed to be more effective than those previously synthesised in the Fishwick group.

Through utilisation of previous inhibitory activity assays numerous model systems were built and compared to find that which best matched empirical evidence. These differed in the settings and arrangements of the computationally modelled enzymatic systems, culminating in a total of fourteen models being compared (these can be seen in *Table 2* in section **2.2.2.4**). These were statistically analysed using the coefficient of determination and Kendall rank correlation coefficient. That which scored a coefficient of determination value closest to 1 and a Kendall rank correlation coefficient closest to -1 was selected, using standard deviation to judge whether the difference in these values from those of other models was statistically significant. This model was then taken forward for use in molecular design.

Docking results showed that molecules featuring a polar terminal moiety were expected to show greater inhibition of the VIM-2 target structure. Therefore these particular molecules were the aim of synthesis. These additional results were intended to then be used to refine the docking model for future work.

4.2.2 Synthetic development of thiol-based inhibitors

Previously identified thiol-based inhibitors in the Fishwick group reported by Cain *et al.* showed inhibitory activity in MBLs comparable to known inhibitors (*i.e.* captopril), and so were an ideal point of further development¹⁵⁰. At the start of the project it was noted that none of these inhibitors featured polar moieties on the R group attached *via* a Suzuki reaction (*Fig. 63*). This was especially poignant, as these functionalities were expected to enhance the activity of the inhibitors through interactions with polar residues in the active sites of those enzymes targeted.

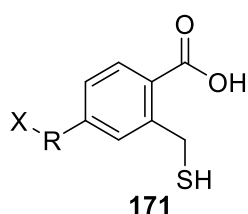


Figure 63. No compounds of this form were made in the original series by Cain, where R represents an aryl group and X represents a polar moiety that can interact with side-chains in enzymatic active sites for improved binding.

New synthetic routes were designed based on late-stage diversification of the series. The progress in these routes gave rise to development of a number of novel compounds featuring a thiolactone moiety. Unfortunately at the final stage of synthesis this particular route proved unworkable, despite thorough and repeated attempts *via* differing means.

Thus, further synthetic routes were developed. These routes sacrificed late-stage diversification but this was deemed ultimately necessary. However, it was seen that the installation of a chemical group bearing a terminal polar moiety on the desired portion of the molecule caused many reaction steps that were not expected to be troublesome to fail. As such, only one final compound in this series was successfully synthesised.

4.2.3 Biological results

Despite the expected binding of the one successfully synthesised molecule in this series (**4.2**, *Fig. 64*) to the target site the biological results were disappointing and far worse than expected from docking studies. Due to the small amount of **4.2** synthesised it was not possible to unequivocally confirm the structure of the tested target molecule. Therefore these results suggest that further investigation of using this compound class as effective inhibitors of MBLs, and in fact of metalloenzymes in general, is required.

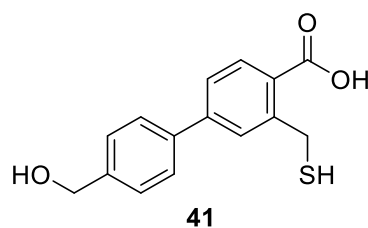


Figure 64. The structure of compound 4.2, the only successfully synthesised thiol-based inhibitor.

4.3 Dithiocarboxylates

4.3.1 Fragment validation

The dithiocarboxylate moiety was successfully synthesised in its simplest aryl form, dithiobenzoic acid. To improve the stability of dithiobenzoic acid this was further transformed to its salt form, sodium dithiobenzoate (**153**, *Fig. 65*). When tested in four B1 MBL subtypes, VIM-1, VIM-2, IMP-1 and NDM-1, **153**

showed inhibition comparable to a known inhibitor, captopril. Due to this effective inhibition it was decided to further extend this series to further investigate the dithiocarboxylate group as an effective moiety for metalloenzyme inhibition.

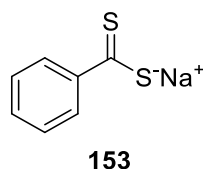


Figure 65. The structure of **153**, the first and simplest aryl dithiocarboxylate salt compounds made.

4.3.2 Synthetic development

A short synthetic route was chosen to ensure synthesis was a simple and quick process. This was eventually shortened even further through purchasing pre-made Grignard reagents, as generation of Grignard reagents had proved difficult with some substrates.

The main development of the synthesis for these compounds was in the rapid purification and isolation. On many substrates the dithiocarboxylate moiety proved very fragile. Additionally work-up conditions that worked for one substrate would often need to be changed when performing the same reaction on a different substrate, meaning constant innovation was required. There was also an intolerance to column chromatography for the dithiocarboxylate group on some substrates. The culmination of all this resulted in synthesis being more time-consuming than expected. As such, synthesis resulted in the production of six final compounds.

4.3.3 *In silico* design for further elaboration of the series

Docking studies were initially done in a VIM-2 crystal structure (PDB ID: 5K48) looking at the binding of simple fragments. The previous thiol-based ligands were used as a guide since they bore some similarity to the newly envisaged dithiocarboxylates. Active site coordination was observed and docking poses appeared similar to those of the crystal structure ligand. As the crystal structure ligand featured a thiol moiety, which is somewhat similar to the dithiocarboxylate moiety, this gave confidence in the docking poses. Thus once biological activity of the initial fragment was seen, docking studies were extended to explore different substrate structures.

Due to the entirely novel nature of these compounds when applied to MBLs, as well as the recondite nature of their synthetic tractability and stability, it was decided that design would be more focused on a broad selection of substrates.

As such, digital libraries of available Grignard reagents were requested from major manufacturers. Fluorochem was able to provide these. KNIME workflow software was used with RDKit and Schrödinger Maestro nodes to complete a virtual reaction of these Grignard reagents to the target dithiocarboxylic acid bearing molecules, followed by subsequent docking into MBL crystal structure grids. This informed the choice of selected materials to be purchased once further filtered for variety and cost. This large-scale docking based approach proved as an effective tool for the use of commercial compound libraries.

4.3.4 Biological activity

The first compound assayed, sodium dithiobenzoate (**153**, *Fig. 66*), yielded very successful results in all four B1 MBL subtypes tested. Comparable inhibition to captopril, a known inhibitor of these enzymes, was seen. This was further supported with the results of testing of sodium {3'-chloro-[1,1'-biphenyl]-3-carbothioyl}sulfanide (**126**, *Fig. 66*), which showed similar inhibition to **153** despite lower purity.

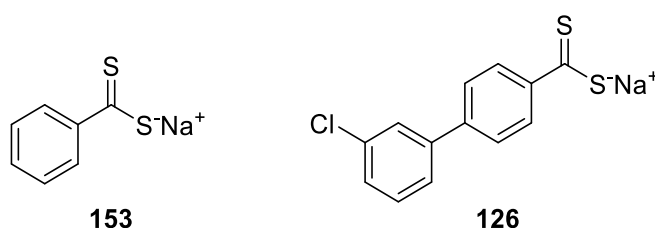


*Figure 66. Compounds **153** and **126** showed effective inhibition in MBLs, comparable to known inhibitor captopril.*

The compounds sent for the second round of assay testing showed inhibition lower than that which was expected from the IC₅₀ results seen in first round of testing. This is mostly attributed to the degradation of these compounds. However, there was some useful information gained from these assays. Firstly, the lower IC₅₀ results of **153** in the second assay provides evidence that dithiocarboxylate degradation products do not inhibit B1 MBLs, or at least inhibit them much more poorly than **153** itself. Secondly, results for **126** were

even better than seen in the first round of assays, which indicates that this compound may be a suitable for further synthetic elaboration.

4.3.5 Stability & degradation

These compounds have been seen to degrade in a multitude of ways. Whilst there seems to be some hypotheses on how the substrate affects this degradation there is little evidence to lend any unequivocal support. It has proved immensely difficult to purify and isolate these compounds. It has also been seen that they will degrade in a nitrogen atmosphere at a low temperature. Hopefully the data gained in these endeavours will contribute to further elucidation of the stability of this potentially powerful functional group.

The main source of degradation seen in these studies was *via* nucleophilic attack of the dithiocarbonyl, be that by an external source or another molecule of the same compound. Large oligomers were seen in the analysis of degradation products of **131** (Fig. 67).

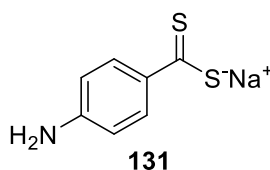


Figure 67. The structure of compound **131**, which was used for degradation studies of dithiocarboxylate salts. It was found oligomers of this compound readily formed.

4.4 Future work

4.4.1 Thiol-based inhibitors

The investigation into these compounds by this work has elucidated two main points: 1) synthesis of thiol-based inhibitors bearing a substrate featuring an addition terminal polar moiety is not trivial; 2) these inhibitors may not be as potent as expected from docking studies.

Therefore a complete synthetic route redesign is recommended for any future investigation of these compounds. The current route has been thoroughly investigated through a variety of different permutations and has been found lacking in every case. Therefore it does not seem prudent to recommend continuing with this series until a more productive route is discovered.

4.4.2 Dithiocarboxylates

The data gained through the enzymatic assays of these compounds is encouraging for the development of a series of MBL inhibiting compounds. The activity of a fragment that rivals known inhibitors provides a basis for the use of the dithiocarboxylate moiety as a “warhead” in the design of future metalloenzyme inhibitors.

The second round of biology assays showed **126** to be the best candidate compound to follow up on. It also provided further evidence that dithiocarboxylate degradation products do not inhibit B1 MBLs.

Unfortunately synthesis of these compounds is thoroughly challenging, due to the fragility of the dithiocarboxylate moiety itself. This stability appears to be extremely substrate dependent, so the exploration of various structures to discover which proves to be the most stable would be a valuable endeavour to aid the further use of this group in medicinal chemistry.

Immediate recommendations for further exploration of this group would be to test the most simple aryl fragment, sodium dithiobenzoate (**153**), in other metalloenzyme targets, be these other MBLs or entirely different targets.

Prior to synthetic elaboration of these compounds into drug-like molecules it is essential that further studies to explain and tune the stability of the dithiocarboxylate moiety be conducted.

Chapter 5

Experimental

General information

Computational

All computational work involving Schrödinger software was completed in the Schrödinger Maestro GUI. Preparation of ligands for docking was performed using the Schrödinger LigPrep module, using the following settings: OPLS3e or OPLS4 forcefields (noted in text); generating possible states at target pH 7.0 ± 2.0 ; adding metal binding states *via* Schrödinger Epik; all other settings were set to their default state. The A chain was selected and used for all imported proteins. Protein preparation was performed *via* the Schrödinger Protein Preparation Wizard, using the default settings; all waters were removed from the crystal structures used unless otherwise noted. Grid generation was performed *via* Schrödinger Receptor Grid Generation using the default settings; no constraints were used unless noted in the text; rotatable groups were enabled for all residues immediately flanking the active site pocket. Unless denoted in the text, computational docking was performed using the Schrödinger Glide software package, using the following settings: XP (extra precision); add Epik state penalties to docking scores; perform post-docking minimization (number of poses per ligand to include: 10, threshold for rejecting minimized pose: 0.50 kcal/mol); all other settings were set to their default state. All poses were examined within the Schrödinger Maestro GUI. PyMOL was used for the generation of images.

Synthetic chemistry

All solvents and reagents were obtained from commercial suppliers and used without further purification. Solvents used were HPLC or analytical grade. Thin layer chromatography was performed on aluminium backed silica gel supplied by Merck, visualised using an ultraviolet lamp. Normal-phase flash-column chromatography was performed using silica gel 60 (40-63 μm particles). Automated normal-phase flash-column chromatography was performed on a Biotage® Isolera™ One machine using Biotage® Sfär columns of varying

sizes between 5 g and 100 g. Automated reverse-phase flash-column chromatography was performed using C18 silica columns. Microwave syntheses were performed using an Anton Parr Monowave 50 reactor. Hydrogen and carbon NMR data were collected on a Bruker Avance III 500. All shifts were recorded against an internal standard of tetramethyl silane. Solvents used for NMR (chloroform-*d*, methanol-*d*₄ and DMSO-*d*₆) were obtained from Sigma-Aldrich. ¹H NMR data is reported in the following format: ppm (splitting pattern, coupling constant (Hz), number of protons, proton assignment). Signal assignments were deduced with the aid of TopSpin, MestReNova, DEPT 135, COSY, HSQC and HMBC. LC-MS (liquid chromatography-mass spectrometry) data were recorded on a Donex Ultimate 3000 LC system with a MeCN/H₂O +0.1% formic acid gradient. HRMS data were recorded using a Bruker MaXis impact spectrometer using electron spray ionisation. Infrared spectra were recorded on a Perkin-Elmer one FTIR spectrometer.

Biology

The inhibitory activity of compounds against representative B1 subfamily MBLs [obtained according to previously reported production and purification procedures: VIM-1²¹⁴, VIM-2, NDM-1 and IMP-1²¹⁵] was determined using a fluorogenic assay monitoring the enzymatic breakdown of the cephalosporin probe FC5²¹⁵. The FC5/meropenem assays were conducted at room temperature in clear-bottomed Greiner 384 black well microplates (FC5) or Greiner 96 well UV star microplates (meropenem), using a ClarioStar or PHERAstar FS microplate reader (BMG LabTech). Representative β-lactamases were tested at the following concentrations: VIM-1, 100 pM; NDM-1, 20 pM; IMP-1, 20 pM; and VIM-2, 500 pM. The concentration of FC5 employed was 5 μM for all enzymes. IMP-1, VIM-1, VIM-2 and NDM-1 inhibition assays were screened in “MBL buffer” (50 mM HEPES, pH 7.2, 1 μM ZnSO₄, 1 μg mL⁻¹ BSA, 0.01% v/v Triton X-100). The initial rates of reaction (measured after 10 min pre-incubation of the NSPC with the enzyme) were assessed by monitoring the fluorescence intensity at λ_{ex} = 380 nm and λ_{em} = 460 nm. Following the determination of initial rates of reaction, the data were fitted using a four-parameter function: log (inhibitor) vs. response,

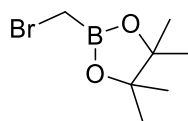
variable slope in GraphPad Prism 6 to obtain IC₅₀ values^{81,215}. These assays were conducted by Dr Karina Calvopina at the University of Oxford²⁰².

Experimental notes

The compounds in this section are denoted by their compound name in the form **RHX**, where X is a number. This numbering represents the compound codes in the laboratory documents that accompany this work. For those compounds listed in the experimental section that are also noted in the manuscript, the corresponding compound number as referenced in the manuscript will be noted in the compound title in brackets. The compounds have been ordered according to their laboratory compound code.

The inclusion of novel compounds lacking complete characterisation and unequivocal identification was ultimately rationalised with the belief that the analysis and characterisation provided could be of use to future scientists should further enterprise be deemed worthwhile. These compounds are denoted with a *.

RH1 (4) - 2-(Bromomethyl)-4,4,5,5-tetramethyl-1,3,2-dioxaborolane¹⁵²



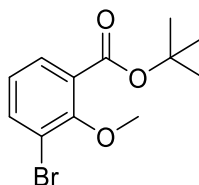
n-Butyllithium (1.60 M in *n*-hexane, 28.1 mL, 4.50 mmol) was added to a solution of dibromomethane (3.86 mL, 5.50 mmol) and triisopropyl borate (11.5 mL, 5.00 mmol) in dry THF (20 mL) under nitrogen at -100 °C over 1 hr. The solution was stirred at -100 °C for a further 1 hr then allowed to reach RT. Methanesulfonic acid (4.17 mL, 4.50 mmol) was added to the solution at 0 °C and the solution was stirred for 1 hr. Pinacol (5.32 g, 4.50 mmol) was added to the solution at 0 °C and the solution was stirred for 16 hrs, being allowed to reach RT. The crude product was purified *via* vacuum distillation to afford the title compound as a colourless oil.

Yield: 8.82 g, 39.9 mmol, 73%

¹H NMR (400 MHz, CDCl₃): 2.59 (s, 2H, CH₂), 1.29 (s, 12H, CH₃)

Data consistent with literature values¹⁵².

RH2 (6) - *Tert*-butyl 3-bromo-2-methoxybenzoate¹⁵²



3-Bromo-2-methoxybenzoic acid (1.00 g, 4.33 mmol) was dissolved in DCM (20 mL), then oxalyl chloride (3.00 mL, 35.5 mmol) and DMF (cat., 4 drops) were added. The solution was stirred for 2 hrs at RT and then concentrated *in vacuo*. The concentrated solution was dissolved in *tert*-butanol (20 mL) and stirred at 80 °C for 48 hrs. The solution was concentrated and then dry-loaded onto a column, then purified *via* normal-phase flash-column chromatography (petrol/ethyl acetate), affording the title compound as a colourless oil.

Yield: 801 mg, 2.79 mmol, 64%

R_f: 0.85 (4:1, Petrol/EtOAc)

¹H NMR (400 MHz, CDCl₃): 7.66 (dd, *J* 7.9 & 1.9, 2H, 4/6-H), 7.01 (t, *J* 7.9, 1H, 5-H), 3.92 (s, 3H, 1-H), 1.60 (s, 9H, 2-CH₃)

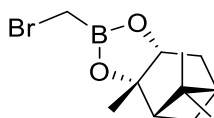
¹³C NMR (100 MHz, CDCl₃): 165.0, 156.4, 136.7, 130.5, 129.2, 125.1, 119.1, 82.3, 62.2, 28.4

IR: ν_{max} /cm⁻¹: 2978, 2940, 1720

m/z (ES): Found: MNa⁺ 309.0097; C₁₂H₁₅BrO₃ requires MNa⁺ 309.0097

Data consistent with literature values¹⁵².

RH3 (5) - (1S,2S,6R,8S)-4-(bromomethyl)-2,9,9-trimethyl-3,5-dioxaboratricyclo[6.1.1.0^{2,6}]decane¹⁵²



2-(Bromomethyl)-4,4,5,5-tetramethyl-1,3,2-dioxaborolane (6.32 g, 28.6 mmol) and (+)-pinanediol (14.6 g, 85.8 mmol) were dissolved in THF (25 mL) and stirred at RT for 48 hrs. The solution was concentrated and redissolved in ethyl acetate (25 mL) then washed with water (25 mL). The aqueous layer was extracted with ethyl acetate and the organic layers were combined and concentrated. The organics were dry loaded onto a column and purified *via* normal-phase flash-column chromatography (petrol/ethyl acetate) to give the title compound as a colourless oil.

Yield: 6.32 g, 23.2 mmol, 81%

R_f: 0.54 (19:1, Petrol/EtOAc)

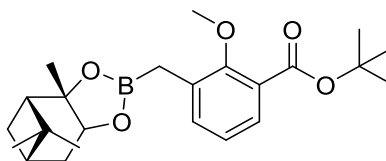
¹H NMR (400 MHz, CDCl₃): 4.37 (dd, *J* 9.1 & 1.9, 1H, 6-H), 2.63 (s, 2H, CH₂Br), 2.30 (m, 2H, 7ax.-H & 10ax.-H), 2.08 (t, *J* 5.2, 1H, 1-H), 1.92 (t, *J* 2.5, 1H, 7eq.-H), 1.91 (dt, 1H, 8-H), 1.42 (s, 3H, 2-CH₃), 1.29 (s, 3H, 9ax.-CH₃), 1.20 (d, *J* 10.9, 1H, 10eq.-H), 0.84 (s, 3H, 9eq.-CH₃)

¹³C NMR (100 MHz, CDCl₃): 87.1, 78.9, 51.4, 39.6, 38.4, 35.4, 28.6, 27.2, 26.5, 24.2

IR: ν_{max} /cm⁻¹: 2971, 2919, 2871

Data consistent with literature values¹⁵².

RH5 (7) - *Tert*-butyl 2-methoxy-3-[[[(1*R*,6*S*,8*R*)-6,9,9-trimethyl-3,5-dioxa-4-boratricyclo[6.1.1.0^{2,6}]decan-4-yl]methyl]benzoate¹⁵²



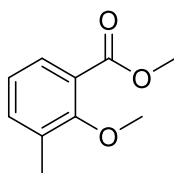
Tert-butyl 3-bromo-2-methoxybenzoate (100 mg, 0.35 mmol) and (1*S*,2*S*,6*R*,8*S*)-4-(bromomethyl)-2,9,9-trimethyl-3,5-dioxa-4-boratricyclo[6.1.1.0^{2,6}]decane (115 mg, 0.42 mmol) were dissolved in THF (10 ml) and the solution was cooled to -100 °C. *n*-Butyllithium (1.6 M, 0.54 ml, 0.86 mmol) was added dropwise over 1 hour and the solution was stirred for 72 hours, being allowed to reach RT. The solution was concentrated *in vacuo*, water (5 mL) was added and extracted with DCM (3x 5 mL). The organic layers were combined and dried (MgSO₄) then concentrated *in vacuo* to afford an amber oil. This was purified *via* normal-phase flash-column chromatography to give the title compound as an amber oil.

Yield: 20 mg, 0.05 mmol, 14%

*R*_f: 0.50 (DCM)

LC-MS (ES): Found: MK⁺ 439.26 - 439.27; C₂₃H₃₃BO₅ requires MK⁺ 439.21

RH7 - Methyl 2-methoxy-3-methylbenzoate



3-Methyl salicylic acid (1.00 g, 6.57 mmol) and potassium carbonate (3.63 g, 26.3 mmol) were dissolved in acetone (100 mL) and dimethyl sulphate (2.73 mL, 26.3 mmol) was added. The solution was stirred at 60 °C for 16 hrs. The solution was allowed to cool to RT and the solvent was removed *in vacuo*. The residue was redissolved in water (100 mL) and extracted with ethyl acetate (3 x 50 mL). The organics were combined and washed with water (50 mL) and brine (2 x 20 mL), then dried (MgSO₄) and concentrated *in vacuo*. The product was purified *via* normal-phase flash-column chromatography, affording the title compound as a colourless oil.

Yield: 1.18 g, 6.52 mmol, 99%

R_f: 0.29 (4:1, Petrol/EtOAc)

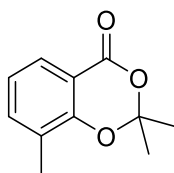
¹H NMR (400 MHz, CDCl₃): 7.63 (d, *J* 7.7, 1H, 4-H), 7.34 (d, *J* 7.4, 1H, 6-H), 7.05 (t, *J* 7.7, 1H, 5-H), 3.91 (s, 3H, 1-CO₂CH₃), 3.83 (s, 3H, 2-OCH₃), 2.32 (s, 3H, 3-CH₃)

¹³C NMR (100 MHz, CDCl₃): 167.1, 158.6, 135.3, 132.9, 129.3, 124.8, 123.7, 61.7, 52.3, 16.2

IR: $\nu_{\max}/\text{cm}^{-1}$: 2950, 1725, 1591

m/z (ES): Found: MNa⁺ 203.0679; C₁₀H₁₂O₃ requires MNa⁺ 203.0679

RH8 (11) - 2,2,8-Trimethyl-2,4-dihydro-1,3-benzodioxin-4-one



3-Methyl salicylic acid (1.00 g, 6.57 mmol) was dissolved in TFA (4 mL) and stirred, then acetone (3.00 mL, 32.9 mmol) in TFAA (3 mL) was added at 0 °C. The solution was stirred overnight at RT. Toluene (20 mL) was added to the solution and it was concentrated *in vacuo*. The residue was dissolved in ethyl acetate (20 mL) and sodium bicarbonate (20 mL), then extracted with ethyl acetate (3 x 20 mL). The organics were combined and dried (MgSO₄), filtered and concentrated *in vacuo*. The product was purified *via* normal-phase flash-column chromatography, affording the title compound as a translucent brown oil which formed a translucent brown crystal when left overnight.

Yield: 980 mg, 5.10 mmol, 78%

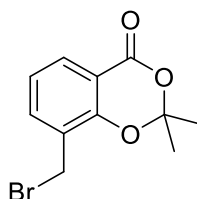
¹H NMR (400 MHz, CDCl₃): 7.79 (d, *J* 7.7, 1H, 7-**H**), 7.39 (d, *J* 7.5, 1H, 6-**H**), 7.00 (t, *J* 7.6, 1H, 5-**H**), 2.22 (s, 3H, 8-**CH**₃), 1.73 (s, 6H, 2-**CH**₃)

¹³C NMR (100 MHz, CDCl₃): 161.7, 154.4, 137.5, 127.3, 126.9, 122.2, 113.4, 106.2, 26.1, 15.2

IR: $\nu_{\max}/\text{cm}^{-1}$: 3005, 2993, 2950, 1725, 1688, 1596

m/z (ES): Found: MH⁺ 193.0859; C₁₁H₁₂O₃ requires MH⁺ 193.0859

RH9 (12) – 8-(Bromomethyl)-2,2-dimethyl-2,4-dihydro-1,3-benzodioxin-4-one



2,2,8-Trimethyl-2,4-dihydro-1,3-benzodioxin-4-one (4.48 g, 23.3 mmol), *N*-bromosuccinimide (4.56 g, 25.6 mmol), and benzyl peroxide (395 mg, 1.63 mmol) were dissolved in acetonitrile (60 mL). The solution was stirred at 80 °C for 3 hrs, then allowed to cool to RT. The solution was diluted with diethyl ether (30 mL), then washed with water (2 x 30 mL) and brine (30 mL). The organics were combined and dried (MgSO₄), filtered and concentrated *in vacuo*. The crude product was recrystallised from ethanol, affording the title compound as colourless rectangular crystals.

Yield: 3.51 g, 12.9 mmol, 56%

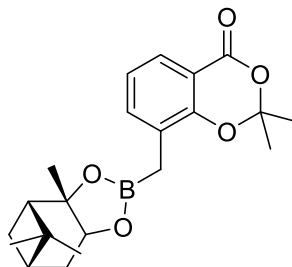
¹H NMR (400 MHz, CDCl₃): 7.93 (dd, *J* 7.8 & 1.5, 1H, 7-H), 7.59 (dd, *J* 7.6 & 1.4, 1H, 6-H), 7.09 (t, *J* 7.7, 1H, 5-H), 4.48 (s, 2H, CH₂Br), 1.78 (s, 6H, 2-CH₃)

¹³C NMR (100 MHz, CDCl₃): 160.8, 154.3, 137.2, 130.4, 126.9, 122.7, 114.4, 107.1, 26.3, 26.1

IR: $\nu_{\max}/\text{cm}^{-1}$: 3036, 2991, 2943, 1730, 1597

m/z (ES): Found: MNa⁺ 292.9784; C₁₁H₁₂O₃ requires MNa⁺ 292.9784

RH10 (13) - 2,2-dimethyl-8-[[[(1*S*,2*S*,8*S*)-2,9,9-trimethyl-3,5-dioxa-4-boratricyclo[6.1.1.0^{2,6}]decan-4-yl]methyl]-2,4-dihydro-1,3-benzodioxin-4-one



8-(Bromomethyl)-2,2-dimethyl-2,4-dihydro-1,3-benzodioxin-4-one (1.08 g, 4.00 mmol), bis[(+)-pinanediolato]diboron (1.72 g, 4.80 mmol) and potassium acetate (1.57 g, 4.00 mmol) were dissolved in 1,4-dioxane (15 mL) and the solution was degassed with argon for 15 mins. Bis(triphenylphosphine)palladium(II) dichloride (160 mg, 0.22 mmol) was added to the solution and the reaction mixture was degassed with argon for a further 30 mins. The solution was heated to reflux and stirred overnight under argon, then allowed to cool to room temperature and concentrated *in vacuo*, aided by azeotroping with ethyl acetate (22.5 mL). The residue was redissolved in ethyl acetate (25 mL) and filtered through celite. The filtrate was then concentrated and purified *via* automated normal-phase flash-column chromatography. The appropriate fractions were combined and concentrated under reduced pressure, affording the title compound as a colourless oil.

Yield: 1.38 g, 3.73 mmol, 93%

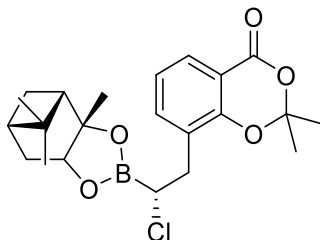
¹H NMR (400 MHz, CDCl₃): 7.74 (dd, *J* 7.8 & 1.6, 1H, 7-H), 7.39 (dd, *J* 7.5 & 1.6, 1H, 6-H), 6.98 (t, *J* 7.6, 1H, 5-H), 4.24 (dd, *J* 8.7 & 1.9, 1H, 6'-H), 2.28 (m, 1H, 7'ax.-H), 2.18 (m, 1H, 10ax.-H), 2.00 (t, *J* 5.8, 1H, 1'-H), 1.88 (m, 1H, 8'-H), 1.78 (ddd, *J* 14.7, 3.4 & 1.9, 1H, 7'eq.-H), 1.70 (d, *J* 6.8, 6H, 2-CH₃), 1.55 (s, 2H, ArCH₂), 1.35 (s, 3H, 2-CH₃), 1.25 (s, 3H, 9ax.-H), 1.11 (d, *J* 10.8, 1H, 10eq.-H), 0.80 (s, 3H, 9eq.-H)

¹³C NMR (100 MHz, CDCl₃): 161.8, 153.9, 137.1, 128.3, 126.6, 122.3, 113.4, 106.2, 86.1, 78.1, 51.4, 39.5, 38.3, 35.5, 28.8, 27.2, 26.5, 26.2, 25.9, 24.1

IR: ν_{max} /cm⁻¹: 2919, 2872, 1736, 1597

m/z (ES): Found: MH⁺ 371.2024; C₂₁H₂₇BO₅ requires MH⁺ 371.2024

RH11 (14) - 8-[(2*R*)-2-chloro-2-[(1*S*,2*S*,8*S*)-2,9,9-trimethyl-3,5-dioxa-4-boratricyclo[6.1.1.0^{2,6}]decan-4-yl]ethyl]-2,2-dimethyl-2,4-dihydro-1,3-benzodioxin-4-one



DCM (1.24 mL, 19.3 mmol) was added to THF (20 mL) and *n*-butyllithium (2.50 M, 4.94 mL, 12.4 mmol) was added dropwise over the course of 30 mins at -100 °C. The solution was then left to stir at 100 °C for 1 hr, producing a colourless turbid solid. 2,2-dimethyl-8-[(1*S*,2*S*,8*S*)-2,9,9-trimethyl-3,5-dioxa-4-boratricyclo[6.1.1.0^{2,6}]decan-4-yl]methyl]-2,4-dihydro-1,3-benzodioxin-4-one (2.86 mL, 7.72 mmol) was dissolved in THF (10 mL) and added dropwise to the reaction mixture at -100 °C, causing the solution to turn yellow. The solution was stirred at -100 °C for 30 mins. ZnCl₂ (1.90 M, 3.25 mL, 6.18 mmol) was then added in one portion dropwise. The solution was left to stir for 16 hours, being allowed to reach RT. The solution was then cooled to 0 °C and NH₄Cl (77 mL) was added. The solution was then stirred at 0 °C for 30 mins. The organics were extracted with ethyl acetate (3 x 10 mL) and combined, then washed with brine and dried with MgSO₄. The solids were filtered off and the filtrate was concentrated and purified *via* automated normal-phase flash-column chromatography. The appropriate fractions were combined and concentrated under reduced pressure, affording the title compound as a pale yellow oil.

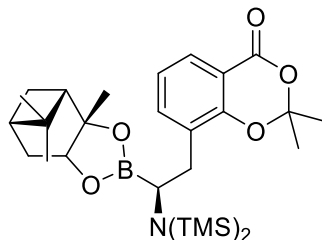
Yield: 1.28 g, 3.35 mmol, 43%

¹H NMR (400 MHz, CDCl₃): 7.87 (dd, *J* 7.8 & 1.7, 1H, 7-**H**), 7.49 (dd, *J* 7.5 & 1.6, 1H, 6-**H**), 7.05 (t, *J* 7.8, 1H, 5-**H**), 4.35 (dd, *J* 8.8 & 2.0, 1H, 6'-**H**), 3.71 (m, 1H, ClCH), 3.15 (m, 2H, ArCH₂), 2.35 (m, 2H, 7'**ax.-H**), 2.06 (t, *J* 5.5, 1'-**H**), 1.91 (m, 1H, 8'-**H**), 1.86 (ddd, *J* 14.7 & 3.3 & 2.0, 1H, 7'**eq.-H**), 1.75 (d, *J* 1.7, 6H, 2'-CH₃), 1.29 (s, 2H, 9**ax.-H**), 1.06 (d, *J* 11.2, 1H, 10**eq.-H**), 0.83 (s, 3H, 9**eq.-H**)

^{13}C NMR (100 MHz, CDCl_3): 161.4, 154.5, 137.9, 128.6, 127.3, 122.3, 113.8, 106.6, 87.2, 78.9, 51.3, 39.5, 38.5, 35.3, 34.1, 28.6, 26.5, 26.2, 26.1, 24.2

LC-MS (ES): Found: MH^+ 419.1 - 419.2; $\text{C}_{22}\text{H}_{28}\text{BClO}_5$ requires MH^+ 419.1791

RH12 (15) - 8-[(2S)-2-[bis(trimethylsilyl)amino]-2-[(1S,2S,8S)-2,9,9-trimethyl-3,5-dioxa-4-boratricyclo[6.1.1.0^{2,6}]decan-4-yl]ethyl]-2,2-dimethyl-1,3-benzodioxin-4-one*

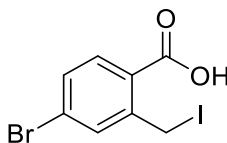


8-[(2R)-2-chloro-2-[(1S,2S,8S)-2,9,9-trimethyl-3,5-dioxa-4-boratricyclo[6.1.1.0^{2,6}]decan-4-yl]ethyl]-2,2-dimethyl-2,4-dihydro-1,3-benzodioxin-4-one (195 mg, 0.46 mmol) was dissolved in dry THF (7 mL) under nitrogen. The solution was cooled to -100 °C and LiHMDS (1M, 0.33 mL, 33 mmol) was added dropwise. The solution was stirred for 16 hrs, being allowed to reach RT. The solution was concentrated *in vacuo* and partially redissolved in hexane (20 mL). The solid were removed in celite *via* vacuum filtration and washed with hexane (2x 20 mL). The filtrate was collected and concentrated *in vacuo*, yielding a pale yellow oil. This was carried forward crude, due to instability.

Yield: 93 mg (crude)

LC-MS (ES): Found: MH⁺ 399.9 - 400.0; C₂₂H₃₀BNO₅ requires MH⁺ 400.2290

RH15 (80) – 4-Bromo-2-(iodomethyl)benzoic acid¹⁵²



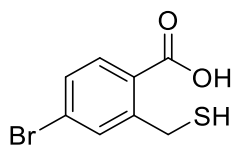
5-Bromophthalide (2.00 g, 9.40 mmol) was dissolved in DCM (50 mL), stirred and heated to 40 °C. Iodotrimethylsilane (2.50 mL, 14.1 mmol) was gradually added and the solution was stirred at 40 °C for 18 hrs. Water was added and a colourless solid precipitated out, which was isolated *via* hot filtration. The colourless solid was purified *via* automated normal-phase flash-column chromatography. The appropriate fractions were combined and concentrated under reduced pressure, affording the title compound as a colourless solid. The compound was carried forward to the next step crude.

Yield: 1.90 g, 5.57 mmol, 59%

R_f: 0.17 (1:1, Petrol/EtOAc)

¹H NMR (600 MHz, (CD₃)₂CO): 7.93 (d, *J* 8.5, 1H, 6-H), 7.78 (d, *J* 2.0, 1H, 5-H), 7.60 (dd, *J* 8.4 & 2.1, 1H, 3-H), 5.07 (s, 2H, 2-CH₂)

RH16 (81) – 4-Bromo-2-(sulfanylmethyl)benzoic acid¹⁵²



Thiourea (56.0 mg, 0.86 mmol) was dissolved in THF (3 mL), stirred and the resulting solution was heated to reflux. 4-Bromo-2-(iodomethyl)benzoic acid (250 mg, 0.78 mmol) was added and the solution was mixed for 16 hrs. The solution was allowed to cool and solvent was removed. The solid residue was redissolved in aqueous sodium hydroxide solution (2 M, 10 mL) and stirred at reflux for 2 hrs. The solution was allowed to cool and then acidified to pH 2 using aqueous hydrochloric acid solution (2 M) dropwise, causing a colourless solid to precipitate out. The solid was collected *via* vacuum filtration.

Yield: 70.0 mg, 0.28 mmol, 36%

R_f: Baseline (1:1, Petrol/EtOAc)

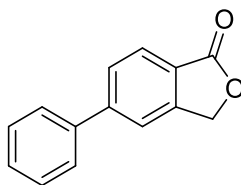
¹H NMR (500 MHz, (CD₃)₂SO): 13.28 (s, 1H, 1-COOH), 7.81 (d, *J* 8.4, 1H, 6-H), 7.74 (d, *J* 2.1, 1H, 3-H), 7.59 (dd, *J* 8.4 & 2.1, 1H, 5-H), 4.06 (d, *J* 8.5, 2H, 2-CH₂), 2.92 (t, *J* 8.5, 1H, SH)

¹³C NMR (125MHz, (CD₃)₂SO): 167.5, 146.1, 133.2, 132.7, 129.9, 128.3, 125.6, 25.7

m/z (ES): Found: M⁻ 244.9258; C₈H₇BrO₂S requires M⁻ 244.9277

Data consistent with literature values¹⁵².

RH19 (82) - 5-Phenyl-1,3-dihydro-2-benzofuran-1-one¹⁵²



5-Bromophthalide (2.00 g, 9.4 mmol), phenylboronic acid (1.26 g, 10.3 mmol), potassium carbonate (3.90 g, 28.6 mmol) and palladium tetrakis (580 mg, 0.5 mmol) were put in an RBF which was then argon flushed. Degassed dry THF was added to the RBF containing solids and the solution was stirred at reflux under argon for 16 hours. The solution was allowed to cool to RT and the solids were removed with celite then washed with water. The filtrate was collected and concentrated *in vacuo*, then purified *via* automated normal phase column chromatography (0 – 50% EtOAc in petrol), affording the product as a cream coloured powder.

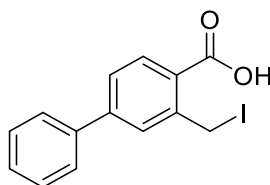
Yield: 590 mg, 2.80 mmol, 30%

¹H NMR (500 MHz, (CD₃)₂SO): 8.00 (s, 1H, 7-H), 7.96 (d, 1H, *J* 8.1, 6-H), 7.92 (d, 1H, *J* 8.1, 4-H), 7.80 (d, 2H, *J* 7.7, 3'/5'-H), 7.57 (t, 2H, *J* 7.7, 2'/6'-H), 7.50 (t, 1H, *J* 7.3, 4'-H), 5.51 (s, 2H, CH₂)

¹³C NMR (125MHz, (CD₃)₂SO): 168.6, 145.6, 143.9, 139.9, 131.5, 129.6, 128.6, 127.5, 127.3, 125.4, 125.0, 61.7

LC-MS (ES): Found: MH⁺ 210.7; C₁₄H₁₀O₂ requires MH⁺ 211.0754

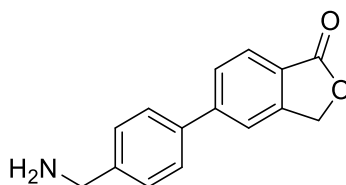
RH20 (83) - 3-(Iodomethyl)-[1,1'-biphenyl]-4-carboxylic acid¹⁵²



5-Bromophthalide (590 mg, 2.81 mmol) was dissolved in DCM (5 mL), stirred and heated to 40 °C. Iodotrimethylsilane (0.60 mL, 4.21 mmol) was gradually added and the solution was stirred at 40 °C for 18 hrs. Water was added and a colourless solid precipitated out, which was isolated *via* hot filtration. The colourless solid was purified *via* automated normal-phase flash-column chromatography. The appropriate fractions were combined and concentrated under reduced pressure, affording the title compound as an off-white solid. The compound was immediately carried forward to the next step crude.

Yield: 774 mg (crude)

RH21 (91) - 5-[4-(Aminomethyl)phenyl]-1,3-dihydro-2-benzofuran-1-one



Triethylamine (0.33 mL, 2.35 mmol) was added to ethanol (5 mL) and the solution was degassed with nitrogen for 30 mins. 5-Bromophthalide (100 mg, 0.47 mmol), 4-aminobenzylboronic acid hydrochloride salt (88.0 mg, 0.47 mmol) and bis(triphenylphosphine)palladium(II) dichloride (35.0 mg, 0.05 mmol) were placed in an RBF and this was flushed with nitrogen for 30 mins. The solution was added to the solids and the mixture was heated and stirred under nitrogen for 16 hrs. The solution was allowed to cool to RT. DCM and methanol were added to dissolve the precipitate and the solution was filtered through celite, then washed with ethanol. The remaining ethanol was removed under reduced pressure and the compound was purified *via* automated reverse-phase flash-column chromatography. The appropriate fractions were combined and concentrated under reduced pressure, affording the title compound as a colourless solid.

Yield: 53.0 mg, 0.22 mmol, 47%

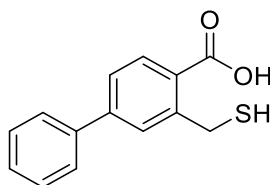
R_f: 0.73 (3:2, Petrol/EtOAc)

¹H NMR (500 MHz, (CD₃)₂SO): 8.02 (s, 1H, 7-H), 7.97 (d, J 8.0, 1H, 6-H), 7.93 (dd, J 8.0 & 1.3, 1H, 4-H), 7.82 (d, J 8.4, 2H, 3'/5'-H), 7.61 (d, J 8.4, 2H, 2'/6'-H), 5.51 (s, 2H, O-CH₂), 4.03 (s, 2H, NH₂-CH₂)

¹³C NMR (125 MHz, (CD₃)₂SO): 170.4, 165.0, 148.3, 145.5, 138.2, 138.1, 129.1, 127.7, 127.3, 125.4, 124.0, 120.9, 69.9, 42.9

m/z (ES): Found: MH⁺ 240.1019; C₁₅H₁₃NO₂ requires MH⁺ 240.1019

RH22 (29) - 3-(Sulfanylmethyl)-[1,1'-biphenyl]-4-carboxylic acid¹⁵²



Thiourea (192 mg, 2.52 mmol) was dissolved in THF (10 mL), stirred and the resulting solution was heated to reflux. 3-(Iodomethyl)-[1,1'-biphenyl]-4-carboxylic (774 mg, crude) was added and the solution was stirred for 16 hrs. The solution was allowed to cool and solvent was removed *in vacuo*. The solid residue was redissolved in aqueous sodium hydroxide solution (2 M, 10 mL) and stirred at reflux for 2 hrs. The solution was allowed to cool and then acidified to pH 2 using aqueous hydrochloric acid solution (2 M) dropwise, causing a colourless solid to precipitate out. The solid was collected *via* vacuum filtration.

Yield: Not obtained

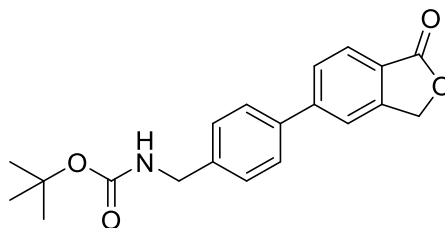
¹H NMR (500 MHz, (CD₃)₂SO): 7.98 (d, *J* 8.4, 1H, 5-H), 7.80 (d, *J* 2.1, 1H, 2-H), 7.77 (d, *J* 7.6, 2H, 3'/5'-H), 7.68 (dd, *J* 8.2 & 1.9, 1H, 6-H), 7.54 (t, *J* 7.8, 2H, 2'/6'-H), 7.46 (t, *J* 7.3, 1H, 4'-H), 4.16 (d, *J* 8.4, 2H, CH₂), 2.88 (t, *J* 8.4, 1H, SH)

¹³C NMR (125MHz, (CD₃)₂SO): 168.5, 144.9, 144.1, 139.2, 132.1, 129.5, 129.4, 128.8, 128.2, 127.4, 125.5, 26.9

LC-MS (ES): Found: M⁻ 242.4; C₁₄H₁₂O₂S requires M⁻ 243.0485

Data consistent with literature values.¹⁵²

RH24 (87) - Tert-butyl N-[[4-(1-oxo-1,3-dihydro-2-benzofuran-5-yl)phenyl]methyl]carbamate



Triethylamine (0.07 mL, 0.50 mmol) was added to ethanol (2.5 mL) and the solution was degassed with nitrogen for 30 mins. 5-Bromophthalide (43.0 mg, 0.20 mmol), 4-(Boc-aminomethyl)benzeneboronic acid (50.0 mg, 0.20 mmol) and bis(triphenylphosphine)palladium(II) dichloride (7.00 mg, 0.01 mmol) were placed in an RBF and this was flushed with nitrogen for 30 mins. The solution was added to the solids and the mixture was heated and stirred under nitrogen for 16 hrs. The solution was allowed to cool to RT. DCM was added to dissolve the precipitate and the solution was filtered through celite, then washed with water. The solution was dried and filtered under reduced pressure. The compound was purified *via* automated reverse-phase flash-column chromatography. The appropriate fractions were combined and concentrated under reduced pressure, affording the title compound as a colourless solid.

Yield: 39.0 mg, 0.11 mmol, 57%

R_f: 0.27 (3:2, Petrol/EtOAc)

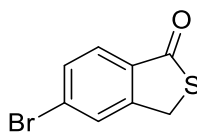
¹H NMR (500 MHz, CDCl₃): 7.95 (d, *J* 8.0, 1H, 7-H), 7.71 (d, *J* 8.0, 1H, 6-H), 7.64 (s, 1H, 4-H), 7.57 (d, *J* 8.1, 2H, 3'/5'-H), 7.40 (d, *J* 8.1, 2H, 2'/6'-H), 5.35 (s, 2H, NH₂-CH₂), 4.37 (d, *J* 5.7, 2H, O-CH₂), 1.47 (s, 9H, Boc-H)

¹³C NMR (125 MHz, (CD₃)₂SO): 170.6, 156.5, 148.8, 147.1, 141.5, 138.6, 128.4, 128.3, 127.8, 125.8, 124.9, 121.3, 78.5, 70.0, 44.0, 43.9, 28.2

IR: ν_{max} /cm⁻¹: 3374, 2974, 2934, 2507, 1752, 1678, 1619, 1516

m/z (ES): Found: MH⁺ 340.1543; C₂₀H₂₁NO₄ requires MH⁺ 340.1543

RH27 (84) – 5-Bromo-1,3-dihydro-2-benzothiophen-1-one*



4-Bromo-2-(sulfanylmethyl)benzoic acid (70.0 mg, 0.28 mmol) was added to TFA (3 mL) and stirred at reflux for 3 hrs. TFA was removed *in vacuo* and the product was afforded as a yellow solid.

Yield: 65.0 mg, 0.28 mmol, quantitative

R_f: 0.94 (4:1, DCM/MeOH)

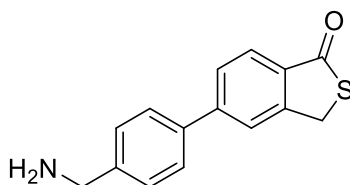
¹H NMR (500 MHz, (CD₃)₂SO): 8.04 (d, *J* 1.0, 1H, 7-H), 7.79 (dd, *J* 8.3 & 1.7, 1H, 4-H), 7.69 (d, *J* 8.3, 1H, 6-H), 4.72 (s, 2H, 3-H)

¹³C NMR (125 MHz, (CD₃)₂SO): 196.4, 149.9, 134.1, 131.3, 130.1, 128.0, 124.4, 34.1

IR: ν_{max} /cm⁻¹: 3014, 2970, 2946, 1739, 1671, 1590

HPLC: T_r = 4.34 (94% rel. area)

RH40 (151) - 5-[4-(Aminomethyl)phenyl]-1,3-dihydro-2-benzothiophen-1-one



Triethylamine (0.23 mL, 1.65 mmol) was added to ethanol (10 mL) and the solution was degassed with nitrogen for 30 mins. 5-Bromo-1,3-dihydro-2-benzothiophen-1-one (150 mg, 0.66 mmol), 4-aminobenzylboronic acid hydrochloride salt (123 mg, 0.66 mmol) and bis(triphenylphosphine)palladium(II) dichloride (49.0 mg, 0.07 mmol) were placed in an RBF and this was flushed with nitrogen for 30 mins. The solution was added to the solids and the mixture was heated and stirred under nitrogen for 16 hrs. The solution was allowed to cool to RT. DCM and methanol were added to dissolve the precipitate and the solution was filtered through celite, then washed with ethanol. The solution was reduced and the obtained solids were stirred in ethyl acetate for 15 mins. The solution was filtered under reduced pressure and a yellow solid was obtained. The compound was purified *via* automated reverse-phase flash-column chromatography. The appropriate fractions were combined and concentrated under reduced pressure, affording the title compound as yellow solid.

Yield: 69.0 mg, 0.27 mmol, 41%

R_f: 0.12 (20:1, EtOAc/Sat. NH₃ in MeOH)

¹H NMR (500 MHz, D₂O): 7.81 (d, *J* 8.7, 1H, 4-H), 7.74 (d, *J* 7.3, 2H, 6/7-H), 7.66 (d, *J* 8.2, 2H, 3'/5'-H), 7.47 (d, *J* 8.2, 2H, 2'/6'-H), 5.33 (s, 2H, 3-H), 4.11 (s, 2H, NH₂-CH₂)

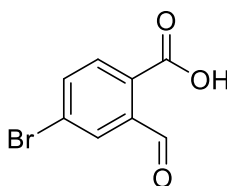
¹³C NMR (125 MHz, D₂O): 174.5, 168.4, 149.4, 147.2, 140.6, 134.1, 130.6, 129.1, 129.0, 126.6, 124.7, 121.8, 72.0, 43.5

IR: ν_{\max} /cm⁻¹: 2943, 2781, 1744, 1584

HPLC: T_r = 2.33 (100% rel. area)

m/z (ES): Found: MH⁺ 256.0791; C₁₅H₁₃NOS requires MH⁺ 256.0791

RH43 (105) - 4-Bromo-2-formylbenzoic acid²¹⁶



5-Bromophthalide (1.00 g, 4.70 mmol), NBS (1.00 g, 5.64 mmol) and AIBN (0.04 g, 0.24 mmol) were placed in an RBF that was then flushed with nitrogen. Dry 1,2-dichloroethane (20 mL) was added to the flask and it was stirred under nitrogen at 85 °C whilst being irradiated with a UV lamp for 2 hrs. The solution was allowed to cool to RT, stored at 8 °C for 16 hrs, then the solution was stirred in an ice-salt bath for 30 mins. The solids were collected *via* vacuum filtration and washed with ice-cold DCM. Solvents were removed under reduced pressure. Aqueous sodium hydroxide solution (2 M, 20 mL) was added to the solids and the solution was stirred at RT for 1 hr, forming a colourless precipitate. The solution was neutralised with aqueous hydrochloric acid solution (2 M) and the precipitate was removed *via* vacuum filtration. The filtrate was washed with ethyl acetate. The aqueous solution was acidified to pH 1 with aqueous hydrochloric acid solution (2 M) dropwise, stirred and the precipitate was collected *via* vacuum filtration. The precipitate was washed with aqueous hydrochloric acid solution (0.5 M) and air-dried, giving the product as a colourless solid.

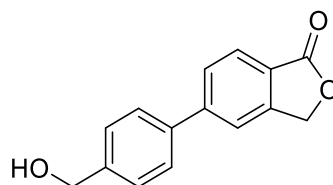
Yield: 350 mg, 1.53 mmol, 33%

*R*_f: 0.33 (4:1, EtOAc/MeOH)

¹H NMR (500 MHz, D₂O): 10.17 (s, 1H, COOH), 8.02 (s, 1H, 3-H), 7.86 (d, *J* 8.0, 1H, 5-H), 7.52 (d, *J* 8.0, 1H, 6-H)

m/z (ES): (Found: M⁻ 226.9334; C₈H₅BrO₃ requires M⁻ 226.9349)

RH44 (95) – 5-[4-(Hydroxymethyl)phenyl]-1,3-dihydro-2-benzofuran-1-one



Triethylamine (0.08 mL, 0.58 mmol) was added to ethanol (5 mL) and the solution was degassed with nitrogen for 30 mins. 5-Bromophthalide (50.0 mg, 0.24 mmol), 4-(hydroxymethyl)phenylboronic acid (35.0 mg, 0.24 mmol) and bis(triphenylphosphine)palladium(II) dichloride (17.0 mg, 0.03 mmol) were placed in an RBF and this was flushed with nitrogen for 30 mins. The solution was added to the solids and the mixture was heated 80 °C and stirred under nitrogen for 16 hrs. The solution was allowed to cool to RT. DCM was added to dissolve the precipitate and the solution was filtered through celite, then washed with ethanol. The solution was dried and filtered under reduced pressure. The compound was purified *via* automated normal-phase flash-column chromatography followed by automated reverse-phase flash-column chromatography. The appropriate fractions were combined and concentrated under reduced pressure, affording the title compound as a colourless solid.

Yield: 50.0 mg, 0.21 mmol, 88%

R_f: 0.5 (EtOAc)

¹H NMR (500 MHz, CD₃OD): 7.95 (d, *J* 8.0, 1H, 7-H), 7.88 (s, 1H, 6-H), 7.87 (d, *J* 8.0, 1H, 4-H), 7.73 (d, *J* 8.2, 2H, 3'/5'-H), 7.52 (d, *J* 8.2, 2H, 2'/6'-H), 5.46 (s, 2H, HO-CH₂), 4.71 (s, 2H, O-CH₂)

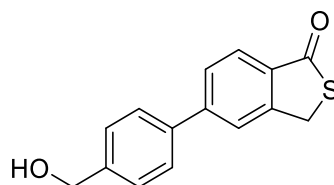
¹³C NMR (125 MHz, CD₃OD): 173.5, 149.9, 148.8, 143.6, 140.0, 129.4, 128.8, 128.7, 126.8, 125.4, 122.0, 71.6, 64.9

IR: ν_{\max} /cm⁻¹: 3488, 3033, 2864, 2590, 1739, 1614

HPLC: T_r = 3.06 (78% rel. area)

m/z (ES): Found: MH⁺ 241.0859; C₁₅H₁₂O₂S requires MH⁺ 241.0859

RH45 (152) – 5-[4-(Hydroxymethyl)phenyl]-1,3-dihydro-2-benzothiophen-1-one



Triethylamine (0.08 mL, 0.58 mmol) was added to ethanol (5 mL) and the solution was degassed with nitrogen for 30 mins. 5-Bromo-1,3-dihydro-2-benzothiophen-1-one (53.0 mg, 0.24 mmol), 4-(hydroxymethyl)phenylboronic acid (35.0 mg, 0.24 mmol) and bis(triphenylphosphine)palladium(II) dichloride (17.0 mg, 0.03 mmol) were placed in an RBF and this was flushed with nitrogen for 30 mins. The solution was added to the solids and the mixture was heated and stirred under nitrogen for 16 hrs. The solution was allowed to cool to RT. DCM was added to dissolve the precipitate and the solution was filtered through celite, then washed with ethanol. The solution was dried and filtered under reduced pressure. The compound was purified *via* automated normal-phase flash-column chromatography followed by automated reverse-phase flash-column chromatography. The appropriate fractions were combined and concentrated under reduced pressure, affording the title compound as an off-white solid.

Yield: 8.00 mg, 0.02 mmol, 13%

R_f : 0.56 (EtOAc)

^1H NMR (500 MHz, CD_3OD): 7.94 (s, 1H, 7-H), 7.85 (d, J 8.1, 1H, 6-H), 7.82 (d, J 8.1, 1H, 4-H), 7.74 (d, J 8.2, 2H, 3'/5'-H), 7.52 (d, J 8.2, 2H, 2'/6'-H), 4.71 (s, 2H, HO- CH_2), 4.67 (s, 2H, S- CH_2)

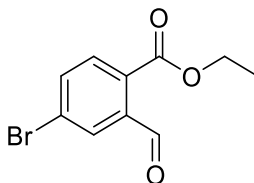
^{13}C NMR (125 MHz, CD_3OD): 199.8, 150.2, 147.8, 143.6, 139.8, 135.7, 128.8, 128.6, 128.2, 126.2, 124.8, 64.9, 35.5

IR: $\nu_{\text{max}}/\text{cm}^{-1}$: 3412, 3139, 3051, 2922, 2851, 1747, 1656, 1594

HPLC: T_r = 3.70 (97% rel. area)

m/z (ES): Found: MH^+ 257.0631; $\text{C}_{15}\text{H}_{12}\text{O}_2\text{S}$ requires MH^+ 257.0631

RH46 (106) – Ethyl 4-bromo-2-formylbenzoate



4-Bromo-2-formylbenzoic acid (250 mg, 1.10 mmol), iodoethane (0.18 mL, 2.20 mmol) and potassium carbonate (304 mg, 2.20 mmol) were added to acetone (50 mL) and the solution was stirred at 60 °C for 16 hrs. Solvents were removed under reduced pressure and the residue was redissolved in DCM (20 mL), water (20 mL) and brine (10 mL). The DCM layer was extracted and the aqueous portions were extracted with DCM. The organics were combined and washed with brine (20 mL) then dried (MgSO₄), filtered and concentrated under reduced pressure, affording the title compound as a pale yellow oil.

Yield: 109 mg, 0.42 mmol, 39%

R_f: 0.37 (4:1, Petrol/EtOAc)

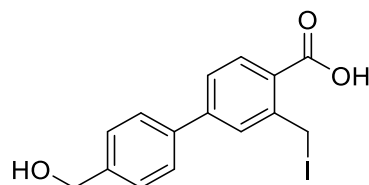
¹H NMR (500 MHz, CDCl₃): 10.57 (s, 1H, COOH), 7.99 (d, *J* 2.1, 1H, 3-H), 7.83 (d, *J* 8.3, 1H, 6-H), 7.72 (dd, *J* 8.3 & 2.1, 1H, 5-H), 4.41 (q, *J* 7.2, 2H, CH₃-CH₂), 1.39 (t, *J* 7.2, 3H, CH₂-CH₃)

¹³C NMR (125 MHz, CDCl₃): 190.8, 165.6, 138.6, 135.9, 132.2, 131.4, 130.9, 127.7, 62.3, 14.4

IR: ν_{max} /cm⁻¹: 3096, 2975, 2938, 2903, 2654, 1704, 1607

m/z (ES): Found: Mna⁺ 278.9627; C₁₀H₉BrO₃ requires Mna⁺ 278.9627

RH48 (96) – 4'-(Hydroxymethyl)-3-(iodomethyl)-[1,1'-biphenyl]-4-carboxylic acid



5-[4-(Hydroxymethyl)phenyl]-1,3-dihydro-2-benzofuran-1-one (300 mg, 1.25 mmol) was added to dry DCM (50 mL) under nitrogen. The solution was heated to 40 °C and stirred. Iodotrimethylsilane (0.27 mL, 1.87 mmol) was added dropwise and the solution was stirred at 40 °C for 3 hrs. The solution was allowed to cool to RT and then quenched with water. The organics were extracted, then dried using MgSO₄, filtered and dry-loaded onto silica. The compound was purified *via* automated normal-phase flash-column chromatography. The appropriate fractions were combined and concentrated under reduced pressure, affording the title compound as a brown solid.

Yield: 356 mg, 0.97 mmol, 77%

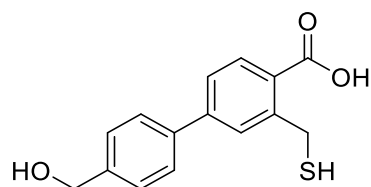
R_f: 0.7 (EtOAc)

¹H NMR (500 MHz, CDCl₃): 7.98 (d, *J* 7.9, 1H, 7-H), 7.73 (d, *J* 7.9, 1H, 6-H), 7.65 (s, 1H, 4-H), 7.55 (d, *J* 8.4, 2H, 3'/5'-H), 7.50 (d, *J* 8.4, 2H, 2'/6'-H), 5.38 (s, 2H, I-CH₂), 4.52 (s, 2H, HO-CH₂)

¹³C NMR (125 MHz, CDCl₃): 171.1, 147.6, 146.9, 140.2, 139.4, 129.7, 128.6, 128.2, 126.4, 125.0, 120.7, 69.8, 4.9

IR: ν_{max} /cm⁻¹: 3029, 2924, 1743, 1617

RH49 (41) - 4'-(Hydroxymethyl)-3-(sulfanylmethyl)-[1,1'-biphenyl]-4-carboxylic acid*



4'-(Hydroxymethyl)-3-(iodomethyl)-[1,1'-biphenyl]-4-carboxylic acid (300 mg, 0.81 mmol) and thiourea (69.0 mg, 0.9 mmol) were added to THF (25 mL) and the solution was stirred at 70 °C for 16 hrs. The solvent was removed under reduced pressure and the solid residue was redissolved in aqueous sodium hydroxide solution (2 M, 25 mL), then stirred at 100 °C for 24 hrs. The solution was allowed to cool to RT and acidified to pH 1 with aqueous hydrochloric acid solution (2 M) dropwise, causing a precipitate to form. The precipitate was collected *via* vacuum filtration and purified *via* automated reverse-phase flash-column chromatography. The appropriate fractions were combined and concentrated under reduced pressure, affording the title compound as an off-white solid.

Yield: 15.0 mg, 0.05 mmol, 6%

R_f: 0 (20:1, EtOAc/Sat. NH₃ in MeOH)

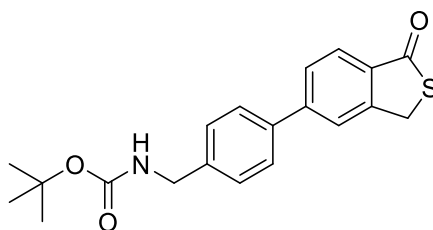
¹H NMR (500 MHz, (CD₃)₂SO): 8.00 (s, 1H, 7-H), 7.95 (d, *J* 8.0, 1H, 6-H), 7.92 (dd, *J* 8.0 & 1.2, 4-H), 7.77 (d, *J* 8.3, 2H, 3'/5'-H), 7.50 (d, *J* 8.3, 2H, 2'/6'-H), 5.50 (s, 2H, HS-CH₂), 5.32 (t, *J* 5.7, 1H, O-H), 4.61 (d, *J* 5.4, 2H, HO-CH₂)

¹³C NMR (125 MHz, (CD₃)₂SO): 170.5, 148.3, 145.9, 143.2, 137.2, 127.6, 127.2, 127.0, 125.4, 123.7, 120.8, 69.9, 62.5

IR: ν_{max} /cm⁻¹: 3327, 3068, 2919, 2855, 1743, 1685, 1616

HPLC: T_r = 3.08 (76% rel. area)

RH50 – *Tert*-butyl N-([4-(1-oxo-1,3-dihydro-2-benzothiophen-5-yl)phenyl]methyl)carbamate



Triethylamine (0.23 mL, 1.65 mmol) was added to ethanol (10 mL) and the solution was degassed with nitrogen for 30 mins. 5-Bromo-1,3-dihydro-2-benzothiophen-1-one (150 mg, 0.66 mmol), 4-(Boc-aminomethyl)benzeneboronic acid (181 mg, 0.72 mmol) and bis(triphenylphosphine)palladium(II) dichloride (49.0 mg, 0.07 mmol) were placed in an RBF and this was flushed with nitrogen for 30 mins. The solution was added to the solids and the mixture was heated and stirred under nitrogen for 16 hrs. The solution was allowed to cool to RT. DCM was added to dissolve the precipitate and the solution was filtered through celite, then washed with water. The solution was dried and filtered under reduced pressure. The compound was purified *via* automated normal-phase flash-column chromatography. The appropriate fractions were combined and concentrated under reduced pressure, affording the title compound as a yellow solid.

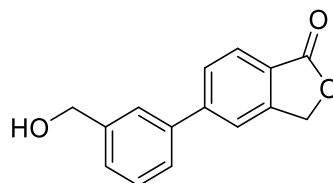
Yield: 167 mg, 0.47 mmol, 71%

*R*_f: 0.71 (EtOAc)

¹H NMR (500 MHz, (CD₃)₂SO): 8.03 (s, 1H, 3-H), 7.88 (d, *J* 8.1, 1H, 6-H), 7.82 (d, *J* 8.1, 1H, 5-H), 7.78 (d, *J* 8.0, 2H, 10-H), 7.42 (d, *J* 8.0, 2H, 9-H), 4.76 (s, 2H, 12-H), 4.23 (d, *J* 6.0, 2H, 7-H), 1.45 (s, 9H, Boc-H)

¹³C NMR (125 MHz, (CD₃)₂SO): 196.9, 155.8, 148.8, 145.1, 140.9, 136.9, 133.7, 127.7, 127.2, 126.6, 124.9, 123.4, 77.9, 43.1, 34.5, 28.3

RH52 - 5-[3-(Hydroxymethyl)phenyl]-1,3-dihydro-2-benzofuran-1-one



Triethylamine (2.11 mL, 15.0 mmol) was added to ethanol (50 mL) and the solution was degassed with nitrogen for 30 mins. 5-Bromophthalide (1.27 g, 5.98 mmol), 3-(hydroxymethyl)phenylboronic acid (1.00 g, 6.58 mmol) and bis(triphenylphosphine)palladium(II) dichloride (0.41 g, 0.59 mmol) were placed in an RBF and this was flushed with nitrogen for 30 mins. The solution was added to the solids and the mixture was heated to 80 °C and stirred under nitrogen for 16 hrs. The solution was allowed to cool to RT. DCM was added to dissolve the precipitate and the solution was filtered through celite, then washed with ethanol. The solution was dried and filtered under reduced pressure. The compound was purified *via* automated normal-phase flash-column chromatography. The appropriate fractions were combined and concentrated under reduced pressure, affording the title compound as a colourless solid.

Yield: 365 mg, 1.52 mmol, 25%

R_f: 0.26 (2:3, Petrol/EtOAc)

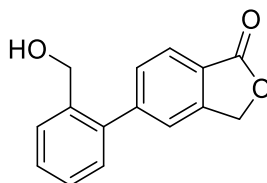
¹H NMR (500 MHz, CD₃OD): 7.97 (d, *J* 8.0, 1H, 7-H), 7.90 (s, 1H, 4-H), 7.88 (dt, *J* 8.0 & 0.7, 1H, 6-H), 7.74 (s, 1H, 2'-H), 7.65 (dt, *J* 7.6 & 1.6, 1H, 6'-H), 7.51 (t, *J* 7.6, 1H, 5'-H), 7.46 (d, *J* 7.7, 1H, 4'-H), 5.48 (s, 2H, HO-CH₂), 4.73 (s, 2H, O-CH₂)

¹³C NMR (125 MHz, CD₃OD): 210.2, 173.5, 149.8, 149.1, 144.0, 141.3, 130.4, 129.5, 128.4, 127.6, 127.2, 126.8, 125.6, 122.2, 71.6, 65.1, 30.8

IR: ν_{\max} /cm⁻¹: 3468, 3447, 3001, 2970, 2922, 2368, 1736, 1618

m/z (ES): Found: MH⁺ 241.0854; C₁₅H₁₂O₂S requires MH⁺ 241.0859

RH53 - 5-[2-(Hydroxymethyl)phenyl]-1,3-dihydro-2-benzofuran-1-one



Triethylamine (2.38 mL, 16.9 mmol) was added to ethanol (50 mL) and the solution was degassed with nitrogen for 30 mins. 5-Bromophthalide (1.45 g, 6.79 mmol), 2-(hydroxymethyl)phenylboronic acid cyclic monoester (1.00 g, 7.47 mmol) and bis(triphenylphosphine)palladium(II) dichloride (0.48 g, 0.68 mmol) were placed in an RBF and this was flushed with nitrogen for 30 mins. The solution was added to the solids and the mixture was heated to 80 °C and stirred under nitrogen for 16 hrs. The solution was allowed to cool to RT. DCM was added to dissolve the precipitate and the solution was filtered through celite, then washed with ethanol. The solution was dried and filtered under reduced pressure. The compound was purified *via* automated normal-phase flash-column chromatography. The appropriate fractions were combined and concentrated under reduced pressure, affording the title compound as an off-white solid.

Yield: 727 mg, 3.03 mmol, 45%

R_f: 0.31 (1:2, Petrol/EtOAc)

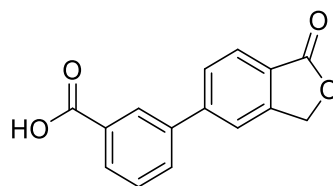
¹H NMR (500 MHz, CD₃OD): 7.84 (dt, *J* 7.9 & 0.4, 1H, 7-**H**), 7.56 (dt, *J* 2.2 & 0.8, 1H, 3'-**H**), 7.52 (dm, *J* 7.8, 2H, 4/6-**H**), 7.36 (td, *J* 7.6 & 1.5, 1H, 5'-**H**), 7.31 (td, *J* 7.5 & 1.4, 1H, 4'-**H**), 7.22 (dd, *J* 7.6 & 1.2, 1H, 6'-**H**), 5.35 (s, 2H, HO-CH₂), 4.42 (s, 2H, O-CH₂)

¹³C NMR (125 MHz, CD₃OD): 210.2, 173.5, 149.8, 149.1, 149.0, 141.5, 139.8, 131.7, 130.9, 130.3, 129.7, 128.9, 126.1, 125.6, 124.6, 71.6, 63.0, 30.8

IR: ν_{max} /cm⁻¹: 3431, 3025, 2971, 2940, 2889, 1735, 1615

m/z (ES): Found: MH⁺ 241.0854; C₁₅H₁₂O₂S requires MH⁺ 241.0859

RH55 (99) - 3-(1-Oxo-1,3-dihydro-2-benzofuran-5-yl)benzoic acid



Triethylamine (1.92 mL, 13.7 mmol) was added to ethanol (40 mL) and the solution was degassed with nitrogen for 30 mins. 5-Bromophthalide (1.17 g, 5.48 mmol), 3-carboxyphenylboronic acid (1.00 g, 6.03 mmol) and bis(triphenylphosphine)palladium(II) dichloride (0.39 g, 0.55 mmol) were placed in an RBF and this was flushed with nitrogen for 30 mins. The solution was added to the solids and the mixture was heated to 80 °C and stirred under nitrogen for 16 hrs. The solution was allowed to cool to RT. The solution was filtered through celite, then washed with ethanol. The solution was acidified to pH 5 with aqueous hydrochloric acid solution (2 M) dropwise, causing a colourless precipitate to form. The precipitate was filtered off to give the title compound as a colourless powder.

Yield: 1.17 g, 4.62 mmol, 84%

R_f: 0.42 (9:1, DCM/MeOH)

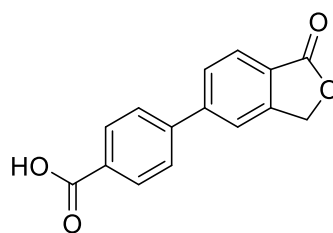
¹H NMR (500 MHz, (CD₃)₂SO): 8.86 (t, *J* 1.6, 1H, 2'-H), 8.61 (ddd, *J* 7.4, 1.6 & 1.2, 1H, 6'-H), 8.52 (ddd, *J* 7.7, 2.0 & 1.0, 1H, 7-H), 8.51 (dd, *J* 1.2, & 0.9, 1H, 6-H), 8.45 (t, *J* 0.9, 1H, 4-H), 8.40 (s, 1H, 5'-H), 8.18 (td, *J* 7.8 & 0.5, 1H, 4'-H), 5.98 (s, 2H, O-CH₂)

¹³C NMR (125 MHz, (CD₃)₂SO): 176.9, 159.0, 142.4, 142.1, 140.1, 140.0, 139.0, 138.7, 136.1, 132.0, 80.1, 55.9

IR: ν_{\max} /cm⁻¹: 3181, 2970, 1734, 1618

m/z (ES): Found: MNa⁺ 277.0465; C₁₅H₁₀O₄ requires MNa⁺ 277.0471

RH56 (97) - 4-(1-Oxo-1,3-dihydro-2-benzofuran-5-yl)benzoic acid



Triethylamine (1.92 mL, 13.7 mmol) was added to ethanol (40 mL) and the solution was degassed with nitrogen for 30 mins. 5-Bromophthalide (1.17 g, 5.48 mmol), 4-carboxyphenylboronic acid (1.00 g, 6.03 mmol) and bis(triphenylphosphine)palladium(II) dichloride (0.39 g, 0.55 mmol) were placed in an RBF and this was flushed with nitrogen for 30 mins. The solution was added to the solids and the mixture was heated to 80 °C and stirred under nitrogen for 16 hrs. The solution was allowed to cool to RT. The solution was filtered through celite, then washed with ethanol. The solution was acidified to pH 5 with aqueous hydrochloric acid solution (2 M) dropwise, causing a colourless precipitate to form. The precipitate was filtered off to give the title compound as a colourless solid.

Yield: 1.10 g, 4.33 mmol, 79%

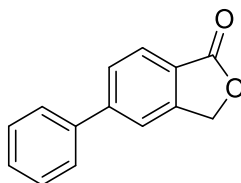
R_f: 0.33 (9:1, DCM/MeOH)

¹H NMR (500 MHz, CD₃OD): 7.86 (d, *J* 8.2, 2H, 2'/6'-H), 7.75 (d, *J* 7.9, 1H, 4-H), 7.67 (d, *J* 9.5, 2H, 6/7-H), 7.58 (d, *J* 8.2, 2H, 3'/5'-H), 5.30 (s, 2H, O-CH₂)

IR: $\nu_{\text{max}}/\text{cm}^{-1}$: 2970, 2669, 2548, 1753, 1685, 1607

m/z (ES): Found: MH⁺ 255.0656; C₁₅H₁₀O₄ requires MH⁺ 255.0652

RH57 (82) - 5-Phenyl-1,3-dihydro-2-benzofuran-1-one¹⁵²



Triethylamine (2.62 mL, 18.7 mmol) was added to ethanol (20 mL) and the solution was degassed with nitrogen for 30 mins. 5-Bromophthalide (1.59 g, 7.48 mmol), phenylboronic acid (1.00 g, 8.23 mmol) and bis(triphenylphosphine)palladium(II) dichloride (0.53 g, 0.75 mmol) were placed in an RBF and this was flushed with nitrogen for 30 mins. The solution was added to the solids and the mixture was heated to 80 °C and stirred under nitrogen for 16 hrs. The solution was allowed to cool to RT. DCM was added to dissolve the precipitate and the solution was filtered through celite, then washed with ethanol. The solution was dried and filtered under reduced pressure. The compound was purified *via* automated normal-phase flash-column chromatography and the appropriate fractions were combined and concentrated under reduced pressure, affording the title compound as a colourless solid.

Yield: 783 mg, 3.72 mmol, 50%

R_f: 0.16 (4:1, Petrol/EtOAc)

¹H NMR (500 MHz, CDCl₃): 7.97 (d, *J* 8.2, 1H, -H), 7.74 (dt, *J* 8.0 & 0.7, 1H, -H), 7.67 (q, *J* 0.7, 1H, 4-H), 7.61 (m, 2H, -H), 7.49 (m, 2H, -H), 7.43 (tt, *J* 7.4 & 1.4, -H), 5.37 (s, 2H, O-CH₂)

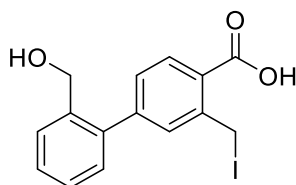
¹³C NMR (125 MHz, (CD₃)₂SO): 180.7, 158.9, 157.4, 150.3, 139.7, 139.1, 138.6, 138.0, 135.9, 135.1, 131.6, 80.1

IR: ν_{max} /cm⁻¹: 3567, 3467, 3015, 2970, 2356, 2333, 1746, 1654

m/z (ES): Found: MNa⁺ 233.0572; C₁₅H₁₀O₄ requires MNa⁺ 233.0573

Data consistent with literature values¹⁵².

RH60 - 2'-(Hydroxymethyl)-3-(iodomethyl)-[1,1'-biphenyl]-4-carboxylic acid



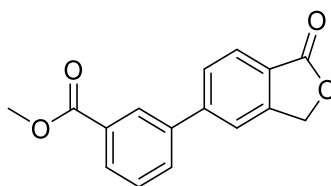
5-[2-(Hydroxymethyl)phenyl]-1,3-dihydro-2-benzofuran-1-one (600 mg, 2.50 mmol) was added to dry DCM (20 mL) under nitrogen. The solution was heated to 40 °C and stirred. Iodotrimethylsilane (1.33 mL, 3.75 mmol) was added dropwise and the solution was stirred at 40 °C for 16 hrs. The solution was allowed to cool to RT and then quenched with water. The organics were extracted, then dried, filtered and dry-loaded onto silica. The compound was purified *via* automated normal-phase flash-column chromatography. The appropriate fractions were combined and concentrated under reduced pressure. These were then further purified *via* automated reverse-phase flash-column chromatography and then the appropriate fractions were combined and concentrated under reduced pressure, affording the title compound as a brown solid. The crude product was used without further purification.

Yield: Crude, 209 mg

R_f: 0.26 (1:1, Petrol/EtOAc)

¹H NMR (500 MHz, CD₃OD): 7.96 (d, *J* 8.0, 1H, -H), 7.68 (dd, *J* 1.4 & 0.8, 1H, -H), 7.64 (t, *J* 0.7, 1H, -H), 7.57 (m, 1H, -H), 7.37 (m, 2H, -H), 7.21 (m, 1H, -H), 5.45 (s, 2H, HO-CH₂), 4.46 (s, 2H, I-CH₂)

RH62 - Methyl-3-(1-oxo-1,3-dihydro-2-benzofuran-5-yl)benzoate



3-(1-Oxo-1,3-dihydro-2-benzofuran-5-yl)benzoic acid (100 mg, 0.39 mmol) was placed in an RBF and the flask was flushed with nitrogen. DMF (2 mL) was added and the solution was heated to 40 °C. Thionyl chloride (2 mL) was added dropwise and the solution was stirred for 16 hrs. The solution was allowed to cool to RT and thionyl was removed under reduced pressure. Methanol was added and the solution was stirred at RT for 1 hr. The solvent was removed under reduced pressure and the solid residue was redissolved in DCM (10 mL). The solution was washed with lithium chloride solution and the solvent was removed under reduced pressure, affording the title compound as a colourless powder.

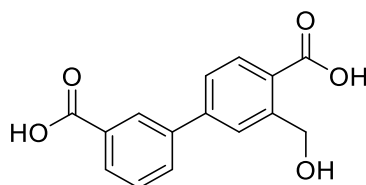
Yield: 77.0 mg, 0.29 mmol, 74%

*R*_f: 0.7 (EtOAc)

¹H NMR (500 MHz, CD₃OD): 8.26 (t, *J* 1.7, 1H, 2'-H), 8.00 (dt, *J* 7.7 & 1.5, 1H, 6'-H), 7.88 (d, *J* 7.7, 2H, 6/7-H), 7.82 (s, 1H, 4-H), 7.78 (d, *J* 8.0, 1H, 4'-H), 7.55 (t, *J* 7.8, 1H, 5'-H), 5.37 (s, 2H, O-CH₂), 3.87 (s, 3H, COO-CH₃)

¹³C NMR (125 MHz, CD₃OD): 173.3, 168.3, 150.0, 147.8, 141.7, 133.3, 132.5, 130.7, 130.7, 129.6, 129.5, 127.0, 126.1, 122.4, 71.6, 53.0

RH69 (104) – 3'-(Hydroxymethyl)-[1,1'-biphenyl]-3,4'-dicarboxylic acid



Methyl-3-(1-oxo-1,3-dihydro-2-benzofuran-5-yl)benzoate (100 mg, 0.39 mmol) was added to aqueous sodium hydroxide solution (2 M, 5 mL) and the solution was stirred at 100 °C for 24 hrs. The solution was allowed to cool to RT and acidified to pH 1 with aqueous hydrochloric acid solution (2 M) dropwise, causing a precipitate to form. The precipitate was filtered off, affording the title compound as a colourless solid.

Yield: 106 mg, 0.39 mmol, quantitative

*R*_f: 0.23 (1:1, EtOAc/MeOH)

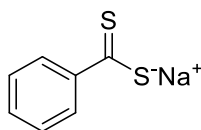
¹H NMR (500 MHz, D₂O): 8.18 (t, *J* 1.7, 1H, 2'-H), 7.87 (m, 2H, 4'/6'-H), 7.77 (d, *J* 1.2, 1H, 4-H), 7.70 (dd, *J* 8.1 & 1.7, 1H, 6-H), 7.68 (d, *J* 7.9, 1H, 7-H), 7.57 (t, *J* 7.8, 1H, 5'-H), 4.82 (s, 2H, HO-CH₂, obscured by D₂O)

¹³C NMR (125 MHz, D₂O): 177.4, 175.7, 141.6, 140.1, 138.8, 137.3, 137.2, 129.9, 129.3, 128.5, 127.6, 127.1, 126.4, 63.1

IR: *v*_{max}/cm⁻¹: 3469, 3058, 2550, 1739, 1680, 1607

m/z (ES): Found: M⁻ 271.0604; C₁₅H₁₂O₅ requires M⁻ 271.0612

RH73 (153) - Sodium benzenecarbothioylsulfanide



Magnesium turnings (122 mg, 5.00 mmol) and iodine (69.0 mg, 0.25 mmol) were placed in an RBF which was then nitrogen flushed. THF (10 mL) and bromobenzene (0.58 mL, 5.50 mmol) were added and the solution was heated to 60 °C and stirred under nitrogen until magnesium was consumed. The solution was cooled to 0 °C and carbon disulfide (0.30 mL, 5.00 mmol) was added dropwise. The solution was stirred overnight under nitrogen, being allowed to reach RT. The solution was acidified to pH 1 with aqueous hydrochloric acid solution (2 M) dropwise and extracted with toluene (2 x 10 mL), then dried (MgSO₄) and filtered. The solvent was removed under reduced pressure and sodium hydride (60% in mineral oil, 180 mg, 4.5 mmol) was added to the flask, which was then flushed with nitrogen and cooled to 0 °C. Toluene was added and the solution was stirred overnight, being allowed to reach RT. An orange crystalline solid precipitated out, which was then filtered and retrieved, affording the title compound as orange crystals.

Yield: 230 mg, 1.31 mmol, 24%

¹H NMR (500 MHz, D₂O): 7.93 (dd, *J* 8.4 & 1.2, 2H, 2'/6'-H), 7.45 (tt, *J* 7.4 & 1.3, 1H, 4-H), 7.33 (tt, *J* 7.3 & 1.6, 2H, 3'/5'-H)

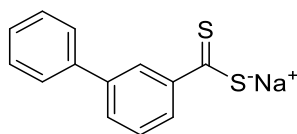
¹³C NMR (125 MHz, D₂O): 258.3, 153.6, 130.2, 127.6, 125.9

IR: $\nu_{\text{max}}/\text{cm}^{-1}$: 3384, 3192, 3070, 2070, 1607

HPLC: *T_r* = 5.71 (86% rel. area)

m/z (ES): Found: *M*⁻ 152.9828; C₇H₆S₂ requires *M*⁻ 152.9838

RH83 (154) - Sodium {[1,1'-biphenyl]-3-carbothioyl}sulfanide



Magnesium turnings (47.0 mg, 1.95 mmol) and iodine (51.0 mg, 0.20 mmol) were placed in an RBF which was then nitrogen flushed. THF (10 mL) and 3-bromobiphenyl (358 μ L, 2.15 mmol) were added and the solution was heated to 60°C and stirred under nitrogen until magnesium was consumed. The solution was cooled to 0 °C and carbon disulfide (234 μ L, 3.90 mmol) was added dropwise. The solution was stirred overnight under nitrogen, being allowed to reach RT. The solution was acidified to pH 1 with aqueous hydrochloric acid solution (2 M) dropwise and extracted with toluene (2 x 10 mL), then dried (MgSO_4) and filtered. The solvent was removed under reduced pressure and sodium hydride (60% in mineral oil, 78.0 mg, 1.95 mmol) was added to the flask, which was then flushed with nitrogen and cooled to 0 °C. Toluene was added and the solution was stirred overnight, being allowed to reach RT. An orange crystalline solid precipitated out, which was then filtered and retrieved, affording the title compound as orange crystals.

Yield: 13.0 mg, 0.05 mmol, 3%

^1H NMR (500 MHz, D_2O): 8.24 (t, J 1.8, 1H, 4-H), 7.96 (ddd, J 7.8, 1.7 & 1.0, 1H, 4'-H), 7.75 (m, 3H, 2/5/6-H), 7.54 (t, J 7.8, 2H, 2'/6'-H), 7.45 (m, 2H, 3'/5'-H)

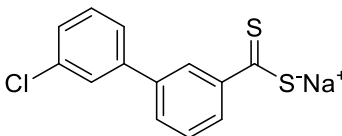
^{13}C NMR (125 MHz, D_2O): 257.7, 154.2, 140.2, 139.7, 129.1, 128.5, 128.2, 127.8, 127.0, 125.0, 124.4

IR: $\nu_{\text{max}}/\text{cm}^{-1}$: 3347, 3061, 2791, 2703, 1589, 1559

HPLC: T_r = 5.840 (49% rel. area) (sample degraded)

m/z (ES): Found: M^- 229.0158; $\text{C}_7\text{H}_6\text{S}_2$ requires M^- 229.0159

RH85 (126) - Sodium {3'-chloro-[1,1'-biphenyl]-3-carbothioyl}sulfanide



3-Bromo-3'-chlorobiphenyl (500 mg, 1.87 mmol), magnesium turnings (41.0 mg, 1.70 mmol) and iodine (43.0 mg, 0.17 mmol) were placed in an RBF which was then nitrogen flushed. THF (15 mL) was added and the solution was heated to 60 °C and stirred under nitrogen until magnesium was consumed. The solution was cooled to 0 °C and carbon disulfide (102 μ L, 1.70 mmol) was added dropwise. The solution was stirred overnight under nitrogen, being allowed to reach RT. The solution was acidified to pH 1 with aqueous hydrochloric acid solution (2 M) dropwise and extracted with toluene (2 x 10 mL), then dried (MgSO_4) and filtered. The solution was dry-loaded on to silica deactivated with 0.1% triethylamine in DCM and purified *via* automated normal-phase flash-column chromatography. The appropriate fractions were combined and the solvent was removed under reduced pressure. Sodium hydride (60% in mineral oil, 38.0 mg, 1.53 mmol) was added to the flask, which was then flushed with nitrogen and cooled to 0 °C. Toluene was added and the solution was stirred overnight, being allowed to reach RT. An orange crystalline solid precipitated out, which was then filtered and retrieved, affording the title compound as orange crystals.

Yield: 122 mg, 0.43 mmol, 23%

^1H NMR (500 MHz, D_2O): 8.15 (t, J 1.7, 1H, 2'-H), 7.95 (dt, J 7.9 & 1.1, 1H, 4'-H), 7.61 (t, J 1.7, 1H, 5'-H), 7.55 (ddt, J 36.4, 7.8 & 1.2, 2H, 3/5-H), 7.37 (td, J 7.9 & 1.7, 2H, 2/6-H), 7.32 (dt, J 7.9 & 1.4, 1H, 6'-H)

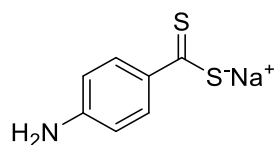
^{13}C NMR (125 MHz, D_2O): 257.1, 153.9, 141.9, 138.3, 134.1, 130.3, 128.5, 128.2, 127.4, 126.8, 125.5, 125.2, 124.5

IR: $\nu_{\text{max}}/\text{cm}^{-1}$: 3414, 3059, 1591, 1562

HPLC: T_r = 6.91 (60% rel. area) (sample degraded)

m/z (ES): Found: M^- 262.9761; $\text{C}_7\text{H}_6\text{S}_2$ requires M^- 262.9761

RH97 (131) - Sodium (4-aminobenzenecarbothioyl)sulfanide



4-(Bis(trimethylsilyl)amino)phenyl magnesium bromide solution (0.5 M in THF, 10 mL) was added to toluene (10 mL) in an RBF under nitrogen. The solution was cooled to 0°C and carbon disulfide (330 μ L, 5.50 mmol) was added dropwise. The solution was stirred overnight under nitrogen, being allowed to reach RT. The solution was cooled to 0 °C and acidified to pH 1 with aqueous hydrochloric acid solution (2 M) dropwise, then stirred for 1 hr. The organics were extracted with toluene (2 x 10 mL), then dried (MgSO_4) and filtered. The solvent was removed under reduced pressure and sodium hydride (60% in mineral oil, 78.0 mg, 1.95 mmol) was added to the flask, which was then flushed with nitrogen and cooled to 0 °C. Toluene was added and the solution was stirred overnight, being allowed to reach RT. An orange crystalline solid had precipitated out, which was then filtered and retrieved. The product was purified *via* automated reverse-phase flash-column chromatography and the appropriate fractions were combined and concentrated under reduced pressure, affording the title compound as a red crystalline solid.

Yield: 282 mg, 1.47 mmol, 29%

^1H NMR (500 MHz, D_2O): 8.18 (dt, J 8.7 & 2.1, 2H, 3/5-H), 6.70 (dt, J 8.7 & 2.1, 2H, 2/6-H)

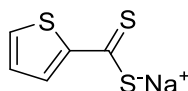
^{13}C NMR (125 MHz, D_2O): 252.9, 150.8, 142.6, 129.2, 113.8

IR: $\nu_{\text{max}}/\text{cm}^{-1}$: 3357, 3307, 3195, 2978, 2933, 2658, 1621, 1590

HPLC: $T_r = 2.52$ (94% rel. area)

m/z (ES): Found: M^- 167.9939; $\text{C}_7\text{H}_6\text{S}_2$ requires M^- 167.9947

RH101 (132) - Sodium (thiophene-2-carbothioyl)sulfanide*



2-Thienyl magnesium bromide solution (1 M in THF, 5 mL) was added to toluene (10 mL) in an RBF under nitrogen. The solution was cooled to 0°C and carbon disulfide (330 μ L, 5.50 mmol) was added dropwise. The solution was stirred overnight under nitrogen, being allowed to reach RT. The solution was cooled to 0 °C and acidified to pH 1 with aqueous hydrochloric acid solution (2 M) dropwise, then stirred for 1 hr. The organics were extracted with toluene (2 x 10 mL), then dried (MgSO_4) and filtered. The solvent was removed under reduced pressure and sodium hydride (60% in mineral oil, 180 mg, 4.50 mmol) was added to the flask, which was then flushed with nitrogen and cooled to 0 °C. Toluene was added and the solution was stirred overnight, being allowed to reach RT. A red crystalline solid precipitated out, which was then filtered and retrieved. The product was purified *via* automated reverse-phase flash-column chromatography and the appropriate fractions were combined and concentrated under reduced pressure, affording the title compound as deep red crystals.

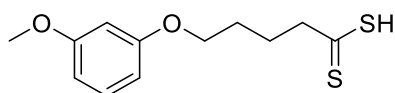
Yield: Not obtained, product degraded.

^1H NMR (500 MHz, D_2O): 7.87 (d, J 2.7, 1H, 3-H), 7.61 (d, J 4.5, 1H, 5-H), 7.10 (t, J 3.6, 1H, 4-H)

^{13}C NMR (125 MHz, D_2O): 239.5, 158.3, 134.4, 129.2, 128.8

HPLC: T_r = 1.48 (50% rel. area) (sample degraded)

RH104 (140) - 5-(3-Methoxyphenoxy)pentanedithioic acid



Neat carbon disulphide (0.5 mL, 17 mmol) was placed in a nitrogen flushed RBF and (4-(3-methoxyphenoxy)butyl magnesium chloride solution (0.5 M in THF, 1 mL) was added dropwise. Upon addition of the Grignard reagent the solution changed from colourless to yellow. The solution was stirred for 1 hr at RT under nitrogen. Aqueous hydrochloric acid solution (2 M, 0.4 mL) was added, causing a precipitate to form and causing the solution to change colour to a deep red. The solution was stirred for 15 mins. A further portion of aqueous hydrochloric acid solution (2 M, 0.4 mL) was added and the solution was stirred for a further 15 mins, over which time the precipitate dissolved. The product was extracted with toluene (3 x 10 mL) and the organics were combined and the solvent was removed. The product was dry-loaded onto deactivated silica with 0.1% triethylamine in DCM for automated normal-phase flash-column chromatography and the appropriate fractions were combined and concentrated under reduced pressure, affording the title compound as an orange-brown oil.

Yield: 37 mg, 0.14 mmol, 28%

^1H NMR (500 MHz, CDCl_3): 7.18 (t, J 8.1, 1H, 2-H), 6.50 (ddt, J 8.1, 2.4 & 0.7, 2H, 1,3-H), 6.46 (t, J 2.4, 1H, 4-H), 3.97 (t, J 6.2, 2H, 5'-H), 3.79 (s, 3H, O-CH₃), 3.07 (t, J 7.5, 2H, 2'-H), 2.02 (p, J 7.5, 2H, 3'-H), 1.87 (m, 2H, 4'-H)

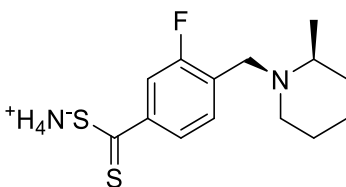
^{13}C NMR (125 MHz, D_2O): 237.9, 160.9, 160.2, 129.9, 106.7, 106.3, 101.0, 67.3, 55.3, 52.8, 28.1, 27.1

IR: $\nu_{\text{max}}/\text{cm}^{-1}$: 2998, 2935, 2869, 2834, 1587

HPLC: T_r = 0.30 (88% rel. area)

m/z (ES): Found: M^- 255.0518; $\text{C}_7\text{H}_6\text{S}_2$ requires M^- 255.0519

RH106 (142) - Ammonium {3-fluoro-4-[(2-methylpiperidin-1-yl)methyl]benzenecarbothioyl}sulfanide*



Neat carbon disulphide (0.5 mL, 17 mmol) was placed in a nitrogen flushed RBF and 3-fluoro-4-[(2-methyl-1-piperidino)methyl]phenyl magnesium bromide solution (0.25 M in THF, 2 mL) was added dropwise. Upon addition of the Grignard reagent the solution changed from colourless to yellow. The solution was stirred for 1 hr at RT under nitrogen. Aqueous hydrochloric acid solution (2 M, 5 drops mL) was added, causing a precipitate to form and causing the solution to change colour to a deep red. The solvent was removed *in vacuo* and methanolic ammonia was added. The solution was stirred at RT for 1 hr. The product was extracted with water (3 x 10 mL) and the aqueous layers were combined and the solvent was removed. The product was washed with toluene and ethyl acetate, affording the title compound as an off-white solid.

Yield: 33 mg, 0.11 mmol, 22%

¹H NMR (500 MHz, DMSO/D₂O): Unassignable, product degraded in NMR solvents.

¹³C NMR (125 MHz, DMSO/D₂O): Unassignable, product degraded in NMR solvents.

IR: $\nu_{\max}/\text{cm}^{-1}$: 3331, 2483, 1634, 1437

HPLC: $T_r = 0.28$ (78% rel. area)

LC-MS (ES): Found: M^- 281.74; C₁₄H₁₈FNS₂ requires M^- 281.0792

List of References

1. Woese, C. R., Kandler, O. & Wheelis, M. L. Towards a natural system of organisms: proposal for the domains Archaea, Bacteria, and Eucarya. *Proc. Natl. Acad. Sci.* **87**, 4576–4579 (1990).
2. Greening, C. & Lithgow, T. Formation and function of bacterial organelles. *Nat. Rev. Microbiol.* **18**, 677–689 (2020).
3. Rogers, K. & Kadner, R. Bacteria. *Encyclopædia Britannica*.
4. NIAID's albums. *Flickr* /photos/niaid/albums/.
5. Beveridge, T. Use of the Gram stain in microbiology. *Biotech. Histochem.* **76**, 111–118 (2001).
6. Silhavy, T. J., Kahne, D. & Walker, S. The Bacterial Cell Envelope. *Cold Spring Harb. Perspect. Biol.* **2**, a000414–a000414 (2010).
7. Antebi, Y. E., Nandagopal, N. & Elowitz, M. B. An operational view of intercellular signaling pathways. *Curr. Opin. Syst. Biol.* **1**, 16–24 (2017).
8. Davies, J. A., Anderson, G. K., Beveridge, T. J. & Clark, H. C. Chemical mechanism of the Gram stain and synthesis of a new electron-opaque marker for electron microscopy which replaces the iodine mordant of the stain. *J. Bacteriol.* **156**, 837–845 (1983).
9. Thairu, Y., Usman, Y. & Nasir, I. Laboratory perspective of gram staining and its significance in investigations of infectious diseases. *Sub-Sahar. Afr. J. Med.* **1**, 168 (2014).
10. Schwechheimer, C. & Kuehn, M. J. Outer-membrane vesicles from Gram-negative bacteria: biogenesis and functions. *Nat. Rev. Microbiol.* **13**, 605–619 (2015).
11. Lambert, P. A. Cellular impermeability and uptake of biocides and antibiotics in Gram-positive bacteria and mycobacteria. *J. Appl. Microbiol.* **92**, 46S-54S (2002).
12. Framingham State University, Massachusetts, USA & Zhivich, A. Fighting bacterial resistance: approaches, challenges, and opportunities in the

- search for new antibiotics. Part 1. Antibiotics used in clinical practice: mechanisms of action and the development of bacterial resistance. *Microbiol. Indep. Res.* **4**, 31–51 (2017).
13. Blair, J. M. A., Webber, M. A., Baylay, A. J., Ogbolu, D. O. & Piddock, L. J. V. Molecular mechanisms of antibiotic resistance. *Nat Rev Micro* **13**, 42–51 (2015).
 14. Delcour, A. H. Outer membrane permeability and antibiotic resistance. *Biochim. Biophys. Acta BBA - Proteins Proteomics* **1794**, 808–816 (2009).
 15. Pagès, J.-M., James, C. E. & Winterhalter, M. The porin and the permeating antibiotic: a selective diffusion barrier in Gram-negative bacteria. *Nat. Rev. Microbiol.* **6**, 893–903 (2008).
 16. Silver, L. L. A Gestalt approach to Gram-negative entry. *Bioorg. Med. Chem.* **24**, 6379–6389 (2016).
 17. Vergalli, J. *et al.* Porins and small-molecule translocation across the outer membrane of Gram-negative bacteria. *Nat. Rev. Microbiol.* **18**, 164–176 (2020).
 18. Du, D. *et al.* Multidrug efflux pumps: structure, function and regulation. *Nat. Rev. Microbiol.* **16**, 523–539 (2018).
 19. Munita, J. M. & Arias, C. A. Mechanisms of Antibiotic Resistance. in *Virulence Mechanisms of Bacterial Pathogens, Fifth Edition* (eds. Kudva, I. T. *et al.*) 481–511 (American Society of Microbiology, 2016). doi:10.1128/microbiolspec.VMBF-0016-2015.
 20. Du, D. *et al.* Structure of the AcrAB–TolC multidrug efflux pump. *Nature* **509**, 512–515 (2014).
 21. Long, K. S., Poehlsgaard, J., Kehrenberg, C., Schwarz, S. & Vester, B. The Cfr rRNA Methyltransferase Confers Resistance to Phenicol, Lincosamides, Oxazolidinones, Pleuromutilins, and Streptogramin A Antibiotics. *Antimicrob. Agents Chemother.* **50**, 2500–2505 (2006).

22. Tomlinson, J. H., Thompson, G. S., Kalverda, A. P., Zhuravleva, A. & O'Neill, A. J. A target-protection mechanism of antibiotic resistance at atomic resolution: insights into FusB-type fusidic acid resistance. **6**, 19524 (2016).
23. Shaikh, S., Fatima, J., Shakil, S., Rizvi, S. Mohd. D. & Kamal, M. A. Antibiotic resistance and extended spectrum beta-lactamases: Types, epidemiology and treatment. *Spec. Issue Biol. Asp. Glob. Health Issues* **22**, 90–101 (2015).
24. Macheboeuf, P., Contreras-Martel, C., Job, V., Dideberg, O. & Dessen, A. Penicillin Binding Proteins: key players in bacterial cell cycle and drug resistance processes. *FEMS Microbiol. Rev.* **30**, 673–691 (2006).
25. Holmes, A. H. *et al.* Understanding the mechanisms and drivers of antimicrobial resistance. *The Lancet* **387**, 176–187 (2016).
26. Soucy, S. M., Huang, J. & Gogarten, J. P. Horizontal gene transfer: building the web of life. *Nat. Rev. Genet.* **16**, 472–482 (2015).
27. Chatterjee, S., Mondal, A., Mitra, S. & Basu, S. *Acinetobacter baumannii* transfers the blaNDM-1 gene via outer membrane vesicles. *J. Antimicrob. Chemother.* **72**, 2201–2207 (2017).
28. Llosa, M., Gomis-Ruth, F. X., Coll, M. & Cruz, F. de la. Bacterial conjugation: a two-step mechanism for DNA transport. *Mol. Microbiol.* **45**, 1–8 (2002).
29. Johnston, C., Martin, B., Fichant, G., Polard, P. & Claverys, J.-P. Bacterial transformation: distribution, shared mechanisms and divergent control. *Nat. Rev. Microbiol.* **12**, 181–196 (2014).
30. Xia, G. & Wolz, C. Phages of *Staphylococcus aureus* and their impact on host evolution. *Infect. Genet. Evol.* **21**, 593–601 (2014).
31. Chiang, Y. N., Penadés, J. R. & Chen, J. Genetic transduction by phages and chromosomal islands: The new and noncanonical. *PLOS Pathog.* **15**, e1007878 (2019).

32. Chen, J. *et al.* Genome hypermobility by lateral transduction. *Science* **362**, 207–212 (2018).
33. WHO | How to stop antibiotic resistance? Here's a WHO prescription. WHO <http://www.who.int/mediacentre/commentaries/stop-antibiotic-resistance/en/>.
34. Lowe, D. & 2016. A Plan For New Antibiotics. *In the Pipeline* <http://blogs.sciencemag.org/pipeline/archives/2016/05/13/a-plan-for-new-antibiotics> (2016).
35. Davies, J. & Davies, D. Origins and Evolution of Antibiotic Resistance. *Microbiol. Mol. Biol. Rev.* **74**, 417–433 (2010).
36. Smith, P. A. & Romesberg, F. E. Combating bacteria and drug resistance by inhibiting mechanisms of persistence and adaptation. *Nat. Chem. Biol.* **3**, 549–556 (2007).
37. Smith, P. W., Watkins, K. & Hewlett, A. Infection control through the ages. *Am. J. Infect. Control* **40**, 35–42 (2012).
38. Torok, E., Moran, E. & Cooke, F. *Oxford Handbook of Infectious Diseases and Microbiology*. (OUP Oxford, 2009).
39. Domagk, G. Ein Beitrag zur Chemotherapie der bakteriellen Infektionen. *DMW - Dtsch. Med. Wochenschr.* **61**, 250–253 (1935).
40. Colebrook, L., Kenny, M., & The members of the honorary staff of St. Charlotte's Hospital. Treatment with Prontosil of Puerperal Infections: Due to Haemolytic Streptococci. *The Lancet* **228**, 1319–1322 (1936).
41. Kaempffert, W. New control for infections: the chemical given to F.D. Roosevelt Jr. for streptococcus hailed as important discovery. *New York Times* (1936).
42. Wainwright, M. & Kristiansen, J. E. On the 75th anniversary of Prontosil. *Dyes Pigments* **88**, 231–234 (2011).
43. Greenwood, D. CHAPTER 1 - Historical introduction. in *Antibiotic and Chemotherapy (Ninth Edition)* (eds. Finch, R. G., Greenwood, D., Norrby,

- S. R. & Whitley, R. J.) 2–9 (W.B. Saunders, 2010). doi:10.1016/B978-0-7020-4064-1.00001-4.
44. Greenwood, D. CHAPTER 29 - Sulfonamides. in *Antibiotic and Chemotherapy (Ninth Edition)* (eds. Finch, R. G., Greenwood, D., Norrby, S. R. & Whitley, R. J.) 337–343 (W.B. Saunders, 2010). doi:10.1016/B978-0-7020-4064-1.00029-4.
45. Fleming, A. On the Antibacterial Action of Cultures of a Penicillium, with Special Reference to their Use in the Isolation of B. influenzae. *Br. J. Exp. Pathol.* **10**, 226–236 (1929).
46. Chain, E. *et al.* Penicillin as a Chemotherapeutic Agent. *The Lancet* **236**, 226–228 (1940).
47. Abraham, E. P. *et al.* Further Observations on Penicillin. *The Lancet* **238**, 177–189 (1941).
48. Debono, M. *et al.* A21978C, a complex of new acidic peptide antibiotics. Isolation, chemistry, and mass spectral structure elucidation. *J. Antibiot. (Tokyo)* **40**, 761–777 (1987).
49. Alder, J. D. Daptomycin, a new drug class for the treatment of Gram-positive infections. *Drugs Today* **41**, 81 (2005).
50. Saga, T. & Yamaguchi, K. History of Antimicrobial Agents and Resistant Bacteria. *J. Jpn. Med. Assoc.* **52**, 103–108 (2009).
51. Emmerson, A. M. The quinolones: decades of development and use. *J. Antimicrob. Chemother.* **51**, 13–20 (2003).
52. Ribeiro da Cunha, Fonseca, & Calado. Antibiotic Discovery: Where Have We Come from, Where Do We Go? *Antibiotics* **8**, 45 (2019).
53. Silver, L. L. Challenges of Antibacterial Discovery. *Clin. Microbiol. Rev.* **24**, 71–109 (2011).
54. Centers for Disease Control and Prevention, Office of Infectious Disease. *Antibiotic resistance threats in the United States - Report.* <http://www.cdc.gov/drugresistance/threat-report-2013> (2013).

55. Payne, D. J., Gwynn, M. N., Holmes, D. J. & Pompliano, D. L. Drugs for bad bugs: confronting the challenges of antibacterial discovery. *Nat. Rev. Drug Discov.* **6**, 29–40 (2007).
56. Lipinski, C. A., Lombardo, F., Dominy, B. W. & Feeney, P. J. Experimental and computational approaches to estimate solubility and permeability in drug discovery and development settings1PII of original article: S0169-409X(96)00423-1. The article was originally published in *Advanced Drug Delivery Reviews* 23 (1997) 3–25.1. *Adv. Drug Deliv. Rev.* **46**, 3–26 (2001).
57. Butler, M. S. & Paterson, D. L. Antibiotics in the clinical pipeline in October 2019. *J. Antibiot. (Tokyo)* (2020) doi:10.1038/s41429-020-0291-8.
58. U.S. Food and Drug Administration. FDA approves new antibacterial drug to treat complicated urinary tract infections as part of ongoing efforts to address antimicrobial resistance. (2019).
59. Piddock, L. J. The Global Antibiotic Research and Development Partnership (GARDP): a not-for-profit antibiotic development organisation. *Lancet Infect. Dis.* **18**, 1304–1305 (2018).
60. World Health Organization. *Antibacterial agents in clinical development: an analysis of the antibacterial clinical development pipeline - Report.* (2019).
61. U.S. Department of Health and Human Services, CDC. *Antibiotic Resistance Threats in the United States - Report.* (2019).
62. World Health Organization. *Antibacterial agents in preclinical development: an open access database - Report.* (2019).
63. Barber, M. & Rozwadowska-Dowzenko, M. Infection by Penicillin-resistant Staphylococci. *The Lancet* **252**, 641–644 (1948).
64. Sun, D., Jeannot, K., Xiao, Y. & Knapp, C. W. Editorial: Horizontal Gene Transfer Mediated Bacterial Antibiotic Resistance. *Front. Microbiol.* **10**, (2019).

65. Zhang, Q.-Q., Ying, G.-G., Pan, C.-G., Liu, Y.-S. & Zhao, J.-L. Comprehensive Evaluation of Antibiotics Emission and Fate in the River Basins of China: Source Analysis, Multimedia Modeling, and Linkage to Bacterial Resistance. *Environ. Sci. Technol.* **49**, 6772–6782 (2015).
66. Qiao, M., Ying, G.-G., Singer, A. C. & Zhu, Y.-G. Review of antibiotic resistance in China and its environment. *Environ. Int.* **110**, 160–172 (2018).
67. Yocum, R. R., Waxman, D. J., Rasmussen, J. R. & Strominger, J. L. Mechanism of penicillin action: penicillin and substrate bind covalently to the same active site serine in two bacterial D-alanine carboxypeptidases. *Proc. Natl. Acad. Sci. U. S. A.* **76**, 2730–2734 (1979).
68. Spratt, B. G. The mechanism of action of penicillin. *Sci. Prog. 1933-* **65**, 101–128 (1978).
69. Sauvage, E., Kerff, F., Terrak, M., Ayala, J. A. & Charlier, P. The penicillin-binding proteins: structure and role in peptidoglycan biosynthesis. *FEMS Microbiol. Rev.* **32**, 234–258 (2008).
70. Massova, I. & Mobashery, S. Kinship and Diversification of Bacterial Penicillin-Binding Proteins and β -Lactamases. *Antimicrob. Agents Chemother.* **42**, 1–17 (1998).
71. Brem, J. *et al.* Structural basis of metallo- β -lactamase, serine- β -lactamase and penicillin-binding protein inhibition by cyclic boronates. *Nat. Commun.* **7**, 12406 (2016).
72. Ghuysen, J. M. Serine Beta-Lactamases and Penicillin-Binding Proteins. *Annu. Rev. Microbiol.* **45**, 37–67 (1991).
73. Stewart, A. C. *et al.* Clinical Variants of New Delhi Metallo- β -Lactamase Are Evolving To Overcome Zinc Scarcity. *ACS Infect. Dis.* (2017) doi:10.1021/acsinfecdis.7b00128.

74. Wang, D. Y., Abboud, M. I., Markoulides, M. S., Brem, J. & Schofield, C. J. The road to avibactam: the first clinically useful non- β -lactam working somewhat like a β -lactam. *Future Med. Chem.* **8**, 1063–1084 (2016).
75. Abboud, M. I. *et al.* Interaction of Avibactam with Class B Metallo- β -Lactamases. *Antimicrob. Agents Chemother.* **60**, 5655–5662 (2016).
76. Ambler, R. P. The structure of β -lactamases. *Philos. Trans. R. Soc. Lond. B Biol. Sci.* **289**, 321–331 (1980).
77. Bush, K. & Jacoby, G. A. Updated Functional Classification of β -Lactamases. *Antimicrob. Agents Chemother.* **54**, 969–976 (2010).
78. Silveira, M. C. *et al.* Systematic Identification and Classification of β -Lactamases Based on Sequence Similarity Criteria: β -Lactamase Annotation. *Evol. Bioinforma.* **14**, 117693431879735 (2018).
79. Singh, R., Saxena, A. & Singh, H. Identification of group specific motifs in Beta-lactamase family of proteins. *J. Biomed. Sci.* **16**, 109 (2009).
80. Tooke, C. L. *et al.* β -Lactamases and β -Lactamase Inhibitors in the 21st Century. *J. Mol. Biol.* **431**, 3472–3500 (2019).
81. Bush, K. & Bradford, P. A. Interplay between β -lactamases and new β -lactamase inhibitors. *Nat. Rev. Microbiol.* **17**, 295–306 (2019).
82. Cohen, S. M. A Bioinorganic Approach to Fragment-Based Drug Discovery Targeting Metalloenzymes. *Acc. Chem. Res.* **50**, 2007–2016 (2017).
83. Valdez, C. E., Smith, Q. A., Nechay, M. R. & Alexandrova, A. N. Mysteries of Metals in Metalloenzymes. *Acc. Chem. Res.* **47**, 3110–3117 (2014).
84. Ulmer, D. D. & Vallee, B. L. Structure and Function of Metalloenzymes. in *Bioinorganic Chemistry* vol. 100 187–218 (American Chemical Society, 1971).
85. McCall, K. A., Huang, C. & Fierke, C. A. Function and mechanism of zinc metalloenzymes. *J. Nutr.* **130**, 1437S–46S (2000).

86. Cai, Y. *et al.* High Prevalence of Metallo- β -Lactamase-Producing *Enterobacter cloacae* From Three Tertiary Hospitals in China. *Front. Microbiol.* **10**, 1610 (2019).
87. Kaur, A. & Singh, S. Prevalence of Extended Spectrum Betalactamase (ESBL) and Metallobetalactamase (MBL) Producing *Pseudomonas aeruginosa* and *Acinetobacter baumannii* Isolated from Various Clinical Samples. *J. Pathog.* **2018**, 1–7 (2018).
88. Turton, J. F. *et al.* High-Resolution Analysis by Whole-Genome Sequencing of an International Lineage (Sequence Type 111) of *Pseudomonas aeruginosa* Associated with Metallo-Carbapenemases in the United Kingdom. *J. Clin. Microbiol.* **53**, 2622–2631 (2015).
89. Murzin, A. G., Brenner, S. E., Hubbard, T. & Chothia, C. SCOP: a structural classification of proteins database for the investigation of sequences and structures. *J. Mol. Biol.* **247**, 536–540 (1995).
90. Baier, F. & Tokuriki, N. Connectivity between Catalytic Landscapes of the Metallo- β -Lactamase Superfamily. *J. Mol. Biol.* **426**, 2442–2456 (2014).
91. Bebrone, C. Metallo- β -lactamases (classification, activity, genetic organization, structure, zinc coordination) and their superfamily. *Biochem. Pharmacol.* **74**, 1686–1701 (2007).
92. Carfi, A. *et al.* The 3-D structure of a zinc metallo- β -lactamase from *Bacillus cereus* reveals a new type of protein fold. *EMBO J.* **14**, 4914–4921 (1995).
93. Pettinati, I., Brem, J., Lee, S. Y., McHugh, P. J. & Schofield, C. J. The Chemical Biology of Human Metallo- β -Lactamase Fold Proteins. *Trends Biochem. Sci.* **41**, 338–355 (2016).
94. Palzkill, T. Metallo- β -lactamase structure and function. *Ann. N. Y. Acad. Sci.* **1277**, 91–104 (2013).
95. Galleni, M. *et al.* Standard Numbering Scheme for Class B β -Lactamases. *Antimicrob. Agents Chemother.* **45**, 660–663 (2001).

96. Meini, M.-R., Llarrull, L. I. & Vila, A. J. Overcoming differences: The catalytic mechanism of metallo- β -lactamases. *FEBS Lett.* **589**, 3419–3432 (2015).
97. Bebrone, C. *et al.* The Structure of the Dizinc Subclass B2 Metallo- β -Lactamase CphA Reveals that the Second Inhibitory Zinc Ion Binds in the Histidine Site. *Antimicrob. Agents Chemother.* **53**, 4464–4471 (2009).
98. De Vriendt, K. *et al.* Monitoring the Zinc Affinity of the Metallo- β -Lactamase CphA by Automated nanoESI-MS. *J. Am. Soc. Mass Spectrom.* **17**, 180–188 (2006).
99. Fonseca, F. *et al.* Biochemical Characterization of Sfh-I, a Subclass B2 Metallo- β -Lactamase from *Serratia fonticola* UTAD54. *Antimicrob. Agents Chemother.* **55**, 5392–5395 (2011).
100. Hinchliffe, P. *et al.* Cross-class metallo- β -lactamase inhibition by bisthiazolidines reveals multiple binding modes. *Proc. Natl. Acad. Sci.* **113**, E3745–E3754 (2016).
101. Crowder, M. W., Walsh, T. R., Banovic, L., Pettit, M. & Spencer, J. Overexpression, Purification, and Characterization of the Cloned Metallo- β -Lactamase L1 from *Stenotrophomonas maltophilia*. *Antimicrob. Agents Chemother.* **42**, 921–926 (1998).
102. Docquier, J.-D. *et al.* CAU-1, a Subclass B3 Metallo- β -Lactamase of Low Substrate Affinity Encoded by an Ortholog Present in the *Caulobacter crescentus* Chromosome. *Antimicrob. Agents Chemother.* **46**, 1823–1830 (2002).
103. Wachino, J. *et al.* Structural Insights into the Subclass B3 Metallo- β -Lactamase SMB-1 and the Mode of Inhibition by the Common Metallo- β -Lactamase Inhibitor Mercaptoacetate. *Antimicrob. Agents Chemother.* **57**, 101–109 (2013).
104. Felici, A. & Amicosante, G. Kinetic analysis of extension of substrate specificity with *Xanthomonas maltophilia*, *Aeromonas hydrophila*, and

- Bacillus cereus metallo-beta-lactamases. *Antimicrob. Agents Chemother.* **39**, 192–199 (1995).
105. Horsfall, L. E. *et al.* Broad antibiotic resistance profile of the subclass B3 metallo- β -lactamase GOB-1, a di-zinc enzyme: Metallo- β -lactamase GOB-1. *FEBS J.* **278**, 1252–1263 (2011).
106. Mercuri, P. S. *et al.* Biochemical Characterization of the FEZ-1 Metallo- β -Lactamase of Legionella gormanii ATCC 33297T Produced in Escherichia coli. *Antimicrob. Agents Chemother.* **45**, 1254–1262 (2001).
107. Dal Peraro, M., Vila, A. J., Carloni, P. & Klein, M. L. Role of Zinc Content on the Catalytic Efficiency of B1 Metallo β -Lactamases. *J. Am. Chem. Soc.* **129**, 2808–2816 (2007).
108. Cornaglia, G. *et al.* Appearance of IMP-1 metallo- β -lactamase in Europe. *The Lancet* **353**, 899–900 (1999).
109. Rolain, J. M., Parola, P. & Cornaglia, G. New Delhi metallo-beta-lactamase (NDM-1): towards a new pandemia? *Clin. Microbiol. Infect.* **16**, 1699–1701 (2010).
110. Poirel, L. *et al.* Characterization of VIM-2, a Carbapenem-Hydrolyzing Metallo- β -Lactamase and Its Plasmid- and Integron-Borne Gene from a Pseudomonas aeruginosa Clinical Isolate in France. *Antimicrob. Agents Chemother.* **44**, 891–897 (2000).
111. Kazmierczak, K. M. *et al.* Multiyear, Multinational Survey of the Incidence and Global Distribution of Metallo- β -Lactamase-Producing Enterobacteriaceae and Pseudomonas aeruginosa. *Antimicrob. Agents Chemother.* **60**, 1067–1078 (2016).
112. Yotsuji, A. Properties of Novel 3-Lactamase Produced by Bacteroides fragilis. *Antimicrob Agents Chemother* **24**, 5 (1983).
113. Osano, E., Horii, T., Ito, H. & Yoshimura, F. Molecular Characterization of an Enterobacterial Metallo 1-Lactamase Found in a Clinical Isolate of

- Serratia marcescens That Shows Imipenem Resistance. *Antimicrob Agents Chemother* **38**, 8 (1994).
114. Mojica, M. F., Bonomo, R. A. & Fast, W. B1-Metallo-beta-Lactamases: Where do we stand? *Curr. Drug Targets* **17**, 1029–1050 (2016).
115. Yatsuyanagi, J. *et al.* Class 1 Integron Containing Metallo- β -Lactamase Gene blaVIM-2 in Pseudomonas aeruginosa Clinical Strains Isolated in Japan. *Antimicrob. Agents Chemother.* **48**, 626–628 (2004).
116. Zafer, M. M., Al-Agamy, M. H., El-Mahallawy, H. A., Amin, M. A. & El Din Ashour, S. Dissemination of VIM-2 producing Pseudomonas aeruginosa ST233 at tertiary care hospitals in Egypt. *BMC Infect. Dis.* **15**, 122 (2015).
117. Moyo, S. *et al.* Identification of VIM-2-Producing Pseudomonas aeruginosa from Tanzania Is Associated with Sequence Types 244 and 640 and the Location of blaVIM-2 in a TniC Integron. *Antimicrob. Agents Chemother.* **59**, 682–685 (2015).
118. Edelstein, M. V. *et al.* Spread of extensively resistant VIM-2-positive ST235 Pseudomonas aeruginosa in Belarus, Kazakhstan, and Russia: a longitudinal epidemiological and clinical study. *Lancet Infect. Dis.* **13**, 867–876 (2013).
119. Peña, C. *et al.* Nosocomial spread of Pseudomonas aeruginosa producing the metallo- β -lactamase VIM-2 in a Spanish hospital: clinical and epidemiological implications. *Clin. Microbiol. Infect.* **13**, 1026–1029 (2007).
120. Villegas, M. V. *et al.* First Detection of Metallo- β -Lactamase VIM-2 in Pseudomonas aeruginosa Isolates from Colombia. *Antimicrob. Agents Chemother.* **50**, 226–229 (2006).
121. Yong, D. *et al.* Characterization of a New Metallo- β -Lactamase Gene, blaNDM-1, and a Novel Erythromycin Esterase Gene Carried on a Unique

- Genetic Structure in *Klebsiella pneumoniae* Sequence Type 14 from India. *Antimicrob. Agents Chemother.* **53**, 5046–5054 (2009).
122. Khan, A. U., Maryam, L. & Zarrilli, R. Structure, Genetics and Worldwide Spread of New Delhi Metallo- β -lactamase (NDM): a threat to public health. *BMC Microbiol.* **17**, 101 (2017).
123. Kumarasamy, K. K. *et al.* Emergence of a new antibiotic resistance mechanism in India, Pakistan, and the UK: a molecular, biological, and epidemiological study. *Lancet Infect. Dis.* **10**, 597–602 (2010).
124. Prunotto, A., Bahr, G., González, L. J., Vila, A. J. & Dal Peraro, M. Molecular Bases of the Membrane Association Mechanism Potentiating Antibiotic Resistance by New Delhi Metallo- β -lactamase 1. *ACS Infect. Dis.* (2020) doi:10.1021/acinfecdis.0c00341.
125. López, C., Ayala, J. A., Bonomo, R. A., González, L. J. & Vila, A. J. Protein determinants of dissemination and host specificity of metallo- β -lactamases. *Nat. Commun.* **10**, 3617 (2019).
126. Kirby, W. M. M. Extraction of a Highly Potent Penicillin Inactivator from Penicillin Resistant Staphylococci. *Science* **99**, 452–453 (1944).
127. Hakenbeck, R. & Coyette, J. Resistant penicillin-binding proteins. *Cell. Mol. Life Sci. CMLS* **54**, 332–340 (1998).
128. Therrien, C. & Levesque, R. C. Molecular basis of antibiotic resistance and β -lactamase inhibition by mechanism-based inactivators: perspectives and future directions. *FEMS Microbiol. Rev.* **24**, 251–262 (2000).
129. Zhanel, G. G. *et al.* Cefiderocol: A Siderophore Cephalosporin with Activity Against Carbapenem-Resistant and Multidrug-Resistant Gram-Negative Bacilli. *Drugs* **79**, 271–289 (2019).
130. Ito-Horiyama, T. *et al.* Stability of Novel Siderophore Cephalosporin S-649266 against Clinically Relevant Carbapenemases. *Antimicrob. Agents Chemother.* **60**, 4384–4386 (2016).

131. Ehmann, D. E. *et al.* Avibactam is a covalent, reversible, non- β -lactam β -lactamase inhibitor. *Proc. Natl. Acad. Sci.* **109**, 11663–11668 (2012).
132. Drawz, S. M. & Bonomo, R. A. Three Decades of β -Lactamase Inhibitors. *Clin. Microbiol. Rev.* **23**, 160–201 (2010).
133. Black, J. A., Thomson, K. S., Buynak, J. D. & Pitout, J. D. D. Evaluation of β -Lactamase Inhibitors in Disk Tests for Detection of Plasmid-Mediated AmpC β -Lactamases in Well-Characterized Clinical Strains of *Klebsiella* spp. *J. Clin. Microbiol.* **43**, 4168–4171 (2005).
134. Nishida, K. *et al.* In Vitro and In Vivo Activities of Syn2190, a Novel β -Lactamase Inhibitor. *Antimicrob. Agents Chemother.* **43**, 1895–1900 (1999).
135. Lomovskaya, O. *et al.* Vaborbactam: Spectrum of Beta-Lactamase Inhibition and Impact of Resistance Mechanisms on Activity in Enterobacteriaceae. *Antimicrob. Agents Chemother.* **61**, e01443-17, e01443-17 (2017).
136. King, D. T., Sobhanifar, S. & Strynadka, N. C. J. One ring to rule them all: Current trends in combating bacterial resistance to the β -lactams. *Protein Sci.* **25**, 787–803 (2016).
137. Jorgensen, S. C. J. & Rybak, M. J. Meropenem and Vaborbactam: Stepping up the Battle against Carbapenem-resistant Enterobacteriaceae. *Pharmacother. J. Hum. Pharmacol. Drug Ther.* **38**, 444–461 (2018).
138. Hecker, S. J. *et al.* Discovery of a Cyclic Boronic Acid β -Lactamase Inhibitor (RPX7009) with Utility vs Class A Serine Carbapenemases. *J. Med. Chem.* **58**, 3682–3692 (2015).
139. Cahill, S. T. *et al.* Cyclic Boronates Inhibit All Classes of β -Lactamases. *Antimicrob. Agents Chemother.* **61**, e02260-16, e02260-16 (2017).
140. Liu, B. *et al.* Discovery of Taniborbactam (VNRX-5133): A Broad-Spectrum Serine- and Metallo- β -lactamase Inhibitor for Carbapenem-Resistant Bacterial Infections. *J. Med. Chem.* **63**, 2789–2801 (2020).

141. Venatorx Pharmaceuticals, Inc. *A Phase 3, Randomized, Double-blind, Active Controlled Noninferiority Study Evaluating the Efficacy, Safety, and Tolerability of Cefepime/VNRX-5133 in Adults With Complicated Urinary Tract Infections (cUTI), Including Acute Pyelonephritis*. <https://clinicaltrials.gov/ct2/show/NCT03840148> (2021).
142. Cefepime-Taniborbactam. Venatorx Pharmaceuticals <https://www.venatorx.com/cefepime-taniborbactam/>.
143. Ju, L.-C., Cheng, Z., Fast, W., Bonomo, R. A. & Crowder, M. W. The Continuing Challenge of Metallo- β -Lactamase Inhibition: Mechanism Matters. *Trends Pharmacol. Sci.* **39**, 635–647 (2018).
144. Khan, N. H. *et al.* A DNA aptamer reveals an allosteric site for inhibition in metallo- β -lactamases. *PLOS ONE* **14**, e0214440 (2019).
145. Yang, Y. *et al.* Discovery of a Novel Natural Allosteric Inhibitor That Targets NDM-1 Against Escherichia coli. *Front. Pharmacol.* **11**, 1531 (2020).
146. Kurosaki, H. *et al.* Probing, Inhibition, and Crystallographic Characterization of Metallo- β -lactamase (IMP-1) with Fluorescent Agents Containing Dansyl and Thiol Groups. *ChemMedChem* **1**, 969–972 (2006).
147. Sabath, L. D. & Abraham, E. P. Zinc as a Cofactor for Cephalosporinase from Bacillus cereus 569. *Biochem. J.* **98**, 11C-13C (1966).
148. Krajnc, A. *et al.* Bicyclic Boronate VNRX-5133 Inhibits Metallo- and Serine- β -Lactamases. *J. Med. Chem.* **62**, 8544–8556 (2019).
149. Brem, J. *et al.* Structural Basis of Metallo- β -Lactamase Inhibition by Captopril Stereoisomers. *Antimicrob. Agents Chemother.* **60**, 142–150 (2016).
150. Cain, R. *et al.* In silico fragment based design identifies subfamily B1 metallo- β -lactamase inhibitors. *J. Med. Chem.* (2017) doi:10.1021/acs.jmedchem.7b01728.

151. Kurosaki, H. *et al.* Irreversible Inhibition of Metallo- β -lactamase (IMP-1) by 3-(3-Mercaptopropionylsulfanyl)propionic Acid Pentafluorophenyl Ester. *Angew. Chem. Int. Ed.* **44**, 3861–3864 (2005).
152. Cain, R. Design and synthesis of metallo- β -lactamase inhibitors. (University of Leeds, 2015).
153. Reddy, R., Glinka, T., Totrov, M., Hecker, S. & Rodny, O. Boronic Acid Derivatives and Therapeutic Uses Thereof. (2016).
154. Matteson, D. S. & Ray, R. Directed chiral synthesis with pinanediol boronic esters. *J. Am. Chem. Soc.* **102**, 7590–7591 (1980).
155. Thomas, S. P., French, R. M., Jheengut, V. & Aggarwal, V. K. Homologation and alkylation of boronic esters and boranes by 1,2-metallate rearrangement of boron ate complexes. *Chem. Rec.* **9**, 24–39 (2009).
156. Leonori, D. & Aggarwal, V. K. Reagent-Controlled Lithiation–Borylation. in *Synthesis and Application of Organoboron Compounds* (eds. Fernández, E. & Whiting, A.) 271–295 (Springer International Publishing, 2015). doi:10.1007/978-3-319-13054-5_9.
157. Home - Schofield Group. <http://schofield.chem.ox.ac.uk/>.
158. Parkova, A. *et al.* Broad Spectrum β -Lactamase Inhibition by a Thioether Substituted Bicyclic Boronate. *ACS Infect. Dis.* **6**, 1398–1404 (2020).
159. Mollard, C. *et al.* Thiomandelic Acid, a Broad Spectrum Inhibitor of Zinc β -Lactamases: Kinetic and Spectroscopic Studies * 210. *J. Biol. Chem.* **276**, 45015–45023 (2001).
160. Olsen, L. *et al.* New leads of metallo- β -lactamase inhibitors from structure-based pharmacophore design. *Bioorg. Med. Chem.* **14**, 2627–2635 (2006).

161. Greenlee, M. L. *et al.* Synthesis and SAR of thioester and thiol inhibitors of IMP-1 Metallo- β -Lactamase. *Bioorg. Med. Chem. Lett.* **9**, 2549–2554 (1999).
162. Heinz, U. *et al.* Coordination Geometries of Metal Ions in D- or L-Captopril-inhibited Metallo- β -lactamases*. *J. Biol. Chem.* **278**, 20659–20666 (2003).
163. Yusof, Y., Tan, D. T. C., Arjomandi, O. K., Schenk, G. & McGeary, R. P. Captopril analogues as metallo- β -lactamase inhibitors. *Bioorg. Med. Chem. Lett.* **26**, 1589–1593 (2016).
164. Li, N. *et al.* Simplified captopril analogues as NDM-1 inhibitors. *Bioorg. Med. Chem. Lett.* **24**, 386–389 (2014).
165. Mata, P. *et al.* SPROUT: 3D Structure Generation Using Templates. *J. Chem. Inf. Comput. Sci.* **35**, 479–493 (1995).
166. Gillet, V. J. *et al.* SPROUT: Recent developments in the de novo design of molecules. *J. Chem. Inf. Comput. Sci.* **34**, 207–217 (1994).
167. Richter, M. F. & Hergenrother, P. J. The challenge of converting Gram-positive-only compounds into broad-spectrum antibiotics. *Ann. N. Y. Acad. Sci.* **1435**, 18–38 (2019).
168. Maia, E. H. B., Assis, L. C., de Oliveira, T. A., da Silva, A. M. & Taranto, A. G. Structure-Based Virtual Screening: From Classical to Artificial Intelligence. *Front. Chem.* **8**, 343 (2020).
169. Anderson, A. C. The Process of Structure-Based Drug Design. *Chem. Biol.* **10**, 787–797 (2003).
170. Waterhouse, A. *et al.* SWISS-MODEL: homology modelling of protein structures and complexes. *Nucleic Acids Res.* **46**, W296–W303 (2018).
171. Ferreira, L., dos Santos, R., Oliva, G. & Andricopulo, A. Molecular Docking and Structure-Based Drug Design Strategies. *Molecules* **20**, 13384–13421 (2015).

172. Scapin, G., Potter, C. S. & Carragher, B. Cryo-EM for Small Molecules Discovery, Design, Understanding, and Application. *Cell Chem. Biol.* **25**, 1318–1325 (2018).
173. Lin, X., Li, X. & Lin, X. A Review on Applications of Computational Methods in Drug Screening and Design. *Molecules* **25**, 1375 (2020).
174. *Schrödinger Release 2020-3: Glide*, Schrödinger, LLC, New York, NY, 2018.
175. Roos, K. *et al.* OPLS3e: Extending Force Field Coverage for Drug-Like Small Molecules. *J. Chem. Theory Comput.* **15**, 1863–1874 (2019).
176. Eldridge, M. D., Murray, C. W., Auton, T. R., Paolini, G. V. & Mee, R. P. Empirical scoring functions: I. The development of a fast empirical scoring function to estimate the binding affinity of ligands in receptor complexes. *J. Comput. Aided Mol. Des.* **11**, 425–445 (1997).
177. Friesner, R. A. *et al.* Glide: A New Approach for Rapid, Accurate Docking and Scoring. 1. Method and Assessment of Docking Accuracy. *J. Med. Chem.* **47**, 1739–1749 (2004).
178. Friesner, R. A. *et al.* Extra Precision Glide: Docking and Scoring Incorporating a Model of Hydrophobic Enclosure for Protein–Ligand Complexes. *J. Med. Chem.* **49**, 6177–6196 (2006).
179. Sherman, W., Day, T., Jacobson, M. P., Friesner, R. A. & Farid, R. Novel Procedure for Modeling Ligand/Receptor Induced Fit Effects. *J. Med. Chem.* **49**, 534–553 (2006).
180. Lu, C. *et al.* OPLS4: Improving Force Field Accuracy on Challenging Regimes of Chemical Space. *J. Chem. Theory Comput.* **17**, 4291–4300 (2021).
181. Kendall tau Rank Correlation - Free Statistics and Forecasting Software (Calculators) v.1.2.1.
https://www.wessa.net/rwasp_kendall.wasp#cite.

182. Jones, G., Willett, P., Glen, R. C., Leach, A. R. & Taylor, R. Development and validation of a genetic algorithm for flexible docking. *J. Mol. Biol.* **267**, 727–748 (1997).
183. Pagadala, N. S., Syed, K. & Tuszynski, J. Software for molecular docking: a review. *Biophys. Rev.* **9**, 91–102 (2017).
184. Jones, G., Willett, P. & Glen, R. C. Molecular recognition of receptor sites using a genetic algorithm with a description of desolvation. *J. Mol. Biol.* **245**, 43–53 (1995).
185. Case: What is the difference between the GoldScore, ChemScore, ASP and ChemPLP scoring functions provided with GOLD? - The Cambridge Crystallographic Data Centre (CCDC). <https://www.ccdc.cam.ac.uk/support-and-resources/support/case/?caseid=5d1a2fc0-c93a-49c3-a8e2-f95c472dcff0>.
186. Liu, J., Kimmel, K., Dao, K., Liu, Y. & Qi, M. Identification and Elimination of an Unexpected Catalyst Poison in Suzuki Coupling. *Org. Process Res. Dev.* **22**, 111–116 (2018).
187. Semple, J. E. *et al.* Trisubstituted Nitrogen Modulators of Tyrosine Phosphatases. (2006).
188. Olah, G. A. & Narang, S. C. Iodotrimethylsilane—a versatile synthetic reagent. *Tetrahedron* **38**, 2225–2277 (1982).
189. Kim, R., Kuduk, S. D., Liverton, N. & Zhuo, G. Ethyldiamine Orexin Receptor Antagonists. (2016).
190. Zhang, X. & Cao, S. Recent advances in the synthesis and CF functionalization of gem-difluoroalkenes. *Tetrahedron Lett.* **58**, 375–392 (2017).
191. Fleischer, M. Ueber das Sulfobenzol und Disulfobenzol. *Justus Liebigs Ann. Chem.* **140**, 234–242 (1866).

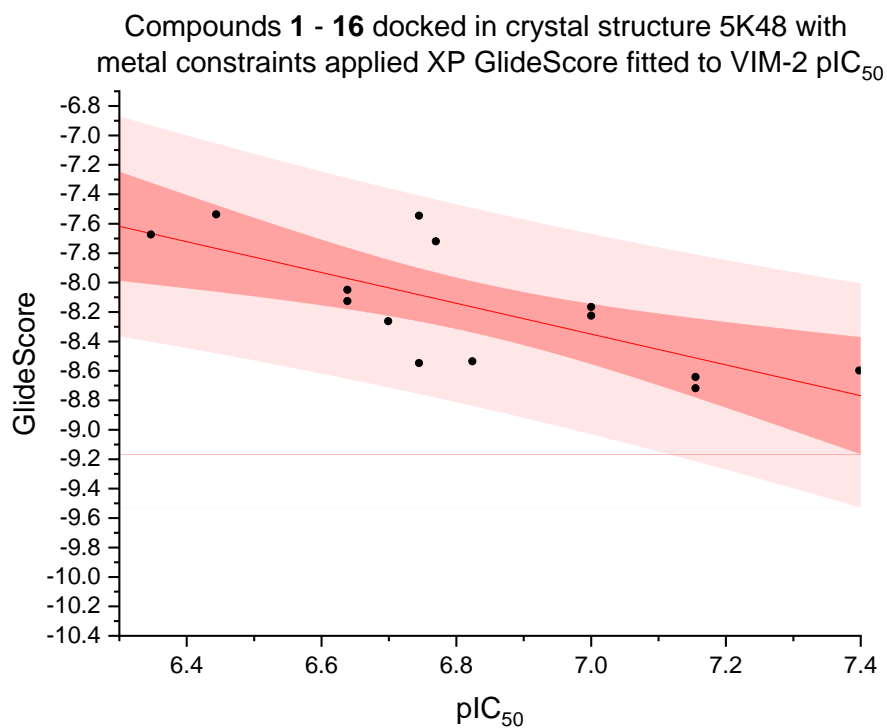
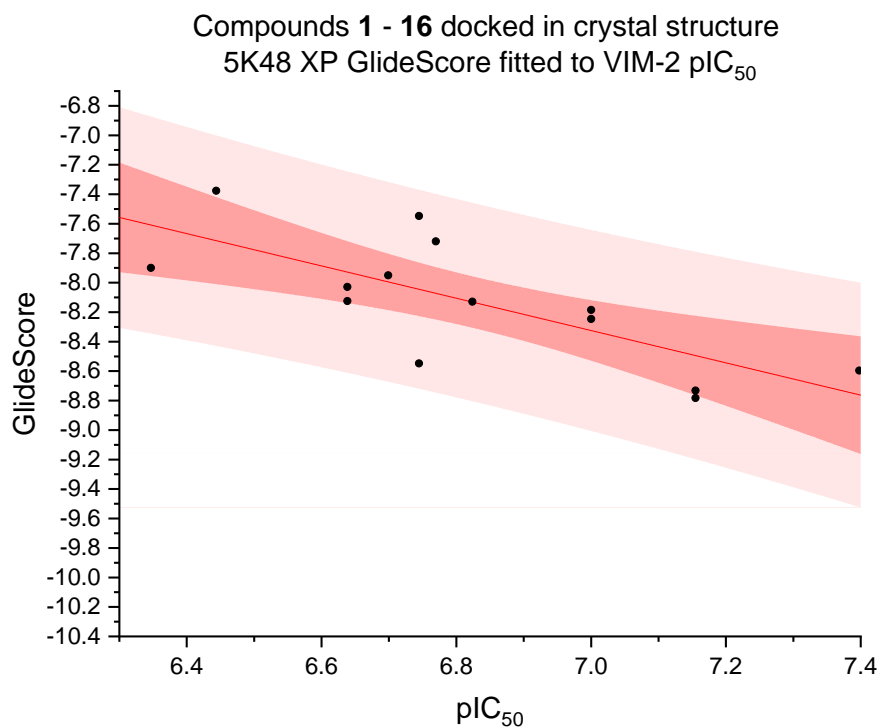
192. Grote, J. *et al.* Dithiocarboxylic Acids: An Old Theme Revisited and Augmented by New Preparative, Spectroscopic and Structural Facts. *Chem. – Eur. J.* **24**, 2626–2633 (2018).
193. Thomas, C. S. *et al.* Pyridine-2,6-Dithiocarboxylic Acid and Its Metal Complexes: New Inhibitors of New Delhi Metallo- β -Lactamase-1. *Mar. Drugs* **18**, 295 (2020).
194. Kato, S. *et al.* A Convenient Preparation Method of Anhydrous Lithium, Potassium, Rubidium and Cesium Dithiocarboxylates. *Z. Für Naturforschung B* **35**, 458–462 (1980).
195. Crampton, M. R. Acidity and hydrogen-bonding. in *The Thiol Group* (1974) 379–415 (John Wiley & Sons, Ltd, 1974). doi:10.1002/9780470771310.ch8.
196. Bordas, B., Sohar, P., Matolcsy, G. & Berencsi, P. Synthesis and antifungal properties of dithiocarboxylic acid derivatives. II. Novel preparation of 2-alkylamino-1-cyclopentene-1-dithiocarboxylic acids and some of their derivatives. *J. Org. Chem.* **37**, 1727–1730 (1972).
197. Cruz, J. C.-D. L., Ureña-Núñez, F., Morales-Juárez, J., Pastor-Medrano, J. & Gómez-Espinosa, R. M. Synthesis of IIB group derived of N-methyl caprolactam-3-dithiocarboxylic acid complexes: thermal properties. *J. Coord. Chem.* **61**, 3253–3259 (2008).
198. Zhang, E. *et al.* NOTA analogue: A first dithiocarbamate inhibitor of metallo- β -lactamases. *Bioorg. Med. Chem. Lett.* **28**, 214–221 (2018).
199. Wang, M.-M. *et al.* Dithiocarbamates: Efficient metallo- β -lactamase inhibitors with good antibacterial activity when combined with meropenem. *Bioorg. Med. Chem. Lett.* **28**, 3436–3440 (2018).
200. Ge, Y. *et al.* Dithiocarbamate as a Valuable Scaffold for the Inhibition of Metallo- β -Lactamases. *Biomolecules* **9**, 699 (2019).
201. Kumar, R. A. *et al.* Strain-Promoted 1,3-Dithiolium-4-olates–Alkyne Cycloaddition. *Angew. Chem. Int. Ed.* **58**, 14544–14548 (2019).

202. KarinaCalvopina - Schofield Group.
<http://schofield.chem.ox.ac.uk/karinacalvopina.aspx>.
203. Tan, J., Akakura, M. & Yamamoto, H. The Supersilyl Group as a Carboxylic Acid Protecting Group: Application to Highly Stereoselective Aldol and Mannich Reactions. *Angew. Chem. Int. Ed.* **52**, 7198–7202 (2013).
204. Berthold, M. R. *et al.* KNIME: The Konstanz Information Miner. in *Data Analysis, Machine Learning and Applications* (eds. Preisach, C., Burkhardt, H., Schmidt-Thieme, L. & Decker, R.) 319–326 (Springer, 2008). doi:10.1007/978-3-540-78246-9_38.
205. RDKit. <http://www.rdkit.org/>.
206. Christen, M.-O. [32] Anethole dithiolethione: Biochemical considerations. in *Methods in Enzymology* vol. 252 316–323 (Academic Press, 1995).
207. Ishii, A. & Nakayama, J. Carbodithioic Acid Esters. in *Chalcogenocarboxylic Acid Derivatives: -/-* (ed. Kato, S.) 181–225 (Springer, 2005). doi:10.1007/b101009.
208. van Berkel, S. S. *et al.* Assay Platform for Clinically Relevant Metallo- β -lactamases. *J. Med. Chem.* **56**, 6945–6953 (2013).
209. Jones, R. N., Wilson, H. W., Novick, W. J., Barry, A. L. & Thornsberry, C. In vitro evaluation of CENTA, a new beta-lactamase-susceptible chromogenic cephalosporin reagent. *J. Clin. Microbiol.* **15**, 954–958 (1982).
210. Shannon, K. & Phillips, I. β -Lactamase detection by three simple methods: Intralactam, nitrocefin and acidimetric. *J. Antimicrob. Chemother.* **6**, 617–621 (1980).
211. Goddard, J.-P. & Reymond, J.-L. Enzyme assays for high-throughput screening. *Curr. Opin. Biotechnol.* **15**, 314–322 (2004).

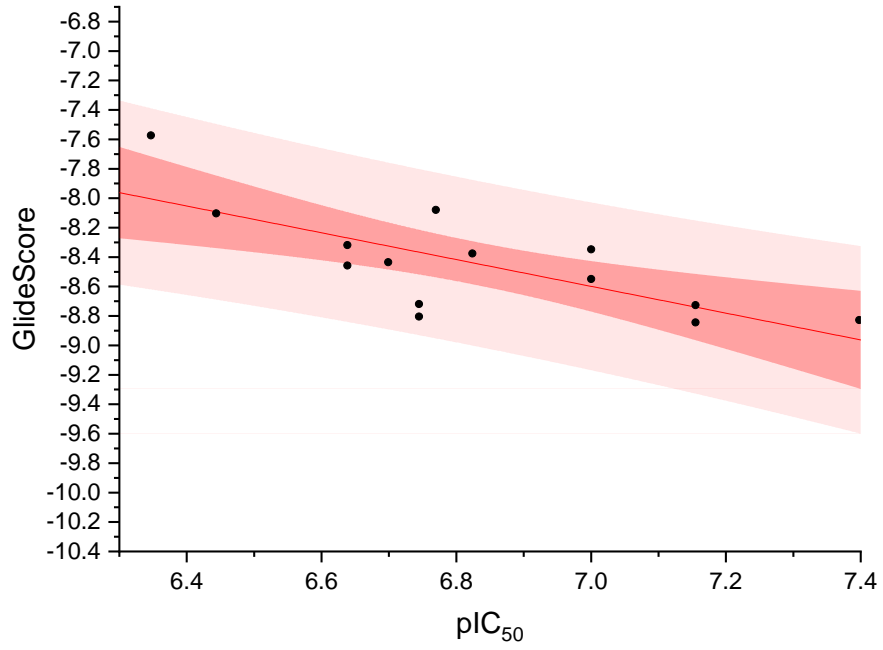
212. Farley, A. J. M. *et al.* Structural Basis of Metallo- β -lactamase Inhibition by N-Sulfamoylpyrrole-2-carboxylates. *ACS Infect. Dis.* **7**, 1809–1817 (2021).
213. Murphy, T. A. *et al.* Crystal Structure of *Pseudomonas aeruginosa* SPM-1 Provides Insights into Variable Zinc Affinity of Metallo- β -lactamases. *J. Mol. Biol.* **357**, 890–903 (2006).
214. Perez, F., Endimiani, A., Hujer, K. M. & Bonomo, R. A. The continuing challenge of ESBLs. *Curr. Opin. Pharmacol.* **7**, 459–469 (2007).
215. Evans, B. A. & Amyes, S. G. B. OXA β -Lactamases. *Clin. Microbiol. Rev.* **27**, 241–263 (2014).
216. He, Y. *et al.* Highly Enantioselective Synthesis of 2,3-Dihydro-1H-imidazo[2,1-a]isoindol-5(9bH)-ones via Catalytic Asymmetric Intramolecular Cascade Imidization–Nucleophilic Addition–Lactamization. *Org. Lett.* **16**, 6366–6369 (2014).

Appendix

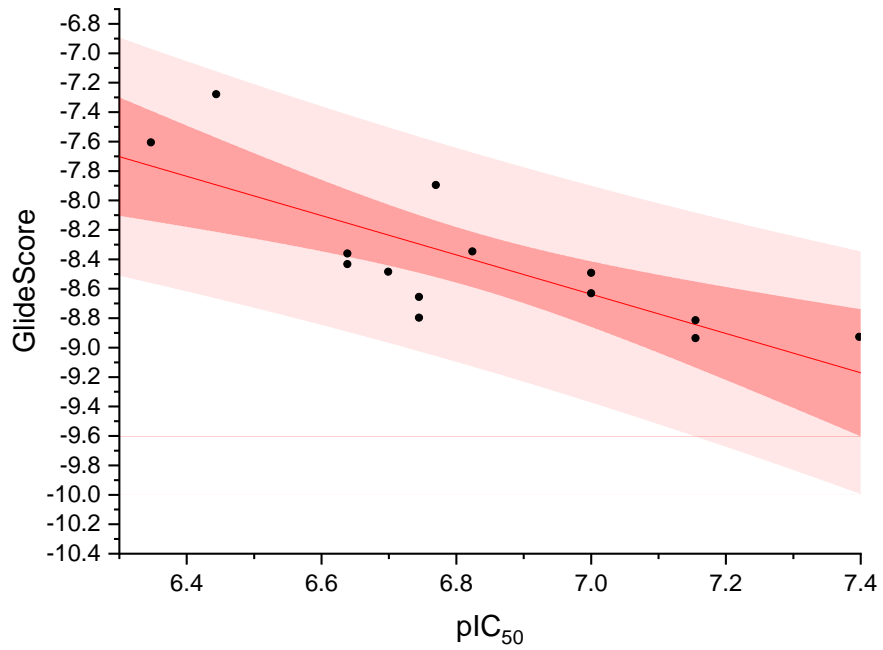
Linear regression analysis plots



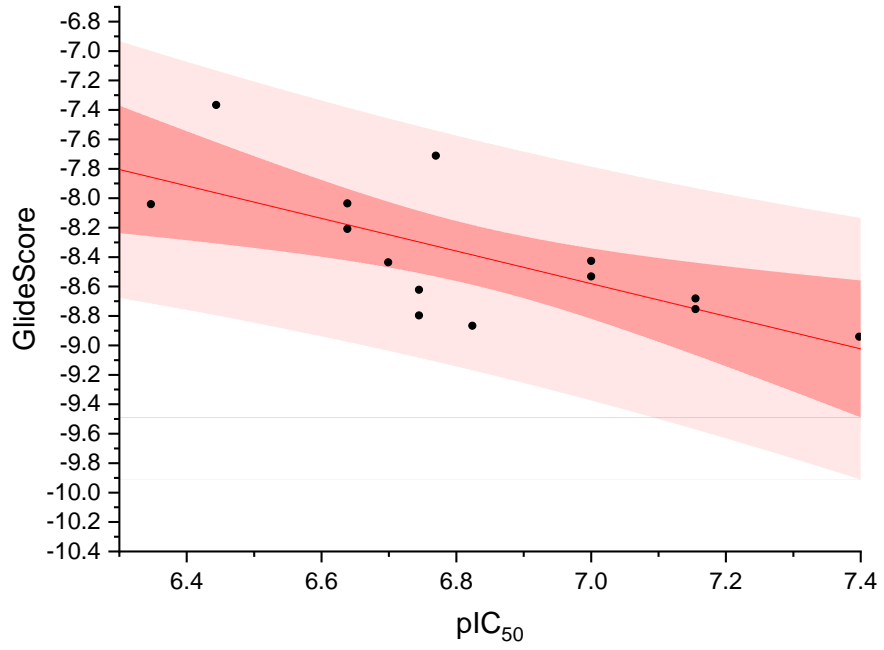
Compounds **1 - 16** docked in crystal structure 5K48 XP with waters 438 and 558 included GlideScore fitted to VIM-2 pIC_{50}



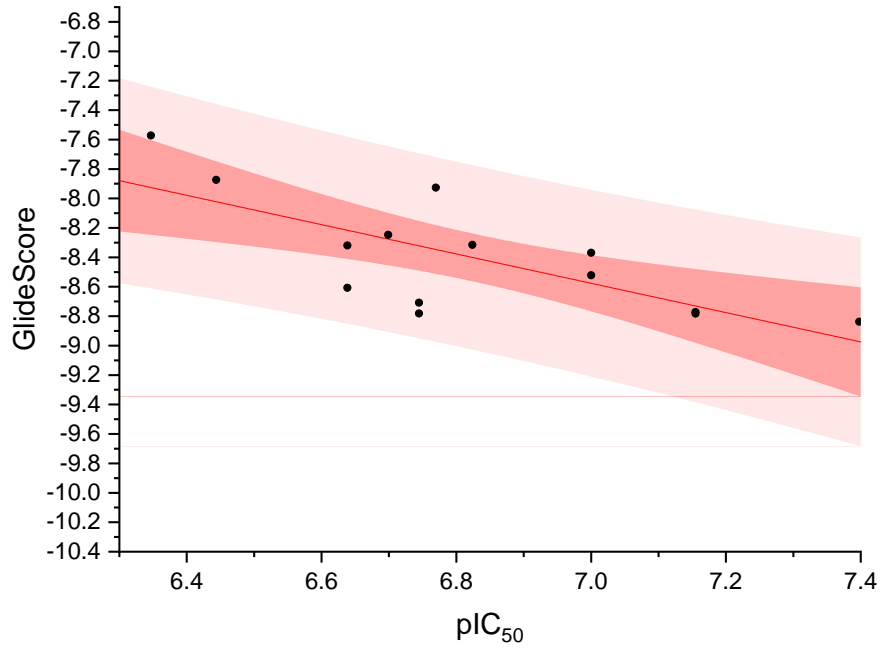
Compounds **1 - 16** docked in crystal structure 5K48 XP with water 438 included GlideScore fitted to VIM-2 pIC_{50}



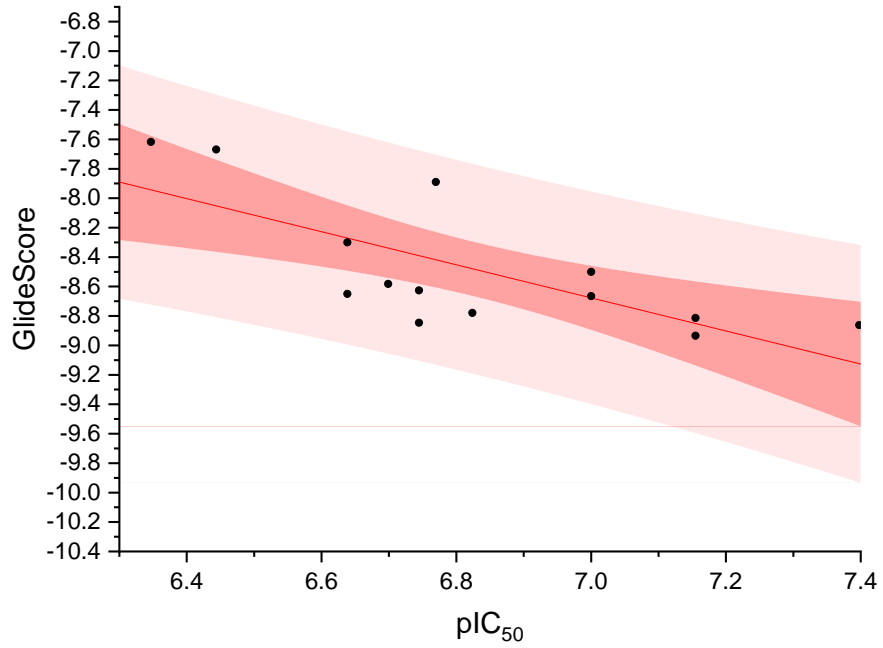
Compounds **1 - 16** docked in crystal structure 5K48 XP with water 558 included GlideScore fitted to VIM-2 pIC₅₀



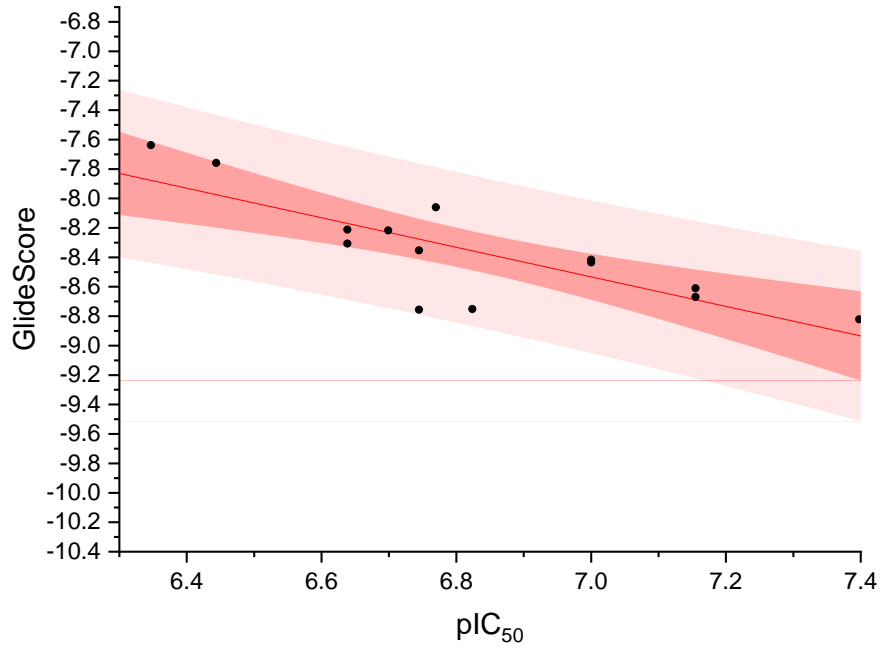
Compounds **1 - 16** docked in crystal structure 5K48 with metals constraints applied and waters 438 and 558 included XP GlideScore fitted to VIM-2 pIC₅₀



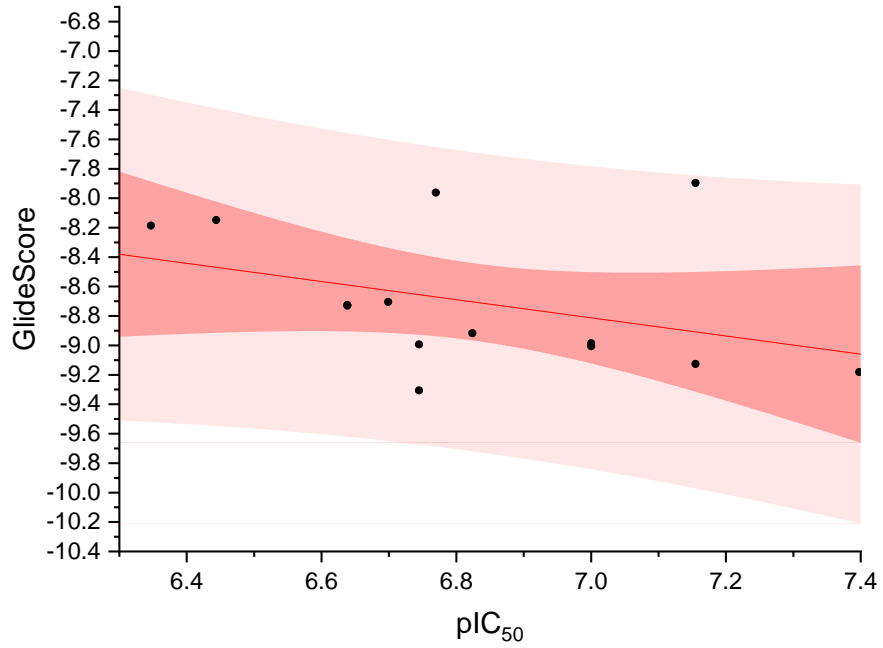
Compounds **1 - 16** docked in crystal structure 5K48 with metals constraints applied and water 438 included XP GlideScore fitted to VIM-2 pIC_{50}



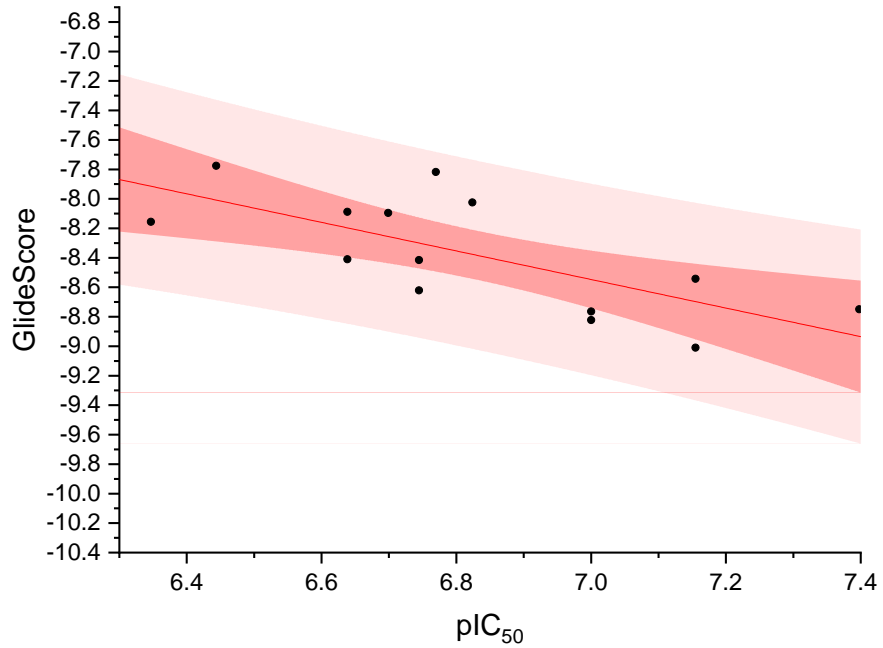
Compounds **1 - 16** docked in crystal structure 5K48 with metal constraints applied and water 558 included XP GlideScore fitted to VIM-2 pIC_{50}



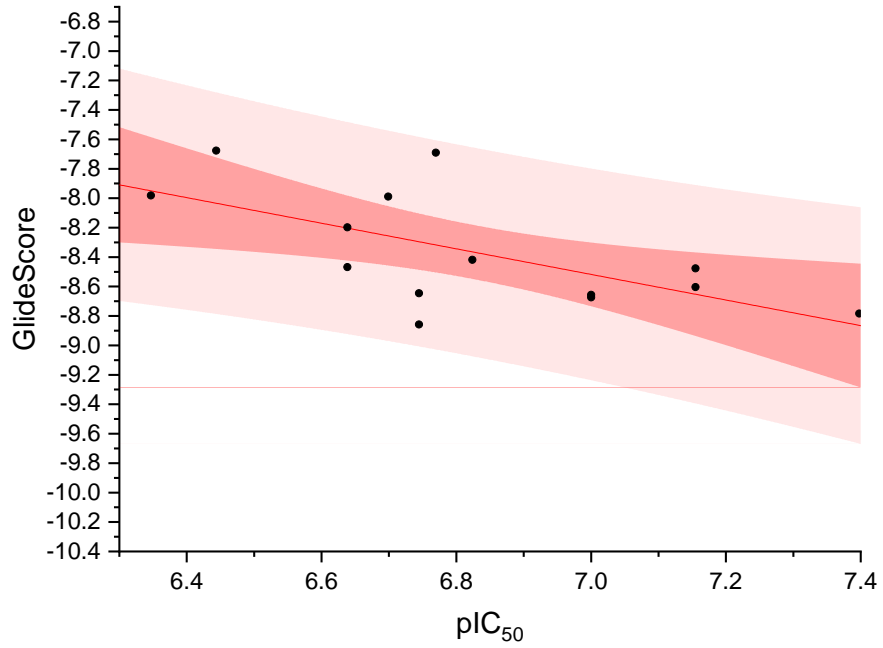
Compounds **1** - **16** docked in crystal structure 5K48 with waters 438 and 558 included and manually orientated XP GlideScore fitted to VIM-2 pIC_{50}



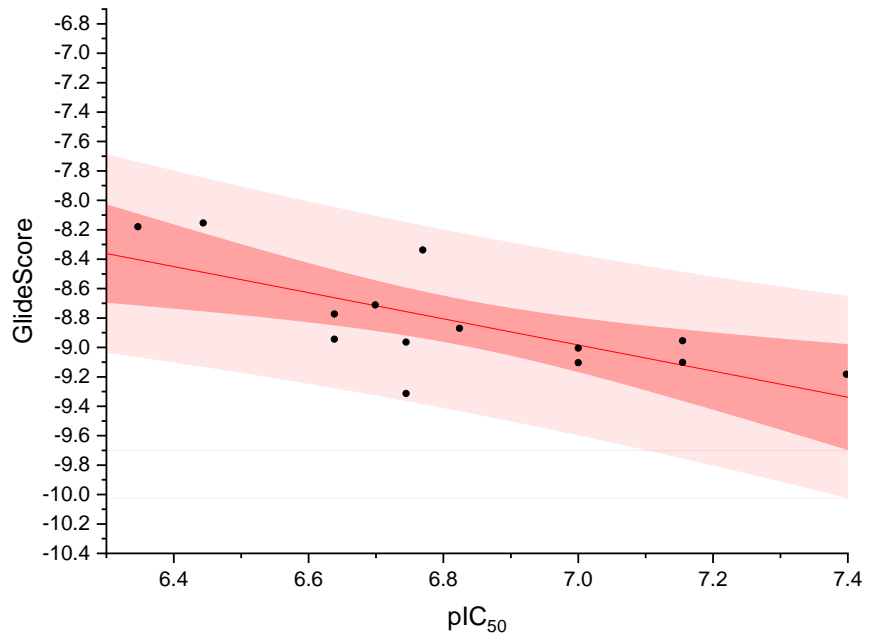
Compounds **1** - **16** docked in crystal structure 5K48 with water 438 included and manually orientated XP GlideScore fitted to VIM-2 pIC_{50}



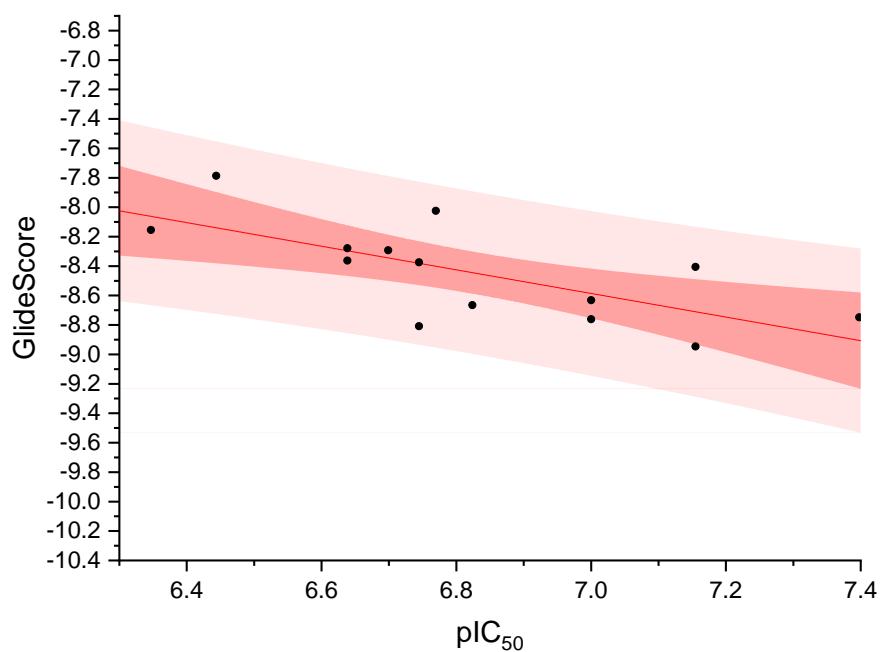
Compounds **1 - 16** docked in crystal structure 5K48 with water 538 included and manually orientated XP GlideScore fitted to VIM-2 pIC_{50}



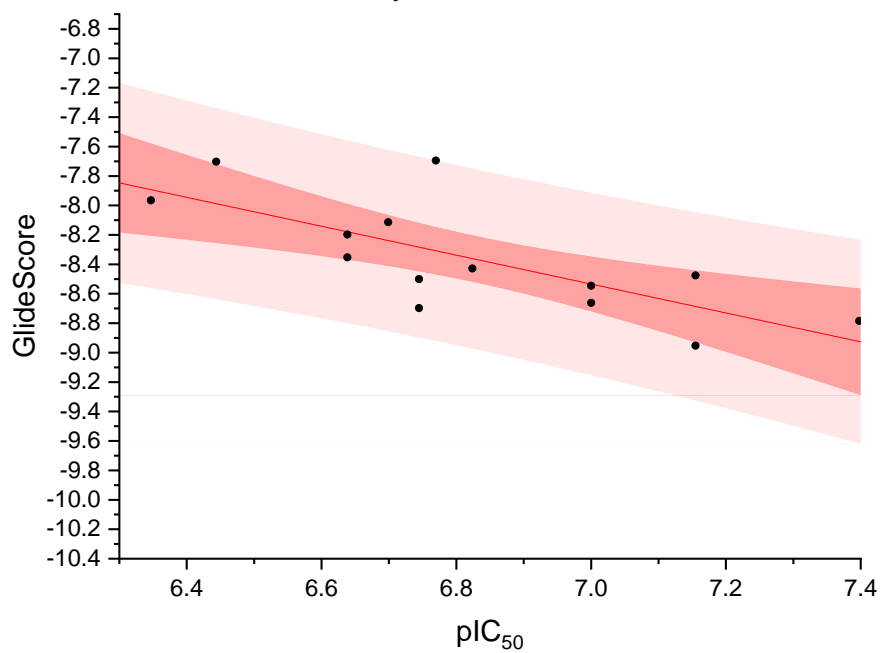
Compounds **1 - 16** docked in crystal structure 5K48 with metal constraints applied and waters 438 and 558 included and manually orientated XP GlideScore fitted to VIM-2 pIC_{50}



Compounds **1** - **16** docked in crystal structure 5K48 with metal constraints applied and water 438 included and manually orientated XP GlideScore fitted to VIM-2 pIC_{50}



Compounds **1** - **16** docked in crystal structure 5K48 with metals constraints applied and water 558 included and manually orientated XP GlideScore fitted to VIM-2 pIC_{50}



Compounds **1** - **16** docked in crystal structure
5K48 GoldScore fitted to VIM-2 pIC_{50}

